



**UNIVERSITY OF ALMERÍA**

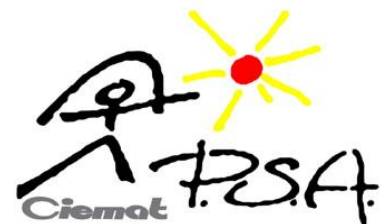
**Department of Chemical Engineering**

**OPERATING STRATEGIES FOR THE APPLICATION  
OF THE PHOTO-FENTON PROCESS TO REMOVE  
PERSISTENT POLLUTANTS**

**IRENE CARRA RUIZ**

**PhD THESIS**

**ALMERÍA 2014**







**Universidad de Almería**  
**Departamento de Ingeniería Química**

# **ESTRATEGIAS DE OPERACIÓN PARA LA APLICACIÓN DEL PROCESO FOTO-FENTON PARA ELIMINAR CONTAMINANTES PERSISTENTES**

Memoria presentada para aspirar al grado de Doctor por:

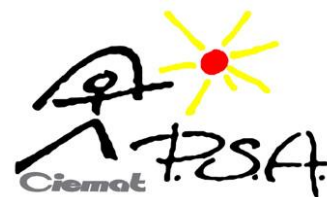
**IRENE CARRA RUIZ**

Fdo. Irene Carra Ruiz

## **DIRECTORES DE TESIS:**

**Dr. Don Sixto Malato Rodríguez**  
Investigador Titular OPI CIEMAT  
Ministerio de Economía y  
Competitividad

**Dr. Don José Antonio Sánchez Pérez**  
Catedrático del Departamento de  
Ingeniería Química  
Universidad de Almería





---

*“Most people say that it is the intellect which makes a great scientist. They are wrong: it is character”.*

***Albert Einstein***

---



## ACKNOWLEDGEMENTS

I would like to acknowledge the Ministerio de Educación, Cultura y Deporte for my FPU scholarship (AP2010-3218) and the funding for my placement in Cranfield University (EST13/00224),

To my supervisors José Antonio and Sixto for their help, advice and guidance during these years,

To my colleagues in the University of Almería and CIESOL. I can't help myself from giving a special thanks to Grace for her friendship and for simply being herself,

To the friends I made during my placement at Cranfield University. It was for a short time, but the experience of my PhD wouldn't have been the same without you.

Thanks to my family and friends. Words fall short to thank you for the last three years and more.

---





---

**TABLE OF CONTENTS**

<b>INDEX OF FIGURES.....</b>	<b>i</b>
<b>INDEX OF TABLES.....</b>	<b>v</b>
<b>ABSTRACT.....</b>	<b>vii</b>
<b>RESUMEN.....</b>	<b>xi</b>
<b>THESIS FRAMEWORK.....</b>	<b>xv</b>
<b>OBJECTIVES AND WORK PLAN SCHEME.....</b>	<b>xvii</b>
<b>1. INTRODUCTION.....</b>	<b>1</b>
<b>1.1 European Legislation –The Water Framework Directive .....</b>	<b>3</b>
<b>1.2 Spanish Legislation on water.....</b>	<b>5</b>
1.2.1 Water Reclamation Law.....	8
1.2.2 Waste Control Tax.....	9
1.2.3 Sanitary Tax.....	10
<b>1.3 Advanced Oxidation Processes.....</b>	<b>14</b>
1.3.1 UV photolysis.....	14
1.3.2 Hydrogen peroxide photolysis.....	15
1.3.3 Heterogeneous photocatalysis.....	15
1.3.4 Persulphate systems.....	16
<b>1.4 The photo-Fenton process.....</b>	<b>17</b>
1.4.1 Process and reactions.....	17
1.4.2 Factors affecting the operation of the process.....	18
1.4.3 Photo-Fenton-like processes.....	24
1.4.4 Control and monitoring of the photo-Fenton process through dissolved oxygen.....	26
1.4.5 Variables affecting costs in the photo-Fenton process.....	27
1.4.6 Solar photoreactors for water treatment applications.....	30
<b>2. EXPERIMENTAL.....</b>	<b>37</b>
<b>2.1 Model pollutants.....</b>	<b>41</b>

---

---

<b>2.2 Water matrices</b> .....	<b>39</b>
<b>2.3 Reagents</b> .....	<b>42</b>
2.3.1 Analysis.....	42
2.3.2 Experiments.....	42
<b>2.4 Analytical techniques</b> .....	<b>43</b>
2.4.1 Dissolved Organic Carbon (DOC) .....	43
2.4.2 Pollutant concentration determination by Ultra Performance Liquid Chromatography with diode array detector (UPLC/DAD).....	44
2.4.3 Ionic Chromatography (IC) .....	45
2.4.4 Dissolved iron measurement.....	47
2.4.5 Hydrogen peroxide measurement.....	48
2.4.6 Persulphate measurement.....	49
2.4.7 Chemical Oxygen Demand (COD).....	50
<b>2.5 Pilot Plants and laboratory scale experiments</b> .....	<b>50</b>
2.5.1 Compound Parabolic Collector (CPC).....	50
2.5.2 Flat-reflector photoreactor.....	51
2.5.3 The Raceway Pond Reactor.....	52
2.5.4 Solar box.....	53
<b>2.6 Experimental set-up</b> .....	<b>54</b>
2.6.1 Preparation of pollutant and simulated wastewater solutions.....	54
2.6.2 Photo-Fenton experimental procedure.....	55
2.6.3 UV lamps.....	56
<b>3. RESULTS AND DISCUSSION</b> .....	<b>59</b>
<b>3.1 Strategies to remove medium concentration of pollutant at natural pH...</b>	<b>61</b>
3.1.1 Use of iron complexes.....	61
3.1.2 Iron dosage strategy.....	76
<b>3.2 Strategies to remove micropollutants</b> .....	<b>87</b>
3.2.1 Iron dosage for micropollutant removal.....	88
3.2.2 Interrelation between iron concentration and irradiance.....	100
3.2.3 Modelling of the irradiance saturation effect.....	116
3.2.4 Raceway ponds as novel technology for micropollutant removal.....	122
3.2.4.1 Micropollutant removal in pilot plant scale raceway pond.....	122
3.2.4.2 Monitoring of transformation products.....	132

---

3.2.5 Use of lamps to run the photo-Fenton process.....	146
3.2.5.1 UVC low pressure amps.....	146
3.2.5.2 UVC high intensity LED.....	159
<b>4. CONCLUSIONS.....</b>	<b>169</b>
<b>5. CONCLUSIONES.....</b>	<b>175</b>
<b>6. REFERENCES.....</b>	<b>181</b>
<b>7. GLOSSARY.....</b>	<b>201</b>
<b>8. SCIENTIFIC PRODUCTION.....</b>	<b>205</b>

---



---

**INDEX OF FIGURES**

- Figure 1.1** Treated and reclaimed water (a) in Spain from 2004 to 2011; (b) and in 2011 in each Spanish region (data obtained from the National Institute of Statistic, update 2014).
- Figure 1.2** Simplified scheme of the redox iron cycle in the photo-Fenton process
- Figure 1.3** Operating strategy to treat wastewater based on pollutant concentration
- Figure 1.4** Parabolic trough collector plant at the Solar Platform of Almería
- Figure 1.5** CPC pilot plant at the Solar Platform of Almería
- Figure 1.6** (a) CPC design and (b) CPC with concentrating factor of one
- Figure 1.7** Transmittance of different materials for the manufacture of photoreactor tubes
- Figure 1.8** Transmittance of  $\text{Fe}^{3+}$  dissolved in water
- Figure 1.9** Design parameters to define row separation for minimum shadowing of collectors
- Figure 1.10** RPR for microalgal mass culture in the University of Almería
- Figure 1.11** Scheme and dimensions of an RPR (Chisti et al., 2007)
- Figure 2.1** Shimadzu analyser used for DOC measurement
- Figure 2.2** UPLC-DAD (Agilent Technologies 1200 series)
- Figure 2.3** Metrohm 881 Compact IC pro system
- Figure 2.4** Pilot plant CPC
- Figure 2.5** Flat-reflector photoreactor
- Figure 2.6** 360-L Raceway Pond Reactor
- Figure 2.7** Operating scheme in the SunTest CPS+ solar box with (a) the plate reactor, and (b) the stirred tank reactor
- Figure 2.8** Scheme of the UVC low pressure lamp system
- Figure 3.1** Chemical structure of ferrous D-gluconate, ferrous lactate and deferoxamine mesylate
- Figure 3.2** Acetaminophen degradation in a pilot plant at initial neutral pH using iron sulphate (a) and D-gluconate (b) (100 mg/L acetaminophen DOC, 20 mg/L  $\text{Fe}^{2+}$ , 1270 mg/L  $\text{H}_2\text{O}_2$ ).
- Figure 3.3** Acetaminophen degradation in a pilot-plant dosing  $\text{H}_2\text{O}_2$  twice and using iron sulphate at pH 2.8 (a) at initial neutral pH (b) and D-gluconate at initial neutral pH (c) (50 mg/L acetaminophen DOC, 20 mg/L  $\text{Fe}^{2+}$ ).

- Figure 3.4** Acetaminophen degradation in a pilot plant applying continuous H<sub>2</sub>O<sub>2</sub> addition and using iron sulphate as the iron source at initial neutral pH (50 mg/L acetaminophen DOC, 20 mg/L Fe<sup>2+</sup>).
- Figure 3.5** Results after applying the photo-Fenton process to real wastewater effluent enriched with acetaminophen and using two H<sub>2</sub>O<sub>2</sub> additions at initial neutral pH (50 mg/L acetaminophen DOC, 20 mg/L Fe<sup>2+</sup>).
- Figure 3.6** Chemical structure of oxamyl, methomyl, imidacloprid, pyrimethanil and dimethoate.
- Figure 3.7** Results obtained after 1h of solar photo-Fenton and dark Fenton with 50 mg DOC/L and 650 mg H<sub>2</sub>O<sub>2</sub>/L; at pH 2.8 with one initial iron addition of 20 mg Fe/L (a); at initial neutral pH with four additions of 5 mg Fe/L (b) and five additions of 20-20-10-10-10 mg Fe/L (c). The arrows point out the time of addition.
- Figure 3.8** Variation in the maximum DOC removal rate, calculated using illuminated time, with the mean dissolved iron concentration in the period of maximum mineralization rate.
- Figure 3.9** Treatment of real wastewater with solar photo-Fenton at (a) pH 2.8 with one iron addition of 20 mg/L using wastewater type I; and at initial neutral pH with iron additions 20-20-10-10-10 mg/L using wastewater type I (b, c) and II (d).
- Figure 3.10** Acetamiprid, thiabendazole and imazalil chemical structure.
- Figure 3.11** Impact of bicarbonates on ACTM, TBZ and IMZ degradation by photo-Fenton at natural pH using three iron additions of 20 mg Fe/L each (20x3). The arrows point out the time of addition.
- Figure 3.12** Acetamiprid, hydrogen peroxide and iron concentration profiles during solar photo-Fenton and Fenton run with sequential iron
- Figure 3.13** pH profiles for sequential iron dosage
- Figure 3.14** Continuous iron dosage effect on the solar photo-Fenton and Fenton process
- Figure 3.15** pH profiles for continuous iron dosage
- Figure 3.16** Acetamiprid degradation in the plate reactor and solar box with demineralised water (dark Fenton and 5, 15, 20 and 30 W<sub>UV</sub>/m<sup>2</sup>)
- Figure 3.17** Thiabendazole degradation profiles at 1 and 5 mg Fe/L and 1 mg Fe/L for imazalil in the plate reactor and solar box in demineralised water (dark Fenton and 5, 15, 20 and 30 W<sub>UV</sub>/m<sup>2</sup>)
- Figure 3.18** Acetamiprid degradation in simulated water at pilot plant scale under

different operating conditions of iron concentration and irradiance.

- Figure 3.19** Hydrogen peroxide consumption profiles in simulated water at pilot plant scale under different operating conditions of iron concentration and irradiance.
- Figure 3.20** Influence of irradiance and iron concentration on the acetamiprid and thiabendazole degradation kinetic constant,  $k'$ .
- Figure 3.21** Mass of acetamiprid ( $C_0 = 100 \mu\text{g/L}$ ) degraded at different light path lengths in stirred tank reactor: at 5 cm height (total volume 0.4 L) and 10 cm height (total volume 0.8 L)
- Figure 3.22** Experimental (dots) and predicted (lines) profiles for ACTM, TBZ and IMZ oxidation and hydrogen peroxide consumption for the model validation (runs 3, 5 and 10)
- Figure 3.23** Acetamiprid degradation by solar photo-Fenton and Fenton with 1, 5.5 and 10 mg Fe/L ( $24 \pm 3 W_{UV}/\text{m}^2$  and  $28 \pm 2 \text{ }^\circ\text{C}$ ).
- Figure 3.24** Thiabendazole degradation by solar photo-Fenton and Fenton with 1 mg Fe/L ( $24 W_{UV}/\text{m}^2$  and  $28 \pm 2 \text{ }^\circ\text{C}$ ).
- Figure 3.25** Hydrogen peroxide concentration profiles during pesticide degradation by solar photo-Fenton and Fenton with 1, 5.5 and 10 mg Fe/L
- Figure 3.26** Acetamiprid degradation and hydrogen peroxide consumption in simulated secondary effluent by solar photo-Fenton in 15 cm liquid-depth-RPR with 5.5 and 10 mg Fe/L, and in 5 cm diameter-CPC with 5.5 mg Fe/L
- Figure 3.27** Details of thiabendazole degradation ( $100 \mu\text{g/L}$ ) in deionised water and natural pH by Fenton with iron dosing (5-5-10-20 mg/L) for TPs identification. Samples for TPs analysis are marked by arrows
- Figure 3.28** Evolution of TPs formed during thiabendazole degradation by Fenton
- Figure 3.29** Thiabendazole degradation in MBR effluent treated by Fenton and photo-Fenton at initial neutral pH; in MBR effluent at pH 2.8 by photo-Fenton; and in deionised water at pH 2.8 by photo-Fenton
- Figure 3.30** Acetamiprid and thiabendazole degradation and hydrogen peroxide consumption after 120 min of solar photo-Fenton ( $14 W/\text{m}^2$ )
- Figure 3.31** Acetamiprid and thiabendazole degradation in industrial effluent by (a) solar photo-Fenton ( $15 W/\text{m}^2$ ) and (b) Fenton in the RPR
- Figure 3.32** Time profile of acetamiprid (a) and thiabendazol (b) and their respective TPs during photo-Fenton treatment of the SBR effluent in the agro-food industry

- Figure 3.33** Acetamiprid degradation in deionised water and by UV (10, 20, 27 W/m<sup>2</sup>); UV/TiO<sub>2</sub> (50, 100, 200 mg TiO<sub>2</sub>/L); UV/H<sub>2</sub>O<sub>2</sub> (25, 50, 100 mg/L); UV/H<sub>2</sub>O<sub>2</sub>/Fe (1mg Fe/L at pH 2.8 and 50 mg H<sub>2</sub>O<sub>2</sub>/L at natural pH), H<sub>2</sub>O<sub>2</sub>/Fe (1 mg Fe/L and 50 mg H<sub>2</sub>O<sub>2</sub>/L at natural pH); UV/PS (25, 50, 100 mg PS/L); UV/PS/Fe (50 mg PS/L and 1 mg Fe/L)
- Figure 3.34** Acetamiprid degradation in synthetic water by UV (10, 20, 27 W/m<sup>2</sup>); UV/TiO<sub>2</sub> (50, 100, 200 mg TiO<sub>2</sub>/L); UV/H<sub>2</sub>O<sub>2</sub> (25, 50, 100 mg/L); UV/H<sub>2</sub>O<sub>2</sub>/Fe (1mg Fe/L at pH 2.8 and 50 mg H<sub>2</sub>O<sub>2</sub>/L at natural pH), H<sub>2</sub>O<sub>2</sub>/Fe (1 mg Fe/L and 50 mg H<sub>2</sub>O<sub>2</sub>/L at natural pH); UV/PS (25, 50, 100 mg PS/L); UV/PS/Fe (50 mg PS/L and 1 mg Fe/L)
- Figure 3.35** Acetamiprid degradation profiles in CAS effluent at 20 W/m<sup>2</sup> by direct photolysis (UV), UV/H<sub>2</sub>O<sub>2</sub> (50 mg H<sub>2</sub>O<sub>2</sub>/L), UV/H<sub>2</sub>O<sub>2</sub>/Fe (1mg Fe/L natural pH and 50 mg H<sub>2</sub>O<sub>2</sub>/L), UV/PS (50, 100 mg PS/L), UV/PS/Fe (50 mg PS/L and 1 mg Fe/L)
- Figure 3.36** Acetamiprid degradation in the presence of 10 mg DOC/L of (a) humic acids; (b) lignin-derivative; and (c) lauryl sulphate at 20 W/m<sup>2</sup> by direct photolysis (UV), UV/H<sub>2</sub>O<sub>2</sub> (50 mg H<sub>2</sub>O<sub>2</sub>/L), UV/H<sub>2</sub>O<sub>2</sub>/Fe (1mg Fe/L natural pH and 50 mg H<sub>2</sub>O<sub>2</sub>/L at natural pH), UV/PS (50, 100 mg PS/L), UV/PS/Fe (50 mg PS/L and 1 mg Fe/L)
- Figure 3.37** Acetamiprid degradation in the (a) LED system and (b) LPL system at natural pH with one and sequencing iron additions every 30 seconds at a H<sub>2</sub>O<sub>2</sub>:Fe ratio of 4:1 and 2:1
- Figure 3.38** Acetamiprid degradation in the UVC-LED system using 1, 2 and 3 mg Fe/L and a H<sub>2</sub>O<sub>2</sub>:Fe ratio of 2:1 and 4:1 in synthetic secondary effluent at pH 2.8
- Figure 3.39** Model validation for acetamiprid degradation in the LED system with a H<sub>2</sub>O<sub>2</sub>:Fe ratio of 2:1 (3 mg Fe/L) and 4:1 (1 mg Fe/L)



**INDEX OF TABLES**

<b>Table 1.1</b>	Water Framework Directive and amendments (2014 update)
<b>Table 1.2</b>	List of priority substances in the field of water policy (Annex X of the WFD updated by Directive 2013/39/EU)
<b>Table 1.3</b>	Sanitary tax equations in the Spanish Autonomous Communities regulation for industrial wastewater
<b>Table 1.4</b>	Tax amounts resulting from the application of the ST equations in the regions which consider water pollution parameters to a treated effluent from a juice and soup industry
<b>Table 1.5</b>	Common iron complexes and chelates used for Fenton and photo-Fenton applications
<b>Table 1.6</b>	Common heterogeneous iron catalysts used for Fenton and photo-Fenton applications
<b>Table 2.1</b>	Model pollutants
<b>Table 2.2</b>	Natural water properties
<b>Table 2.3</b>	Simulated secondary effluent properties
<b>Table 2.4</b>	UPLC-DAD methods for the detection of the model compounds.
<b>Table 2.5</b>	Retention times for anions detected by IC
<b>Table 3.1</b>	Acetaminophen degradation at natural pH (except when indicated) applying photo-Fenton for 2 h at laboratory scale (initial concentration of 20 mg·L <sup>-1</sup> Fe and 1270 mg·L <sup>-1</sup> H <sub>2</sub> O <sub>2</sub> )
<b>Table 3.2</b>	Operating conditions and results obtained after 60 min for the solar photo-Fenton process applied to demineralised and real wastewater
<b>Table 3.3</b>	Real wastewater anion characterization
<b>Table 3.4</b>	Acetamidrid, thiabendazole and imazalil degradation and hydrogen peroxide consumption at the end of the experiment (45 min)
<b>Table 3.5</b>	Operating conditions at pilot plant scale.
<b>Table 3.6</b>	Zero-order kinetic constant (M·min <sup>-1</sup> ) for hydrogen peroxide consumption in deionised and simulated water for all assayed conditions.
<b>Table 3.7</b>	Experimental conditions for identification and validation runs
<b>Table 3.8</b>	Reaction scheme for the model
<b>Table 3.9</b>	Kinetic expressions for each reaction in the model
<b>Table 3.10</b>	Mass balances on the system for the model

<b>Table 3.11</b>	Model parameters in $\text{mM}^{-1} \text{s}^{-1}$
<b>Table 3.12</b>	Kinetic constants for ACTM and $\text{H}_2\text{O}_2$
<b>Table 3.13</b>	Experimental conditions for the degradation experiments
<b>Table 3.14</b>	Experimental conditions used with 1-L reactors
<b>Table 3.15</b>	Structure of acetamiprid transformation products analyzed by LC-QqLIT-MS
<b>Table 3.16</b>	Structure of thiabendazole transformation products analyzed by LC-QqLIT-MS
<b>Table 3.17</b>	Operating conditions assayed in deionised and simulated water with the low pressure lamps
<b>Table 3.18</b>	Acetamiprid pseudo-first order degradation constants in DW, SW and CAS water for each operating condition and consumed $\text{H}_2\text{O}_2$ or PS.
<b>Table 3.19</b>	CAS effluent properties
<b>Table 3.20</b>	Operating conditions assayed
<b>Table 3.21</b>	Model parameters and fitting

## ABSTRACT

The presence of persistent pollutants in water bodies has encouraged the scientific community to investigate advanced water processes which degrade them. Wastewater treatment plants are often based on biological processes as secondary treatment. Nevertheless, these systems are not sufficient to remove non-biodegradable contaminants or contaminants at a very low concentration. As a result, recalcitrant compounds can be detected in rivers, lakes and other aquatic systems. Stronger types of treatment are therefore required. Advanced Oxidation Processes (AOPs) have gained the reputation over the last few decades of being effective in this regard. Amongst them, homogeneous photocatalysis, or the photo-Fenton process, has been reported as being successful in the removal of organic pollutants. Nonetheless, its application at commercial scale has not yet become widespread.

This study investigated the application of several operating strategies to carry out the solar-driven photo-Fenton process. It was comprised by two parts: (i) the oxidation of pollutants in the mg/L range (medium concentration level) and (ii) in the µg/L range (micropollutants). For medium concentration of pollutants, the first strategy proposed was the use of the complexes iron d-gluconate, iron lactate and fertilizer ferroactive, and the iron chelate deferoxamine mesylate to operate the process at natural pH and mineralise 0.5 mM acetaminophen (50 mg DOC/L) in a compound parabolic collector (CPC). The strategy was compared with the addition of ferrous iron salt. Results showed that the addition of ferrous salt was analogous or better than the use of iron complexes. Based on these results, the dosage of iron salt was further investigated at pilot plant scale and under realistic conditions as secondary wastewater was used as an example of complex matrix where model contaminants were added. The removal of 50 mg DOC/L of a mixture of five commercial pesticides - Vydate® (10% w/v oxamyl), Metomur® (20% w/v methomyl), Couraze® (20% w/v imidacloprid), Perfekthion® (40% dimethoate) and Scala® (40% w/v pyrimethanil)- was evaluated

under different iron dosage strategies, paying special attention to iron concentration per dose and addition time. Complete pesticide removal and up to 50% mineralisation were achieved.

For the study of micropollutant removal, sequential and continuous iron salt dosage strategies were also applied. All the strategies used to operate the photo-Fenton process at micropollutant level were evaluated using a mixture of pesticides found in the effluent of an agro-food industry: acetamiprid, thiabendazole and imazalil, each at a concentration of 100 µg/L. Sequential and continuous iron salt dosages were investigated at pilot plant scale in a flat-reflector tubular photoreactor. Continuous dosage provided the shortest degradation time in real wastewater (15 min and 80 mg Fe/L in total).

At micropollutant level, the interrelationship between iron concentration and UV solar light was also studied. These two factors are the key variables in photoreactor design and process operation. Iron concentration was varied between 1-20 mg/L and UV-light between 5-30 W/m<sup>2</sup>. The experimentation was carried out in deionised water and simulated secondary effluent as well as at laboratory and pilot plant scale. Results indicated that above 15 W<sub>UV</sub>/m<sup>2</sup> and a light path length of 5 cm (the most commonly used path for this type of application) iron concentration limited the process and there was irradiance excess under these conditions. It was concluded that wider path lengths of more than 5 cm (typical of CPC) are recommended since more wastewater volume can be treated with a higher process rate per surface unit. A simplified model was also suggested to corroborate the phenomenology observed.

These conclusions led to the proposal of raceway pond reactors (RPRs) as a new technology for the application of solar photo-Fenton as tertiary treatment wastewater. RPRs are extensive photoreactors traditionally used for microalgal mass culture. A 360-L RPR was used to study the degradation of commercial formulations of

acetamiprid and thiabendazole (100 µg/L each) in water from the supply network in CIESOL and in simulated secondary effluent. Iron concentration (1-10 mg/L) and liquid depth (5-15 cm) were studied as process variables. A process time of 40 min was needed to treat 360 L until complete pollutant degradation was achieved. A higher treatment capacity per surface area than for CPC was obtained (48 mg/h·m<sup>2</sup> with 5.5 mg Fe/L and 15 cm liquid depth compared to 29 mg/h·m<sup>2</sup> for the same iron concentration in the CPC), proving the feasibility of using RPRs for micropollutant removal. Transformation products of thiabendazole and acetamiprid, the two most persistent model micropollutants, were detected in collaboration with the Environmental Analysis and Water Treatment research group in the CIESOL. They were monitored at laboratory scale and during the treatment of real agro-food wastewater in the RPR thanks to the use of highly sensitive liquid chromatography-triple quadrupole-linear ion trap-mass spectrometry (LC-QqLiT-MS/MS).

With the strategies learned, the operation of the photo-Fenton process was also studied under artificial light during a three-month placement at Cranfield University, UK. Firstly, UVC low pressure lamps were used to compare the performance of the photo-Fenton process with other AOP systems such as persulphate, hydrogen peroxide photolysis and heterogeneous photocatalysis to remove the most persistent model pollutant, acetamiprid. Results indicated that photo-Fenton and UVC/persulphate were the most effective AOPs tested in real wastewater. Secondly, high intensity UVC light emitting diodes (LEDs) were also tested as low energy-consuming technology for photo-Fenton applications, with high intensity LEDs emerging as a promising and novel technology for lamp-driven photo-Fenton.

Most of the work presented in this Ph.D. thesis showed that the efficient operation of solar-driven photo-Fenton is possible. The results indicated that iron dosage could be an effective strategy to operate the solar photo-Fenton process at natural pH to oxidise either mg/L or µg/L of pollutants. At micropollutant level,

irradiance requirements are not high, so extensive and low-cost photoreactors such as RPRs can be used. They demonstrate a high treatment capacity and this finding involves an approach to commercial scale application. Finally, lamp-driven photo-Fenton is also a promising process thanks to high intensity LEDs.

## RESUMEN

La presencia de contaminantes orgánicos persistentes en sistemas acuosos ha impulsado a la comunidad científica a investigar en nuevos procesos con el fin de degradarlos. Las plantas de tratamiento de aguas residuales constan de sistemas biológicos como tratamiento secundario. Sin embargo, estos sistemas no son suficientes para eliminar contaminantes no biodegradables o tóxicos en concentraciones muy bajas. Como consecuencia, se han detectado compuestos persistentes en ríos, lagos y otros sistemas acuosos. Por tanto, son necesarios tratamientos más enérgicos. Los Procesos de Oxidación Avanzada (PPOA) han surgido en las últimas décadas y se presentan como tratamientos efectivos en este sentido. Entre ellos, se ha demostrado que la fotocatalisis homogénea o proceso foto-Fenton es eficaz en la eliminación de contaminantes orgánicos. No obstante, su aplicación a escala comercial aún no se ha extendido.

En este trabajo se ha investigado la aplicación de distintas estrategias de operación para llevar a cabo el proceso foto-Fenton con radiación solar. El estudio tiene dos partes: (i) la oxidación de contaminantes en el nivel de mg/L (nivel medio de concentración); (ii) y en el nivel de µg/L (microcontaminantes). Para concentración media de contaminantes, la primera estrategia propuesta fue el uso de los complejos d-gluconato y lactato de hierro, y el fertilizante ferroactive y el quelato de hierro mesilato de deferoxamina para operar el proceso a pH natural y mineralizar 0.5 mM de acetaminofén (50 mg COD/L) en un fotorreactor tubular provisto de un colector parabólico compuesto (CPC). Esta estrategia se comparó con la adición secuencial de sulfato ferroso. Dichas adiciones de sal de hierro dieron resultados similares o mejores que el uso de los complejos de hierro. En base a estos resultados, se estudió la dosificación de sal de hierro en planta piloto y en condiciones reales, ya que se utilizó efluente de secundario como ejemplo de matriz de agua compleja a la que se añadieron los contaminantes. Se evaluó la eliminación de 50 mg COD/L de una

mezcla de cinco plaguicidas comerciales - Vydate® (10% m/v oxamilo), Metomur® (20% m/v metomilo), Couraze® (20% m/v imidacloprid), Perfekthion® (40% dimetoato) and Scala® (40% m/v pirimetanil)- con distintas estrategias de dosificación de hierro, prestando especial atención a la concentración de hierro por dosis y al tiempo de adición. Se consiguió la eliminación completa de los plaguicidas y hasta un 50% de mineralización.

Para el estudio de eliminación de microcontaminantes, también se aplicaron estrategias de dosificación de hierro secuencial y continua. Todas las estrategias para operar el proceso foto-Fenton a nivel de microcontaminantes se evaluaron utilizando una mezcla de plaguicidas detectados en el efluente de una industria agroalimentaria: acetamiprid, tiabendazol e imazalil, cada uno en una concentración de 100 µg/L. Las dosificaciones secuencial y continua se estudiaron en planta piloto en un fotorreactor tubular con reflector plano. Con la dosificación continua se obtuvo el tiempo de degradación más corto (15 min y 80 mg Fe/L en total).

A nivel de microcontaminantes también se estudió la relación entre la concentración de hierro y la luz solar ultravioleta. Estos dos factores son clave en el diseño de fotorreactores y en su operación. La concentración de hierro se varió entre 1 y 20 mg/L y la radiación UV entre 5 y 30 W/m<sup>2</sup>. La experimentación se llevó a cabo en agua destilada y en agua simulada de efluente secundario, tanto a escala de laboratorio como en planta piloto. Los resultados indicaron que por encima de 15 W<sub>UV</sub>/m<sup>2</sup> y para un paso óptico de 5 cm (el valor más común para este tipo de aplicación) la concentración de hierro limita el proceso y hay exceso de radiación. Se concluyó que pasos ópticos mayores de 5 cm (típicos para CPC) son recomendables ya que se puede tratar más volumen de agua con mayor velocidad de proceso por unidad de superficie. Se propuso un modelo simplificado para corroborar la fenomenología estudiada.



Estas conclusiones llevaron a proponer a los reactores tipo “raceway” como tecnología para la aplicación de foto-Fenton solar como tratamiento terciario de agua urbana. Los reactores “raceway” son fotorreactores extensivos tradicionalmente aplicados para el cultivo de microalgas. Se utilizó un reactor de 360 L para estudiar la degradación de formulaciones comerciales de acetamiprid y tiabendazol (100 µg/L de cada uno) en agua de red y en agua simulada de efluente secundario. La concentración de hierro (1-10 mg/L) y la profundidad de líquido (5-15 cm) fueron las variables de proceso estudiadas. Se necesitaron 40 min para tratar 360 L y degradar completamente los contaminantes. Se obtuvo una capacidad de tratamiento por unidad de superficie de 48 mg/h·m<sup>2</sup> con 5.5 mg Fe/L y 15 cm de profundidad de líquido en el reactor “raceway” mayor que los 29 mg/h·m<sup>2</sup> para la misma concentración de hierro en un CPC con 5 cm de diámetro de tubo, probando la viabilidad de utilizar reactores “raceway” para la eliminación de microcontaminantes.

En colaboración con el grupo de investigación de Análisis Ambiental y Tratamiento de Agua de CIESOL, se estudió la generación de los productos de transformación de tiabendazol y acetamiprid, los dos contaminantes más persistentes. Este estudio se desarrolló a escala de laboratorio y en el “raceway” durante el tratamiento de agua residual de una industria agroalimentaria gracias al uso de tecnología de alta sensibilidad analítica, LC-QqLiT-MS/MS, de sus siglas en inglés “liquid chromatography-triple quadrupole-linear ion trap-mass spectrometry”.

Finalmente, durante una estancia de tres meses en la Universidad de Cranfield, Reino Unido, se estudió la operación del proceso foto-Fenton con luz artificial. En primer lugar, se utilizaron lámparas UVC de baja presión para comparar el proceso foto-Fenton con otros PPOA como persulfato, fotólisis de peróxido de hidrógeno y fotocatalisis heterogénea para eliminar al contaminante más persistente, acetamiprid. Los resultados indicaron que foto-Fenton y UVC/persulfato fueron los PPOA más efectivos en agua real. En segundo lugar, se probaron diodos emisores de luz (LEDs,

de sus siglas en inglés) como tecnología de bajo consumo para aplicaciones con foto-Fenton utilizando lámparas LED de alta intensidad.

La mayor parte del trabajo presentado en esta tesis muestra que es posible la operación eficiente del proceso foto-Fenton solar. Los resultados indican que la dosificación de hierro podría ser una estrategia efectiva para operar el proceso de foto-Fenton solar a pH natural para oxidar tanto mg/L o  $\mu\text{g/L}$  de contaminantes. A nivel de microcontaminantes, los requerimientos de irradiancia no son grandes, así que puede utilizarse fotorreactores extensivos y de bajo coste como los "raceway". Presentan una alta capacidad de tratamiento y esto implica un acercamiento a la aplicación a escala comercial. Finalmente, el proceso foto-Fenton operado mediante lámparas también es prometedor gracias al uso de LED de alta intensidad.

## THESIS FRAMEWORK

The research presented in this Ph.D. thesis has been carried out in the framework of three projects:

- 1) “Development of new strategies based on solar photocatalysis for water reclamation” (FOTOREG). The aim of the Project was to study new sustainable technologies based on the use of solar energy for water reclamation. It is a coordinated national project between the Solar Platform of Almería and the Chemical Engineering and Analytical Chemistry groups in CIESOL.
- 2) “Combination of intensive technologies for the enhancement of water effluent quality in small and medium-size industries. Design of an integrated process” (AQUAPYME). Its main purpose was to investigate the use of solar photocatalysis to remove persistent pollutants from industrial effluents. It is funded by the Junta de Andalucía in coordination with the agro-food industry “Cítricos del Andarax S.A”.
- 3) “Design of new reactors for solar photo-Fenton applied to water reclamation. Economy, scale and control of the process” (SULAYR). This is a project funded by the Junta de Andalucía with the aim of investigating new photoreactors for solar and lamp-driven photo-Fenton.

This research has been developed in the Department of Chemical Engineering of the University of Almería and CIESOL with the studentship FPU for the formation of teaching staff at universities, awarded by the Spanish Ministry of Education, who also funded a placement for three months at the Water Science Institute in Cranfield University.

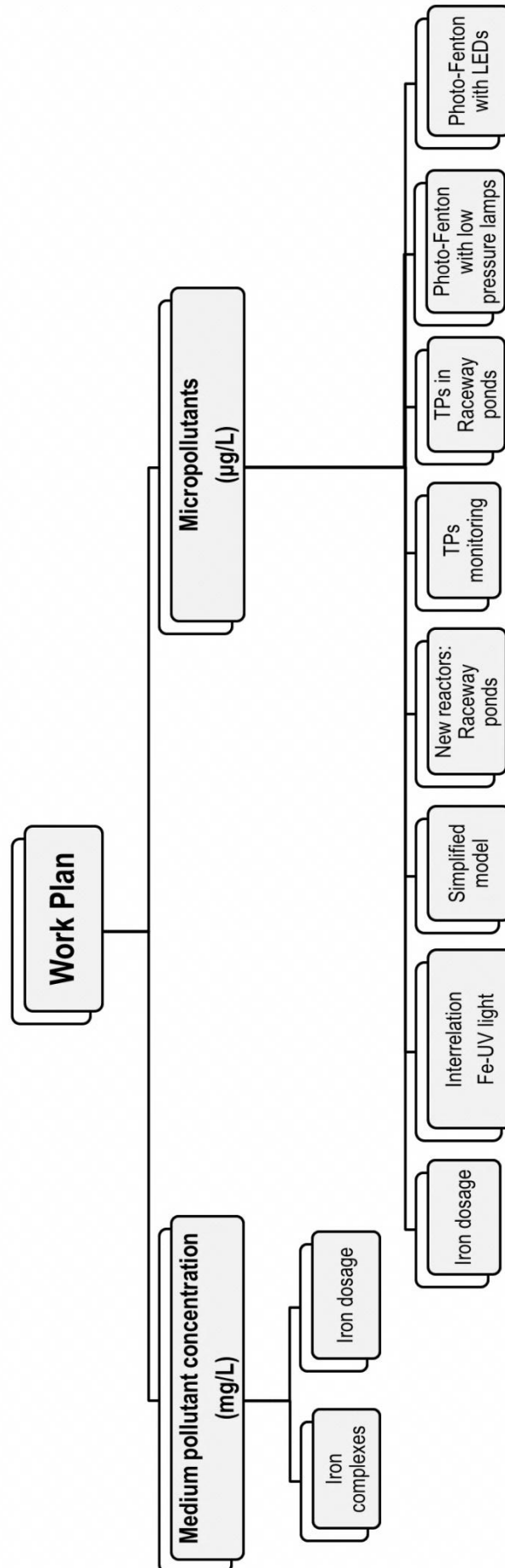


## OBJECTIVES AND WORK PLAN SCHEME

The main objective of this Ph.D. thesis is to investigate and develop new operating strategies to operate the photo-Fenton process to remove persistent pollutants. The photo-Fenton process is a well-known Advanced Oxidation Process which has been proven effective in the removal of organic contaminants. However, its commercial application has not yet been fully established and only a few industrial-scale plants exist worldwide. Finding a successful operating strategy would help this technology to become more widespread at a commercial level. The investigation was carried out based on pollutant concentration: on the one hand, to treat effluents with medium concentration of pollutants (mg/L range); and on the other hand, to remove micropollutants ( $\mu\text{g/L}$  range). To this end, specific objectives were developed:

- Operate the process at natural pH. Firstly, the use of organic iron complexes was proposed, followed by an operating strategy based on the dosage of iron salt.
- Study the interrelationship between iron concentration-irradiance to better understand the UV-light requirement as a function of the supplied amount of catalyst (iron). This would help with photoreactor design and, therefore, process operation.
- Investigate a simplified model able to simulate the phenomenology of pollutant degradation based on irradiance and iron concentration.
- Propose a new photoreactor design, with a lower cost and more feasible from an operating point of view.

A scheme of the work plan carried out in this thesis is presented below.



# ***INTRODUCTION***

---





## **1. INTRODUCTION**

Approximately 70% of the planet is covered by water. However, only 3% of it is fresh water. In addition, not all fresh water is available for human use since two-thirds of it forms part of icecaps and glaciers (USGS, 2014). Furthermore, human activities affect water systems, which include rivers, lakes, aquifers and wetlands, which subsequently become stressed. The main factors behind water stress are pollution, climate change, agriculture and population growth (WWF, 2014).

Pollution comes from many sources such as pesticides, which become part of water effluents through agriculture or agrofood industries. Other common sources are untreated urban wastewater and industrial wastewater. As a result of the excessive generation of carbon dioxide and other greenhouse gases, the climate is changing. As a consequence, droughts and floods are becoming more frequent in some places. These and other changes are giving rise to a decrease in available water. Agriculture is one of the activities which consumes the most water and inefficiencies in irrigation technologies increase water waste. Therefore, aquifers, rivers and lakes are quickly drying up. Countries like China, the United States or Spain are getting close to their water resource limits. Population growth is also one of the reasons behind freshwater scarcity. The increase in the population as well as industrial development is generating further water stress (WWF, 2014).

To decrease the generation of polluted water and improve water reclamation techniques, the European Union (EU) has set up a legislative framework through the Water Framework Directive (WFD). Every member of the EU has to meet the goals established in the WFD and in the future may include more restrictive measures. To that effect, innovative processes and technologies for water treatment such as Advanced Oxidation Processes (AOPs) should be developed. The combination of these processes with other well-established ones such as biological treatments and the use of solar light as source of energy for AOPs can provide a potential solution for water pollution.

### **1.1 European Legislation –Water Framework Directive**

Human activities and population growth have brought about an increase in pressure on water resources in Europe. The European Union established the Water Framework Directive (WFD) in 2000 to ensure the protection of water bodies ('Directive 2000/60/EC of the European Parliament and of the Council establishing a framework

for the Community action in the field of water policy'). It is explicitly aimed at the protection of surface waters, transitional waters, coastal waters and groundwater. The specific purposes of the WFD are:

- Prevent and enhance the aquatic systems
- Promote sustainable water use
- Control and reduce discharges containing priority substances
- Reduce groundwater pollution
- Mitigate flood and drought effects by maintaining the good quality of groundwater, marine and surface waters

The WFD has been amended over the years by different acts, presented in Table 1.1. It was also complemented by more specific EU laws: the Environmental Quality Standards Directive (2008), the Marine Strategy Framework Directive (2008), the Floods Directive (2007), the Groundwater Directive (2006), the Bathing Water Directive (2006), the Drinking Water Directive (1998) and the Urban Wastewater Directive (1991).

**Table 1.1.** Water Framework Directive and amendments (2014 update).

<b>Acts</b>	<b>Measures</b>
Directive 2000/60/EC of the European Parliament and of the Council establishing a framework for the Community action in the field of water policy	First approach at water protection in river basins
Decision No 2455/2001/EC of the European Parliament and of the Council of 20 November 2001	Lists 33 priority substances dangerous to the environment; 20 are priority hazardous substances and should be out of the environment in less than 20 years; other 13 are subject to review as possible priority hazardous substances
Directive 2008/105/EC of the European Parliament and of the Council of 16 December 2008	Lays down the environmental quality standards for priority substances and sets the limits for the 33 priority substances and 8 other compounds
Directive 2009/31/EC of the European Parliament and of the Council of 23 April 2009	Amendment for the injection of CO <sub>2</sub> into saline aquifers for the purposes of geological storage
Directive 2013/39/EU of the European Parliament and of the Council Text with EEA relevance of 12 August 2013	Update for the list of priority substances

With the establishment of the WFD a healthy status in all water bodies is expected by 2015. At the moment, the chemical status of 25% of groundwater is poor due to human activities. If further measures are not taken by this time, 47% of EU surface waters will not be up to the required standard (European Commission, 2014).

Concern about the presence of pollutants in water bodies is also expressed in the WFD. The amended version considers a group of priority substances which have been found water bodies and are dangerous to the environment, including organohalogen and organophosphorous compounds, substances which have been proved to possess carcinogenic or mutagenic properties or properties which may affect steroidogenic, thyroid, reproduction or other endocrine-related functions in or via the aquatic environment, persistent hydrocarbons and toxic substances, cyanides, metals, arsenic compounds, biocides, among others (Table 1.2). On a more specific level, the WFD also includes a list of priority substances labelled as “priority hazardous substances” (Table 1.2). According to the WFD, “hazardous substances” are ‘substances or groups of substances that are toxic, persistent and liable to bioaccumulate, and other substances or groups of substances which give rise to an equivalent level of concern’. Specific measures against this list of priority substances have to be adopted to progressively reduce them and, eventually, cease their discharge. The measures needed to adapt to the WFD have to be included in the legislation of each member state of the EU. In the case of Spain, local and national legislation has been established to meet European standards and regulate water management.

## **1.2 Spanish Legislation on water**

In Spain the first water law which involved water management was the Water Law in 1985 (Law, 1985). It was the first one established to manage surface and groundwater in Spain. It also included some points about water pollution, wastewater discharge regulation and the need to control water quality. After that several other regulations were established until in 2001 the Consolidated Water Law (CWL) (Royal Decree, 2001) was published. The CWL unified all the regulations and is currently managing the hydric resources in Spain (Sánchez-Martínez et al., 2011). Nonetheless, the CWL has also been modified over the years to adapt it to the WFD. The CWL has established a general framework for water body regulation, wastewater disposal and the characteristics of discharged effluents and water reclamation. It also includes the regulation for water depuration, reclamation, desalination and saving (Sánchez-

Martínez et al., 2011). One of its main contributions is the Water Reclamation Law that establishes the regulation for reclaimed water in Spain.

**Table 1.2.** List of priority substances in the field of water policy (Annex X of the WFD updated by Directive 2013/39/EU).

No.	CAS number (1)	EU number (2)	Name of priority substance (3)	Identified as priority hazardous substance
1	15972-60-8	240-110-8	Alachlor	
2	120-12-7	204-371-1	Anthracene	X
3	1912-24-9	217-617-8	Atrazine	
4	71-43-2	200-753-7	Benzene	
5	not applicable	not applicable	Brominated diphenylethers	X (4)
6	7440-43-9	231-152-8	Cadmium and its compounds	X
7	85535-84-8	287-476-5	Chloroalkanes, C <sub>10-13</sub>	X
8	470-90-6	207-432-0	Chlorfenvinphos	
9	2921-88-2	220-864-4	Chlorpyrifos	
10	107-06-2	203-458-1	1,2-dichloroethane	
11	75-09-2	200-838-9	Dichloromethane	
12	117-81-7	204-211-0	Di(2-ethylhexyl)phthalate (DEHP)	X
13	330-54-1	206-354-4	Diuron	
14	115-29-7	204-079-4	Endosulfan	X
15	206-44-0	205-912-4	Fluoranthene	
16	118-74-1	204-273-9	Hexachlorobenzene	X
17	87-68-3	201-765-5	Hexachlorobutadiene	X
18	608-73-1	210-168-9	Hexachlorocyclohexane	X
19	34123-59-6	251-835-4	Isoproturon	
20	7439-92-1	231-100-4	Lead and its compounds	
21	7439-97-6	231-106-7	Mercury and its compounds	X
22	91-20-3	202-049-5	Naphthalene	
23	7440-02-0	231-111-4	Nickel and its compounds	
24	not applicable	not applicable	Nonylphenols	X (5)
25	not applicable	not applicable	Octylphenols (6)	
26	608-93-5	210-172-0	Pentachlorobenzene	X
27	87-86-5	201-778-6	Pentachlorophenol	
28	not applicable	not applicable	Polyaromatic hydrocarbons (PAH) (7)	X
29	122-34-9	204-535-2	Simazine	
30	not applicable	not applicable	Tributyltin compounds	X (8)
31	12002-48-1	234-413-4	Trichlorobenzenes	

32	67-66-3	200-663-8	Trichloromethane (chloroform)	
33	1582-09-8	216-428-8	Trifluralin	X
34	115-32-2	204-082-0	Dicofol	X
35	1763-23-1	217-179-8	Perfluorooctane sulfonic acid and its derivatives (PFOS)	X
36	124495-18-7	not applicable	Quinoxifen	X
37	not applicable	not applicable	Dioxins and dioxin-like compounds	X (9)
38	74070-46-5	277-704-1	Aclonifen	
39	42576-02-3	255-894-7	Bifenoxy	
40	28159-98-0	248-872-3	Cybutryne	
41	52315-07-8	257-842-9	Cypermethrin (10)	
42	62-73-7	200-547-7	Dichlorvos	
43	not applicable	not applicable	Hexabromocyclododecanes (HBCDD)	X (11)
44	76-44-8/ 1024-57-3	200-962-3/ 213-831-0	Heptachlor and heptachlor epoxide	X
45	886-50-0	212-950-5	Terbutryn	

<sup>(1)</sup> CAS: Chemical Abstracts Service.

<sup>(2)</sup> EU-number: European Inventory of Existing Commercial Substances (EINECS) or European List of Notified Chemical Substances (ELINCS).

<sup>(3)</sup> Where groups of substances have been selected, unless explicitly noted, typical individual representatives are defined in the context of the setting of environmental quality standards.

<sup>(4)</sup> Only Tetra, Penta, Hexa and Heptabromodiphenylether (CAS -numbers 40088-47-9, 32534-81-9, 36483-60-0, 68928-80-3, respectively).

<sup>(5)</sup> Nonylphenol (CAS 25154-52-3, EU 246-672-0) including isomers 4-nonylphenol (CAS 104-40-5, EU 203-199-4) and 4-nonylphenol (branched) (CAS 84852-15-3, EU 284-325-5).

<sup>(6)</sup> Octylphenol (CAS 1806-26-4, EU 217-302-5) including isomer 4-(1,1',3,3'-tetramethylbutyl)-phenol (CAS 140-66-9, EU 205-426-2).

<sup>(7)</sup> Including benzo(a)pyrene (CAS 50-32-8, EU 200-028-5), benzo(b)fluoranthene (CAS 205-99-2, EU 205-911-9), benzo(g,h,i)perylene (CAS 191-24-2, EU 205-883-8), benzo(k)fluoranthene (CAS 207-08-9, EU 205-916-6), indeno(1,2,3-cd)pyrene (CAS 193-39-5, EU 205-893-2) and excluding anthracene, fluoranthene and naphthalene, which are listed separately.

<sup>(8)</sup> Including tributyltin-cation (CAS 36643-28-4).

<sup>(9)</sup> This refers to the following compounds: 7 polychlorinated dibenzo-p-dioxins (PCDDs): 2,3,7,8-T4CDD (CAS 1746-01-6), 1,2,3,7,8-P5CDD (CAS 40321-76-4), 1,2,3,4,7,8-H6CDD (CAS 39227-28-6), 1,2,3,6,7,8-H6CDD (CAS 57653-85-7), 1,2,3,7,8,9-H6CDD (CAS 19408-74-3), 1,2,3,4,6,7,8-H7CDD (CAS 35822-46-9), 1,2,3,4,6,7,8,9-O8CDD (CAS 3268-87-9); 10 polychlorinated dibenzofurans (PCDFs): 2,3,7,8-T4CDF (CAS 51207-31-9), 1,2,3,7,8-P5CDF (CAS 57117-41-6), 2,3,4,7,8-P5CDF (CAS 57117-31-4), 1,2,3,4,7,8-H6CDF (CAS 70648-26-9), 1,2,3,6,7,8-H6CDF (CAS 57117-44-9), 1,2,3,7,8,9-H6CDF (CAS 72918-21-9), 2,3,4,6,7,8-H6CDF (CAS 60851-34-5), 1,2,3,4,6,7,8-H7CDF (CAS 67562-39-4), 1,2,3,4,7,8,9-H7CDF (CAS 55673-89-7), 1,2,3,4,6,7,8,9-O8CDF (CAS 39001-02-0); 12 dioxin-like polychlorinated biphenyls (PCB-DL): 3,3',4,4'-T4CB (PCB 77, CAS 32598-13-3), 3,3',4',5'-T4CB (PCB 81, CAS 70362-50-4), 2,3,3',4,4'-P5CB (PCB 105, CAS 32598-14-4), 2,3,4,4',5'-P5CB (PCB 114, CAS 74472-37-0), 2,3',4,4',5'-P5CB (PCB 118, CAS 31508-00-6), 2,3',4,4',5'-P5CB (PCB 123, CAS 65510-44-3), 3,3',4,4',5'-P5CB (PCB 126, CAS 57465-28-8), 2,3,3',4,4',5'-H6CB (PCB 156, CAS 38380-08-4), 2,3,3',4,4',5'-H6CB (PCB 157, CAS 69782-90-7), 2,3',4,4',5,5'-H6CB (PCB 167, CAS 52663-72-6), 3,3',4,4',5,5'-H6CB (PCB 169, CAS 32774-16-6), 2,3,3',4,4',5,5'-H7CB (PCB 189, CAS 39635-31-9).

<sup>(10)</sup> CAS 52315-07-8 refers to an isomer mixture of cypermethrin, alpha-cypermethrin (CAS 67375-30-8), beta-cypermethrin (CAS 65731-84-2), theta-cypermethrin (CAS 71697-59-1) and zeta-cypermethrin (52315-07-8).

<sup>(11)</sup> This refers to 1,3,5,7,9,11-Hexabromocyclododecane (CAS 25637-99-4), 1,2,5,6,9,10-Hexabromocyclododecane (CAS 3194-55-6),  $\alpha$ -Hexabromocyclododecane (CAS 134237-50-6),  $\beta$ -Hexabromocyclododecane (CAS 134237-51-7) and  $\gamma$ -Hexabromocyclododecane (CAS 134237-52-8).

### 1.2.1 The Water Reclamation Law

The current version of the CWL includes the Water Reclamation Law (Royal Decree, 2007). It establishes the different uses of reclaimed water and the water quality parameters required for each use. They are classified as follows:

- 1) Urban (e.g. park irrigation, street cleaning)
- 2) Agricultural (e.g. crop irrigation)
- 3) Industrial (e.g. process and cleaning water)
- 4) Leisure activities (e.g. golf course irrigation)
- 5) Environmental activities (e.g. aquifer recharge)

However, reclaimed water cannot be used for human consumption in Spain at the present time and it specifies that the use of water reclamation is prohibited for food industry, hospital facilities, mollusc cultivation in aquaculture, bath water, fountains in public places, cooling towers close to urban activities and any other specific case that the health authority deems appropriate.

For the accepted uses the effluent must be monitored. The parameters evaluated for the use of reclaimed water are:

- 1) Intestinal nematodes
- 2) *Escherichia coli*
- 3) Suspended solids
- 4) Turbidity
- 5) Other criteria: depending on the use, other parameters like total nitrogen, conductivity or metals are evaluated

Nevertheless, there is still a long way to go. Figure 1.1 shows the values of treated and reclaimed water in Spain from 2004 to 2011 (Figure 1.1a) and for each Spanish region in 2011 (Figure 1.1b). It can be seen that there is a great deal of potential for water reclamation, but not all the wastewater is treated to the point of reuse.

Aside from water reclamation, at a national and local level, Spanish regulation also establishes more specifically the requirements for wastewater disposal. Examples of it are the Waste Control Tax and the Sanitary Tax.

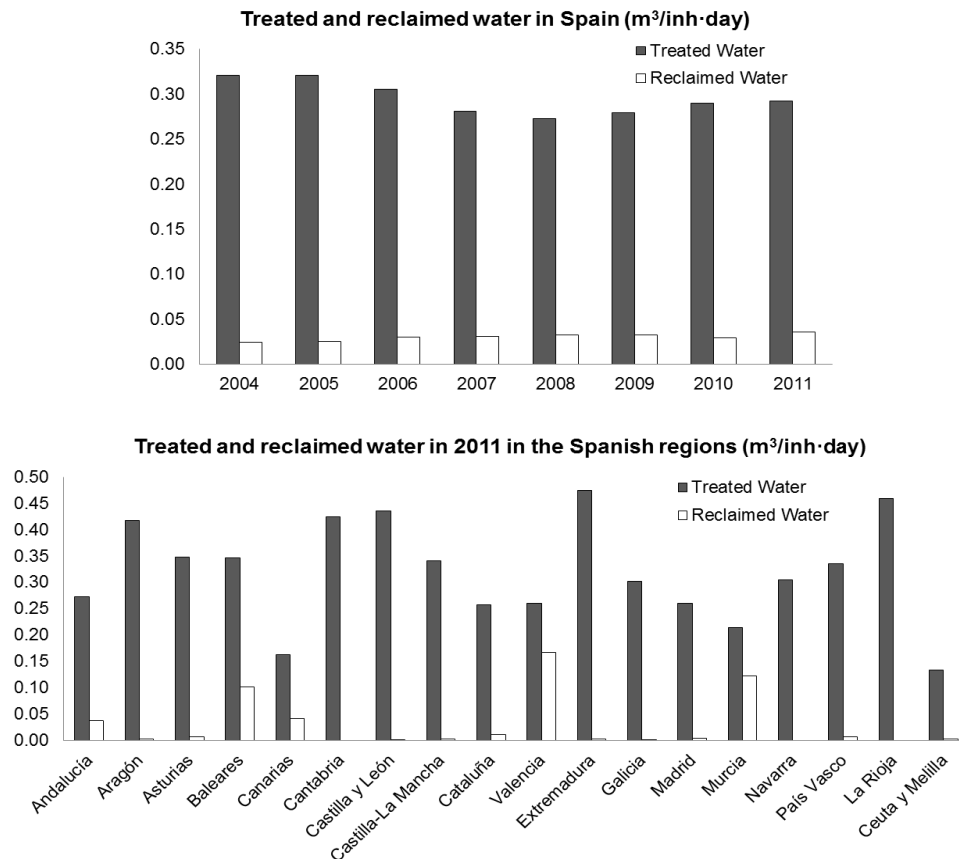


**Figure 1.1.** Treated and reclaimed water (a) in Spain from 2004 to 2011; (b) and in 2011 in each Spanish region (data obtained from the National Institute of Statistic, update 2014).

### 1.2.2 The Waste Control Tax (WCT)

The current version of the CWL also manages wastewater discharges into surface and groundwater through the Waste Control Tax (WCT). Wastewater treatment and proper management of water discharge depend on current legislation. In Spain, there are different taxation models depending on where the effluent is discharged. The WCT regulates discharges into the Hydraulic Public Domain nationwide, which includes surface water (e.g. rivers and lakes) and groundwater.

In the Article 113 of Royal Decree 1/2001 of July 20<sup>th</sup> the Consolidated Water Law establishes that waste discharge into the Hydraulic Public Domain will be taxed with a fee subsequently designated to the study, control, protection and improvement of the natural water body of each river basin district. This tax is fixed in each region in Spain. The WCT amount is the product of the wastewater volume ( $V$ ) and the unitary

price (UP) of waste control (Royal Decree, 2001),  $WTC=V \cdot UP$ . This unitary price depends on the type of wastewater (e.g. industrial or urban wastewater). The unitary price, UP, is calculated by multiplying the basic price per cubic meter by a multiplying coefficient that is established by the current legislation. The coefficient is based on the nature, characteristics and pollution grade of the waste (e.g. industrial water from an agrofood industry), as well as the environmental quality of the receiving environment.

As an example, we could apply the calculation of the WCT to the discharge of the biologically treated effluent of an agrofood industry which produces different types of soup, creams and juices seasonally and that was used in the work plan (Section 2.2). The yearly wastewater volume generated in this industry can be assumed to be  $134,400 \text{ m}^3$ .

In this case, the basic price per cubic meter is fixed at  $0.03005 \text{ €/m}^3$  (basic price for industrial wastewater). A multiplying coefficient is applied to this fixed price which depends on the waste type, waste characteristics, pollution and environmental quality of the water body, attending to Appendix IV of Royal Decree 603/2003 of May 23rd (Decree, 2008). For industrial wastewater and, specifically, for the manufacture of fruit and juices, which has in-situ wastewater treatment and, later discharged to a river, the coefficient would be 0.56. This coefficient would multiply the basic price,  $0.03005 \text{ €/m}^3$  by the yearly wastewater volume,  $134,400 \text{ m}^3$ . For this example, the WCT would be  $WCT=134,400 \cdot 0.03005 \cdot 0.56=2,262 \text{ €/year}$  (Román Sánchez et al., 2011).

### 1.2.3 The Sanitary Tax

Another regulated fee in Spain is the Sanitary Tax (ST). The ST regulates discharges into the sewer network system at a local level. The amount collected is used to finance wastewater treatment costs, necessary for carrying out general services. The aim of the tax is to improve public water treatment and reduce pollution in water. The ST encourages wastewater treatment to diminish discharged pollution. It is a levy used to finance wastewater treatment as well as sanitary activities such as maintenance, operational costs and essential annual investment. Therefore, making use of an effective water treatment can result in potential savings for a company since the ST is reduced (Nemetz, 1980; Steer et al., 2003; Ko et al., 2004).

In Spain, autonomous communities establish their own STs which are applied in each of their provinces. For industrial wastewaters, the ST could penalize water polluters with a fixed amount of tax which does not take into account the pollution load



of the wastewater; or by establishing common parameters used for water characterization in order to calculate the final tax amount, such as the Chemical Oxygen Demand (COD), Biological Oxygen Demand (BOD), nutrient concentrations (total nitrogen, N, and phosphorus, P), inhibitory substances (IS) or heavy metals (HM) and others which are more specific, such as pH or temperature, giving each of them different levels of importance according to the particular regional criteria (Román Sánchez et al., 2014).

The Spanish regions where pollution parameters are regarded as part of the tax equation in Spain are Asturias, Aragón, Cantabria, Cataluña, Galicia, La Rioja, Madrid, Murcia, Navarra and Valencia. The other regions do not take pollution parameters into consideration in their equations. Autonomous communities such as Andalucía apply a fixed amount according to the industry type (Law, 2007). In Table 1.3, the STs of the regions which consider pollution parameters are displayed. The ST equations were taken out of the different regional regulations.

The structure of the STs is generally divided into two terms: firstly, a fixed cost term (FC) which is calculated regardless of the annual volume discharged; secondly, a variable cost term (VC), which is dependent on the wastewater volume. The variable cost usually takes into account the pollution load (PL).

These equations were applied by Román et al., (2014) to the biologically treated effluent of the agrofood industry model which seasonally produces different types of soup, creamy soups and juices, described for the example in the WCT and that was used in the work plan (Section 2.2). For the application of the STs, it was estimated that yearly water consumption for this industry was 193,000 m<sup>3</sup> and the wastewater volume generated was 134,400 m<sup>3</sup>. These values were used as the basis for the yearly cost calculations for the tax. The pollution parameters during one of the seasons were: BOD= 46 g/L; COD= 108 g/L; N total= 3 g/L; Phosphorus= 1 g/L; suspended solids= 61 g/L; conductivity= 3 mS/cm. With these properties the equations of the ST were applied, providing the yearly cost of discharging this effluent in different autonomous communities (Table 1.4).

The costs in Table 1.4 highlight that, for this example, depending on the plant location, there are amount differences of up to 96,221 €/year to discharge the same wastewater- in this case, from 103,751 €/year that a company would have to pay in Madrid down to 7,530 €/year in Cantabria - with a mean value of 35,128 €/year-, which are differences of more than 1000 % for the same industry and the same wastewater,

for different locations all over Spain. These variations are caused by the different parameters being taken into account for each ST and also by the relative weight placed upon them in each region in Spain.

**Table 1.3** Sanitary tax equations in the Spanish Autonomous Communities regulation for industrial wastewater.

Region	Equation to calculate Sanitary Tax cost
Asturias (Law, 1994b)	$ST_{Asturias} (\text{€/year}) = FC + VC \cdot Q_w$ $FC (\text{€/year}) = 60$ $VC (\text{€/m}^3) = 0.12 + 0.4673 \cdot SS + 0.4154 \cdot COD + 2.3814 \cdot N + 4.3416 \cdot P + 0.5247 \cdot C + 0.004 \cdot \Delta T + 0.0239 \cdot HM + 0.0072 \cdot IS$
Aragon (Law, 2001)	$ST_{Aragón} (\text{€/year}) = FC + VC \cdot Q_w$ $FC (\text{€/year}) = 194.75$ $VC (\text{€/m}^3) = 0.396 \cdot SS + 0.551 \cdot COD + 1.082 \cdot N + 4.453 \cdot C + 0.00541 \cdot HM + 0.01286 \cdot IS$
Cantabria (Law, 2002)	$ST_{Cantabria} (\text{€/year}) = FC + VC \cdot Q_w$ $FC (\text{€/year}) = 14.88$ $VC (\text{€/m}^3) = 0.2316 \cdot SS \cdot C_{pSS} + 0.2681 \cdot COD \cdot C_{pCOD} + 0.2925 \cdot N \cdot C_{pN} + 0.5850 \cdot P \cdot C_{pP} + 3.6683 \cdot C \cdot C_{pC} + 0.004595 \cdot IS \cdot C_{pIS} + 0.000048 \cdot \Delta T \cdot C_{p\Delta T}$ $C_{pSS}, C_{pCOD}, C_{pN}, C_{pP}, C_{pC}, C_{pIM}, C_{p\Delta T}$ : peak coefficients for each parameter, defined as the relation between maximum concentration and mean concentration
Madrid (Law, 1993)	$ST_{Madrid} (\text{€/year}) = SC + VC \cdot Q_c$ $SC (\text{€/year}) = 1.254 \cdot (\phi^2 + 5 \phi)$ $\phi (mm) = 200$ $VC (\text{€/m}^3) = 0.5104 \cdot PL$ $PL = 1.1 \cdot SS + COD + 1.65 \cdot BOD$
Galicia (Law, 2010)	$ST_{Galicia} (\text{€/year}) = FC + VC \cdot Q_w$ $FC (\text{€/year}) = 30$ $VC (\text{€/m}^3) = 0.246 \cdot SS + 0.493 \cdot COD + 0.369 \cdot N + 0.74 \cdot P + 3.955 \cdot C + 0.0111 \cdot HM + 0.052 \cdot IS$
Cataluña (Legislative Decree, 2003)	$ST_{Cataluña} (\text{€/year}) = Q_c \cdot (CC + PL)$ $CC (\text{€/m}^3) = 0.134$ $PL (\text{€/m}^3) = [0.406 \cdot SS + 0.8122 \cdot COD + 0.6166 \cdot N + 1.2334 \cdot P + 6.4979 \cdot C + 0.00963 \cdot IS] C_p \cdot C_v \cdot C_w \cdot C_d \cdot C_s \cdot C_r$ $C_v$ : volume coefficient calculated as the relation between wastewater volume and consumed volume $C_p$ : peak coefficient for all parameters defined as the relation between maximum concentration and mean concentration $C_w$ : discharge coefficient; a value of 1.5 is considered for sewer discharges $C_d$ : dilution coefficient, applicable to sea discharges $C_s$ : salinity coefficient
Valencia (Law, 1992)	$ST_{Valencia} (\text{€/year}) = (SC + CC \cdot Q_c) \cdot C_v \cdot C_p \cdot (PL + SPC)$ $SC (\text{€/year}) = 2957.17$ $CC (\text{€/m}^3) = 0.414$ $PL = 0.14 \cdot SS / 0.3 + 0.14 \cdot BOD / 0.3 + 0.18 \cdot COD / 0.5 + 0.07 \cdot N / 0.05 + 0.11 \cdot P / 0.02 + 0.11 \cdot (C - 0.002) / 0.002 + 0.25 \cdot IS / 3$ $SPC$ : specific pollution coefficient applied when HM presence or pH variation exist $C_v$ : volume coefficient calculated as the relation between wastewater volume and consumed volume

Navarra (Law, 1988)	$ST_{Navarra} (\text{€/year}) = 0.169 \cdot Q_w \cdot PL$ $PL = 0.34 \cdot SS / 0.286 + 0.55 \cdot ((COD + 2 \cdot BOD) / 3) / 0.2677 + 0.11 \cdot N / 0.04$		
La Rioja (Law, 2000)	$ST_{Rioja} (\text{€/year}) = 0.35 \cdot PL \cdot Q_w$ $PL = 0.276 \cdot SS / 0.22 + 0.458 \cdot COD / 0.5 + 0.266 \cdot C / 0.0024$		
Murcia (Law, 2000)	$ST_{Murcia} (\text{€/year}) = (SC + (CC \cdot Q_c)) \cdot PL \cdot C_v$ $SC (\text{€/year}) = 30$ $CC (\text{€/m}^3) = 0.34$ $PL = (SS / 0.3 + 2 \cdot COD / 0.333 + 1.3 \cdot N / 0.05 + 2.6 \cdot P / 0.014 + 3 \cdot C / 0.002) / 9.9$ $C_v$ : volume coefficient calculated as the relation between wastewater volume and consumed volume		
*Nomenclature:	$FC = \text{fixed cost}$ $VC = \text{variable cost}$ $Q_w = \text{water flow}$ $PL = \text{pollution load}$ $\phi = \text{pipe diameter}$	$SS = \text{suspended solids}$ $COD = \text{chemical oxygen demand}$ $N = \text{total nitrogen}$ $P = \text{total phosphorus}$	$C = \text{conductivity}$ $T = \text{temperature}$ $HM = \text{heavy metals}$ $IS = \text{inhibitory substances}$

**Table 1.4.** Tax amounts resulting from the application of the ST equations to a treated effluent from an example of juice and soup industry.

<b>Region</b>	<b>(€/year)</b>
Asturias	27,811
Aragón	13,731
Cantabria	7,530
Cataluña	53,248
Galicia	11,099
La Rioja	24,416
Madrid	103,751
Murcia	26,625
Navarra	41,597
Valencia	41,471

The sanitary tax amount and treatment cost determine decisions on wastewater treatment. Therefore, the development of innovative and affordable technologies would encourage water treatment in industries. Moreover, European legislation will become stricter as the list of priority and hazardous substances increase and the need to eliminate them from water bodies becomes critical. As a consequence, effective technologies like AOPs rise as an alternative which needs to be developed before it is widely applied at commercial scale.

### 1.3 Advanced Oxidation Processes

Advanced Oxidation Processes (AOPs) are near ambient temperature and pressure water treatment processes which involve the generation of hydroxyl radicals in sufficient quantity to effective water purification (Malato et al., 2009). Pollutants are oxidised by in-situ generation of highly oxidant hydroxyl radicals ( $E_0=2.8$  V). Other free radicals such as sulphate anion radicals may also be involved when persulphate (PS) is used as an oxidant (Chan and Chu, 2009; Deng and Ezyske, 2011). AOPs can also be classified as photochemical or non-photochemical processes. Examples of the photochemical group are UV/H<sub>2</sub>O<sub>2</sub>, UV/TiO<sub>2</sub>, the photo-Fenton and photo-Fenton-like processes. Conversely, ozonation or the Fenton process are examples of non-photochemical AOPs.

Although all of them have the generation of highly oxidant radicals in common, the way in which they are generated changes from one AOP to another. For instance, both UV/TiO<sub>2</sub> and the photo-Fenton process have been shown to be effective in the removal of a range of pesticides (Gogate and Pandit, 2004; Prieto-Rodriguez et al., 2012) but the fact that the former yields hydroxyl radicals by semiconductor heterogeneous photocatalysis and the latter by iron complexes homogeneous photocatalysis, makes a difference to radical generation efficiency, and therefore in pollutant degradation.

#### 1.3.1 UV photolysis

Strictly speaking, UV photolysis is not considered an AOP since it is not fundamentally based on the generation of highly oxidative radicals. However, it is directly related to AOPs as it is based on UV absorption and radical reactions. It is fundamentally based on the degradation of photolabile pollutants thanks to their ability to absorb UV-light (Equation 1.1). The pollutant molecule reaches an excited state (Pollutant\*) and there is an electron transfer to molecular oxygen (Equation 1.2) (Legrini et al., 1993).



One of its main applications is for drinking water disinfection, but it has also been used to remove persistent compounds such as pesticides identified as priority pollutants by the WFD (Sanches et al., 2010) or pharmaceuticals (Pereira et al., 2007a; Pereira et al., 2007b; Yuan et al., 2009). For this kind of application the UVC range is

the most common since photons have more energy than UVA or UVB. UVC low pressure lamps are specially used for water treatment.

### 1.3.2 Hydrogen peroxide photolysis

This system has been reported as effective in the degradation of micropollutants from wastewater effluents using UV lamps (Keen et al., 2013). This process is also used for disinfection applications (Goswami, 1997; Alkan et al., 2007). This AOP is based on the cleavage of hydrogen peroxide (Equation 1.3). This reaction yields HO<sup>•</sup> by photon absorption.

However, the molar absorption coefficient is low. For instance, at 254 nm it is approximately 25 M<sup>-1</sup> cm<sup>-1</sup> (Virkyte, et al., 2010). This process has been used for the treatment of drinking water to remove, for instance, N-Nitrosodimethylamine (Sharpless et al., 2003) or dibutyl phthalate (Toor et al., 2007). It has also been applied for wastewater treatment to remove compounds such as 4-chlorophenol (Ruppert et al., 1994) or textile effluents (Arslan and Balcioglu, 2001).



### 1.3.3 Heterogeneous photocatalysis

Pollutant degradation by heterogeneous photocatalysis involves the illumination of a semiconductor and the incidence of photons with enough energy on its surface to provoke the migration of electrons (e<sup>-</sup>) from the valence to the conduction band, leaving a charged hole (h<sup>+</sup>) in the valence band, and creating an electron–hole pair (Equation 1.4). Holes oxidise water and hydroxyl groups, yielding hydroxyl radicals that become available for oxidative reactions (Equations 1.5-1.7) or directly oxidise organic compounds adsorbed onto the solid surface. Conduction band electrons can react with oxygen, yielding hydroperoxide radicals, which also oxidise organic matter but have lower oxidation potential (Lee, et al., 2013). As a result, the efficiency of heterogeneous photocatalysis is highly dependent on the available holes on the catalyst surface. The presence of organic matter and anions in complex water matrices can be detrimental to photocatalysis efficiency as they can block or compete for sites on the catalyst surface (Blanco and Malato, 2003).



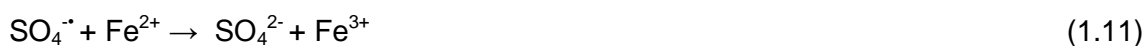
TiO<sub>2</sub> works in the UVA range ( $\lambda < 400$  nm), so it can be carried out under solar radiation (Blanco and Malato, 2003), but the irradiation wavelength range will depend on the band-gap (energetic separation between valence and conduction band) of the semiconductor. Heterogeneous photocatalysis has been successfully applied for the removal of low concentration of pollutants in municipal wastewater effluents (L. Prieto-Rodríguez et al., 2013; Ghatak, 2014).

### 1.3.4 Persulphate systems

These systems generate sulphate radical anions, SO<sub>4</sub><sup>•-</sup>. To generate the radicals, the PS has to be activated. This activation can take place through irradiation (Equation 1.8), direct electron transfer with a transition metal like the ferrous iron (Equation 1.9) or through temperature (Rodriguez et al., 2014). Hydroxyl radicals can also be generated during the process (Equation 1.10). Sulphate radical anions provide the advantage of being highly oxidative ( $E_0=2.6$  V). They have also been reported to be more selective than hydroxyl radicals, with a higher propensity to remove electrons from aromatic rings (Norman et al., 1970).



The inefficient reaction between the sulphate radical anion and ferrous iron may also occur when high concentrations of iron are present (Equation 1.11) (Liang et al., 2004).



Persulphate can be an advantageous oxidising agent when combined with TiO<sub>2</sub> since the sulphate radical anion can be formed by the reaction of persulphate with the photogenerated semiconductor electrons (Equations 1.4 and 1.12) (Blanco et al., 2009).



The sulphate anion radical can react with organic compounds (i) by abstracting a hydrogen atom from saturated carbon; (ii) by adding to unsaturated or aromatic carbon; (iii) and by removing an electron from carboxylate anions and certain neutral molecules (Malato et al., 2009). They can also react with chloride, producing chlorine radicals. Likewise, chlorine radicals can react with organic radicals, yielding chlorinated derivatives (Anipsitakis et al., 2006).

Persulphate has been effectively used in different aqueous systems for the degradation of persistent compounds such as polychlorinated biphenyls (Rastogi et al., 2009), methyl *tert*-butyl ether (Huang et al., 2002), textil dye (Neppolian et al., 2004), cylindrospermopsin (He et al., 2004) or sulfamethoxazole (Ayoub and Ghauch, 2014).

## 1.4 The photo-Fenton process

### 1.4.1 Process and reactions

The photo-Fenton process can make use of  $\lambda < 580$  nm wavelengths, so it can also be solar-driven (Gogate and Pandit, 2004). In this process, the generation of HO<sup>•</sup> is initiated by the reaction between hydrogen peroxide (the reactant) and ferrous iron (the catalyst) (Equation 1.13). In the presence of UV-Vis light, the oxidized catalyst is reduced again (Equation 1.14), resulting in a redox cycle where iron is constantly reduced and oxidized, in turn generating hydroxyl radicals and consuming hydrogen peroxide (Ikehata and El-Din, 2006). The redox cycle is represented in Figure 1.2.



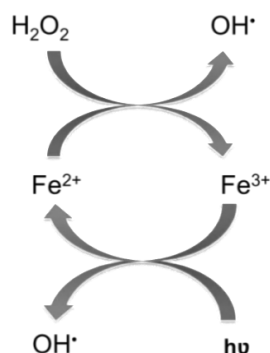
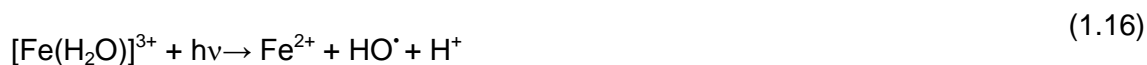


**Figure 1.2.** Simplified scheme of the redox iron cycle in the photo-Fenton process.

Iron reduction can occur through different reactions.  $\text{Fe}^{3+}$  can form complexes with Lewis-base ligands present in the aqueous system (Equation 1.15), for instance, forming aqua-complexes (Equation 1.16) or carboxylate complexes (Equation 1.17). The photoreduction takes place via ligand-to-metal charge transfer reaction (Zepp et al., 1992). The absorption properties of each complex varies, exhibiting different quantum yields, which makes the photo-Fenton process a complex system since it strongly depends on the potential ligands in the water (Pignatello et al. 2006).



Iron reduction can also take place in the dark, although more slowly (Equation 1.18) (Fenton process). As a consequence, this process is especially dependent on light power and iron concentration.



The photo-Fenton process is based on radical reactions, making it more complex. Carbon-centred free radicals ( $\text{R}^{\cdot}$ ) react with dissolved oxygen (Equations 1.19 and 1.20) in what is called the Dorfman mechanism (Dorfman et al., 1962; Kunai et al., 1986). Another reaction is the hydrogen peroxide-hydroxyl radical reaction (Equation 1.21). This reaction is considered inefficient since radicals consume the oxidising agent ( $\text{H}_2\text{O}_2$ ) and do not oxidise the pollutants. Other radical reactions involving hydroperoxide radical or superoxide anion radical may take place (Equations 1.22-1.24) (Pignatello, et al., 2006).





The optimal pH of the process has been reported to be pH 2.8. At this pH iron is soluble and the species  $[Fe(OH)]^{2+}$ , which is the most photoactive of the aquo-complexes, is predominant (Pignatello, 1992).

### 1.4.2 Factors affecting the operation of the process

#### a) Pollutant concentration

The operating strategy is dependent, amongst other things, on the concentration of the pollutant in the wastewater. The photo-Fenton process, as well as many other AOPs, has been studied not as a stand-alone process, but as part of a combined process with other treatments such as biological processes (Oller et al., 2011).

When pollutant concentration is high (in the mg/L range or higher), it has been reported that an efficient operating strategy is to apply the photo-Fenton process as pre-treatment for a biological process such as a sequencing batch reactor (Ballesteros-Martín et al., 2009) or a membrane bioreactor (Sánchez Pérez et al., 2013; Cabrera Reina et al., 2014b). This is the case for many industrial effluents. Such high concentrations of contaminants tend to result in high toxicity, so a pre-treatment with photo-Fenton reduces organic matter load, increases biodegradability and reduce toxicity (Ballesteros-Martín et al., 2010). Consequently the effluent of the pre-treatment can be treated in a biological stage.

The application of photo-Fenton to oxidise high pollutant concentration requires longer process times than when the concentration is low. An additional drawback is that certain organic compounds can form complexes with iron and inactivate it. If the concentration of these compounds is high, it will be detrimental for the process (Malato et al., 2009). Additionally, when pollutant concentration is low we are dealing with micropollutants (below  $\mu\text{g/L}$ ). The concentration of persistent contaminants is so low that there is usually no acute toxicity for a biological system. Therefore, when the

organic load is high and biodegradable and only a small fraction is constituted by micropollutants, an initial treatment should be biological, followed by the photo-Fenton process. It should also be noted that even if micropollutants are not toxic for the biological treatment, they can exhibit acute or chronic toxicity for the receiving environment (Trovó et al., 2010; Li et al., 2010), so an appropriate treatment should be applied for their removal. Another alternative, when the organic load is very low and micropollutants make up a significant fraction of it, would be to combine a pre-concentration stage that increases pollutant concentration, followed by the photo-Fenton process. This strategy has also been reported as effective in the removal of micropollutants (Miralles-Cuevas et al., 2014a). In Figure 1.3 the operating strategy according to the pollutant concentration is shown.

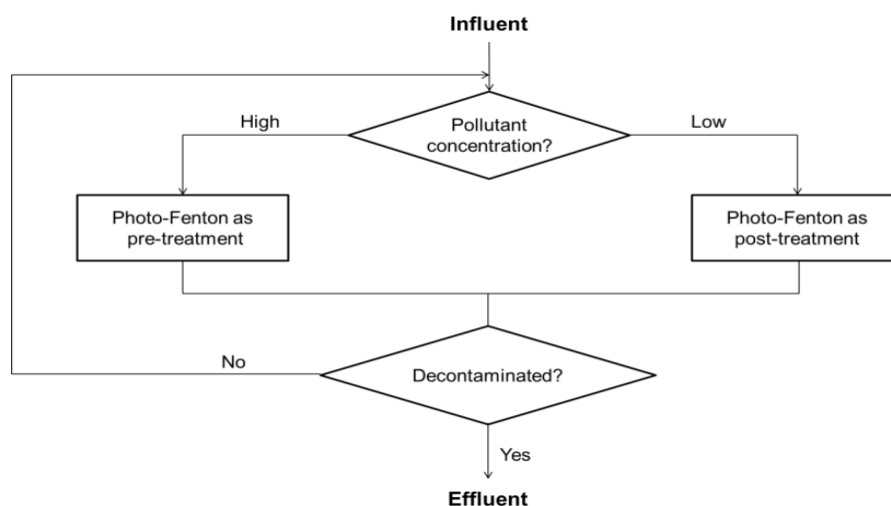


**Figure 1.3.** Operating strategy to treat wastewater as based on pollutant concentration.

## b) Salinity

The effect of the water matrix on the photo-Fenton process is considerable. Ions commonly found in different wastewaters can have negative effects on the formation of hydroxyl radicals and iron complexes. Some anions, such as phosphate, can react with ferrous iron and form an iron complex (Equation 1.25). When ferrous iron is oxidized during the photo-Fenton reactions, ferric iron forms another complex with phosphate and precipitates (Equation 1.26) (Lu et al., 1997).



Chloride anions can form iron complexes that are less photoactive than the iron aqua-complex (Equations 1.27-1.29) and they also act as hydroxyl radical scavengers

(Equation 1.30) (Liao et al., 2001; Laat et al., 2004). The complexes can absorb light and yield chlorine radicals, less oxidant than hydroxyl radicals (Equations 1.31-1.32) (Jayson and Parsons, 1973; Kiwi et al., 2000).



Analogously to chloride, sulphate ions can form iron complexes (Equation 1.33), absorbing photons (Equation 1.34) and generating sulphate radicals. Additionally, sulphate ions can act as hydroxyl radical scavengers (Equation 1.35) (Laat et al., 2004).



The reaction between hydroxyl radicals and chloride or sulphate is more favourable at pH values below 3. Aside from being less reactive, sulphate and chlorine radicals have other negative effects such as having a less efficient use of oxidant.

The presence of carbonates has a negative impact on the photo-Fenton process as well. They can act as hydroxyl radical scavengers, generating less oxidant and reactive species (Equation 1.36) (Buxton et al., 1988). In addition, they create a buffer effect which also affects the process. This is further discussed below.



### c) Alkalinity and pH

As previously described, the optimal pH of the photo-Fenton process has been reported to be pH 2.8 due to iron solubility and predominance of photoactive iron species (Pignatello, 1992). This also happens to be one of its main drawbacks.



The ferric iron ion precipitates in aqueous solution as ferric hydroxide as pH increases (Equation 1.37). However, the chemistry of iron is complex and iron solubility depends, to a great extent, on the solution pH. Many iron oxides have a range of minimum solubility between pH 7-8. As they are amphoteric, they can dissolve at lower or higher pH, yielding cationic or anionic hydroxo species, respectively; although their solubility between pH 6-9 is unclear. Iron solubility is also dependent on the presence of complexing or reducing agents, temperature, and the ionic strength of the solution as well as whether it can occur by dissolution or by chemical reaction (Cornell and Schwertmann, 2003). The presence of inorganic or organic ligands, such as chloride or oxalate, enhances the solubility (Kiwi et al., 2000; Nogueira, et al., 2005a) but competing mechanisms usually affect it. For instance, above pH 5, there is competition between the hydroxyl ion and oxalate for sites in the iron coordination spheres. On the other hand, reducing conditions improve solubility of iron oxides, promoting reductive dissolution. In general, the presence of organic matter affects iron solubility, although it is difficult to say if it enhances or decreases it, due to the complex nature of the organic compounds in wastewater. The effect of ionic strength is also significant. When ionic strength is low, the solubility increases due to the decrease in interionic forces in solution (Cornell and Schwertmann, 2003).

If the aim is to work at neutral or circumneutral pH, alkalinity plays an important role as well. Alkalinity refers to the buffering capacity of water. It measures the water buffering capacity through the amount of acid or base required to neutralise water and maintain a stable pH. Compounds such as carbonates/bicarbonates are commonly present in wastewater effluents and create a buffer, raising pH. Additionally, the carbonate/bicarbonate equilibrium is affected by the presence of other salts or even organic matter. This has an impact on pH adjustment by acid since the amount needed is not easy to predict and varies with the effluent.

#### **d) Temperature**

Temperature plays an important role in the photo-Fenton process and the thermal dependence of the process can be taken into account through the Arrhenius equation (Cabrera Reina et al., 2014a). Increasing temperature usually increases the process rate. For instance, it has been reported that when temperature is increased from 20 °C to 50 °C, there is an improvement in pollutant mineralization by 5

times (Gernjak et al., 2006). There is usually an optimal temperature value for each system. Lin et al. (1997) reported that to treat dyes Blue-G and Black-B the optimal temperature was 30 °C. Below this value, the process rate, measured in terms of COD, decreased. However, high temperatures are not recommended either since they lead to loss of  $\text{Fe}^{2+}$  by precipitation (Lin et al., 1997). Temperatures above 45 °C should be avoided to prevent significant loss of iron by precipitation (Zapata et al., 2010). Another reason is that high temperatures can also lead to higher hydrogen peroxide consumption to reach the same level of decontamination. This is caused by the decomposition of hydrogen peroxide, favoured at high temperatures, and because the reaction in Equation 1.18 is a thermal reaction where hydrogen peroxide is consumed to reduce ferric iron (Malato et al., 2009).

### **1.4.3 Fenton-like processes**

#### **a) Use of iron chelates and complexes**

The drawback of the traditional photo-Fenton process operating pH has encouraged research to be centred on obtaining similar results at neutral pH in order to reduce operating costs and avoid increasing water salinity due to acidification for the treatment and neutralisation for disposal. Considering that iron can form complexes with several Lewis bases, the use of complexing agents would solve the problem of working at pH 2.8. As a consequence, recent studies have been focused on the use of different iron sources. Additionally, the photoreduction of ferric iron (Equation 1.14) when it is forming complexes can take place at longer wavelengths than the iron aquo-complex. Therefore, when the photo-Fenton process is solar-driven, the contribution of these complexes to the photoreduction is greater. As such, the optimal pH of the process changes when iron complexes are used (Malato et al., 2009).

Another important matter that has to do with the iron source are the filter effects in the aqueous system. Usually many substances present in water other than the iron source can absorb photons, creating a light filter. These absorbing species are often the contaminants. In some cases, light absorption by the contaminants can result in direct photolysis, but photolysis tends to have a low quantum yield. This means there is an inefficient photon competing effect between the iron source and other light-absorbing species. Some examples have been found regarding better process performance at higher wavelengths. For instance, it was reported that the use of

sunlight improved vanillin degradation in comparison with medium pressure lamps (Gernjack et al., 2003).

It was also found that medium pressure lamps resulted in a better performance than low pressure lamps in wastewater containing xylydine (Oliveros et al., 1997). It was suggested that this effect was a consequence of the light filters present at lower wavelengths. Therefore, the use of iron complexes which absorb at higher wavelengths would overcome this problem.

To be useful, an iron chelate should display the following characteristics: i) have catalytic activity and be able to generate hydroxyl radicals; ii) and be environmentally safe (Sun and Pignatello, 1992). Complexes such as ethylenediamine-N,N'-disuccinic acid (EDDS) have been often studied as an iron source (Klamerth et al., 2012); ferrioxalate or ferric citrate have also been proposed as alternative iron sources (Safarzadeh-Amiri; Nogueira et al., 2005a).

In Table 1.5 a summary of common iron chelates and complexes reported in the literature as well as the target pollutant is presented. Nonetheless, when the process is applied as a tertiary treatment, iron complexes or chelates should be chosen carefully because they have to be innocuous and add as little dissolved organic carbon (DOC) as possible.

### **b) Heterogeneous photo-Fenton**

Another strategy reported in the literature to operate the photo-Fenton process is the use of heterogeneous catalysts (Pouran et al., In Press), operating similarly to heterogeneous photocatalysis with  $\text{TiO}_2$ . The photocatalysts are often iron oxides supported in materials like silica, alumina or clay. They can also be suspended oxides. Hydrolytic  $\text{Fe}^{3+}$  species have been studied in recent years in this regard, including low-molecular-weight  $\text{Fe}^{3+}$ -OH complexes,  $\text{Fe}^{3+}$  oxides and  $\text{Fe}^{3+}$  hydroxides (Feng and Nasheng, 2000).

The separation of the suspended catalyst is relatively easy and it facilitates working without pH adjustments. However, heterogeneous photocatalysis often exhibits lower reaction rates than homogeneous photocatalysis due to mass transfer limitations and worse light penetration with the suspended catalyst (Pérez Estrada et al., 2005). A summary of common heterogeneous catalysts is shown in Table 1.6.

**Table 1.5.** Common iron complexes and chelates used for Fenton and photo-Fenton applications.

<b>Iron Ligand/chelate</b>	<b>Pollutant</b>	<b>Reference</b>
Citrate	4-chlorophenol	Abida et al., 2012
Citrate	2,4,6-trichlorophenol	Li et al., 2005
Chitosan cross-linked with glutaraldehyde	trichloroethylene	Lee and Lee, 2010
EDDS	4-tert-Butylphenol	Wu et al., 2014a Wu et al., 2014b
EDDS	17 $\beta$ -estradiol Bisphenol A	Huang et al., 2013
EDDS	2,2-bis-(4-hydroxyphenyl)propane	Huang et al., 2012
EDDS, Ferrioxalate, Humic acids	acetaminophen, antipyrine, atrazine, caffeine, carbamazepine, diclofenac, flumequine, hydroxybiphenyl, ibuprofen, isoproturon, ketorolac, ofloxacin, progesterone, sulfamethoxazole, and triclosan	Klamerth et al., 2011; Klamerth et al., 2012
EDTA Nitrilotriacetic acid Oxalic acid Tartaric acid	Sulfamethoxazole	De Luca, et al., 2014
Ferrioxalate	trimethoprim and sulfamethoxazole	Dias et al., 2014
Ferricarboxylate	oxytetracycline	Pereira et al., 2014
Glutamate	nitrobenzene	EIshafei et al., 2010
<sup>a</sup> Hydroxyethyliminodiacetic acid (HEIDA) Picolinic acid Nitrilotriacetic acid Gallic acid Rhodizonic acid Hexaketocyclohexane (HKCH) Tetrahydroxy-1,4quinone (THQ)	2,4-dichlorophenoxyacetic acid	Sun and Pignatello, 1992
Phosphotungstate	Benzoate, methanol	Lee and Sedlak, 2009
Sulfophthalocyanine (FePcS)	2,4,6-trichlorophenol	Sorokin et al., 1995
Tetraamidomacrocyclic complex	pentachlorophenol and 2,4,6-trichlorophenol	Gupta et al., 2002

<sup>a</sup>Only active iron complexes were included

**Table 1.6.** Common heterogeneous iron catalysts used for Fenton and photo-Fenton applications.

Source of iron	Pollutant	Reference
Bismuth ferrite (BiFeO <sub>3</sub> )	Methyl Violet Rhodamine B	An et al., 2013
Goethite	2-chlorophenol	Ortiz de la Plata et al., 2010
Iron clay	Phenol and tyrosol	Abderrahmane et al., 2014
Iron hexacyanoferrate colloids	Rhodamine B	Liu et al., 2010
Iron (Fe <sup>0</sup> ) mesh	Ampicillin and penicillin G	Orbeci et al., 2014
Iron (III) oxide (Fe <sub>2</sub> O <sub>3</sub> )	Bisphenol A	Jiang et al., 2014
Iron supported on alumina powder (Fe <sup>2+</sup> /γ-Al <sub>2</sub> O <sub>3</sub> )	phthalocyanine dyes	Cheng et al., 2014
Iron oxide pillars supported on clay	Phenol	Hadjltaief et al., 2014
Iron oxide supported on sewage sludge derived carbon	Acid Orange II	Tu et al., 2014
Iron supported on TiO <sub>2</sub> /SiO <sub>2</sub>	Orange II	Lam et al., 2009
Iron wolframite complex (LiFe(WO <sub>4</sub> ) <sub>2</sub> )	Methylene blue	Ji et al., 2011
Iron zeolites	Phenol Imidacloprid Dichloroacetic acid	Gonzalez-Olmos et al., 2012
Iron zeolites	Remazol Brilliant Orange	Tekbas et al., 2008
Magnetic nanospinels MFe <sub>2</sub> O <sub>4</sub> (M = Cu, Zn, Ni and Co)	Dye Remazol Black 5	Sharma et al., 2014
Magnetite (Fe <sub>3</sub> O <sub>4</sub> )	Phenol	Minella et al., 2014

#### 1.4.4 Control and monitoring of the photo-Fenton process through dissolved oxygen

The oxidant in the photo-Fenton process is hydrogen peroxide. A hydrogen peroxide concentration which is too low or too high leads to a reduction in the process rate. In the former case, there is lack of oxidant, which is detrimental for the process rate. In the latter case, a too high oxidant concentration favours inefficient reactions. The generation of hydroxyl radicals is proportional to the amount oxidant. In a situation of oxidant excess, radical-radical and radical-oxidant reactions are favoured, which is a non-efficient radical consumption. These ineffective reactions are in most cases



oxygen-generating (Section 1.4.1). Therefore, oxygen concentration can serve as monitoring variable of the process using on-line dissolved oxygen probes (Gernjak et al., 2006). In this sense, dissolved oxygen monitoring has been demonstrated as an adequate tool for detecting inefficient conditions, in which there is either a lack, or an excess, of hydrogen peroxide (Santos-Juanes et al., 2011). Generation of too much oxygen points to inefficient reactions taking place, whereas a decrease in dissolved oxygen concentration may indicate a lack of oxidant. Therefore it can be used to reduce hydrogen peroxide consumption and increase efficiency in degradation.

Dissolved oxygen has been successfully used as a controlled variable to degrade acetaminophen in a concentration of 50-100 mg DOC/L. The controllers used were on/off and anti-windup Proportional & Integral controllers, the latter being the most efficient since it maintained maximum mineralization rates and minimum oxidant consumption at the lowest cost (Ortega-Gómez et al., 2012; Carra et al., 2013). Prieto Rodríguez et al. (2011) studied the use of dissolved oxygen concentration as an indicator of the reaction stage as a function of hydrogen peroxide concentration. This was attempted with a mixture of pesticides (oxamyl, methomyl, imidacloprid, dimethoate and pyrimethanil) in a concentration of 200 mg DOC/L. It was concluded that hydrogen peroxide and dissolved oxygen profiles were related and it was possible to use the results for automatic oxidant dosage. The supply of pure oxygen and air along with hydrogen peroxide was also studied to evaluate if the addition of oxygen would lower hydrogen peroxide consumption (Miralles Cuevas et al., 2014b). However, oxygen dosage actually increases the generation of  $\text{HO}_2^{\cdot}$ , resulting in a longer process time and oxidant consumption.

That said, the optimisation of the automatic dosage and the improving of dissolved oxygen probes are still unfinished tasks. Moreover, this strategy to monitor and control the process can only be used when the aim is to remove high pollutant concentration. For micropollutants, hydrogen peroxide requirements are much lower and the concentration of dissolved oxygen is not enough to be monitored by the probes.

#### **1.4.5 Variables affecting costs in the photo-Fenton process**

The main drawback of AOPs is their high cost in comparison with biological treatments. This cost difference is caused not only by the type of treatment itself, but also by the nature of the effluent and the treatment volume, which is usually on a

smaller scale for AOPs. For instance, the estimated cost for treating wastewater containing 500 mg/L of alpha-methyl-phenylglycine (MPG) applying solar photo-Fenton has been found to be 14.1 €/m<sup>3</sup> (Muñoz et al., 2008) in contrast with 0.25 €/m<sup>3</sup> for the activated sludge treatment cost with nutrient removal for domestic wastewater (Hernández Sancho et al., 2011). Nevertheless, the combination of AOP-biological systems according to the strategy suggested in Section 1.4.2.a based on pollutant concentration can reduce the costs of the AOP stage. Even so, the cost of the AOP is still higher than the biological process.

The economic assessment should include amortization and operating costs. Amortization costs may include costs associated with the land and equipment, so design parameters have a strong influence on them. If the cost of the land is disregarded, reaction time to achieve the desired goal is the variable with the largest impact on amortization costs as it affects the size of the photoreactor, in the case of solar photo-Fenton, surface of solar collectors.

In the estimation of the operating costs, hydrogen peroxide concentration is the most important factor, given that this reactant is used in large amounts (Sánchez Pérez et al., 2013). This is linked to how hydrogen peroxide is supplied since the dosage strategy can reduce oxidant consumption, as explained in Section 1.4.4. How the hydrogen peroxide is supplied also affects reaction rates, and, consequently, the overall operation costs. For instance, it has been reported that the treatment of 0.5 mM of paracetamol by solar photo-Fenton would incur a cost of 1.32 €/m<sup>3</sup> if hydrogen peroxide was added in one addition at the beginning of the treatment; but if a PI controller is used with dissolved-oxygen as a controlled variable to add hydrogen peroxide when needed, the cost is reduced to 1.15 €/m<sup>3</sup> (Carra et al., 2013). Other variables affecting operating costs would be the acid amount to adjust pH in case the process is run at acidic pH and iron salt when the concentration used is high. An economic assessment of the process is also of interest when iron complexes are used. Duran et al. (2014) estimated that the operating costs of treating 50 mg DOC/L of antipyrine with ferrioxalate in a CPC semi-industrial pilot plant was 1.56 €/m<sup>3</sup>.

When carrying out an economic assessment, it is important to bear in mind that only taking into account operating costs is of use when comparing results as part of the same experimental work. However, when comparing other experimental results or considering a more realistic situation, considering hydrogen peroxide consumption as

the only economic variable may lead to errors. The treatment time should always be considered as long with other reagents employed in the process (Carra et al., 2013).

The possibility of linking the economic and environmental factor with an integrated environmental-economic index (EEI) (Muñoz et al., 2008) has also been suggested. It is designed for comparing processes in a simplified way. It has been applied for a case study to make a comparison between ozonation, solar- and lamp-driven photo-Fenton for the treatment of 2500 m<sup>3</sup>/yr of industrial wastewater with 500 mg/L alpha-methyl-phenylglycine. The application of the EEI pointed out that, from an integrated environmental and economic point of view, solar-driven photo-Fenton was preferable in comparison with lamp-driven photo-Fenton or ozonation (Muñoz et al., 2008).

#### **1.4.6 Solar photoreactors for water treatment applications**

##### **a) Concentrating reactors. The Parabolic Trough Concentrator.**

The first solar photoreactors for photochemical applications were based on designs used for solar thermal processes since the hardware required was similar (Dillert et al., 1999). However, certain modifications had to be made. The solar thermal design is aimed at maximising the fluid temperature, collecting as many photons as possible, from any wavelength. In the case of photochemical applications, the aim is to collect high energy photons in the UV and part of the visible in the case of the photo-Fenton process (up to 600 nm). As a consequence, the absorber has to let the UV radiation in. Furthermore, as the aim is not to maximise temperature, no insulation is needed (Malato et al., 2002). Specifically, the first photoreactors for photochemical applications were based on a parabolic-trough concentrator (PTC) and mainly applied for heterogeneous photocatalysis (Figure 1.4).

PTCs were already a developed technology and they could be adapted for photochemical processes. They have a cylinder which receives a large amount of photons per unit volume (Figure 1.4). The absorber tube could be replaced by a Pyrex glass one to let UV radiation in (Goswami, 1997). It is easy to handle and control the liquid being treated. However, they are expensive, use only direct radiation and have low optic and quantum efficiency (Malato et al., 1997; Alfano et al., 2000). As they focus only direct radiation, the diffuse component is not used. This is a major drawback since clouds and dust increase the fraction of diffuse radiation.



**Figure 1.4.** Parabolic trough collector plant at the Solar Platform of Almería.

Consequently, non-concentrating collectors are a better alternative since they can use diffuse radiation and operate in cloudy conditions, while a trough system is not able to.

#### **b) Non-concentrating reactors. The Compound Parabolic Collector (CPC).**

Different non-concentrating systems were designed (Bahnemann, 2004). Research focused on flat-plate photoreactors like the Double Skin Sheet Reactor (DSSR) and the Thin Film Fixed Bed Reactor (TFFBR). The DSSR is a rectangular-shaped reactor with a flat and transparent box of PLEXIGLAS® with channels dividing it. The water is pumped through the channels. It was also designed for heterogeneous photocatalysis applications, adding  $\text{TiO}_2$  in suspended form, meaning it had to be removed after the treatment (van Well et al., 1997). The TFFBR was designed for heterogeneous photocatalysis applications as well. It is formed by an inclined plate and coated with  $\text{TiO}_2$ . Water is washed over it, forming a thin film to favour contact between the catalyst and water (Bockelmann et al., 1995).

However, flat plate reactors require more photoreactor area than concentrating reactors. This would increase the operating pressure of a system in a full-scale plant and the materials would have to be able to withstand it. Also, the materials should be inert to outdoor corrosion and be able to endure long exposure times to solar light. As a consequence, the idea of developing these reactors was abandoned.

In the search for a solar photoreactor it should be kept in mind that it has to be effective in the collection of UV radiation and it should allow being able to work at ambient temperature to avoid loss of volatile compounds. It should also be easy to

build and economical. Considering this, the use of tubular photoreactors was suggested since tubes are available in different sizes and materials that let UV radiation in the system.

To this end, Compound Parabolic Collectors (CPCs) were proposed. They are a combination of parabolic concentrators and static flat systems. CPCs concentrate solar radiation; they are static and can collect diffuse radiation (Ajona et al., 2000). They are constituted by borosilicate tubes with an involute reflective surface around them made of aluminium. They provide a concentrating ratio close to one and their design allows the collection of direct and diffuse radiation. The beams reflected reach the back of the tubes so that most of the tube is illuminated. From an operating point of view, water is easy to pipe. All these characteristics lead to a good performance for solar photochemical applications and make them the most frequently used reactors for solar photochemical processes. Figure 1.5 shows a photo of a CPC pilot plant.

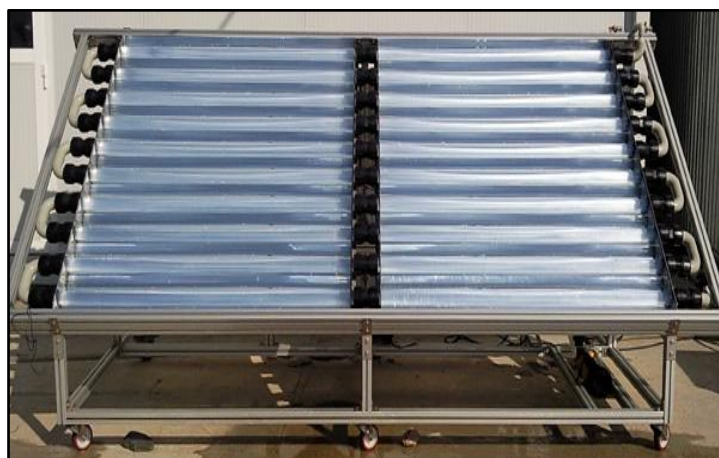


**Figure 1.5.** CPC pilot plant at the Solar Platform of Almería.

The angle of acceptance in the CPC ( $\theta_a$  in Figure 1.6a) is usually between  $60^\circ$  and  $90^\circ$ . This interval allows the collection of direct and a large part of diffuse radiation. When the angle is  $90^\circ$ , the aperture area of the collector is  $2\pi r$  and the concentrating factor is one (Figure 1.6b). In this case, all direct and diffuse radiation that reaches the surface can be collected. As a consequence, CPCs are designed with this angle value, which makes them optically efficient. As in the case of flat-plate collectors, the maximum yearly efficiency is normally obtained at the same collector angle inclination as the local latitude (Malato et al., 2013).

Two important design factors are the reflective surface and the tubular photoreactor. In non-concentrating systems, the quality requirements of the reflective surface in terms of surface imperfections are lower than in PTCs. This is an advantage

for manufacturing them since costs decrease (Blanco et al., 2003). The material must be highly reflective for UV radiation. Reflecting surfaces of aluminium are traditionally used. Aluminium is highly reflective in the UV range, with a reflectivity of 92% at 385 nm. To protect them from outdoor conditions the surface is often electropolished anodised aluminium or organic plastic coated with aluminium.

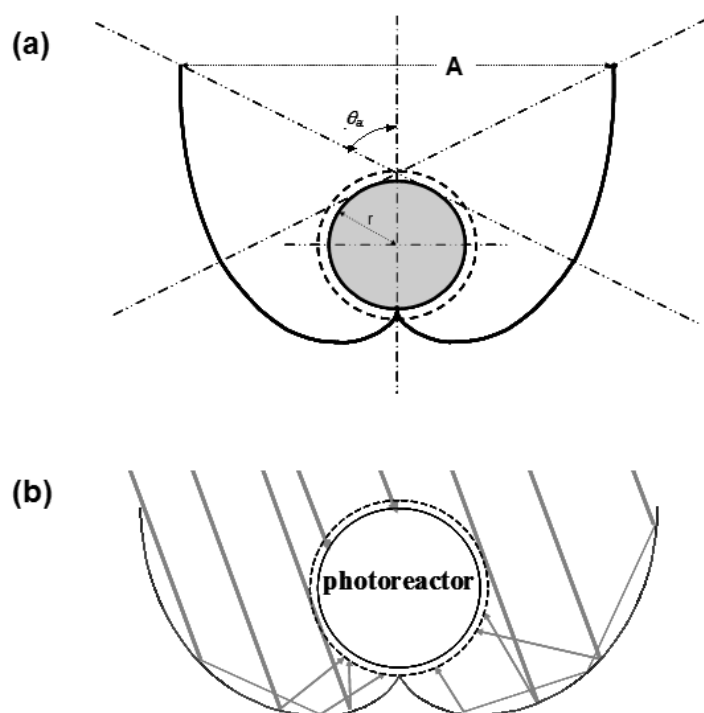


**Figure 1.6.** (a) CPC design and (b) CPC with concentrating factor of one.

Regarding the photoreactor, it has to be transparent for UV radiation whilst providing low pressure drop and good mass transfer in the system. It should also be resistant to the temperatures in the system in summer and working pH. It should be inert to the compounds in the water (contaminants, catalyst and oxidant). Some of the materials which meet these conditions for the tubular reactor are shown in Figure 1.7. The best transmission is given by quartz. However, its high cost makes it unviable for this application.

Fluoropolymers like polytetrafluoroethylene (PTFE) could make good materials for photoreactors due to their low cost, UV stability, good transmittance, resistance and inertness. However, the pressure in the system would necessitate thick tube walls due to their lack of rigidity, which lowers the UV transmittance. Glass is another choice. Standard glass contains iron, so it filters out part of the UV radiation, but borosilicate glass has poor transmission properties in the UV. Its higher resistance to pressure drops in full-scale plants makes it a better alternative as photoreactor material.

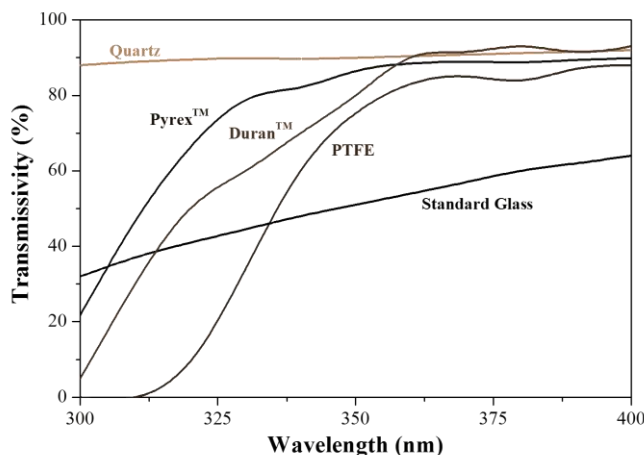


**Figure 1.7.** Transmittance of different materials for the manufacture of photoreactor tubes.

The other important factor in photoreactor design is the tube diameter. It must be guaranteed that all photons get into the tube and react with all the catalyst molecules. This will depend on the catalyst concentration and irradiance value as well. In the conventional photo-Fenton process, the absorbing species is  $\text{Fe}^{3+}$  at pH 2.8. Figure 1.8 shows the transmittance of ferric sulphate at that pH and at 350 nm for different tube diameters (Malato et al., 2013). However, these values can change due to the different complexes formed by ferric iron during the photo-Fenton process. Experimental optimal values between 0.5-0.2 mM were found for different photoreactors and wastewater matrices (Fallmann, et al., 1999; Gernjak, et al., 2003; Zapata et al., 2009).

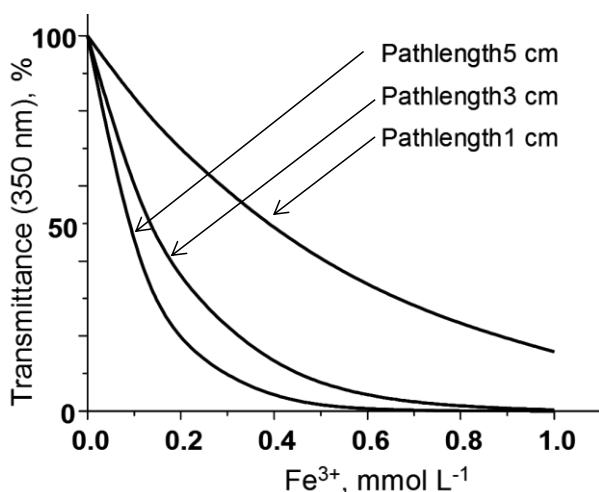


**Figure 1.8.** Transmittance of  $\text{Fe}^{3+}$  dissolved in water.

Another matter is the design of a full-scale plant where several rows of CPCs have to be included. In this case, it is recommendable to use the angle of sunlight at

noon on December 21<sup>st</sup>, when the sun elevation is the lowest in the northern hemisphere, to separate the rows explained in Figure 1.9 (Malato et al., 2013).

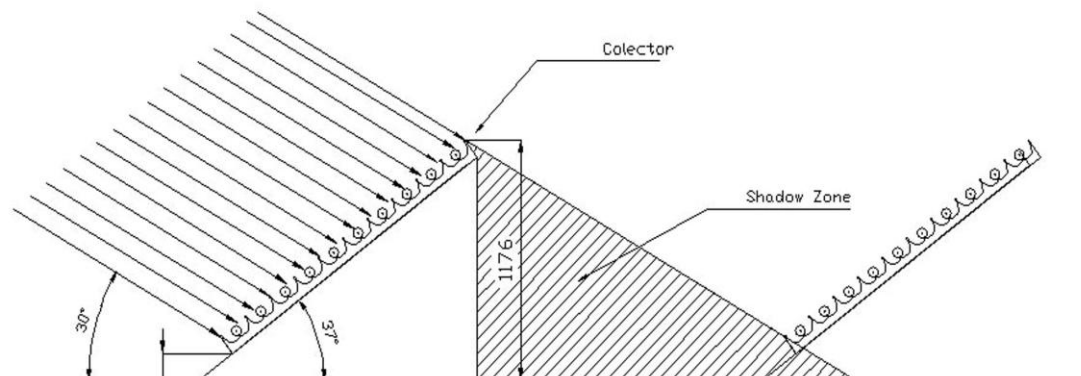


**Figure 1.9.** Design parameters to define row separation for minimum shadowing of collectors.

### **c) Solar photoreactors for other applications. Raceway Pond Reactors (RPRs)**

There are photoreactor designs for other kind of applications. Such is the case in the Raceway Pond Reactors (RPRs) or “high-rate ponds”. They were also called Oswald ponds after their inventor, W. J. Oswald. He based their design on the idea of lagoons where a degree of biological oxidation of wastewater was accomplished as well as the photosynthetic growth of organisms like algae. When organic matter in the wastewater is oxidised by bacteria,  $\text{CO}_2$ ,  $\text{NH}_4$  and water are produced. In the presence of solar energy, this is useful for algal photosynthesis, which produces dissolved oxygen. At the same time, the dissolved oxygen produced can be used in the bacterial oxidation of organic matter. Therefore, dissolved oxygen is consumed to oxidise organic matter as soon as it is produced by algal photosynthesis (Oswald and Gotaas, 1957). This technology is suitable for the Mediterranean area or arid areas in general (Bontoux and Picot, 1994). It is aimed at the sanitation of small communities due to its simple operation in comparison with conventional wastewater treatments like activated sludge. It is also effective in the removal of nutrients (nitrogen and phosphorus). The RPRs are frequently combined with sedimentation ponds (Green et al., 1995).

The wastewater treatment varies during the day and night according to the photosynthetic activity. Dissolved oxygen and pH are highest at midday and lowest at night, even going through anoxic periods (Picot et al., 1993; El Ouarghi et al., 2000),



night aeration has to be increased to satisfy the oxygen demand of aerobic microorganisms. The low pH at night also reduces nutrient removal due to volatilisation and precipitation processes (Cromar et al., 1996). As a result, organic matter removal changes throughout the day. Nevertheless, diurnal variations in the operation of RPR do not affect the overall reliability of wastewater treatment (García et al., 2006).

However, although RPRs were initially designed to treat wastewater, they are better known for their application for microalgae mass culture. They started to be used for this application after World War II (Becker, 1994) and now RPR technology is well established at a large scale to grow algae (Lee 1997; Molina Grima et al., 1999). Microalgae are used for aquaculture, human nutrition products, cosmetics and carotenoids amongst others (Spolaore et al., 2006). For instance, some strains of *Scenedesmus* have been reported to produce lutein and other pigments (Fernández Sevilla, 2010). Microalgae can also produce biodiesel in RPRs reaching up to 12,000 L/ha-year (Schenk et al., 2008). A typical algae culture raceway is shown in Figure 1.10.

The RPR is constituted by channels in a closed loop. It can work with liquid depths of 25-30 cm. The system is mixed by a paddlewheel and with dimensions as shown in the scheme in Figure 1.11 and it can be configured with multiple bends to save energy for recirculation (Chisti, 2007). The surface area varies depending on the use: for algal biomass production the area can be of around 0.5 ha; however, for wastewater treatment by bacterial oxidation in combination with photosynthesis, the area can reach 2.5 ha (Chisti, 2007).



**Figure 1.10.** RPR for microalgal mass culture in the University of Almería.

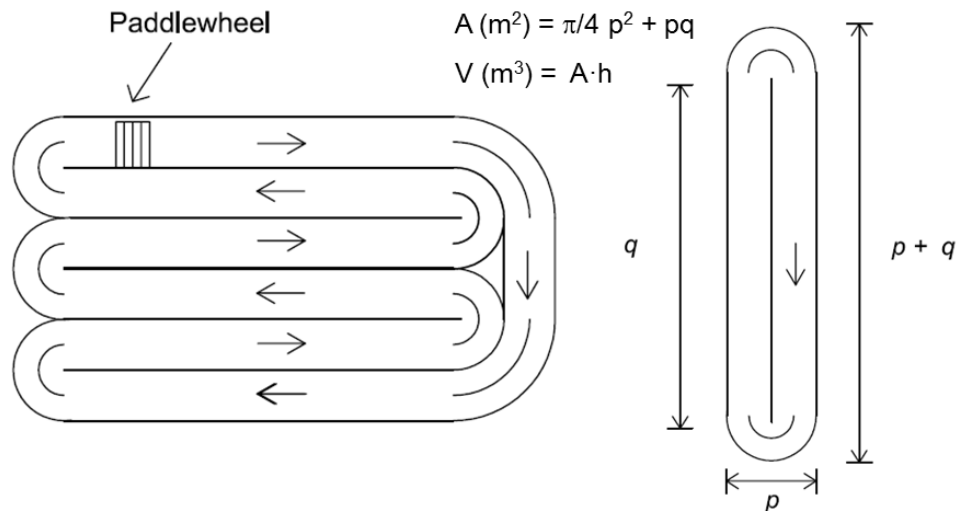


**Figure 1.11.** Scheme and dimensions of an RPR (Chisti et al., 2007).

The bottom is flat, with a surface area,  $A$ , calculated as:

$$A = \pi/4 \cdot p^2 + p \cdot q \quad (1.38)$$

Where  $p$  and  $q$  are the dimensions shown in Figure 1.11, with a common  $p/q$  ration of 10 or more. If the ratio is too low, there are disturbances in the flow due to the closeness of the bends. The volume also depends on the surface area and the liquid depth,  $h$ . The surface to volume ratio is taken as a design parameter and for microalgae culture applications it is commonly set to  $1/h$ . Commercial RPRs are made of concrete covered by a plastic lining, resistant to UV light and RPRs are usually designed with semi-circular ends, as shown in Figure 1.11. They also include baffles to avoid dead zones and ensure homogeneous flow (Chisti et al., 2007).

Photoreactors installed in CPCs focus are closed systems, which allow more control over the process variables and make good use of solar irradiance. In contrast, RPRs are extensive reactors which allow the treatment of large volumes of wastewater, using less photons per photoreactor volume unit than CPCs, but which could make the operation of the photo-Fenton process in continuous mode more feasible and with lower-cost when applied to a low concentration of contaminants. The key of using each photoreactor would mainly depend on the demand of photons to treat a specific wastewater and treatment time.

# ***EXPERIMENTAL***

---

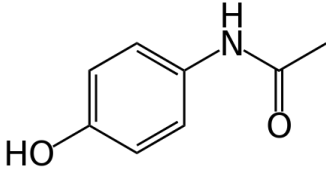
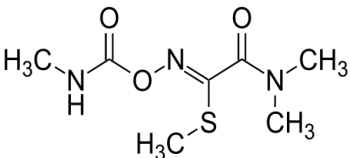
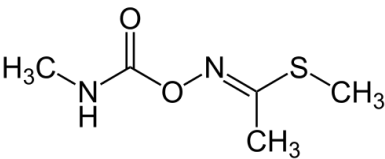
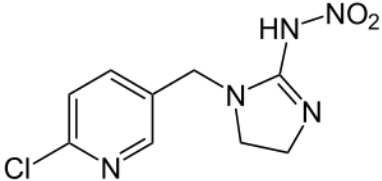
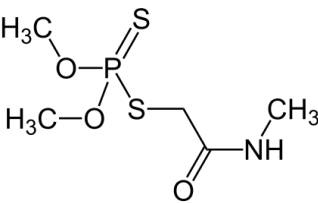


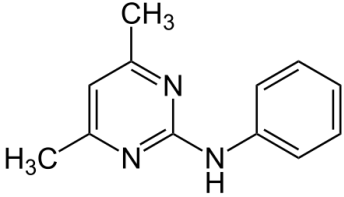
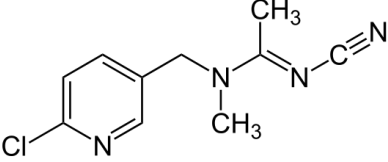
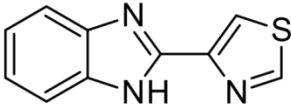
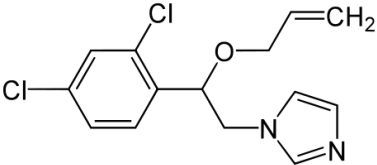
## 2. EXPERIMENTAL

### 2.1 Model pollutants

The model pollutants selected were acetaminophen, as common drug detected in water effluents, and the pesticides oxamyl, methomyl, imidacloprid, dimethoate, pyrimethanil, acetamiprid, thiabendazol and imazalil due to their diverse uses in agriculture. Commercial formulations of the pesticides were also used. The properties of the model pollutants and the commercial formulations used are shown in Table 2.1.

**Table 2.1.** Model pollutants.

Name:	Acetaminophen/ paracetamol	
Mol. weight:	151.17 g/mol	
Formula:	C <sub>8</sub> H <sub>9</sub> NO <sub>2</sub>	
CAS num:	103-90-2	
Solubility in water:	12.78 g/L (20 °C)	
Use:	Analgesic and antipyretic	
Name:	Oxamyl	
Mol. weight:	219.26 g/mol	
Formula:	C <sub>7</sub> H <sub>13</sub> N <sub>3</sub> O <sub>3</sub> S	
CAS num:	23135-22-0	
Solubility in water:	280 g/L (25 °C)	
Commercial formulation:	Vydate® (10% w/v oxamyl)	
Use:	insecticide/acaricide/n ematicide	
Name:	Methomyl	
Mol. weight:	162.21 g/mol	
Formula:	C <sub>5</sub> H <sub>10</sub> N <sub>2</sub> O <sub>2</sub> S	
CAS num:	16752-77-5	
Solubility in water:	58 g/L (25 °C)	
Commercial formulation:	Metomur® (20%, w/v, methomyl)	
Use:	Carbamate insecticide	
Name:	Imidacloprid	
Mol. weight:	255.66 g/mol	
Formula:	C <sub>16</sub> H <sub>22</sub> ClN <sub>3</sub> O	
CAS num:	138261-41-3	
Solubility in water:	0.51 g/L (20 °C)	
Commercial formulation:	Couraze® (20% w/v imidacloprid)	
Use:	Neocotinoid	
Name:	Dimethoate	
Mol. weight:	229.26 g/mol	
Formula:	C <sub>5</sub> H <sub>12</sub> NO <sub>3</sub> PS <sub>2</sub>	
CAS num:	60-51-5	
Solubility in water:	25 g/L (25 °C)	
Commercial formulation:	Perfektion® (40% w/v dimethoate)	
Use:	Organophosphate insecticide	

Name:	Pyrimethanil	
Mol. weight:	199.25 g/mol	
Formula:	C <sub>12</sub> H <sub>13</sub> N <sub>3</sub>	
CAS num:	53112-28-0	
Solubility in water:	0.121 g/L (25 °C)	
Commercial formulation:	Scala® (40% w/v pyrimethanil)	
Use:	Fungicide	
Name:	Acetamiprid	
Mol. weight:	222.68 g/mol	
Formula:	C <sub>12</sub> H <sub>11</sub> ClN <sub>4</sub>	
CAS num:	135410-20-7	
Solubility in water:	2.95 g/L (25 °C)	
Commercial formulation:	EPIK® (20% w/w)	
Use:	Neonicotinoid	
Name:	Thiabendazole	
Mol. weight:	201.25 g/mol	
Formula:	C <sub>10</sub> H <sub>7</sub> N <sub>3</sub> S	
CAS num:	148-79-8	
Solubility in water:	50 mg/L (25 °C)	
Commercial formulation:	Textar 60® (60% w/v)	
Use:	Fungicide and parasiticide	
Name:	Imazalil or enilconazole	
Mol. weight:	297.18 g/mol	
Formula:	C <sub>14</sub> H <sub>14</sub> Cl <sub>2</sub> N <sub>2</sub> O	
CAS num:	35554-44-0	
Solubility in water:	1.4 g/L (20 °C)	
Use:	Fugicide	

## 2.2 Water matrices

The experimental work was carried out in deionised water, natural water, synthetic water and real wastewater. Deionised water was obtained from the demineralisation system at CIESOL (electric conductivity < 10 µS/cm, Cl<sup>-</sup> = 0.3 mg/L, SO<sub>4</sub><sup>2-</sup> = 0.2 mg/L, DOC < 0.5 mg/L). Natural water distributed through the plumbing network in CIESOL was used as a first step for optimising variables and checking protocols under more realistic conditions than deionised water but not as complex as real wastewater, which was left as last step. The properties of natural water are presented in Table 2.2.

On the other hand, for studies that required similar water properties for comparison purposes, a simulated effluent from secondary treatment was used, following the recipe by Zhang et al. (2007). The base of the recipe was fresh standard water (OECD, 1999). All the compounds are shown in Table 2.3.

**Table 2.2.** Natural water properties.

Parameter	Concentration (mg/L)
Sulphate	30 ± 4.5
Chloride	206 ± 10
Nitrite	<0.2
Nitrate	<0.3
pH	7.9 ± 0.2
Conductivity	0.9 ± 0.1 mS/cm

\*Other anions were below the limit of detection of ionic chromatography

**Table 2.3.** Simulated secondary effluent properties.

	mg/L	CAS num
<b>Organic compounds</b>		
Beef extract powder	1.8	-
Peptone	2.7	-
Humic salt	4.3	68131-04-4
Sodium lignin sulfonate	2.4	8061-51-6
Sodium lauryle sulphate	0.9	151-21-3
Acacia gum powder	4.7	9000-01-5
Arabic acid	5.0	32609-14-6
<b>Salts</b>		
NaHCO <sub>3</sub>	96.0	144-55-8
CaSO <sub>4</sub> ·2H <sub>2</sub> O	60.0	10101-41-4
MgSO <sub>4</sub>	60.0	7487-88-9
KCl	4.0	7447-40-7
(NH <sub>4</sub> ) <sub>2</sub> SO <sub>4</sub>	23.6	7783-20-2
K <sub>2</sub> HPO <sub>4</sub>	7.0	7758-11-4

For the experiments in real wastewater, effluent from biological treatment was taken from three wastewater treatment plants (WWTPs): from the urban wastewater treatment plant (UWWTP) “El Bobar”, in Almería; from the WWTP situated in-campus in the nursery in the University of Almería; and from the in-situ industrial wastewater treatment plant (IWWTP) in the agro-food industry Cítricos del Andarax S.A.

The first WWTP treats municipal wastewater generated in Almería with an activated sludge system as final step before discharging the water to the sea. The

second WWTP is comprised by a membrane bioreactor with a treatment capacity of 1 m<sup>3</sup>/day to treat the wastewater generated in the nursery building in-campus. The third plant has a sequencing batch reactor (SBR) as final step before discharging the water to the sewer network and a capacity of 450 m<sup>3</sup>/day. The industry produces different types of soup, creams and juices, so wastewater variability is high due to seasonal changes in product production in the industry.

The effluent from the same WWTP was taken in different seasons, so the properties presented certain variability. For this reason, the specific properties are presented with the results in the Results and Discussion Section.

## **2.3 Reagents**

### **2.3.1 Analysis**

Ultrapure water was obtained from a Millipore Milli-Q® system. It was used for preparation of analytical standards and eluents in liquid and ionic chromatography. Chromatographic standards of acetaminophen, oxamyl, methomyl, imidacloprid, dimethotote, pyrimethanil, acetamiprid, thiabendazole and imazalil were obtained from Sigma-Aldrich. Acetonitrile and methanol were used as solvents in liquid chromatography and were acquired with HPLC grade. Sulphuric acid (95-97%) and sodium carbonate (reagent grade) were used for ionic chromatography. Ammonium metavanadate, o-phenantroline, ammonium acetate and acetic acid were reagents employed for the determination of dissolved iron and hydrogen peroxide concentrations and were obtained in reagent grade.

### **2.3.2 Experiments**

Iron sulphate heptahydrated (FeSO<sub>4</sub>·7H<sub>2</sub>O), hydrogen peroxide (30% w/v), were used systematically for the photo-Fenton experiments. Commercial formulations of pesticides were also obtained: Textar® 60-T (60% w/v thiabendazole) and EPIK® (20 % w/w acetamiprid) were supplied by Tecnidex S. A. Vydate® (10% w/v oxamyl), Metomur® (20%, w/v, methomyl), Couraze® (20% w/v imidacloprid), Perfektion® (40% w/v dimethoate) and Scala® (40% w/v pyrimethanil) were obtained from local suppliers. The standard-grade pesticides and acetaminophen were also used for the experiments. Sodium bisulfite was also used from Panreac at laboratory grade to act as hydrogen peroxide scavenger. Iron D-gluconate and lactate and deferoxamine mesylate were provided by Sigma-Aldrich and ferroactive fertiliser was obtained from a



local supplier. Titanium dioxide Degussa P25 was used for heterogeneous photocatalysis.

## 2.4 Analytical techniques

### 2.4.1 Dissolved Organic Carbon (DOC)

The Dissolved Organic Carbon (DOC) is the Total Organic Carbon (TOC) measurement in a filtered sample. DOC determinations were carried out in a Shimadzu TOC-V CPH analyser with TNM-1 analyser, calibrated with standard solutions of potassium phthalate. The instrument is equipped with a Shimadzu ASI-V autosampler. A picture of the instrument is shown in Figure 2.1. It measures Total Carbon (TC) and Total Inorganic Carbon (TIC). The TOC is calculated as the difference between TC and TIC.



**Figure 2.1.** Shimadzu analyser used for DOC measurement.

The TC measurement is based on the combustion of the aqueous sample on a platinum catalyst supported on aluminium oxide spheres, converting all carbon into  $\text{CO}_2$ . The combustion takes place in the combustion chamber at  $680\text{ }^\circ\text{C}$ . The combustion gas is transported by a carrier gas and fed into an infrared detector for analysis of the  $\text{CO}_2$  concentration.

The TIC concentration is measured by injecting 25% w/v phosphoric acid to the sample so that carbonate and bicarbonates are liberated as  $\text{CO}_2$ . The  $\text{CO}_2$  concentration is measured by the same detector as for the TC concentration.

The calibration of the instrument for the measurement of TC was made using standard solutions of potassium phthalate at different concentrations. For the

calibration of TIC, standard solutions of sodium hydrogen carbonate were used. The analyser has an automatic statistical quality control based on the standard deviation limits set (1%). If the error in the measurement did not meet the quality control standard, the samples were re-injected automatically. To avoid obstructions in the instrument, samples were filter before the analysis, so the measurement corresponds to DOC.

#### 2.4.2 Pollutant concentration determination by Ultra Performance Liquid Chromatography with diode array detector (UPLC/DAD)

The concentration of the model pollutants was measured by UPLC in an Agilent Technologies 1200 Series instrument (Figure 2.2).



**Figure 2.2.** UPLC-DAD (Agilent Technologies 1200 series).

The instrument has a column oven, degasser, autosampler and diode array detector (UV-Vis detection). The sample is injected by the autosampler. The sample is pumped through the system in laminar regime to avoid vertical mixing and passes through the column. The pressure along the column is high compared with conventional HPLC due to the small size of the particles (higher performance than conventional columns with particles  $> 4 \mu\text{m}$ ) filling the column, high flow and column length, varying from 50 to 250 bar in the methods employed (400 bar maximum allowed pressure in the system). The compounds generate a signal in the UV-Vis detector and the signal is registered in the software (Agilent ChemStation®). The concentration of each compound is then obtained through calibration curves calculated from the standards.

The column used throughout the experimental work was a reverse phase column (Agilent XDB-C18, 50-4.6 mm and 1.8  $\mu\text{m}$ ). The eluents used were acetonitrile and ultrapure water with 1% v/v formic acid. Each sample was filtered with 0.22  $\mu\text{m}$  syringe filters before the analysis. The compounds are held in the column depending on their affinity to form bonds with the C18 column. If their affinity for the column is not high, they will go through the column in the eluent and have short retention times.

Method 1 was used for the determination of the mixture of pesticides oxamyl, dimethoate, imidacloprid, pyrimethanil and methomyl; and Method 2 allowed measuring acetamiprid, thiabendazole and imazalil. The specifications of the methods and limits of detection (LOD) are shown in Table 2.4.

**Table 2.4.** UPLC-DAD methods for the detection of the model compounds.

UPLC-DAD methods			
<b>Method 1</b>			
Isocratic, 15% acetonitrile			
20 $\mu\text{L}$ sample volume; 1.5 mL/min			
Compound	Retention time (min)	Wavelength (nm)	LOD (mg/L)
Dimethoate	2.80	210	5
Pyrimethanil	9.95	265	1
Methomyl	1.02	234	2
Oxamyl	0.83	234	2
Imidacloprid	2.65	265	3
<b>Method 2</b>			
Gradient, 5% acetonitrile (t=0 min) and			
100% acetonitrile (t=12 min);			
100 $\mu\text{L}$ sample volume; 1.0 mL/min			
Compound	Retention time (min)	Wavelength (nm)	LOD ( $\mu\text{g/L}$ )
Acetamiprid	9.6	248	2
Thiabendazole	3.4	300	1
Imazalil	11.4	225	10

### 2.4.3 Ionic Chromatography (IC)

The concentration of anions in water was determined using ion chromatography Metrohm 881 Compact IC pro. The instrument is constituted by a degasser to remove gas bubbles from the eluent and sample through a vacuum chamber; a high pressure pump; an injection valve to connect the eluent and the sample; column heater in the column chamber to ensure stable temperature; a peristaltic pump to pump the sample and eluent; a suppressor module which is in operating mode for the analysis of anions

and removes CO<sub>2</sub> to avoid interferences of the eluent; and an anionic chromatography column (Figure 2.3).



**Figure 2.3.** Metrohm 881 Compact IC pro system.

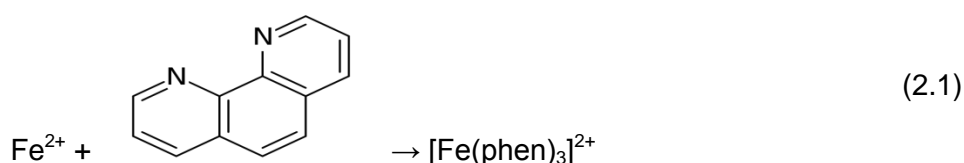
In ionic chromatography the ions in aqueous solution are held in the column through ionic acidic and basic bonds with counter ions. The column is formed by a resin with charged ions as active sites. The system can work with a cationic column, to detect cations in solution, or with an anionic column for anions. In this case, the instrument always worked with an anionic column. The column used was a Metrosep A Supp 7, 250-4.0 mm and 5 µm from Metrohm. The eluent consisted of a solution of Na<sub>2</sub>CO<sub>3</sub>, to compete with the anions for the active sites. The instrument worked with a flow of 0.8 mL/min and the column temperature was set at 45 °C. The retention times for the anions are presented in Table 2.5.

**Table 2.5.** Retention times for anions detected by IC.

Anion	Retention time (min)
Fluoride	5.83
Chloride	9.36
Nitrite	11.49
Bromide	14.64
Nitrate	17.03
Phosphate	24.09
Sulphate	27.09

### 2.4.4 Dissolved iron measurement

The method used in this work to measure dissolved iron (total iron, ferrous and ferric iron) followed the standard method “ISO 6332:1988, Water quality – Determination of iron – Spectrometric method using 1,10-phenantroline”. O-phenantroline reacts with ferrous iron forming an orange-coloured complex, following Reaction 2.1. The complex presents a maximum of absorbance at 510 nm which does not change from pH=3-9, with a molar extinction coefficient of  $\epsilon_{510\text{nm}}=11720 \pm 60$  L/mol-cm. From pH=3-5 the colour of the complex develops rapidly, ensuring a good quantification. Therefore, the measurement is usually made in a buffered solution.



This method serves specifically to measure ferrous iron. Ferric iron does not form a coloured complex with o-phenantroline. During photo-Fenton experiments, most of the dissolved iron exists as ferric iron. A strategy to measure it is to add a reducing agent such as ascorbic acid to reduce ferric iron to ferrous iron. The measured ferrous iron corresponds to total dissolved iron. Measuring ferrous iron before and after adding the reducing agent allows determining the concentration of ferric and ferrous iron as well.

There are metals which can form complexes with o-phenantroline such as  $\text{Zn}^{2+}$ ,  $\text{Cu}^{2+}$  or  $\text{Ni}^{2+}$  or which can precipitate it, like  $\text{Ag}^{2+}$  or  $\text{Hg}^{2+}$ . Nevertheless, these metals are not present in the wastewater effluents treated in this work. In photo-Fenton experiments the main interferences may come from the colour of the own effluent and hydrogen peroxide.

To carry out the determination of iron concentration, a 1 g/L-solution of o-phenantroline and a buffer solution were prepared. The buffer solution was a mixture of ammonium acetate and acetic acid to ensure acidic pH (62.5 g ammonium acetate and 175 mL acetic acid in a 250 mL solution with deionised water). The measurement was carried out attending to the following protocol:

1. The samples are filtered through 0.22  $\mu\text{m}$  syringe filters.
2. 1 mL is taken from the samples and diluted with 4 mL of deionised water.
3. 1 mL of buffer solution is added to the diluted sample.

4. 1 mL of 1,10-phenantroline solution is added and the coloured complex is formed.
5. For non-coloured samples, deionised water can be used as blank. For coloured samples, the blank is prepared following the same steps as for the samples but substituting the o-phenantroline with water sample.
6. The absorbance of the sample can be measured, giving the concentration of ferrous iron.
7. Add the tip of a spatula of ascorbic acid to reduce all ferric iron to ferrous iron. Then measure again the sample. The concentration corresponds to total dissolved iron.

A calibration curve with ferrous iron concentrations from 1 to 30 mg Fe/L was made to obtain the concentration in the experiments. The curve was validated regularly.

If the aim of the measurement is to distinguish between ferric and ferrous iron during an experiment with hydrogen peroxide, the sample should be measured immediately, unless the reaction is stopped by a hydrogen peroxide scavenging agent. Otherwise, the measurement does not have to be made as immediately, but it should be noted that slow iron precipitation tends to occur, even if the sample is filtered beforehand, so the sample should not be left for long unmeasured.

#### 2.4.5 Hydrogen peroxide measurement

Hydrogen peroxide is the oxidising reagent of the photo-Fenton process. Therefore, determining its concentration and consumption during the experiments is essential to evaluate the process. There are different methods to determine hydrogen peroxide concentration, but in this work it was determined through a simple spectrophotometric method developed by Nogueira et al (2005b).

This method is based on the reaction of hydrogen peroxide with metavanadate anion. When both react in acidic solution, the red-orange peroxovanadium cation is formed with maximum absorbance at 450 nm (Reaction 2.2).



For the application of the method, an acidic solution of ammonium metavanadate is prepared, using 0.06 M ammonium metavanadate and 0.36 M sulphuric acid. For the sample analysis, the following protocol is applied:

1. Take a sample volume between 1 and 8 mL, depending on the hydrogen peroxide concentration to ensure accuracy in the method.
2. Add 1.030  $\mu\text{L}$  of the 0.06 M metavanadate solution
3. Add deionised water up to 10 mL
4. Measure in the spectrophotometer at 450 nm, using a blank prepared with the same protocol, but substituting the sample with hydrogen peroxide for sample without it.

The absorbance should be between 0.1-1 to ensure accurate results. The concentration of hydrogen peroxide can be determined through Equation 2.3.

$$[\text{H}_2\text{O}_2] = A_{450} \cdot \frac{V_2}{283 \cdot V_1} \quad (2.3)$$

Where  $V_1$  is the sample volume (mL) and  $V_2$  is the total volume (mL). The concentration is obtained in mM.

#### 2.4.6 Persulphate measurement

Persulphate is another oxidising agent used in AOPs. When it is activated, it gives yield to sulphate anion radicals,  $\text{SO}_4^{2\cdot-}$ . The activation process through radiation, temperature or metal electron transfer is explained in the Introduction (Section 1.3.4). It is traditionally measured through back-titration with thiosulphate (Kolthoff and Carr, 1953). However, this method is not feasible as routine analysis. A recent spectrophotometric method proposed by Liang et al. (2008) was used in this work for the determination of persulphate concentration.

This method is based on the reaction of persulphate and iodide, according to Reaction 2.4. This reaction takes place in 15 min (25 °C) with excess of iodide, forming a yellow complex. The reaction is carried out in the presence of sodium bicarbonate to avoid oxygen-oxidation of iodide.



If the sample presents iron concentration (e.g. as activation compound for persulphate), it may interfere with the measurement of absorbance. The measurement is suggested at 352 nm and if there are interferences by the reagent matrix, at 400 nm. However, at the latter wavelength there might be a reduction in the intensity of the complex absorption.

To measure persulphate with this method, the protocol described by Liang et al. (2008) is:

1. Take 40 mL of sample
2. Add 0.2 g of NaHCO<sub>3</sub>
3. Add 4 g of KI, shake and let equilibrate for 15 min
4. Measure at 352 nm (or 400 nm), preparing a blank with the same protocol with the sample without persulphate

It can be used taking less sample volume and maintaining the relationship of the rest of the reagents.

### **2.4.7 Chemical Oxygen Demand (COD)**

The Chemical Oxygen Demand (COD) is the amount of oxidising agent, expressed as oxygen concentration, required to oxidise organic matter in a sample under certain conditions of temperature and time.

Its measurement is done through the Merck Spectroquant® kit. The kit contains an acidic solution of potassium dichromate, with silver sulphate as catalyst. In the presence of organic matter and after two hours of reaction at 148 °C, the dichromate ion is turned into Cr<sup>3+</sup>, forming a green-coloured solution which can be measured by spectrometry at 445 nm.

To apply the kit, the sample is filtered and added to the kit. The sample volume depends on the range of the kit. The reaction is exothermic but it could be accelerated if heated up. Therefore, the kit is put in a thermo block at 148 °C to keep isothermic and high temperature conditions for 2 h.

## **2.5 Pilot Plants and laboratory scale experiments**

The work was developed in different pilot plants as well as at laboratory scale. Each system is described below.

### **2.5.1 Compound parabolic Collector (CPC)**

A Compound Parabolic Collector (CPC) was one of the pilot plants used. It is constituted by two identical closed loops with two tubes each. The tubes are made of



borosilicate glass over a curved reflector made of aluminum. The absorber tube has an internal diameter of 45 mm. The reflector has a concentration factor of 1 and direct and diffuse radiation is used. The hydraulic circuit involves a continuously stirred spherical-like tank with a centrifugal recirculation pump and connecting tubes made of polyethylene and valves. The samples are taken from the spherical tank.

The system is designed to work in batch mode. The total volume of each loop was 7 L (4.55 L irradiated volume). The pilot plant is located at the Centro de Investigación de la Energía Solar (CIESOL), in Almería, Spain (latitude 36° 50' 24.59" N, longitude 2° 28' 4.52" W). The CPC is set in one module tilted 37° facing south and with a surface of 1 m<sup>2</sup>. A rotameter is installed in the plant, with a measured flow rate of 11 L/min. This results in a Reynolds number close to 30,000 and turbulent regime inside the tubes.

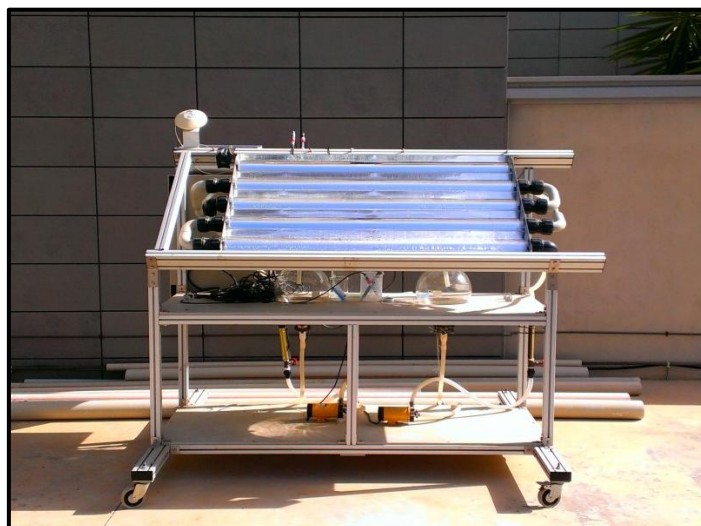


**Figure 2.4.** Pilot plant CPC.

The plant also includes temperature, pH and dissolved oxygen probes and UV radiometer DeltaOhm (LP UVA 02 AV; spectral response 327-384 nm). The probes are connected to a LabJack USB/Ethernet data acquisition device connected to a computer to facilitate the online monitoring of the variables. The system has a peristaltic pump as well for the dosage of reagents in the system.

### **2.5.2 Flat-reflector photoreactor**

This pilot plant is similar to the CPC but with the difference that the reflector surface is flat instead of curved. This fact simplifies the design and cost of the system. It is constituted by four closed loops, with two borosilicate glass tubes per loop. The

hydraulic circuit includes the tubes, the cylindrical tank where the samples are taken, centrifuge pump, valves and connections. The capacity of each loop is also 7 L. It is located in CIESOL, so the plant is also tilted 37° and faces south. The internal diameter of the tubes is 49 mm.

The plant also includes temperature, pH and dissolved oxygen probes and UV radiometer DeltaOhm, LP UVA 02 AV; spectral response 327-384 nm), connected to the same kind of device as the CPC, a LabJack USB/Ethernet data acquisition device connected to a computer to facilitate the online monitoring of the variables. The system has two peristaltic pumps for the dosage of reagents in the system, connected to the online system.

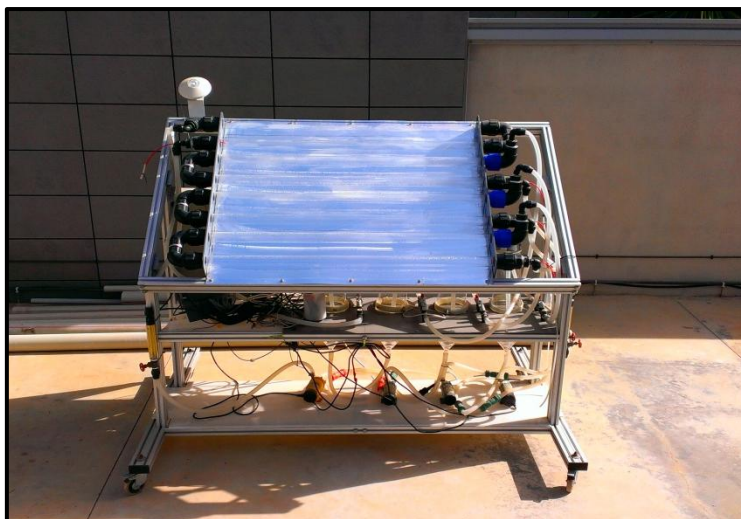


**Figure 2.5.** Flat-reflector photoreactor.

### 2.5.3 The Raceway Pond Reactor

A Raceway Pond Reactor (RPR) pilot plant was also used. It is a reactor with a maximum treatment capacity of 360 L. It is made of fiberglass with a length of 3.85 m and width of 0.64 m. It is separated by a central wall, forming two canals. The RPR includes a paddle wheel connected to an engine to obtain a mixed and homogeneous system. The engine is linked to a variable frequency drive to control the paddles' speed. A scheme of the plant is presented in Figure 2.6.

It is an open system which allows modifying the liquid height from 5 to 15 cm. It presents a recirculation time of 30 s and a mixing time of 2.5 min. The flow is turbulent, with Reynolds numbers between  $6 \cdot 10^5$  and  $7 \cdot 10^5$ , depending on the liquid height. For 5

cm liquid height the capacity of the photoreactor is 120 L; for 10 cm, it is 240 L; and for 15 cm, 360 L. It is also located in CIESOL, facing south. It includes temperature and pH probes as well as a global UV radiometer (DeltaOhm, LP UVA 02 AV) mounted on a horizontal platform.



**Figure 2.6.** 360-L Raceway Pond Reactor.

#### **2.5.4 Solar box**

Experiments were also carried out at laboratory scale. They were run under solar radiation or in a SunTest CPS+ solar box from Atlas. The system presents an emission range from 250 to 765 W/m<sup>2</sup> (complete emission spectrum). It has the advantage of operating the process in controlled conditions of irradiance.

The system can be operated with a stirred tank reactor or with plate reactor placed inside the solar box. The plate reactor is connected to a mixing and recirculation tank (Santos-Juanes et al., 2011). The capacity of the plate reactor system is 3 L, 2 L inside the plate reactor (irradiated volume) and a volume of 1 L in the recirculation tank outside the solar box (dark volume). The liquid height in the plate reactor is 5 cm. A scheme of the operating systems in the solar box is shown in Figure 2.7.

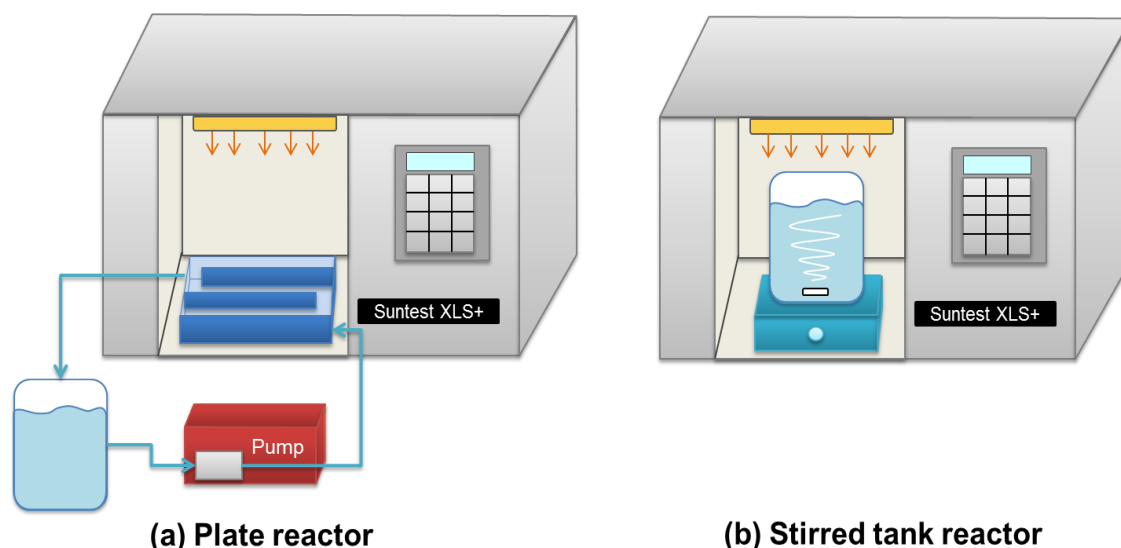


**Figure 2.7.** Operating scheme in the SunTest CPS+ solar box with (a) the plate reactor, and (b) the stirred tank reactor.

## 2.6 Experimental set-up

### 2.6.1 Preparation of pollutant and simulated wastewater solutions

The model pollutants (Table 2.1) were used in different groups:

- Acetaminophen was used as single pollutant. It was usually used in a concentration of 50 mg DOC/L and left to dissolve for at least 0.5 h in deionised water. The compound did not present solubility problems in the concentration range used. 7-L solutions were prepared to work in the CPC.
- Oxamyl, methomyl, imidacloprid, pyrimethanil and dimethoate were always used in their commercial formulations for the experiments (Vydate®, Metomur®, Couraze®, Scala® and Perfektion®, respectively). They were left to dissolve in deionised water or in real wastewater for at least 1 h, although the commercial formulations presented high solubility in water. 7-L solutions were prepared to work in the CPC.
- Acetamiprid, thiabendazole and imazalil were used in deionised water, simulated effluent and real wastewater. They were used in their pure forms to work in the flat-reflector photoreactor (7-L volume). A concentrated solution of the pesticides (10 mg/L) was prepared in methanol with the pesticide standards. Then dilutions were made to obtain 100 µg/L in the 7-L aqueous solution to work in the flat-reflector photoreactor, leaving over 2 h of mixing time.

- For the experiments in the raceway pond, the commercial formulations of acetamiprid (EPIK®) and thiabendazole (TEXTAR®) were used. 10-L solutions were prepared a few hours before the experiments, but no concentrated solutions were needed due to the higher solubility of the commercial formulations.

The simulated effluent (Table 2.3) was usually prepared the day before the experiments to ensure complete solubility of all compounds and was left mixing overnight. The salts were the first to be added to deionised water. When they were completely dissolved, the organic compounds were added to avoid aggregates, especially with calcium sulphate. Only when the compounds were completely dissolved, the pollutants were added to avoid adsorption effects.

### **2.6.2 Photo-Fenton experimental procedure**

The photoreactors were always covered before starting the experiment to prevent photochemical reactions during preparation. The effluent to be treated was always added with the model pollutants already dissolved, except in the case of the raceway operation, where they were dissolved in the reactor. In the tubular reactors the plants were recirculated during the preparation and in the raceway pond the paddle wheel was switched on as well.

The initial sample was taken before adding any other chemical and pH was adjusted immediately to the desired value with sulphuric acid. In case of using iron complexes, pH was added after they were mixed.

For experiments at acidic pH (pH 2.8), iron sulphate was added and left to mix. Then a sample was taken to ensure the iron concentration in solution was as expected. Then hydrogen peroxide was added, beginning the reaction and immediately the reactor was uncovered. Then samples were taken during the experiment regularly to measure iron, hydrogen peroxide and pollutant concentration; while online temperature, pH, UV radiation and dissolved oxygen were monitored online.

For experiments at natural or circumneutral pH, hydrogen peroxide was added first and left to mix. Then a freshly prepared solution of iron sulphate was added to the photoreactor, starting the experiment. At the same time, the reactor was uncovered. When iron dosage was applied, it was made through a peristaltic pump and a silicone

tube which added the iron solution directly to the borosilicate tube of the tubular photoreactor.

After each experiment the tubular photoreactors were cleaned twice with sulphuric or oxalic acid and then with deionised water to avoid contamination from one experiment to the other. The raceway was cleaned similarly.

### 2.6.3 UV lamps

Part of the work plan was developed in the Water Science Institute in Cranfield University (UK). Mercury UVC low pressure lamps (LPL) and UVC low emitting diodes (LEDs) were evaluated as tertiary treatment technology using the photo-Fenton process.

#### a) UVC low pressure lamps system

The UVC experiments were conducted in a Wedeco AG laboratory scale quasi-collimated beam apparatus equipped with three 30 W UVC low pressure lamps emitting monochromatic light at 254 nm. The experiments were carried out in a 250-mL or 25-mL reactor placed under the lamps (Figure 2.8).

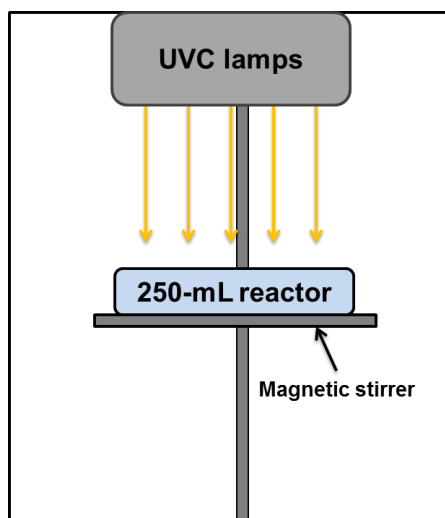


**Figure 2.8.** Scheme of the UVC low pressure lamp system.

Underneath the lamps was a platform where the reactor was placed. The platform could be moved vertically to vary the distance between. UV irradiance was determined to be 10, 20 and 27 W/m<sup>2</sup> when the distance between the lamps and the reactor was 22, 11 and 4 cm, respectively.

The experiments were carried out in deionised water, simulated secondary effluent and using real wastewater from an activated sludge plant on campus.

### **b) UVC-LED system**

The experiments were conducted in a UVC-LED system formed by an UVCLEAN lamp with multi-chip arrays of UV LEDs enclosed in a metal glass package from Sensor Electronic Technology (Columbia, South Carolina) and emitting at 256 nm. It is packaged in a TO-3 can with an internal heat sink. A 25-mL petri dish was placed underneath and was magnetically stirred. The UVC irradiance was determined to be 20 W/m<sup>3</sup>. The experiments were conducted in simulated effluent.





## ***RESULTS AND DISCUSSION***

---



### **3. RESULTS AND DISCUSSION**

#### **3.1 Strategies to remove medium concentration of pollutant at natural pH**

##### **3.1.1 Use of iron complexes**

As previously stated, the efficiency of the photo-Fenton process depends on pH. The optimal pH for this process is 2.8; not only because iron precipitation is avoided but also because the formation of photoactive iron complexes is dependent on pH and the presence of ions (Laat et al., 2004). However, this pH value involves higher operational costs due to the amount of reagent needed to adjust pH along with the consequent environmental impact. All of these reasons have prompted the study of modified photo-Fenton processes in which the initial pH is not so extreme. At neutral pH, though, iron (III) precipitates as hydrous oxyhydroxides ( $\text{Fe}_2\text{O}_3 \cdot n\text{H}_2\text{O}$ ), so  $\text{Fe}^{2+}$  regeneration is prevented (Elshafei et al., 2010). This fact leads to efficiency loss due to catalyst precipitation, but also at higher pH values, some authors have discussed the participation of iron species with higher oxidation states (ferryl ion, Fe (IV)) (Bossmann et al., 1998) and that the reaction mechanism may actually be different from traditional photo-Fenton (Katsoyiannis et al., 2008). In order to escape difficulties associated with pH, modified photo-Fenton systems are studied, using stable iron complexes at neutral pH to improve hydroxyl radical generation and mineralization.

In this Section, acetaminophen was used as model pollutant. Traditional photo-Fenton (pH 2.8) has been applied effectively for the removal of pharmaceuticals such as ibuprofen (Mendez-Arriaga et al., 2010) sulfamethoxazole (González et al., 2007), and acetaminophen, amongst others (Klavarioti et al., 2008). Acetaminophen, also known as paracetamol, is a commonly used analgesic. However, it is not removed by traditional biological systems, usually activated sludge, given that its biodegradability is not very high and its widespread use promotes accumulation in the freshwater environment (Murray et al., 2010). As a result, acetaminophen accumulates in the receiving environment if it isn't specifically removed.

##### **a) Mineralisation at laboratory scale**

At laboratory scale, iron (II) sulphate, iron (II) D-gluconate, deferoxamine mesylate and fertilizer Ferroactiv were used. Each iron source was studied and then the one which gave the best results was evaluated in the 7-L CPC pilot plant.

Iron (II) D-gluconate and lactate (Figure 3.1) are iron complexes often used to treat illnesses related to the lack of iron in the body. Deferoxamine mesylate (Figure 3.1) is a ferric iron chelate, used in medicine for the opposite reason. They were selected because of their solubility in water and innocuous nature. Moreover, their biodegradability makes it particularly interesting given that any quantity remaining after photo-Fenton treatment could be disposed of in conventional wastewater treatment plants. The last selected compound was fertilizer Ferroactiv, which has an active ingredient (FeEDDHA) similar to EDTA, reported as effective to complex iron (Zhoua et al., 2008).

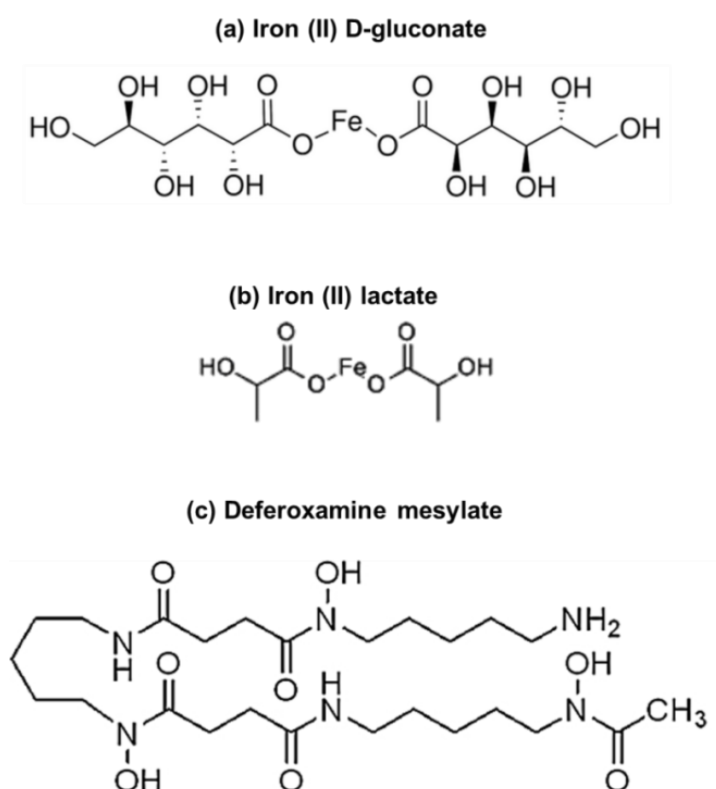


**Figure 3.1.** Chemical structure of ferrous D-gluconate, ferrous lactate and deferoxamine mesylate

The experiments were carried out in the solar box, at constant irradiance. UV radiation was set at  $30 \text{ W/m}^2$  in all cases. Stirred-tank reactors with a 250 mL capacity were used ensuring that illuminated volume was 100%. Acetaminophen concentration was 1 mM, resulting in 100 mg/L DOC. Iron concentration was 20 mg/L, provided as ferrous sulphate, ferrous D-gluconate, ferrous lactate, deferoxamine mesylate or fertilizer. This iron concentration is optimal for CPCs with 5 cm of optical path (Malato et al., 2004). When the iron chelate and complexes were added, DOC concentration increased. Therefore, DOC concentration was 100 mg DOC/L added as

acetaminophen plus ~50, 25, 105, 75 mg DOC/L added as D-gluconate, lactate, deferoxamine mesylate or fertilizer, respectively.

Hydrogen peroxide concentration was twice the amount needed to completely oxidize acetaminophen (1270 mg/L H<sub>2</sub>O<sub>2</sub>) based on the chemical oxygen demand obtained for 1 mM of acetaminophen. Deionised water was used for all experiments. Experiments were carried out adjusting initial pH to 7 and a test was done using iron sulphate at pH to 2.8 as a reference.

In Table 3.1, results after two hours of treatment in the solar box are shown. As expected, the highest mineralization was obtained at pH 2.8 (90%) along with the greatest hydrogen peroxide consumption (97% of initial concentration). Iron salt was used at natural pH as well and nearly 80% paracetamol was mineralized; and despite the fact that the final iron concentration was 46% of the initial concentration, it seemed to be dissolved for enough time to reach a substantial level of mineralization, with reactant consumption similar to the reference (95%). The reasons as to why this successful mineralization value is obtained despite iron precipitation will be discussed later.

Regarding iron complex D-gluconate, the final mineralization (84%) and hydrogen peroxide consumption (97.0%) were comparable to those obtained with iron sulphate at initial pH 7. However, final iron concentration was slightly lower (37%). Iron lactate showed similar iron and hydrogen peroxide profiles, but mineralization was lower (75%), even though the DOC concentration added by the complex was lower than iron D-gluconate (Table 3.1).

The deferoxamine mesylate chelate and the fertilizer gave red colour to water, so iron and hydrogen peroxide measurements were not possible during the tests. Only the sample at 120 min could be measured in the case of the deferoxamine due to loss of colour. The loss of colour was due to the oxidation of the own chelate. In both cases mineralisation was low, 75% and 60% with the deferoxamine and ferroactive, respectively.

Nonetheless, it has to be taken into consideration that final mineralization is expressed in relative terms and that initial DOC varies with the different iron sources. Thus, another approach for studying the reaction efficiency is by comparing the ratio between removed DOC and consumed hydrogen peroxide,  $\Delta\text{DOC}/\Delta\text{H}_2\text{O}_2$ , expressed as a molar rate.

**Table 3.1.** Acetaminophen degradation at natural pH (except when indicated) applying photo-Fenton for 2 h at laboratory scale (initial concentration of 20 mg/L Fe and 1270 mg/L H<sub>2</sub>O<sub>2</sub>).

Iron sources	Initial	Efficiency $\Delta\text{DOC}/\Delta\text{H}_2\text{O}_2$	Mineralization (%)	Dissolved Fe (%)	Consumed H <sub>2</sub> O <sub>2</sub> (%)
	DOC (mg/L)				
Fe <sup>2+</sup> sulphate pH 2.8	100	0.09	90	96	97
Fe <sup>2+</sup> sulphate	100	0.07	80	46	95
Fe <sup>2+</sup> D-gluconate	150	0.10	84	37	97
Fe <sup>2+</sup> lactate	125	0.07	75	36	91
Deferox. mesylate	205	0.13	75	54	96
Ferroactive	175	0.13	60	-	-

The ratio  $\Delta\text{DOC}/\Delta\text{H}_2\text{O}_2$  was highest for the deferoxamine mesylate and the fertilizer, followed by iron D-gluconate, while iron lactate was the iron complex with the lowest efficiency (Table 3.1). However, as the deferoxamine and fertilizer presented colour and high DOC concentration in comparison with acetaminophen concentration, they were disregarded as practical sources of iron. As iron lactate presented low efficiency, only ferrous D-gluconate was selected to be evaluated at pilot plant scale, together with the ferrous sulphate as reference.

### b) Results at pilot plant scale

Pilot-plant scale experimentation was carried out in the CPC in deionized water. Tests were carried out applying the same conditions as in laboratory experiments to study how the change of scale affects the final results. Additionally, the effect of hydrogen peroxide dosage was analysed at pilot-plant scale since how the reactant is dosed can be expected to improve the consumption efficiency (Santos-Juanes et al., 2011) and two sequential additions and continuous dosage were tried. Finally, the results were also tested in real water in order to determine the consistency of the conclusions obtained.

#### One addition of hydrogen peroxide

The same conditions as in the laboratory-scale tests were used (Table 1) to see the effect that the change of scale had on the final results: 1 mM acetaminophen (100

mg/L DOC), 20 mg/L Fe<sup>2+</sup> as iron salt or complexed with D-gluconate, 1270 mg/L H<sub>2</sub>O<sub>2</sub> and initial neutral pH. Figure 3.2 shows dissolved iron, hydrogen peroxide concentration and DOC evolution with real and illuminated time using iron sulphate and D-gluconate under these conditions.

As solar UV radiation is a variable which has a profound effect on the running of the process, it is interesting to compare experiments using normalized time. With Equation 3.1, a combination of the data from several days' experiments and their comparison to other photocatalytic experiments is possible (Malato et al., 2003).

$$t_{30W} = t_{30W,n-1} + \Delta t_n \cdot \frac{\overline{UV}}{30} \cdot \frac{V_i}{V_T} \quad (3.1)$$

for  $\Delta t_n = t_n - t_{n-1}$ ;  $t_0 = 0$ ;  $n=1$

Where  $t_n$  is the experimental time for each sample,  $\overline{UV}$  is the average solar ultraviolet radiation measured during  $\Delta t_n$ , and  $t_{30W}$  is a "normalized illumination time". In this case, time refers to a constant solar UV power of 30 W/m<sup>2</sup> (typical solar UV power on a perfectly sunny day around noon).  $V_T$  is the total water volume loaded in the pilot plant (7 L) and  $V_i$  is the total irradiated volume (4.55 L).

In this set of experiments iron precipitation was more pronounced than in the laboratory. For iron sulphate, the final dissolved iron was 9.1 mg/L in the laboratory test (46%) while it was 4.5 mg/L after 5 minutes in the pilot-plant test (Figure 3.2a). For D-gluconate, iron concentration in the laboratory experiment was 7.4 mg/L while in the pilot-plant test it was 3.8 mg/L (Figure 3.2b). Iron precipitation was caused by the change of reactor, which causes a different illuminated volume (100% in the laboratory-scale experiments and 65% in the pilot plant) and a higher temperature (35-40°C), which favored the formation of Fe(OH)<sub>3</sub> (Grundl et al., 1993). Ferric hydroxides precipitate at a lower pH than ferrous iron because of the low solubility product of ferric iron hydroxide ( $K_S(\text{Fe}(\text{OH})_3) \approx 10^{-37}$ ) and precipitation starts at pH 3.0–3.5 depending on the iron concentration, while the ferrous hydroxides precipitate mainly at a pH up to 6 (Datta, 1981). Precipitation, which also depends on temperature (Sapieszko et al., 1977), is higher and faster as temperature increases from 25 to 80 °C. Furthermore, in the pilot plant there are dark zones (mainly the recirculation tank) where Fe<sup>3+</sup> was not reduced to Fe<sup>2+</sup> and as a result it is more likely that the catalyst precipitates when combining illuminated and dark zones.

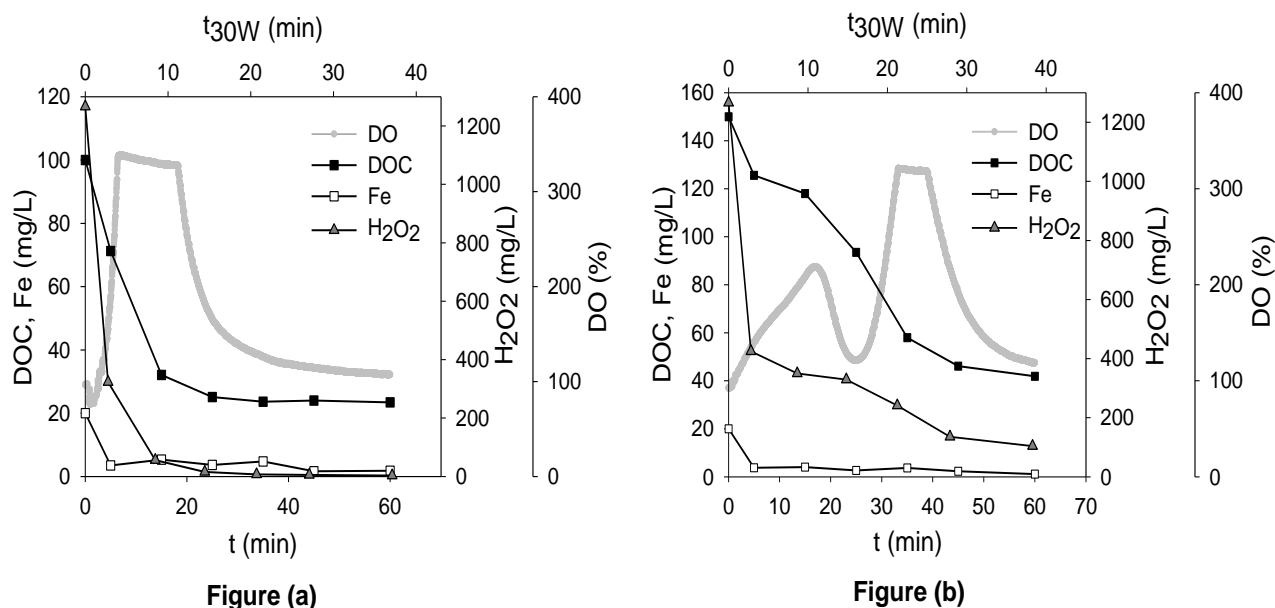


**Figure 3.2.** Acetaminophen degradation in the CPC pilot plant at initial neutral pH using iron sulphate (a) and iron D-gluconate (b) (100 mg/L acetaminophen DOC, 20 mg/L Fe<sup>2+</sup>, 1270 mg/L H<sub>2</sub>O<sub>2</sub>).

When iron sulphate was used (Figure 3.2a), it was active enough to consume most of the total hydrogen peroxide and generate sufficient hydroxyl radicals to mineralize 75% after 15 minutes although the dissolved iron disappeared mainly in the first 5 minutes. From that point on, the reaction progressed at a slower pace since there was not enough H<sub>2</sub>O<sub>2</sub> available. At the end of the test, the final mineralization was 78%. The relevant mineralization level at initial neutral pH (but at low iron concentration in both laboratory and pilot-plant tests) may be due to the fact that acetaminophen degradation by-products could form stable iron complexes (Pignatello et al., 2006). It is well known that the main intermediates formed in photo-Fenton before complete mineralization are carboxylic acids. These organic acids (acetic, formic, pyruvic, maleic, and oxalic acid etc...) are known to form complexes with ferric iron (Faust and Hoigné, 1990), which could cause the free dissolved iron in the solution to decrease after a certain illumination time but, nevertheless, keep the iron dissolved and temporarily slow down its precipitation. Another effect, which is specific to acetaminophen, has already been described in the literature: a reaction pathway for paracetamol degradation was proposed (Almeida et al., 2011) where acetaminophen is attacked by hydroxyl radicals to yield acetamide and hydroquinone. The former could be oxidized to oxamic acid which might form an oxamate complex with Fe<sup>3+</sup>. If it is taken into account that 1mM of acetaminophen (100 mg/L) could yield a maximum of 1mM of oxamate and that the initial iron concentration is 0.35 mM (20 mg/L), it is



possible that said iron complex is sufficiently formed to slow down its precipitation in the first stages of the reaction, despite initial neutral pH. It is necessary to point out that oxidation intermediates are continuously being formed and degraded; but given that oxamate is an equimolar intermediate of acetaminophen, a substantial quantity could be present during the first stages ( $t < 15$  min). The combined effect of oxamate with other organic iron complexes might be responsible for the substantial mineralization taking place during the first 15 minutes with a low concentration of dissolved iron. Moreover, as a result of iron hydrolysis and the production of acidic intermediates (carboxylic acids), pH dropped in both tests to a value of three.

With regard to DO, characteristic profiles were observed when each iron source was used. In the case of iron sulphate (Figure 3.2a), the DO profile first showed a decreasing slope at initial neutral pH, attributed to the Dorfmann mechanism, in which oxygen-consuming reactions take place. Following this, there was an increase in the DO concentration reaching probe saturation; this was due to inefficient reactions consuming hydrogen peroxide because it was in excess. Hydrogen peroxide excess means a higher probability of reaction with hydroxyl radicals that eventually encompasses oxygen generation (Pignatello et al., 2006). When hydrogen peroxide was totally consumed (between 15 and 20 minutes), there was a decrease in the DO concentration until it was in equilibrium with the atmospheric oxygen, also indicating the lack of hydrogen peroxide.

As regards D-gluconate (Figure 3.2b), again hydrogen peroxide consumption was fast in the first 5 minutes, but less so than with iron sulphate after the same time period. The main difference might be related to the presence of D-gluconate complex, which prevents the formation of more active iron complexes. The observed change in the DOC curve slope is also illustrated in the DO profile, which is significantly different from that shown in Figure 3.2a. Firstly, the characteristic decrease in DO concentration related to the Dorfmann mechanism (aromatic ring oxidation), which is observed in Figure 3.2a, did not take place, but DO concentration increased as hydrogen peroxide was consumed. This may mean D-gluconate oxidation mainly occurred first, releasing iron during the first stages ( $t < 15$  min), which was then able to form complexes with the available oxamate and any other organics (carboxylic acids formed from partially mineralized acetaminophen). The decreasing slope (not only in DO, but also in DOC) that followed this step (between 15 and 25 minutes) could then correspond with the Dorfmann mechanism related to oxygen-consuming reactions oxidizing acetaminophen. Following this, there was another increase in the DO, similar to the one shown for iron sulphate, which also reached probe saturation. At the end of the

test, mineralization was similar but significantly slower than with iron sulphate. Results indicated that iron D-gluconate would not be a good choice for avoiding iron precipitation at initial neutral pH as it also avoided the formation of other active iron complexes during the first stages of degradation and therefore D-gluconate decreased the reaction rate compared to iron sulphate at initial neutral pH. Nevertheless, 74% mineralization was achieved and as the results seemed to be seriously affected by the DOC concentration (formation of smaller or larger quantities of carboxylic acids) and  $\text{H}_2\text{O}_2$  concentration. Therefore, more experiments were done to gain insight into this matter.

### Two additions of hydrogen peroxide

The effect of adding hydrogen peroxide sequentially and continuously was studied. For this purpose, acetaminophen concentration was reduced to 0.5 mM (50 mg/L DOC) to diminish hydrogen peroxide consumption that caused saturation of the DO probe. It has been reported by Santos-Juanes et al. (2011) that for acetaminophen mineralization with photo-Fenton at pH 2.8, the molar ratio between  $\text{H}_2\text{O}_2$  and acetaminophen DOC resulting in the highest mineralization rate, and with the least concentration of reactant, is  $[\text{H}_2\text{O}_2]/[\text{DOC}]=1.65$ . For the experiments with two additions, it was made with the first one complying with said molar ratio; the second addition was half that of the first and was made when the DO on-line measurement, together with the spectrophotometric measurement, showed a lack of  $\text{H}_2\text{O}_2$ . A reference test was carried out as well using iron sulphate at pH 2.8.

Results are shown in Figure 3.3. As expected, the dissolved iron concentration was practically constant during the reference test (Figure 3.3a) and final mineralization was 79%. In the case of iron sulphate addition at initial neutral pH (Figure 3.3b), the concentration was above 10 mg/L for more than 10 minutes, which was enough time to carry out substantial mineralization (74%). The fact that iron precipitation is partially avoided during the first period of the test may be explained if it is considered that carboxylic acids are formed faster due to the lower initial acetaminophen concentration, so that both the dissolved Fe and the complexed Fe were active long enough to achieve considerable DOC degradation; and hydrogen peroxide consumption was almost the same in the experiment at pH 2.8 and at initial neutral pH.

Regarding  $\text{H}_2\text{O}_2$ , the reactant consumption was similar in both the reference and at initial neutral pH; and even the second  $\text{H}_2\text{O}_2$  addition was made at practically the same time.

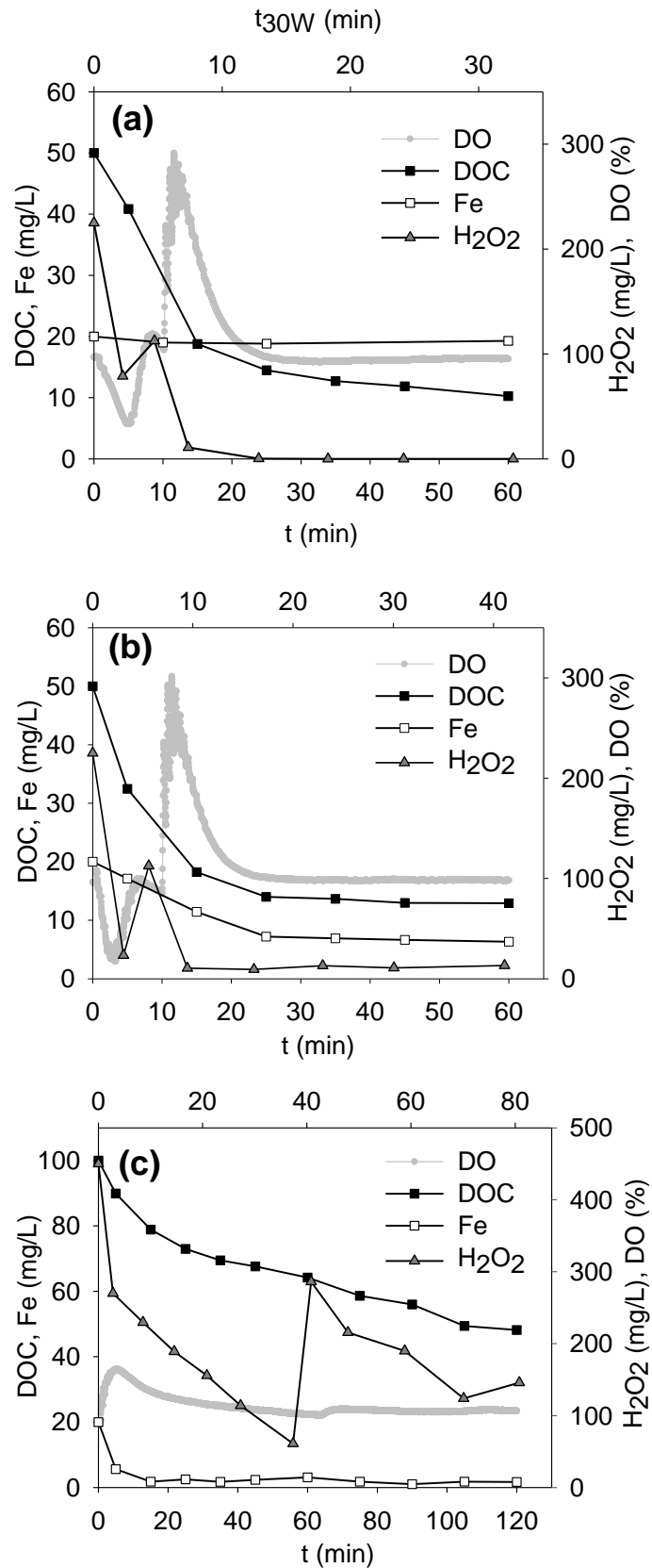


**Figure 3.3.** Acetaminophen degradation in the CPC pilot-plant dosing H<sub>2</sub>O<sub>2</sub> twice and using iron sulphate at pH 2.8 (a) at initial neutral pH (b) and D-gluconate at initial neutral pH (c) (50 mg/L acetaminophen DOC, 20 mg/L Fe<sup>2+</sup>).

The DO profile in these two situations also confirmed that the reaction rate was quite similar. The first minimum, which represents the Dorfmann mechanism, is overlapped for both cases. After that, the second decrease in the slope due to oxygen desorption depicts an absence of hydrogen peroxide, which also happened practically at the same time in both cases. The second addition of hydrogen peroxide is represented in the DO profiles by the second maximum. With regard to the pH, it dropped as before when beginning at initial neutral pH.

### Continuous addition of H<sub>2</sub>O<sub>2</sub>

With regard to experiments in which a continuous hydrogen peroxide addition was made, the reactant (a solution of 17.5 % w/w H<sub>2</sub>O<sub>2</sub>) was added to the mixing tank by means of a peristaltic pump using a flow of 0.34 mL/min during 35 min. The total reactant volume added was negligible in all cases when compared to treated volume (7 L).

Iron sulphate was used in order to analyze its effect on dissolved iron and mineralization; it has been reported by Santos-Juanes et al. (2011) that DO indicates slow H<sub>2</sub>O<sub>2</sub> dosage improves efficiency. Total H<sub>2</sub>O<sub>2</sub> concentration continuously added during the experiment was 310 mg/L, similar to the total amount of hydrogen peroxide added with two additions (338 mg/L).

It was observed that the process rate was slower than in experiments where two additions of H<sub>2</sub>O<sub>2</sub> were applied; this being a result of reactant limitation given that it was dosed and the concentration of H<sub>2</sub>O<sub>2</sub> in water was always lower than in previous tests (Figure 3.4).

It was also confirmed that D-gluconate was detrimental to the process (Figure 3.3c) as DOC mineralization was less (49%), and at a slower rate, than in the experiment shown in Figure 3.2. This means that D-gluconate degradation prevented the formation of more active iron complexes and mineralization was slower than in Figure 3.2b due to the fact that, in this case, the ratio between DOC from D-gluconate and DOC from acetaminophen was higher: 50 mg/L D-gluconate DOC and 50 mg/L acetaminophen DOC means a 1:1 ratio whereas for the operational conditions shown in Figure 3.2b, acetaminophen DOC was 100 mg/L, meaning a ratio of 1:2. The reduction in the process rate was also confirmed by the DO profile which varied with respect to the experiment carried out with only one hydrogen peroxide addition; and also by the delay in the second addition of hydrogen peroxide, which was made later

than with iron sulphate. After considering these results, D-gluconate was disregarded for the subsequent experimental conditions as it decreased the efficiency of the process.

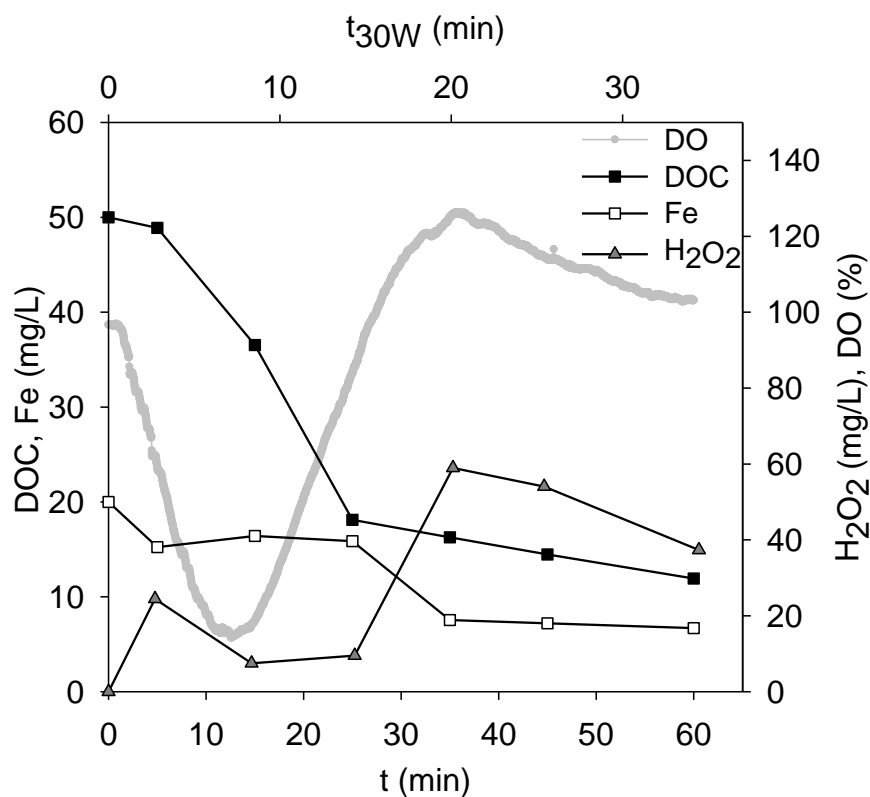


**Figure 3.4.** Acetaminophen degradation in the CPC pilot plant applying continuous H<sub>2</sub>O<sub>2</sub> addition and using iron sulphate as the iron source at initial neutral pH (50 mg/L acetaminophen DOC, 20 mg/L Fe<sup>2+</sup>).

Dissolved iron concentration during this experiment was higher than in the other experiments with the same iron source (Figure 3.4). However, there was still precipitation and pH dropped as previously indicated. This behavior results from the fact that carboxylic acids and oxamate generated as acetaminophen by-products, remained longer in solution because the photo-Fenton global reaction rate (i.e. mineralization rate) was slower - therefore iron can be dissolved over more time. The pH drop also had to do with iron hydrolysis effect. This is further explained in Section 3.1.2. Regarding H<sub>2</sub>O<sub>2</sub> concentration, its consumption was slower but more efficient regarding mineralization than with any other condition tried (Figure 3.4). This statement is also supported by the DO concentration registered, which was always lower than 130% throughout the test. The DO profile also supports the aforementioned reduction in the reaction rate.

With regard to mineralization, a final value of 78% was accomplished. 50% mineralization was achieved at 11 min in  $t_{30W}$ , which was slower in comparison to the two-addition experiments with said source of iron, even though they were similar; this accorded with the reduction in the photo-Fenton global reaction rate. However, even if  $H_2O_2$  consumption was lower and final mineralization was slightly higher for continuous addition, two  $H_2O_2$  additions were considered the best of all the conditions studied since continuous addition took longer to achieve the same mineralization. An alternative could be increasing total  $H_2O_2$  concentration during continuous addition but it would involve a higher consumption, which is the main advantage of this operating mode. Consequently, two additions would be a more advisable strategy.

### Treatment of secondary effluent enriched with acetaminophen

The experience gained was applied to a more complex matrix. A secondary treatment effluent from the WWTP “El Bobar” in Almería was selected as an example of water containing significant ionic strength as well as other natural components which could affect the reaction rate. The DOC of the effluent was 10 mg/L and enriched with 50 mg/L DOC of acetaminophen. The concentrations of the main ions present in the effluent were: 225 mg/L  $HCO_3^-$ , 210 mg/L  $Cl^-$ , 13 mg/L  $PO_4^{3-}$  and 46 mg/L  $SO_4^{2-}$ . Nitrate concentration was negligible. The molar ratio  $[H_2O_2]/[DOC]=1.65$  was also applied to calculate the total amount of hydrogen peroxide needed. Phosphates were completely precipitated in order to avoid iron precipitation as  $Fe(PO_4)$ .

On the other hand, the presence of bicarbonate can decrease the process rate since  $OH^\bullet$  scavenging occurs, as shown in Equation 1.36:



This reaction yields carbonate radicals, but these species are less oxidant and reactive than  $HO^\bullet$  (Buxton et al., 1988). In addition, the presence of bicarbonates causes a buffer effect that prevents pH decrease and thus promotes iron precipitation. Consequently, carbonates were mostly removed with sulfuric acid and the pH was adjusted to 7, so that their effect as buffer and scavengers of hydroxyl radicals was avoided.

During this test, iron precipitation was faster than in the previous experiments using iron sulphate (Figure 3.5) as pH decreased slower than in the other experiments with deionised water but finally pH also dropped to three. Mineralization was also

slower mainly due to the presence of  $\text{Cl}^-$  - since it acts as a radical scavenger yielding chlorine species which are less oxidant than  $\text{HO}^\cdot$  (Kiwi et al., 2010).

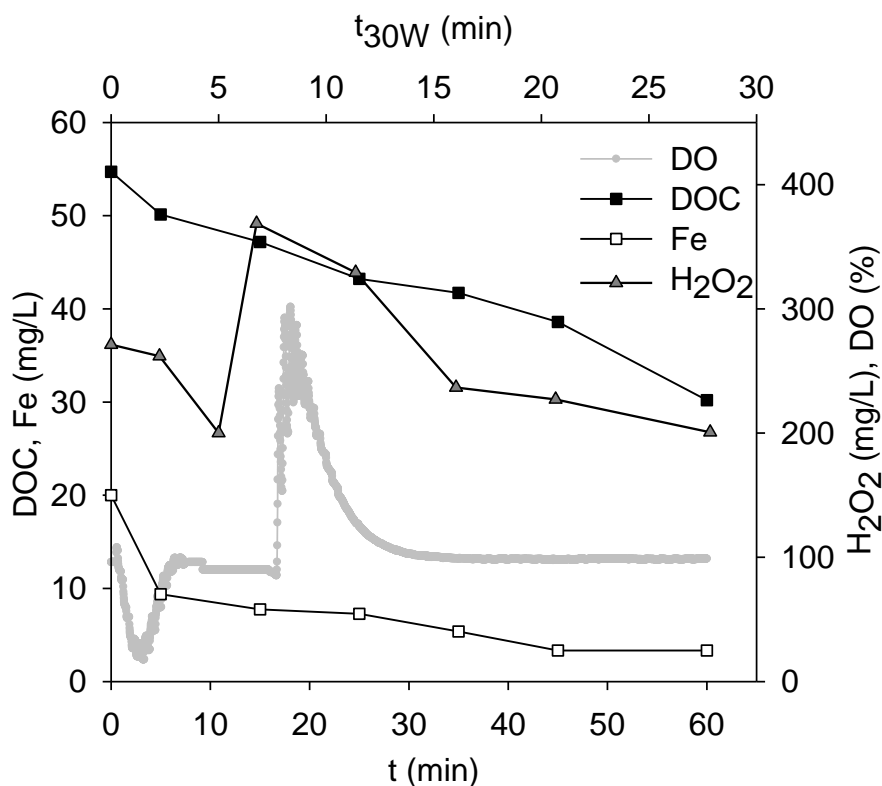


**Figure 3.5.** Results after applying the photo-Fenton process to real wastewater effluent enriched with acetaminophen and using two  $\text{H}_2\text{O}_2$  additions at initial neutral pH (50 mg/L acetaminophen DOC, 20 mg/L  $\text{Fe}^{2+}$ ).

The DO profile registered the Dorfmann mechanism, as illustrated by the two-addition tests in deionised water, but in this case slower. However, after the first maximum, the decrease in DO was less pronounced, meaning that the process was somehow slower and thus agreeing with the negative effect of some ions, as previously explained. Consequently, the second addition was made later than when deionised water was used. The decrease in the process rate was also reflected by slower mineralization. Despite all of this, final mineralization was 45%.

From the different operational conditions studied, it was concluded that the ratio between organic carbon, supplied by an iron complex, and the pollutant, is especially important; and that DOC due to the complex should not be significant with respect to that of the pollutant.

It could also be drawn that it is possible to operate the solar photo-Fenton process at natural pH adding iron salt. On the one hand, organic iron complexes between iron and degradation contaminant by-products can be formed, which could increase process efficiency when initiated at neutral pH. On the other hand, the cost associated to use an iron chelate or complex would be avoided, as well as the need to remove it later from water. Additionally, it is possible that complexes between iron and degradation contaminant by-products could be formed, which could increase process efficiency when initiated at neutral pH.

With regard to H<sub>2</sub>O<sub>2</sub> dosage, results showed that, although continuous addition reduced hydrogen peroxide consumption, the process rate was slower than for sequential additions. It is important to remark that the inorganic composition of wastewater seriously affects not only degradation kinetics, but also H<sub>2</sub>O<sub>2</sub> dosage sequence, being necessary an optimization in a case by case basis.

### 3.1.2 Iron dosage strategy

From the results with the different iron sources, there was interest in further studying the dosage of iron salt as an operating strategy. Also, many studies have been focused on the source of iron itself, but not many have been dedicated to iron dosage in the photo-Fenton process for permitting operation without setting pH at 2.8 by acid addition

The model pollutant was changed to validate the conclusions drawn in Section 3.1.1 and to corroborate that they were not valid only for acetaminophen. In this case, a mixture of five commercial pesticides was used: Commercial formulations of Vydate® (10%, w/v, oxamyl), Metomur® (20%, w/v, methomyl), Couraze® (20%, w/v, imidacloprid), Perfekthion® (40%, w/v, dimethoate) and Scala® (40%, w/v, pyrimethanil) (Figure 3.6). The selected pesticide formulations are commonly employed in Mediterranean intensive agriculture and present toxicity and a recalcitrant nature (Ballesteros-Martín et al., 2009). They were used in a concentration of 50 mg DOC/L, corresponding to 10 mg/L of DOC from each pesticide. The pH was always adjusted to 7. A concentration of 650 mg/L H<sub>2</sub>O<sub>2</sub> (~20 mM) was used so that it was in excess and didn't limit the reaction.

The goal of this work was to study different iron dosage combinations to mineralize the pesticides. The impact of iron concentration and dosage time on the process was analysed. Deionised water was initially used as matrix and then the



results were corroborated in real wastewater. All the experiments were carried out in the CPC.

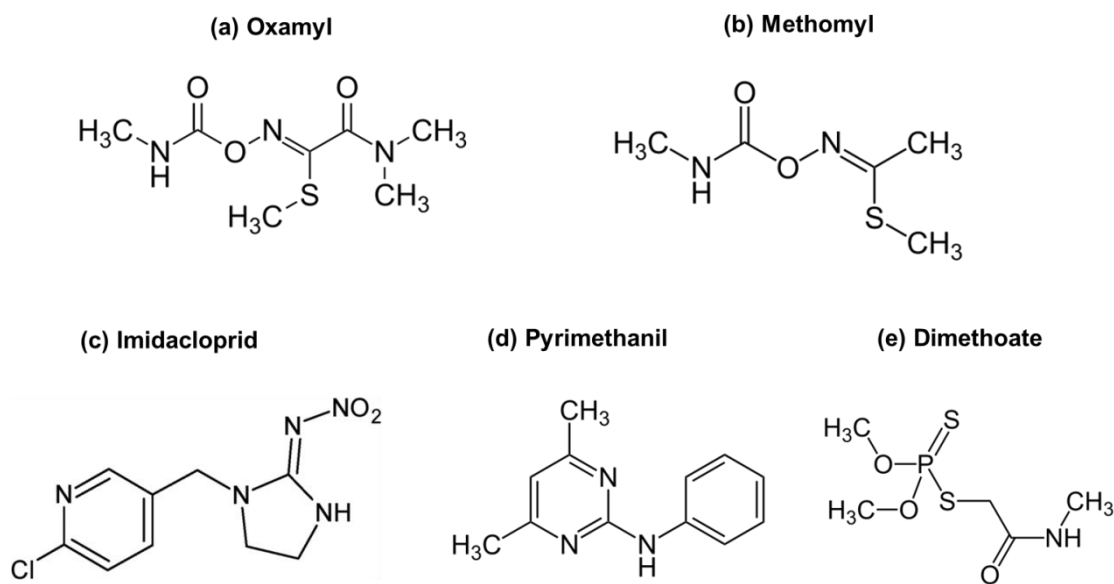


**Figure 3.6.** Chemical structure of oxamyl, methomyl, imidacloprid, pyrimethanil and dimethoate.

### a) The effect of iron concentration and addition time

Different iron dosages were made as ferrous iron salt ( $\text{FeSO}_4 \cdot 7\text{H}_2\text{O}$ ) solutions so that total iron dose per addition in the system would be 5, 10 and/or 20 mg/L  $\text{Fe}^{2+}$ . The additions were made using a peristaltic pump for 30 seconds at 3.5 mL/min. This addition time corresponded to the pilot plant recirculation time, which permitted a rapid homogeneous mixing. At least 5 min (reactor mixing time) passed between additions. The iron additions were made following the scheduled sequences and concentration combinations in Table 3.2, including a reference test at pH 2.8 using a single 20 mg  $\text{Fe}^{2+}$ /L addition. The effect of the dark Fenton reaction in these conditions was studied as well.

Some of the results are presented in Figure 3.7, including the dark Fenton. For the reference at acidic pH (Figure 3.7a) the pesticide active ingredients were almost completely eliminated after 45 min in the dark. Nonetheless, DOC removal barely occurred in the absence of light after 1h pointing out that pesticide molecules were attacked by hydroxyl radicals, but no mineralization took place. In concordance, hydrogen peroxide consumption was slight. These results are in agreement with other research using this pesticide mixture and concentration (Zapata et al., 2009).

**Table 3.2.** Operating conditions and results obtained after 60 min for the solar photo-Fenton process applied to demineralised and real wastewater.

Water matrix	Fe additions (mg/L)	Time of addition (min)	Fe <sub>mean</sub> (mg/L)	pH <sub>0</sub>	Mineralization for pesticide removal (%)	Final mineralization (%)
Deionised	20	0	12.4	2.8	20	52
Deionised	20	0	4.6	7	-	3
Deionised	5-5-5-5	0, 5, 10, 15	4.0	7	-	8
Deionised	10-10-10-10	0, 5, 10, 15	8.4	7	35	52
Deionised	20-20-20-20	0, 5, 10, 15	26.8	7	20	62
Deionised	20-20-10-10	0, 10, 20, 30	10.3	7	44	57
Deionised	20-20-10-10-10	0, 5, 15, 25, 35	19.2	7	20	60
Wastewater type I	20	0	15.8	2.8	25	42
Wastewater type I	20-20-10-10-10	0, 5, 15, 25, 35	12.5	7	28	40
Wastewater type I	20-20-10-10-10	0, 5, 15, 25, 35	16.8	7	27	44
Wastewater type II	20-20-10-10-10	0, 5, 15, 25, 35	13.5	7	24	49

During the photo-Fenton process (Figure 3.7a), progressive iron precipitation was observed as a result of the presence of thiophosphate in the active ingredients (namely, dimethoate). The DOC curve presented an initial shoulder indicating the pesticide mixture required many oxidation steps before mineralization (the average oxidation state was -0.27). Nevertheless, oxidation of all active ingredients took place from the beginning and complete removal was obtained at 20% mineralization (Table 3.2), corresponding to 7.5 min<sub>30W</sub>, which was over six times faster than in the Fenton process.

A first-order kinetic was obtained for the active ingredients removal in the photo-Fenton process (Figure 3.7a). The overall kinetic constant for the pesticides was 0.315

$\text{min}^{-1}_{30W}$ , being methomyl the pesticide which was harder to oxidize followed by imidacloprid, dimethoate, pyrimethanil and oxamyl.

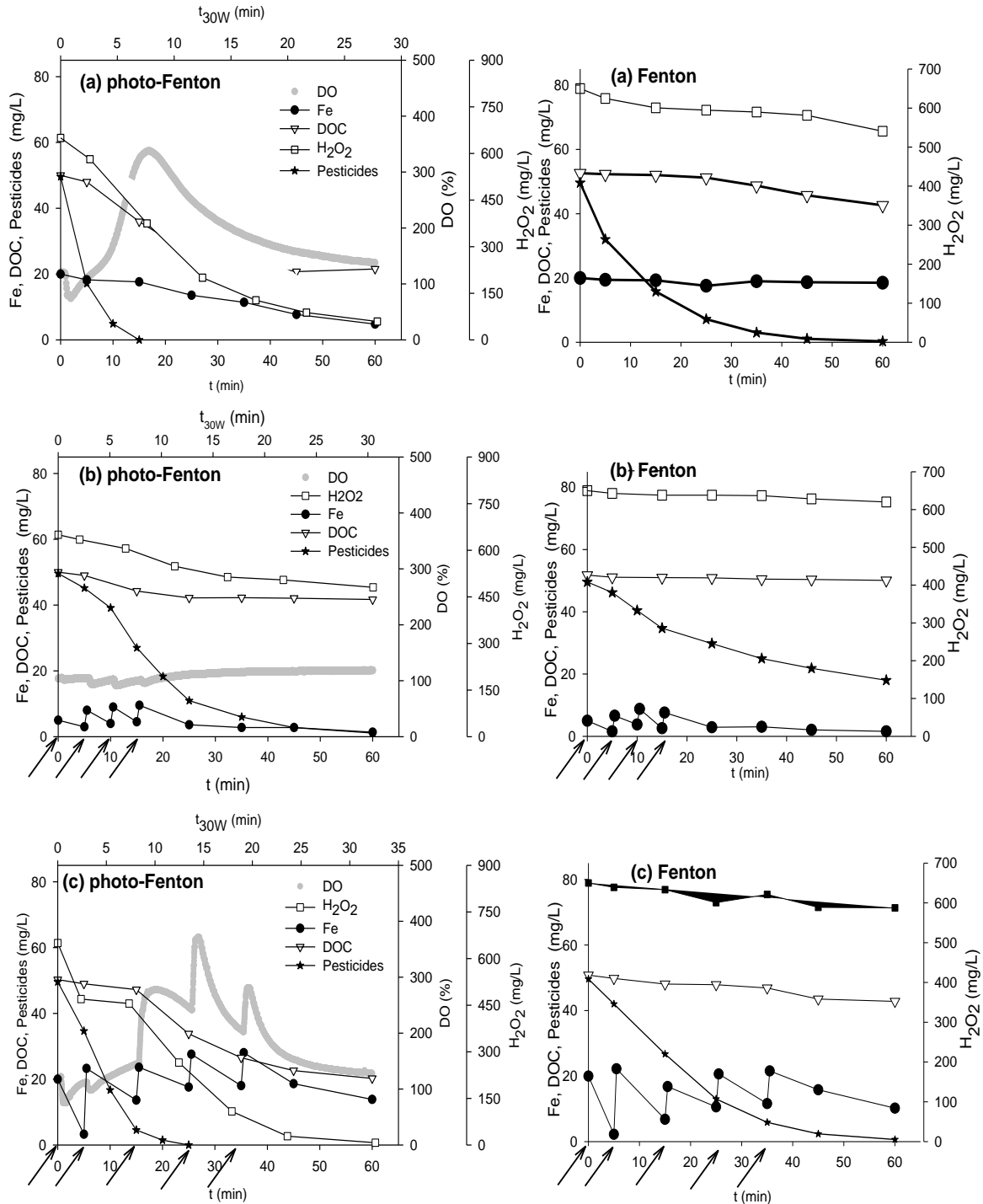


**Figure 3.7.** Results obtained after 1h of solar photo-Fenton and dark Fenton with 50 mg DOC/L and 650 mg  $\text{H}_2\text{O}_2$ /L; (a) at pH 2.8 with one initial iron addition of 20 mg Fe/L; (b) at initial neutral pH with four additions of 5 mg Fe/L and (c) five additions of 20-20-10-10-10 mg Fe/L. The arrows point out the time of addition.

In addition to this, there was a rapid mineralization rate in the linear zone of the DOC curve ( $\sim 1.9$  mg DOC/L $\cdot$ min<sub>30W</sub>) despite the initial shoulder. A 52% mineralization level was achieved (Table 3.2), corresponding to values obtained in other works (Ballesteros-Martín et al., 2009).

Additionally, hydrogen peroxide was quickly consumed at a rate of  $\sim 32$  mg H<sub>2</sub>O<sub>2</sub>/L $\cdot$ min<sub>30W</sub> until the level of dissolved iron was rather low, thus stopping the reaction. Dissolved oxygen (DO) concentration was also registered as the percentage of saturation with air, allowing the monitoring of the reaction since in the photo-Fenton process some reactions can be oxygen-generating and others, oxygen-consuming (Prieto Rodríguez et al., 2011; Santos-Juanes et al., 2011). An initial decrease in the DO concentration was observed. This was due to the Dorfman mechanism (Dorfmann et al., 1962; Kunai et al., 1982), where oxygen-consuming reactions took place associated with the oxidation of aromatic rings (Equations 1.19 and 1.20).



In this instance, the aromatic rings were present in the pesticides' active ingredients. Also, as the pesticide mixture came from commercial formulations, other aromatic compounds could have been present. After the ring-attacking reactions, DO concentration rose to 350 % showing that non-efficient reactions were taking place since oxygen-generating reactions occur in the presence of hydrogen peroxide excess (Santos-Juanes et al., 2011).

Taking into account the results obtained in the reference experiment (Figure 3.7a), the same conditions were used again applying the solar photo-Fenton and dark Fenton processes, but at initial neutral pH (Figure 3.7b). Iron precipitation prevented high mineralization and the active ingredients were not completely oxidized (Table 3.2). To keep a higher dissolved iron concentration, iron additions were proposed as a strategy, maintaining a certain concentration during the process. In Table 3.2, the different iron dosages and a summary of the results after applying the photo-Fenton process to water polluted with the pesticide mixture are presented.

A dosage of four additions of 5 mg Fe<sup>2+</sup>/L was tested (Figure 3.7b) to keep the total amount of added iron to 20 mg/L. In the dark Fenton process, the slower regeneration of Fe<sup>2+</sup> in absence of light resulted in insignificant hydrogen peroxide consumption. Thus, less hydroxyl radicals were yielded and DOC concentration did not change during the process. Nevertheless, the small amounts of radicals generated

were enough to partially oxidize the active ingredients, but more slowly and to a lesser extent than in the photo-Fenton process.

During the iron additions in the solar photo-Fenton process,  $\text{H}_2\text{O}_2$  was consumed but at a slower rate than the reference ( $\sim 9 \text{ mg H}_2\text{O}_2/\text{L}\cdot\text{min}_{30\text{W}}$ ). The DO curve also showed a different response during the additions that will be further discussed later. Nevertheless, when iron additions stopped (15 min), Fe concentration remained under 5 mg/L. The low concentration of iron during the first 15 min resulted in low mineralization (8%) and the active ingredients were not completely eliminated after 60 min of experimentation. Consequently, the overall first-order kinetic constant for the active ingredients removal (Figure 3.7b) was significantly lower than that obtained at pH 2.8:  $0.066 \text{ min}^{-1}_{30\text{W}}$ . The persistence kept the trend showed at acidic pH though (methomyl<imidacloprid<dimethoate<pyrimethanil<oxamyl).

Different sequences were performed: varying iron concentration in the system per addition as well as the time of addition. Thus, the mean concentration of dissolved iron also changed. The time of addition was 5 or 10 min (one or two mixing times in the pilot plant, respectively) and iron concentration per addition was either 10 or 20 mg Fe/L (Table 3.2). The first amount of iron reacted with water molecules in a hydrolysis reaction (Equation 1.37 from the Introduction Section), forming iron hydroxides that precipitated. Hence, iron was no longer available to carry out the photo-Fenton reaction.



A consequence of iron hydrolysis is the increase in the concentration of protons, which are responsible for the drop in pH to three. As this effect always occurs at neutral pH, there was a drop in pH in all conditions assayed from the first addition of iron. As a result, if the first addition was 10 mg Fe/L, iron precipitated to a great extent, and almost instantaneously, due to the hydrolysis reaction. There was almost no iron left to act as a catalyst for the photo-Fenton process and part of the iron of the second addition suffered hydrolysis as well. Consequently, the initial mineralization rate was slowed down. However, when the first addition was 20 mg Fe/L, although iron precipitated as well, there was more dissolved Fe to start the photocatalytic reactions. Such is the case represented in Figure 3.7c, where the first iron addition was 20 mg Fe/L. Fast hydrogen peroxide consumption and active ingredient removal occurred from the beginning, and together with the DO response, showed that the process was active from the first addition onwards.

The time of addition was also critical in the first stages of the process. As iron precipitation in the first addition was always substantial, as previously explained, if the second dose was added after 10 min, the lack of catalyst in the process would be longer. Therefore, the results obtained suggested that the first iron additions had to be made every 5 min instead of 10 min. Variations in the additions led to different mean iron concentrations (Table 3.2) and these were not equally distributed throughout the tests.

As a consequence of the above explanation, it was observed that the first iron addition was essential and the concentration used in said addition greatly affected the mineralization rate. Nevertheless, at least 52% mineralization was achieved when iron additions were used (excepting the sequence 5-5-5-5 mg Fe/L), which is also in agreement with the results obtained in the reference and in similar research (Ballesteros-Martin et al., 2009), as previously discussed. Regarding the active ingredients, mineralization and pesticide removal presented quite different tendencies. While the DOC curve was non-linear, a first-order kinetic was observed for the overall active ingredients concentration (Figure 3.7c) for all operating conditions, as it was for the reference. However, only for the iron sequences 20-20-20-20 and 20-20-10-10-10 mg Fe/L, and for the reference, was a 20% mineralization level needed for complete removal; while the sequences 10-10-10-10 and 20-20-10-10 mg Fe/L required higher levels (35% and 44%, respectively) due to the different average iron concentrations and availability that these dosages led to.

The response of all variables are similar in tendency to the results obtained for the iron sequence 20-20-10-10-10 mg Fe/L (Figure 3.7c) and can be explained over one of the tests. In this case, the first two iron additions were made at intervals of 5 minutes for the reasons mentioned above. In the dark Fenton reaction (Figure 3.7c), DOC removal and hydrogen peroxide consumption were negligible, following the trend observed for the previous operating conditions. Pesticide active ingredients degradation occurred, although taking four times the reaction time needed for complete removal in the presence of 30 W/m<sup>2</sup> of UV light. Average iron concentration during the process was also lower than in the solar photo-Fenton experimentation.

During the photo-Fenton process, after the first addition of 20 mg Fe/L, there was substantial precipitation, but the addition of the second dose after 5 min avoided the process slowing down. This fact is also reflected by H<sub>2</sub>O<sub>2</sub> consumption, as described above. After this, the remaining additions were made every two mixing times (10 minutes), allowing an overall homogeneous iron concentration of ~ 20 mg Fe/L.

Regarding DOC concentration, a more extended shoulder appeared than in the reference (pH 2.8) due to iron precipitation by hydrolysis in the first dosage. Nevertheless, the subsequent iron additions allowed a mineralization rate in the linear zone of  $\sim 2$  mg DOC/L $\cdot$ min<sub>30W</sub>, analogous to the value obtained for the reference. Although it must be taken into account that the linear zone for the reference starts before that with iron additions, working at sequential additions of 20-20-10-10-10 mg Fe/L allows to obtain almost 60% mineralization. Although pesticides removal was slower than the reference at pH 2.8, complete removal was achieved at 20% mineralization as well. The overall first-order kinetic constant was  $0.19 \text{ min}^{-1}_{30W}$ . With respect to hydrogen peroxide, the consumption was rapid and linear from the beginning until it was totally consumed. This rapid consumption from the start supports the idea that initial iron additions should be made at short intervals so that iron can react properly before precipitating. The consumption rate was  $\sim 30$  mg H<sub>2</sub>O<sub>2</sub>/L $\cdot$ min<sub>30W</sub>, again like that of the reference ( $\sim 32$  mg/L $\cdot$ min<sub>30W</sub>).

Concerning DO concentration, there was a first minimum due to the Dorfman mechanism, as occurred under the reference conditions. However, as the iron added in the first dosage mostly precipitated, the oxidation of aromatic rings associated to this mechanism was not completed. So, when the second iron addition was made, there was a second DO decrease, indicating that a new set of aromatic ring attacks were produced. After that, the DO concentration increased, showing that the Dorfman mechanism was finished and that other oxygen-generating reactions predominated. From then on, each iron addition was represented by a maximum in DO concentration. At the moment of each addition, a Fenton effect was observed due to the rapid reaction of Fe<sup>2+</sup> with H<sub>2</sub>O<sub>2</sub> (the Fenton reaction), swiftly generating hydroxyl radicals. Some of these radicals reacted with organic matter, but they reacted with themselves as well, or with H<sub>2</sub>O<sub>2</sub> in inefficient reactions that generated high DO concentrations (Prieto et al., 2011).

The DO curve tendency was similar for all considered iron dosages and even the mineralization level was comparable between operating conditions (Table 3.2). However, the fact that the iron sequences allowed a different average iron concentration for each operating condition resulted in different mineralization levels for complete pesticide removal as well. In fact, only those sequences with the first addition of 20 mg Fe/L and the second addition made after 5 min permitted complete active ingredient removal for the lowest mineralization value (20%), apart from the reference. In addition to this, although the mineralization levels achieved in all cases were alike (except when four 5 mg Fe/L additions were used), the rates of H<sub>2</sub>O<sub>2</sub> consumption and

mineralization in the linear zone were not similar. This was because the iron availability, at any given moment, was different depending on the iron sequence used. Since there was enough UV radiation in all cases (a mean of  $20 \text{ W/m}^2$ ) and an excess of  $\text{H}_2\text{O}_2$ , the process rate was limited by iron or DOC. On the one hand, if the DOC concentration was too low with respect to dissolved iron concentration, the formation of iron complexes with organic matter could be limited. On the other hand, if iron dosages resulted in a prolonged period without iron due to its precipitation, there would be a lack of catalyst to carry out the photo-Fenton process. To evaluate the impact of a limitation of iron on the mineralization rate, said rate ( $r$ , in  $\text{mg DOC/L} \cdot \text{min}_{30\text{W}}$ ) was calculated in the linear zone using the normalized illuminated time ( $t_{30\text{W}}$ ). The dependence of the mineralization rate on average dissolved iron (calculated in the same period as the maximum mineralization rate) is shown in Figure 3.8.

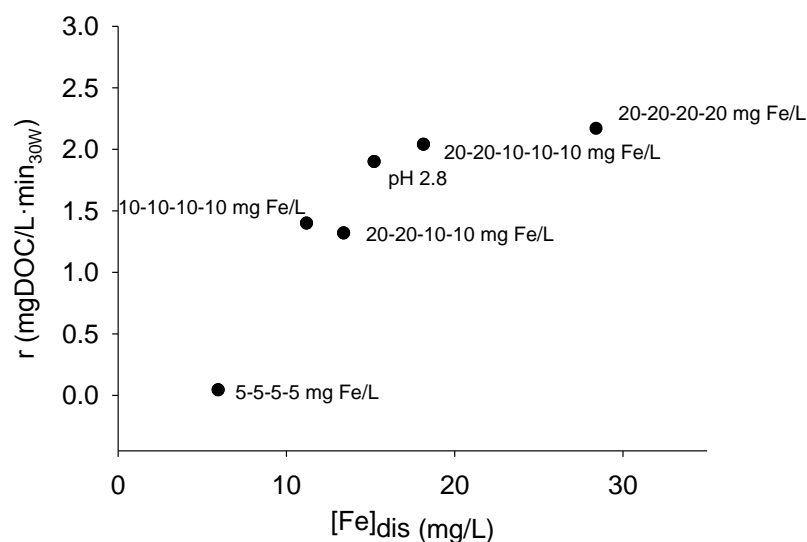


**Figure 3.8.** Variation in the maximum DOC removal rate, calculated using illuminated time, with the mean dissolved iron concentration in the period of maximum mineralization rate.

It was observed that the maximum mineralization rate increased linearly with dissolved iron concentration until saturation; this means the more iron available in the system, the more hydroxyl radicals were generated under these conditions - provided there was enough hydrogen peroxide. However, a saturation effect was detected so that when dissolved iron was above  $\sim 20 \text{ mg/L}$ , there was no tangible improvement in the maximum mineralization rate. As a result, the addition sequence 20-20-10-10-10 mg Fe/L allowed the highest DOC mineralization rate in the linear zone with the least dissolved iron from all experimental conditions assayed at initial neutral pH. This



circumstance, together with the fact that all active ingredients were removed at a mineralization level of 20%, along with the high mineralization level obtained, resulted in this operational condition being selected to evaluate the applicability of iron additions in the solar photo-Fenton process with real wastewater.

### b) Applicability to real wastewater

To check the proposed strategy, experimentation was carried out at natural pH with the iron dosage 20-20-10-10-10 mg Fe/L (0, 5, 15, 25, 35 min) with two real wastewater sources (Table 3.3). Type I was collected on different days from the UWWTP in Almería. Type II was collected from the UWWTP in the in-campus nursery of the University of Almería. A reference was also carried out at pH 2.8 (20 mg Fe/L) with wastewater type I and in that case, phosphates were precipitated with ferric iron.

**Table 3.3.** Real wastewater characterization

	Wastewater type I	Wastewater type II
Variable	Concentration (mg/L)	
DOC	60-66	55
Fluoride	0.02	<DL
Chloride	235	211
Nitrite	0.2	<DL
Nitrate	11.3	5.70
Phosphate	6.4	13.1
Sulphate	113	45.6
Bicarbonate	205-400	215

Wastewater Type I was taken in different days, obtaining the similar anion and DOC concentrations, but different bicarbonate concentration (Table 3.3). This did not affect the reference test at pH 2.8 since bicarbonates were neutralized and all bicarbonates are transformed into CO<sub>2</sub> due to the carbonate equilibrium, but it allowed studying the influence of bicarbonates at natural pH with the selected iron dosage. However, when pH is adjusted around 7, different residual amounts of bicarbonates remain. As a result, bicarbonate concentration at the beginning of the experiments was different for each assay when working at initial neutral pH. Next, the same operational conditions (at initial neutral pH) were used for solar photo-Fenton applied to

wastewater type II. The wastewaters were enriched with 50 mg DOC/L of the pesticide mixture and hydrogen peroxide was added at the beginning (650 mg H<sub>2</sub>O<sub>2</sub> /L).

In Figure 3.9, the results obtained for the two types of wastewater sources are illustrated. During the process at pH 2.8 (Figure 3.9a) the shoulder shown in the DOC curve, characteristic of this pesticide mixture, was more pronounced than in demineralized water as a consequence of the matrix complexity. This meant the global reaction rate was lower, which was also corroborated by the consumption of hydrogen peroxide: the reactant was consumed at a rate of ~9 mg/L·min<sub>30W</sub> while in demineralized water, this value was 3.5 times higher. The DO concentration also reflected that the process was slower. The Dorfman mechanism was registered, but, after the oxygen-consuming reactions ended, the DO response was slow as well until the last part of the experiment. However, despite the decrease in the process rate, final mineralization was 42%.

Solar photo-Fenton at initial neutral pH with iron additions was also applied to the same wastewater source. However, phosphates were not previously removed; the pH was adjusted to 7 and a residual amount of bicarbonates remained: 102 mg/L (Figure 3.9b) and 51 mg/L (Figure 3.9c). Iron added in the first dosages reacted with the remaining bicarbonates and phosphates, precipitating quickly. At the same time, iron hydrolysis occurred, causing pH to drop to three. Therefore, the iron mostly reacted at the beginning with bicarbonates, phosphates and in protonation reactions. Consequently, when the initial bicarbonate concentration was higher (Figure 3.9c), more iron was needed at the beginning.

The DOC curve showed three defined stages. There was an initial decrease in DOC concentration due to the mineralization of the more easily-oxidable organic matter present in the matrix. This stage is less pronounced in the reference test as the process rate at the beginning is faster. After this, a shoulder was shown, reflecting the oxidation of the pesticides' active ingredients, but not mineralization. Finally, an organic matter mineralization stage took place that changed linearly with time.

Regarding H<sub>2</sub>O<sub>2</sub>, the consumption rate was ~16 mg H<sub>2</sub>O<sub>2</sub>/L·min<sub>30W</sub> in both cases, which is approximately half the value obtained in demineralized water, but it is higher than at pH 2.8. The fact that the consumption rate is higher than the reference is due to the iron additions. Each time iron was added to the system, the Fenton reaction took place, consuming H<sub>2</sub>O<sub>2</sub> and generating hydroxyl radicals. As a result, final mineralization in both tests was similar to the reference, approximately 40% and 44% (Table 3.2).

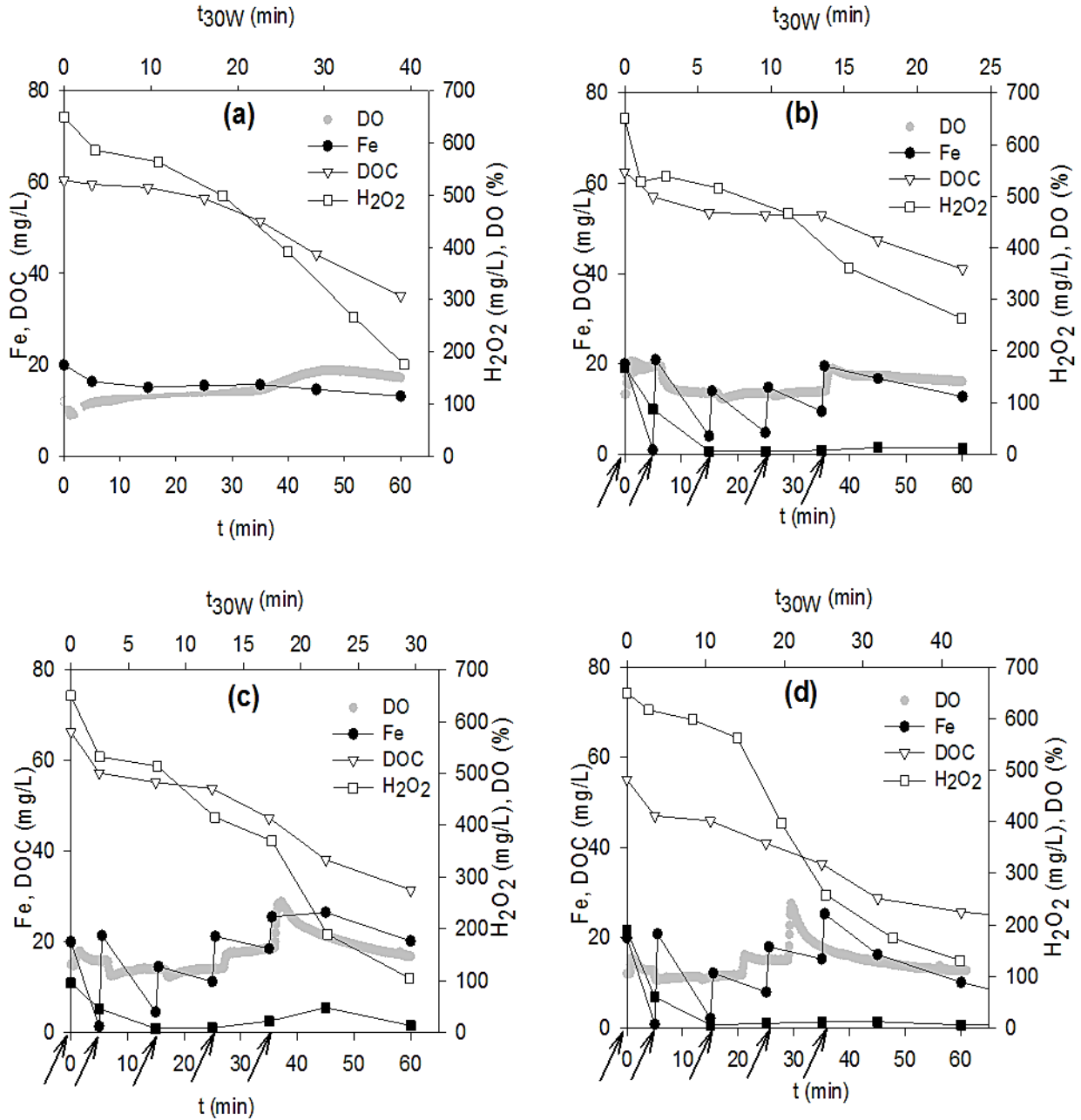


**Figure 3.9.** Treatment of real wastewater with solar photo-Fenton at (a) pH 2.8 with one iron addition of 20 mg/L using wastewater type I; (b, c) and at initial neutral pH with iron additions 20-20-10-10-10 mg/L using wastewater type I; (d) and type II.

With respect to DO concentration, more decreases corresponding to the Dorfman mechanism were observed than with demineralized water. In this way, the presence of carbonates and phosphates slowed down the process, so more iron was needed to complete the reactions associated with this mechanism. Nevertheless, the shape of the DO curves was quite similar and after the Dorfman phenomenon the oxygen-generating reactions predominated, increasing the DO concentration.

The effect of the matrix was also tested using the same operational conditions with another wastewater source (type II). DOC concentration was ~ 5 mg/L. In this case, the residual amount of bicarbonates was 112 mg/L after adjusting pH to 7. The results are represented in Figure 3.9d. DO concentration showed the same tendency as described in previous experiments and the DOC curve showed the same three stages: predominantly rapid oxidation of easily-oxidable matter followed by a plateau representing the initial oxidation of active ingredients and, finally, pesticide mineralization. The mineralization value reached was 49%, slightly higher than with the other wastewater source. However, it must also be considered that the UV radiation received during this test was higher (an average of 25 W/m<sup>2</sup>) and after 30 min of normalized illuminated time, the mineralization achieved was approximately the same in wastewater type I for the same illuminated time (~ 40%) (Figure 3.9.c). This happened despite the fact that the phosphate concentration was higher (twice the value found for the other wastewater source) in this wastewater, so more iron was needed. In this way, the hydrogen peroxide consumption rate was also slower (~6 mg H<sub>2</sub>O<sub>2</sub>/L·min<sub>30W</sub>) since more iron precipitated at the beginning due to the phosphate concentration. Nevertheless, final results for a fixed normalized illuminated time were similar for both types of wastewater. Consequently, the matrix effect was negligible between both wastewaters and the outcomes were analogous. Each iron addition created the Fenton effect earlier described, driving the Fenton reaction that quickly generated hydroxyl radicals. This effect proved more important than the difference in iron or DOC concentrations.

Regarding pesticide removal, a first-order kinetic was observed for overall active ingredient concentration under all operating conditions, as previously described. When complete pesticides removal was achieved, it was found that mineralization reached 24-28%. This indicates that at that point, more than 70% of the initial DOC is still present in the system, and the initial pesticides have been just transformed into an array of reaction byproducts. However, in demineralized water, the mineralization value was 20%, thus the wastewater initial DOC must be added to the pesticide concentration so initial DOC is higher. Consequently, the mineralization level for complete active ingredient removal was also somewhat greater.

The results demonstrated that by adding iron at different steps, it is possible to operate photo-Fenton at initial neutral pH without substantially decreasing the reaction rate compared to photo-Fenton at pH 2.8. Nonetheless, iron consumption would be greater than at pH 2.8 and it should be taken into account that pH could decrease due to iron hydrolysis.

Dosing iron allows different average iron concentrations in the system, thus obtaining different DOC removal and H<sub>2</sub>O<sub>2</sub> consumption rates. Active ingredients can even be removed with dark Fenton dosing iron at pH 7, but at a much slower rate and obtaining negligible mineralization.

Therefore, the protocol for deciding the adequate sequence of iron dosing should be carefully studied on a case by case basis, seeing as not only reaction rate but also iron precipitation is seriously affected by water quality, the initial concentration of contaminants and the final objective (i.e. the elimination of certain compounds or the percentage of mineralization) of the treatment.

### 3.2 Strategies to remove micropollutants

The development of highly sensitive analytical techniques has allowed accurate pollutant detection in urban and industrial wastewaters. Pesticides, drugs, endocrine disruptors and other common substances such as caffeine or nicotine can be easily detected in water effluents (Calderón-Preciado et al., 2011; Ratola et al., 2012). They are the so-called “micropollutants” due to the low concentrations in which they are found (nanograms or micrograms per liter). For the study of operating strategies for micropollutant removal, three pesticides were chosen: acetamiprid (ACTM), thiabendazole (TBZ) and imazalil (IMZ) (Figure 3.10). They are common biocides used in citrus crops (García-Reyes et al., 2008; Fitzgerald and Jay, 2011; McKay et al., 2012).

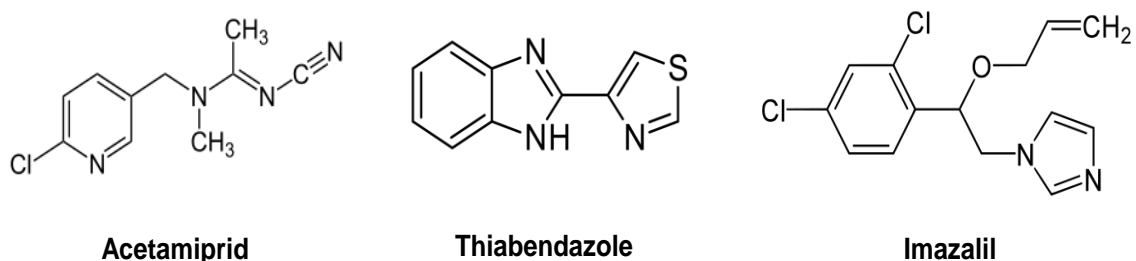


**Figure 3.10.** Acetamiprid, thiabendazole and imazalil chemical structure.

#### 3.2.1 Iron dosage for micropollutant removal

In the Section 3.1.2 it was concluded that iron dosage was effective in the removal of persistent pollutants at medium concentration range. Based on the

experience gained, the same strategy was proposed for micropollutants removal. This time the effect of bicarbonates and the addition mode (sequential or continuous) was evaluated.

On the other hand, wastewater treatments are necessary processes due to the environmental benefits generated by them, but from which direct economic profits are not obtained. Therefore, the decision of implementing a particular treatment or another greatly depends on the costs associated with it. One of the variables which affects the costs of photo-Fenton the most is the reaction time, since it seriously affects the size of the treatment plant and operational costs (Sánchez Pérez et al., 2013). Therefore, iron dosage was applied with the aim of reducing treatment time.

For this study, the mixture formed by ACTM, TBZ and IMZ, 100 µg/L each, was used. The water matrix was the simulated secondary effluent (see Section 2.2) for comparison purposes. Initially, the effect of bicarbonate concentration was studied at laboratory scale in the solar box. Then, accumulated iron, supply times and addition mode (sequential or continuous) were studied at pilot plant scale in the flat-reflector pilot plant.

#### **a) Impact of bicarbonate concentration on pollutant degradation with iron additions**

A 1-L-stirred tank reactor was used and placed inside the solar box and UV radiation was set at 30 W/m<sup>2</sup> except when indicated. To study the effect of bicarbonates, assays were done with 70 mg/L HCO<sub>3</sub><sup>-</sup> and without bicarbonates. Iron was added sequentially every five minutes, which is the mixing time in the flat-reflector pilot plant where results were scaled up. The different iron addition combinations are presented in Table 3.4. The hydrogen peroxide concentration added was 50 mg/L (~1.5 mM) for the experimentation with carbonates and 75 mg/L (~2.2 mM) for the assays without them. The aim was to work with hydrogen peroxide excess to focus the research on the behaviour of the different iron dosages.

So as to check possible pollutant degradation not attributable to photo-Fenton, some preliminary blank assays were carried out including degradation by hydrogen peroxide in the dark and photolysis with hydrogen peroxide. No remarkable degradation was observed for any of the three contaminants. Likewise, direct photolysis and hydrolysis were negligible for the studied pollutants, coinciding with the

information provided by the Environmental Protection Agency (EPA, 2002a; EPA, 2002b; EPA, 2002c).

**Table 3.4.** Acetamiprid, thiabendazole and imazalil degradation and hydrogen peroxide consumption at the end of the experiment (45 min).

Fe additions (mg/L) <sup>a</sup>	Results just after the additions				Results after 45 min			
	ACTM (%)	TBZ (%)	IMZ (%)	H <sub>2</sub> O <sub>2</sub> (mg/L)	ACTM (%)	TBZ (%)	IMZ (%)	H <sub>2</sub> O <sub>2</sub> (mg/L)
<b>With bicarbonates (70 mg/L) – 50 mg/L of H<sub>2</sub>O<sub>2</sub></b>								
20x2	10	43	41	22	10	44	46	32
20x3	40	83	<LOD	30	47	89	<LOD	35
20x3 (14W/m <sup>2</sup> )	44	86	<LOD	31	54	94	<LOD	35
20x3 (Fenton)	32	81	<LOD	28	47	94	<LOD	34
<b>Without bicarbonates – 75 mg/L of H<sub>2</sub>O<sub>2</sub></b>								
5x4	51	95	<LOD	21	69	<LOD	<LOD	28
5x4 (Fenton)	37	81	<LOD	19	46	89	<LOD	22
20x2	55	93	<LOD	14	80	<LOD	<LOD	38
20x2 (Fenton)	49	86	<LOD	23	60	95	<LOD	26
20x3	79	<LOD	<LOD	40	93	<LOD	<LOD	54
20x3 (Fenton)	70	97	<LOD	34	78	<LOD	<LOD	40

<sup>a</sup> Iron additions made every 5 min

The performance of the photo-Fenton process in the solar box on ACTM, TBZ and IMZ degradation is shown in Figure 3.11. To avoid redundancies, only the results obtained after applying three sequential iron dosages of 20 mg Fe/L each (20x3) are shown, which was a representative experimental condition.

When bicarbonates were present (Figure 3.11a), ACTM and TBZ could not be completely removed after 45 min. Every time iron was added, soluble ferrous iron was oxidized to ferric iron, yielding hydroxyl radicals through the Fenton reaction (Equation 1.13). However, ferric iron could not be reduced in the redox cycle through Equation 1.14 due to the presence of bicarbonates and it rapidly precipitated as iron hydroxides in the iron hydrolysis reaction.





Therefore dissolved iron concentration rapidly became close to 1 mg Fe/L. Nevertheless, certain degradation took place since ferrous iron oxidation to form iron hydroxide is rather fast, but so is the reaction between ferrous iron and hydrogen peroxide. Thus, ACTM and TBZ degradation was 40% and 83%. Only IMZ was degraded in 15 min due to its high reactivity towards hydroxyl radicals. After the third iron addition, no further degradation was observed since quantitative iron precipitation occurred. As for hydrogen peroxide, 50 mg/L was initially added and approximately 40% was consumed while iron was being added. After that, the reactant concentration remained practically constant as the reaction was stopped due to the absence of the catalyst.

On the other hand, the process rate was faster when bicarbonates were removed from the water matrix (Figure 3b). To be precise, ACTM degradation was found to be 93% in 45 min and TBZ and IMZ were completely removed in 15 min and 10 min, respectively. The increase in the degradation rate was a result of higher iron concentration during the whole treatment in comparison with the values observed in the presence of bicarbonates. Regarding hydrogen peroxide, close to 30% was consumed, although in this case 75 mg/L was added instead of 50 mg/L to ensure there was not lack of hydroxyl radical due to reactant absence.

To better understand the differences in the micropollutant's degradation when in the presence or absence of bicarbonates it is necessary to analyse the reactions taking place each time and how the iron addition is made. Bicarbonates create a buffer effect around neutral-basic pH which is detrimental to the process, as iron precipitates easily at this pH. Without bicarbonates, when iron is added, it precipitates following the iron hydrolysis reaction (Cornell and Schwertmann, 2003). In this reaction, proton concentration increases, causing pH to drop. This occurs every time iron is added until pH is close to three. Consequently, each iron addition results in higher dissolved iron due to the lowering of pH produced by the earlier addition.

However, when bicarbonates are present in the water matrix, the protons generated by iron hydrolysis react in the carbonate equilibrium to eventually yield CO<sub>2</sub> (Equation 3.2). Therefore, pH is stable until the buffer no longer works due to equilibrium displacement towards carbonic acid. As a result, more iron additions are needed to maintain a certain dissolved concentration when in the presence of bicarbonates. Therefore, bicarbonates prior elimination is consequently recommended by adding acid before adding iron salt.



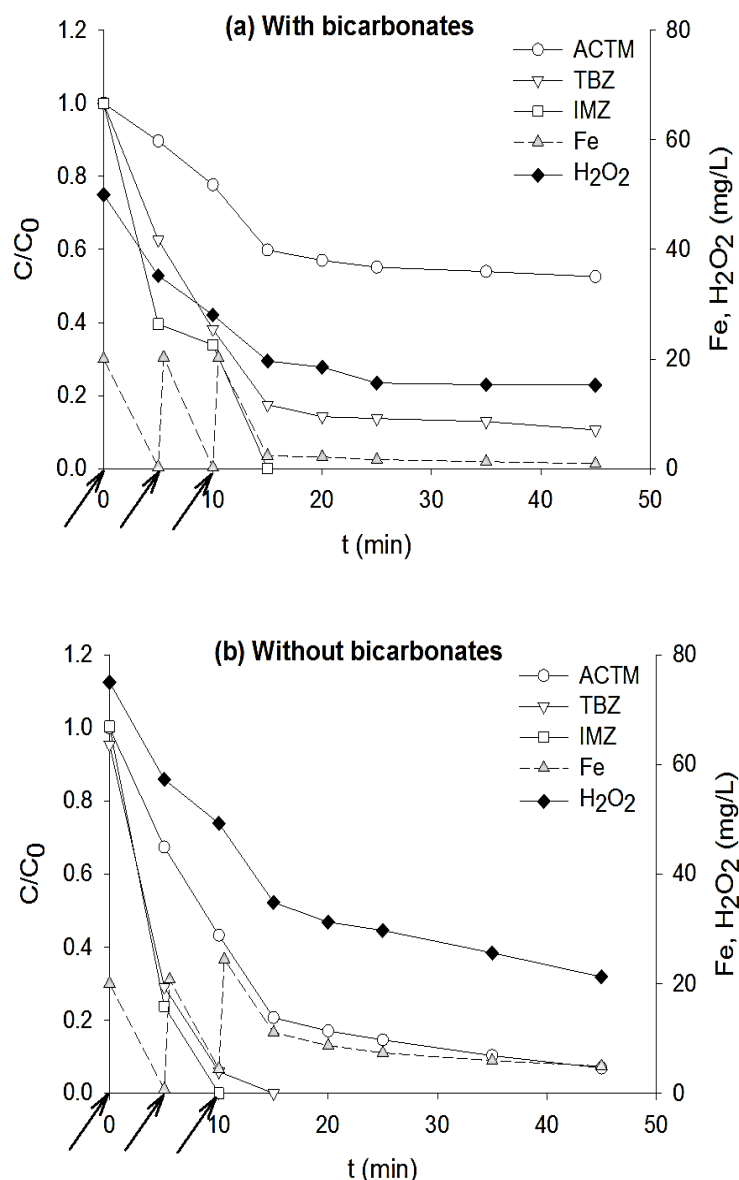


**Figure 3.11.** Impact of bicarbonates on ACTM, TBZ and IMZ degradation by photo-Fenton at natural pH using three iron additions of 20 mg Fe/L each (20x3). The arrows point out the time of addition.

Aside from the assays shown in Figure 3.11, different experimental conditions with and without bicarbonates were investigated. The results are presented in Table 3.4. When bicarbonates were present, initially only two additions of 20 mg Fe/L (20x2) were used in order to limit the iron amount added. However, only 10% ACTM and less than 45% of TBZ and IMZ was removed after adding all the iron. In fact, their degradation was not improved afterwards as observed in the three additions of 20 mg Fe/L. To corroborate the fact that degradation was not improved because only the

reaction between ferrous iron and hydrogen peroxide was taking place, the same addition was applied, but using  $14 \text{ W/m}^2$  and in the dark (Fenton process). Results confirmed that hydroxyl radicals were generated exclusively through the Fenton reaction (Equation 1.13) as degradation was similar in the three radiation conditions.

With respect to hydrogen peroxide, between 32-35 mg/L was consumed in all cases. Moreover, if only the Fenton reaction occurs, for every mol of  $\text{Fe}^{2+}$  added, a mol of  $\text{H}_2\text{O}_2$  is consumed. For the sequential addition of  $20 \times 3 \text{ mg Fe/L}$ , the stoichiometric amount of hydrogen peroxide consumed would be 1.08 mM, which is approximately 36 mg/L. This value matches the experimental consumption observed.

Regarding the outcome obtained without bicarbonates, results presented in Table 3.4 indicate there was a substantial improvement when bicarbonates were removed. Since the process was significantly enhanced, additions with lower amounts of iron were tried to reduce the catalyst concentration. Indeed, with a total amount of 20 mg Fe/L added four times (addition of  $5 \times 4 \text{ mg Fe/L}$ ) a 69% ACTM degradation was achieved in 45 min with the photo-Fenton process and with 40 mg Fe/L ( $20 \times 2 \text{ mg Fe/L}$ ), 80%, almost 7 and 8 times higher than with 60 mg Fe/L ( $20 \times 3 \text{ mg Fe/L}$ ) in the presence of bicarbonates, respectively. It was also noticeable that increasing catalyst concentration two and three times (from  $5 \times 4$  to  $20 \times 2 \text{ mg Fe/L}$  and  $20 \times 3 \text{ mg Fe/L}$ ) gave rise to an increase in final degradation, but not in the same proportion (from 69% to 80% and 93% ACTM degradation).

To ensure that in this case the iron redox cycle was taking place and not only the Fenton reaction was happening, each condition was run in the dark as well (Fenton process). ACTM degradation just after adding all the iron was 37%, 49% and 70% for  $5 \times 4$ ,  $20 \times 2$  and  $20 \times 3 \text{ mg Fe/L}$ , respectively, which was improved in the photo-Fenton process (51%, 55%, 79%, resp.). However, these differences between Fenton and photo-Fenton increased with time until the end of experiment as iron concentration was higher in the presence of UV-Vis: ACTM removal was 60% with the sequence  $20 \times 2$  in the Fenton process and 80% in photo-Fenton.

Regarding TBZ and IMZ, the former was degraded more than 95% in the presence of irradiance after adding all the iron and completely in 45 min; the latter was removed in all conditions. Therefore, as ACTM was the least reactant pollutant, it could be used as target pollutant.

After analysing these results it was concluded that bicarbonates should be removed from the water matrix to obtain significant micropollutant degradation

improvement in short reaction times, despite the fact that the presence of low bicarbonate concentration did not overly affect iron dosage in the photo-Fenton process when dealing with higher pollutant concentration in Section 3.1.2. This may be a consequence of lowering organic matter concentration, which usually helps keep iron dissolved by forming complexes with organic ligands (Birus et al., 1993) and of the different proportion between the generated HO<sup>•</sup> and the organic matter.

### **b) Effect of the iron dosage strategy on micropollutant degradation efficiency**

Based on the results obtained at laboratory scale, bicarbonates were removed from the simulated secondary effluent. Two iron dosage strategies were compared, sequential addition *versus* continuous addition. Both Fenton and solar photo-Fenton processes were compared in the removal of the same micropollutant mixture (100 µg/L of ACTM, TBZ and IMZ each). ACTM was considered the target pollutant since it was the most recalcitrant among the three tested compounds. To ensure hydrogen peroxide excess, 75 mg/L was used in all the sequential additions, but a second addition at half this value was made after 15 min for the sequence 20x4 and also continuous dosage due to the higher iron concentration. The experimental conditions are presented in Table 3.5.

#### Sequential dosage

The results found when sequential additions were made are represented in Figure 3.12. The experimental plan started with the sequence of 20x3 mg Fe/L due to the promising results obtained at laboratory scale. 92% ACTM degradation was achieved after 45 min, and 96% after 75 min, in accordance with those results obtained in the solar simulator at laboratory scale and pointing out that no differences due to the change of reactor or light source were found. The Fenton and photo-Fenton processes showed a similar tendency, but the differences between both were marked after the last addition. Even so, 80% degradation was observed with the Fenton process after 75 min.

To guarantee a faster ACTM removal, another addition of 20 mg Fe/L was made (20x4). For this sequence, ACTM removal was reached in 20 min with solar photo-Fenton; while with Fenton, complete removal was found after 35 min. This result indicates that to remove micropollutants, Fenton is a choice worth studying when the

final use of reclaimed water would permit a high concentration of iron. Finally, only one initial addition was tried as a pulse of 80 mg Fe/L (matching the total amount added for the sequence 20x4 mg Fe/L).

**Table 3.5.** Experimental conditions at pilot plant scale

<b>Fe addition mode</b>	<b>Total Fe (mg/L)</b>	<b>H<sub>2</sub>O<sub>2</sub> (mg/L)<sup>b</sup></b>
<b>Sequential additions<sup>a</sup></b>		
20 mg/L x3	60	75
20 mg/L x3 (Fenton)	60	75
20 mg/L x4	80	75+38
20 mg/L x4 (Fenton)	80	75+38
Pulse	80	75
Pulse (Fenton)	80	75
<b>Continuous dosage</b>		
1 mg/L·min	75	75+38
1 mg/L·min (Fenton)	75	75+38
5 mg/L·min	75	75+38
5 mg/L·min (Fenton)	75	75+38
Exp. Decrease	75	75+38
Exp. decrease (Fenton)	75	75+38
Exp. decrease pH 2.8	75	75+38
Exp. decrease pH 2.8 (Fenton)	75	75+38

<sup>a</sup>Iron additions made every 5 min (mixing time)

<sup>b</sup>2<sup>nd</sup> hydrogen peroxide addition made after 15 min

This particular strategy was followed to determine if adding the same amount in one dosage or distributing it over the course of the experiment would change the results. The profiles in Figure 3.12 indicate that the same amount of catalyst did not allow the same efficiency to be obtained since only 68% ACTM degradation was achieved in 20 min and 90% in 75 min with the solar photo-Fenton. The Fenton process proved even slower (64% and 73% in 20 min and 75 min, resp.).

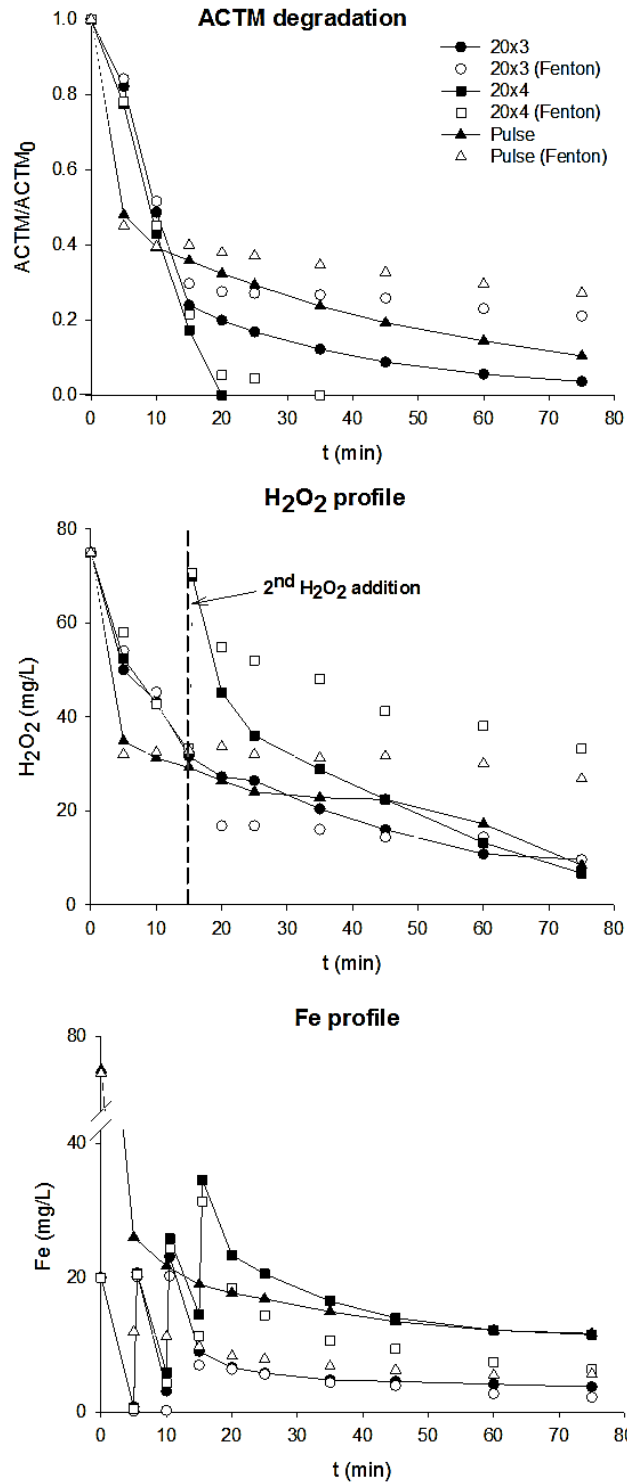


**Figure 3.12.** Acetamiprid, hydrogen peroxide and iron concentration profiles during solar photo-Fenton and Fenton run with sequential iron dosage.

The disparities between strategies were caused by how iron precipitated in each case. When the pulse was tried, a large amount of iron was added at the same time. While iron precipitated, particles formed floccules which favoured even more precipitation. However, when the same amount of iron was dosed four times (20x4

dosage), iron precipitation per addition was not so pronounced, and so precipitation was less favourable than for the pulse. In addition to this, as expected iron hydrolysis caused pH drop to three (Figure 3.13).

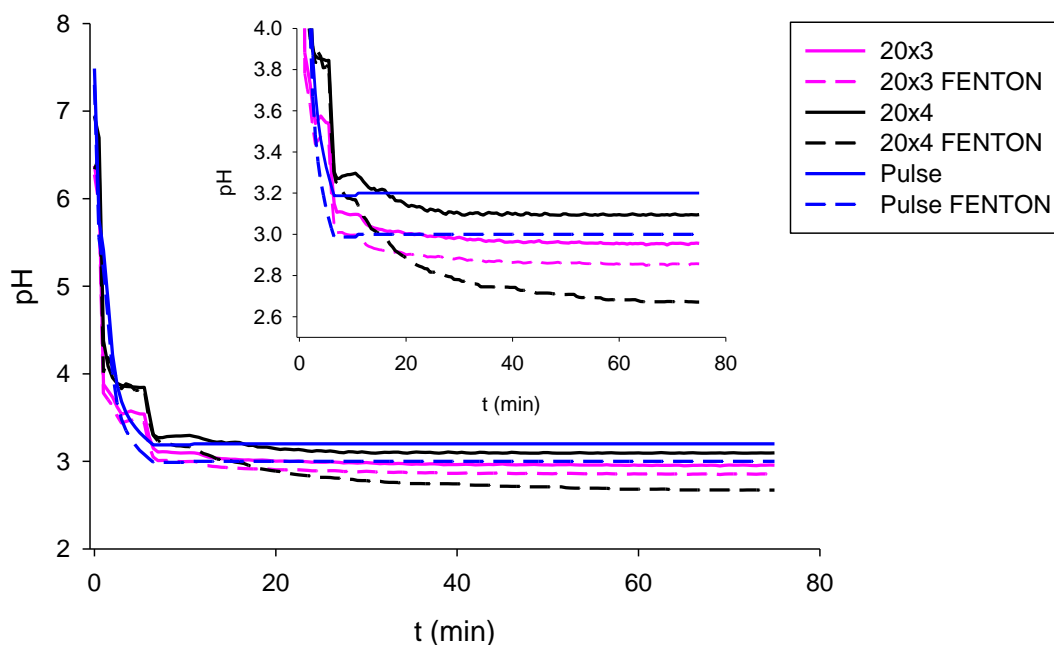


**Figure 3.13.** pH profiles for sequential iron dosage.

As for the other two pollutants, TBZ was removed in 5 min with the pulse of iron in the photo-Fenton process while 95% degradation was achieved in 75 min with Fenton. Regarding the other sequence strategies, removal was reached in 15 min with all of them, regardless of the presence or absence of UV-Vis. IMZ was the most easily oxidized, being removed in 5 min in all cases.

When it came to hydrogen peroxide (Figure 3.12), close to 70 mg/L was consumed in the sequence of Fe 20x3 and with the pulse in the photo-Fenton process to obtain more than 90% ACTM degradation, but not removal. On the other hand, just 60 mg/L of hydrogen peroxide was consumed in the sequence of Fe 20x4 for the photo-Fenton process to achieve removal in 20 min.

Regarding iron profiles (Figure 3.12), during the additions, iron concentration was similar for Fenton and photo-Fenton, as previously mentioned, but after that, faster iron reduction by UV-Vis in the photo-Fenton process partially prevented precipitation. In addition, most of the dissolved iron was  $\text{Fe}^{3+}$ , since  $\text{Fe}^{2+}$  oxidation was instantaneous and the salt reduction, quite slow. Thus, iron was mainly as ferric iron. The profile for the pulse was similar to the one obtained for the 20x4 sequence after 25 min in either

Fenton or photo-Fenton, but ACTM was already much more degraded with the 20x4 strategy as a result of the first few minutes of the reaction. This highlights the significance of how iron is distributed throughout the process.

### Continuous dosage

Bearing in mind the results obtained and that iron dosage is more effective if spread out instead of being added all at once, different continuous dosage strategies were carried out. The effect on ACTM degradation, hydrogen peroxide consumption and iron profiles is illustrated in Figure 3.14.

Firstly, a continuous addition of 1 mg Fe/L·min was made for the duration of the test (75 min), so a total of 75 mg Fe/L was added and equally distributed over the experimental time. ACTM degradation (Figure 3.14) was reached with solar photo-Fenton, albeit rather slowly, in 75 min, and 75% was achieved by Fenton in the same time. In fact, ACTM removal was practically the same during the first 25 min in both processes as hydroxyl radicals were generated mainly through Equation 1.13 until the pH drop caused by iron hydrolysis allowed more iron to be dissolved so that Equation 1.14 could take place.

This is corroborated by the total iron profiles (Figure 3.14), where differences between Fenton and photo-Fenton could be noticed after 60 min, although barely so. Therefore, although this continuous mode was successful in removing ACTM, the reaction time was too long. To shorten it, the same total amount of iron (75 mg/L) was added continuously at 5 mg Fe/L·min for 15 min in Fenton and photo-Fenton so that there was more iron at the beginning. It was observed that initial ACTM degradation was greater in comparison with the previous continuous mode in both processes. Indeed, 85% was removed in just 25 min with solar photo-Fenton and over 75% with Fenton. Nevertheless, for the first, removal was achieved in 60 min, while barely any improvement was observed for the Fenton process after 25 min. As iron was only added for 15 min, slow iron reduction by Fenton drove iron precipitation, whereas faster iron reduction in photo-Fenton generated more hydroxyl radicals.

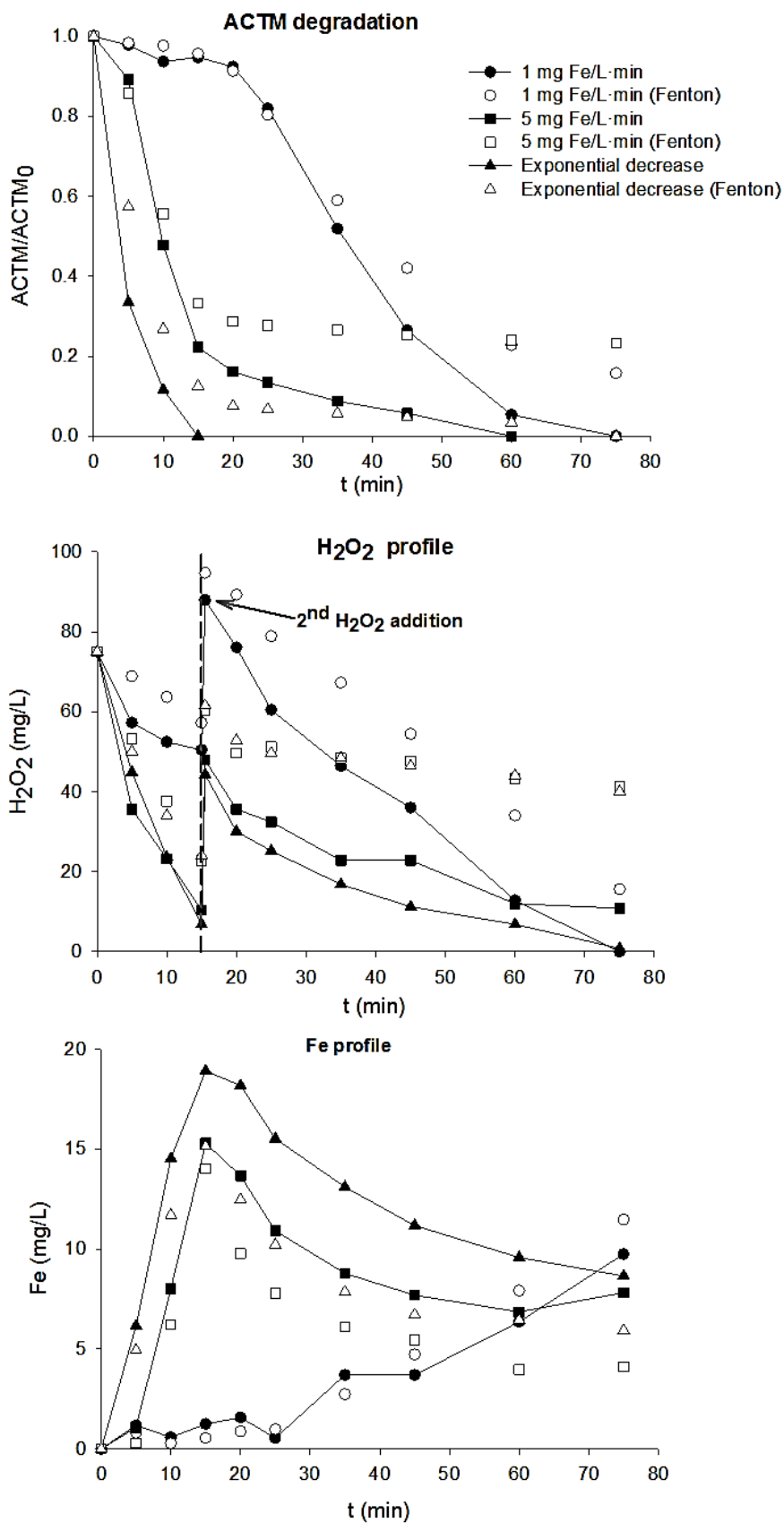
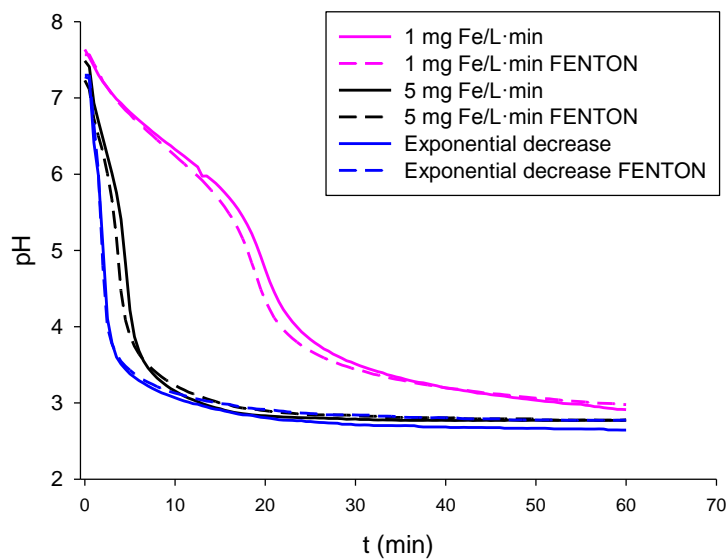


Figure 3.14. Continuous iron dosage effect on the solar photo-Fenton and Fenton process.



To improve the observed results, an exponentially decreasing iron dosage was carried out so that again 75 mg Fe/L was added after 15 min. This type of dosage was justified since iron concentration at the start of the process is important because iron efficiency, understood as the relationship between ACTM degradation and total iron added, is initially lower due to iron precipitation by hydrolysis. Thus, the employed function implied that 40 mg Fe/L was added in the first 5 min. The results pointed out (Figure 3.14) rapid ACTM degradation. Indeed, removal with photo-Fenton was reached in less than 15 min, faster than with any other strategy. With Fenton, 88% degradation was obtained in the same time, but removal was only achieved after 75 min. Thus, this strategy proved to be the best among all those tested. This can be explained if it is taken into account that in photo-Fenton more iron is temporarily dissolved; however, its precipitation is still rapid, so real dissolved iron profiles are difficult to obtain due to mixing time limitation in the pilot plant (5 min). The drop in pH to three due to the hydrolysis also occurred with all strategies (Figure 3.15).

Analogously to the sequence dosage, total iron profiles (Figure 3.14) were practically the same as  $\text{Fe}^{3+}$  profiles. Since these results were the best ones obtained in terms of reaction time, the same iron dosage was applied to both Fenton and photo-Fenton at optimal pH 2.8 as a reference, although results were not included to prevent Figure 3.14 from not being clear enough. ACTM oxidation was rapid and degradation time with photo-Fenton was found to be 10 min, only 5 min less than at natural pH. Regarding the Fenton process, the same removal time was obtained than with photo-Fenton. Also, dissolved iron concentration was greater at pH 2.8 than at natural pH, but the improvement in removal rate was not proportional.



**Figure 3.15.** pH profiles for continuous iron dosage.

With respect to IMZ degradation, it was removed in less than 5 min for all strategies assayed in either Fenton or photo-Fenton with the exception of the dosage of 1 mg Fe/L·min in the Fenton process, where it took 10 min. As for TBZ, the exponentially decreasing dosage at both pHs resulted in a 10-min-process for degradation, regardless of the AOP employed; the 5 mg Fe/L·min dosage took 15 min for both Fenton and photo-Fenton; and the 1 mg Fe/L·min, 45 min. DOC concentration was analysed as in the previous experiments and mineralization also proved to be unimportant. Regarding hydrogen peroxide, two additions were made for all continuous dosage strategies to ensure excess (Figure 3.15) (113 mg/L total).

The results show the necessity to develop different iron dosage strategies to remove micropollutants in short reaction times at natural pH, therefore avoiding the extreme acidification of water at pH 2.8. It should also be pointed out that final neutralisation of the effluent would be required in both cases.

The study indicates that how iron is added during the process is essential to reduce reaction times without affecting overall efficiency. It is necessary to add more at the beginning of the process, distributing it for the first few minutes of reaction, but not adding it all at once since precipitation is favoured at neutral pH. In accordance with this, the continuous dosage allows iron to be better distributed than for sequencing additions given that the latter gave rise to a lack of catalyst between additions. Indeed, the least reactive pollutant, ACTM, was able to be removed in less than 15 min applying an exponentially decreasing iron dosage, obtaining similar results at pH 2.8. In addition, Fenton is a choice worth studying when the final use of reclaimed water would permit a high concentration of iron or as a step to combine with photo-Fenton for cloudy days or continuous operation.

### **3.2.2 Interrelation between iron concentration and irradiance**

The extremely low contaminant concentration may result in differences in the process performance with respect to higher pollutant concentrations (micropollutants versus macropollutants). Knowing that light intensity and Fe concentration are cross-linked when designing solar photoreactors (Kusic et al., 2009; Malato et al., 2004), that solar irradiation changes within certain well-known limits and that it would be advantageous to use as little Fe as possible to permit simple Fe removal after the treatment, it is worth studying the combined effect of Fe concentration and irradiance when dealing with micropollutants by finding which one is the process limiting variable.

The limiting variable is the factor which prevents the overall process from running at a faster rate. There is usually one limiting variable which determines the process rate, however much the levels of the others change. Iron concentration is an operating variable, which can be varied during the process; while UV-irradiance is an environmental variable, uncontrolled in the solar photo-Fenton process but easy to predict in sunny days (Martín et al., 2010).

This Section is focused on study of the combined influence of iron concentration and incident UV radiation on the removal of micropollutants in the photo-Fenton process and its repercussions on the process application. A sound understanding of the relationship between both variables is vital to be able to monitor, operate and design the photo-Fenton process.

The micropollutant mixture -ACTM, TBZ and IMZ-, each at a concentration of 100 µg/L was used. Experimentation was carried out in deionised water in the solar box and simulated secondary effluent in the flat-reflector tubular reactor pilot plant. The process was operated at pH 2.8 to keep iron concentration constant. It was varied between 1-20 mg Fe/L. UV radiation values were changed in the range usually attained in solar photoreactors (5-30 W/m<sup>2</sup>).

#### **a) Interrelation Fe-Irradiance in deionised water**

The plate reactor described in Section 2.5.4 was placed in the solar box (Figure 2.7b). The optical path length was 5 cm, the same diameter as pilot plant photoreactor. It was connected to a mixing and recirculation tank, maintaining the temperature at 35 °C, commonly found in non-concentrating solar photoreactors (Zapata et al., 2009). The volume exposed to irradiation was 2 L and the total volume was 3 L. The experimentation was carried out at pH 2.8 in deionised water so as to avoid interferences in this first stage of the research due to substances present in real water, such as organic matter or ions.

Iron concentration was the operating variable studied and it was varied between three commonly used values in the photo-Fenton process: 1 mg Fe/L, a concentration which can be found in some lakes, rivers and surface waters (De la Cruz et al., 2012) and therefore, the efficiency of which under photo-Fenton conditions would be of some interest; 5 mg Fe/L, a concentration typically used when dealing with micropollutants in the photo-Fenton process in order to avoid iron removal after treatment (legislation

permits disposal at this concentration level) (Klamerth et al., 2013); and 20 mg Fe/L, as this is the optimized concentration when using the photo-Fenton process in photoreactors such as CPCs with a 5-cm path length (Malato et al., 2004; Malato et al. 2009).

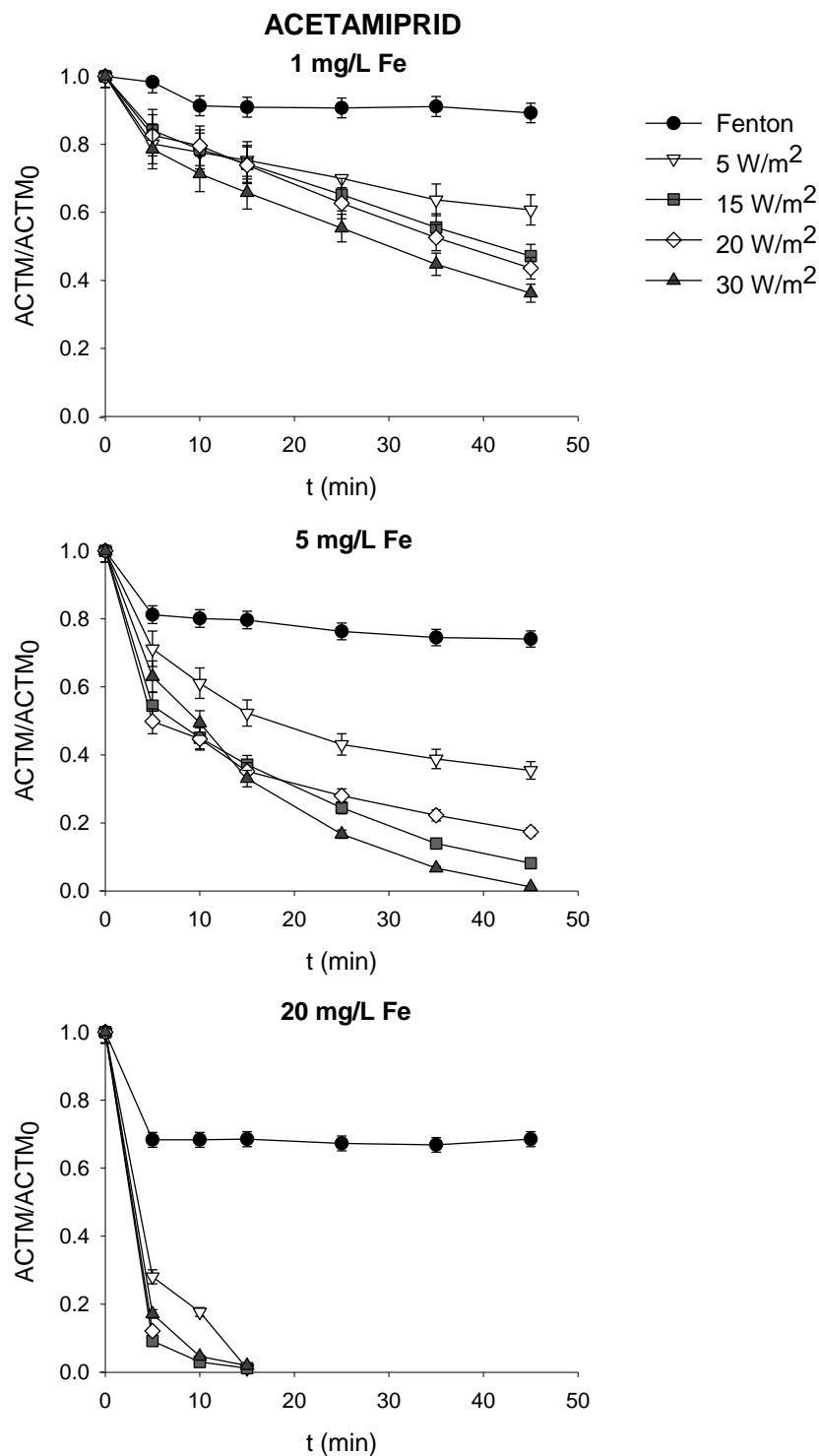


**Figure 3.16.** Acetamiprid degradation in the plate reactor and solar box with deionised water (dark Fenton and 5, 15, 20 and 30 W<sub>UV</sub>/m<sup>2</sup>).

The environmental variable, UV incident radiation ( $I$ ), ranged from low values experienced in winter and cloudy days to higher irradiances commonly found in the Mediterranean area at noon (Blanco Gálvez and Malato, 2003): 5, 15, 20 and 30  $W/m^2$ . The hydrogen peroxide concentration added was 50 mg/L, enough to drive the process without any restriction due to low oxidant concentration and also low enough to avoid scavenging of  $HO^\bullet$  radicals by  $H_2O_2$ . A 'one-factor-at-a-time' strategy was followed, changing an individual variable and keeping the other one constant to find out limitation phenomena and to study reaction kinetics.

The biocide mixture degradation obtained in deionised water is presented in Figures 3.16 and 3.17. The different reactivity between pollutant and hydroxyl radicals resulted in different reaction rates for each biocide. The lowest degradation rate by far was given by ACTM (Figure 3.16). Also, being the slowest contaminant of the selected three to be removed, it could thus be used as the target pollutant, meaning if it was removed, the other pollutants would be as well. Indeed, ACTM was removed in 15 min with 20 mg Fe/L.

Figure 3.17 shows the results with TBZ at 1 and 5 mg Fe/L, and IMZ at 1 mg Fe/L. Experiments with TBZ and IMZ at higher iron concentrations were so fast that it was not possible to obtain consistent kinetic data. Indeed, TBZ could be degraded in 5 min for the highest iron concentration, or under milder conditions (5 mg Fe/L) in 35 min (Figure 3.17); while IMZ presented even faster kinetics, since it could be removed with 1 mg Fe/L after 25 min (Figure 3.17). Although the initial molar concentration differed slightly from one biocide to another due to the different molar weights, the order of magnitude was the same (0.34, 0.50 and 0.45  $\mu M$  for imazalil, thiabendazol and acetamiprid, respectively).

As for the influence of iron concentration on degradation, regardless of the biocide or the irradiance, increasing iron concentration produced a substantial increase in the degradation rate. On the other hand, the influence of incident radiation was more complex. For instance, with 1 mg Fe/L ACTM degradation showed similar degradation profiles for irradiances from 15 to 30  $W/m^2$ ; whilst at 5  $W/m^2$  removal was slower. This could also be appreciated for 5 and even 20 mg Fe/L. Likewise, TBZ removal showed the same effect for 1 and 5 mg Fe/L: increasing irradiance above 15  $W/m^2$  did not improve the degradation rate. The same behaviour could be observed with IMZ for 1 mg Fe/L. Therefore, for the three pollutants, rising UV radiation from 5 to 15  $W/m^2$  gave an increase in reaction rate. But there was a UV-light saturation effect at higher

irradiances (no clear improvement at  $UV > 15 \text{ W/m}^2$ ), regardless of the iron concentration used.

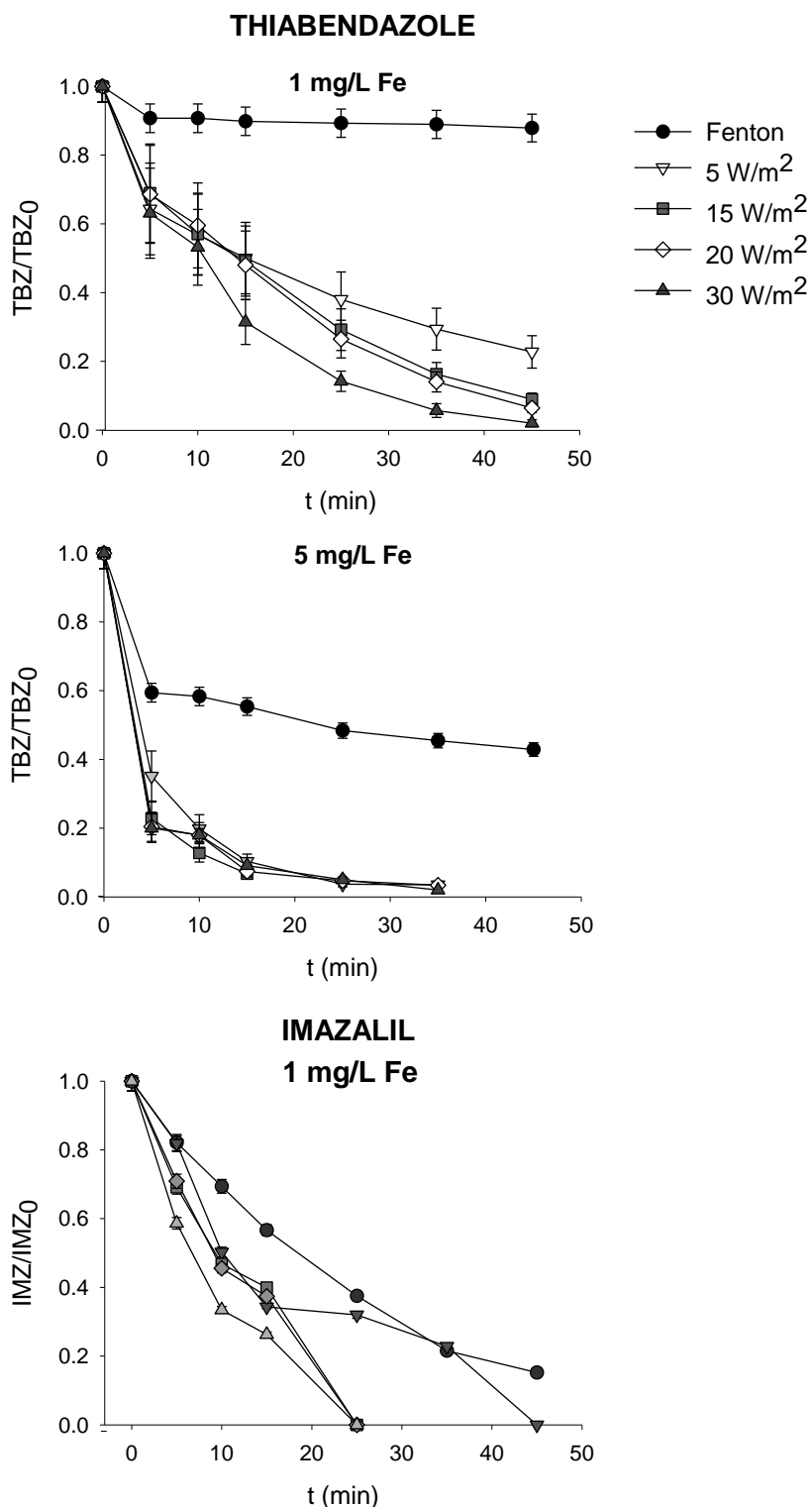


**Figure 3.17.** Thiabendazole degradation profiles at 1 and 5 mg Fe/L and 1 mg Fe/L for imazalil in the plate reactor and solar box in deionised water (dark Fenton and 5, 15, 20 and  $30 \text{ W}_{UV}/\text{m}^2$ ).

The dark Fenton process was also carried out as blank. The reaction involving iron reduction in Fenton is rather slow in comparison to the reduction in the presence of UV-light (Equation 1.14) (Pignatello et al., 2006). Thus, the absence of radiation resulted in low ACTM degradation for 1 mg Fe/L (barely 10% degradation), and although the Fenton effect increased with iron concentration, removal was not achieved in any case. Additionally, as ferric iron reduction in the dark was slow, the HO<sup>•</sup> generation by Fenton occurred mainly at the beginning, yielded by the reaction represented in Equation 1.13. However, dark Fenton degradation was more significant, as the compound was more reactive with hydroxyl radicals. For IMZ, the most reactive compound, there was degradation after 15 min for 5 mg Fe/L, and 5 min for 20 mg Fe/L during dark Fenton.

As for the hydrogen peroxide consumption, the profiles were distributed into three groups which were clearly distinguishable for each iron concentration: a minor consumption rate corresponding to the dark Fenton reaction, followed by photo-Fenton at 5 W/m<sup>2</sup> whilst the greatest consumption rate was produced for irradiances higher than 15 W/m<sup>2</sup>. In fact, from 15 to 30 W/m<sup>2</sup> the hydrogen peroxide consumption profiles were the same, reproducing the effect observed for the biocide degradation profiles. In all the cases, hydrogen peroxide still remained when all the contaminant was degraded, indicating the correct selection of 50 mg/L as initial concentration.

Subsequently, experimentation was carried out at pilot plant scale outdoors, using simulated secondary effluent as a matrix to study the process in more complex and real conditions.

### **b) Interrelation Fe-Irradiance in simulated effluent**

The experimental conditions were the same as in the solar box, although in the simulated secondary effluent so that the matrix was more complex, but without the variability of real wastewater. The pH was set to 2.8; an initial concentration of 50 mg/L H<sub>2</sub>O<sub>2</sub> was used; Fe concentration was 1, 5 and 20 mg Fe/L. As for UV incident radiation, different values were able to be obtained outdoors through the use of meshes which partially filtered solar irradiance: 5, 15, 20 and 30 W/m<sup>2</sup> were able to be achieved with a temperature of 25±2°C. Irradiances from 5 to 15 W/m<sup>2</sup> were especially important since during this interval, irradiance saturation was achieved in deionised water. The meshes consisted of dark cloth with very small pores and homogeneous distribution. Meshes with different pore size were used depending on the irradiance needed in the system (e.g. the mesh with the smallest pore size would be used to

achieve lowest radiation), covering the whole loop. The process was run at noon, when UV irradiance was virtually constant for the duration of the tests. In addition, experimentation was also carried out on a cloudy day with an average irradiation of  $25 \text{ W/m}^2$  and minimum / maximum values of 11 and  $31 \text{ W/m}^2$ , respectively. The average temperature was  $18 \text{ }^\circ\text{C}$ .

Since ACTM could be considered the target pollutant and it was representative of the other two, only ACTM's degradation is shown in Figure 3.18 to avoid repetitive results, but all the experiments were carried out with a mixture of the three contaminants at  $100 \text{ } \mu\text{g/L}$  each. Fenton process was run in the dark for five minutes ( $t = -5 \text{ min}$ ) before photo-Fenton ( $t = 0$ ) to ensure homogeneous mixing. Figure 3.18 illustrates that ACTM degradation curves show an analogous tendency towards the results presented in deionised water. Nevertheless, degradation required longer treatment times in simulated effluent than in deionised water.

For instance, ACTM degradation in deionised water was achieved in 15 min while in simulated effluent it did not even reach it after 75 min using  $20 \text{ mg Fe/L}$  for high radiation values (above  $15 \text{ W/m}^2$ ). For  $5 \text{ mg Fe/L}$ , 93% ACTM degradation was obtained in 45 min in deionised water compared with only 84% in 75 min in simulated effluent. Nonetheless, for  $1 \text{ mg Fe/L}$  over 43% degradation was achieved after 45 min in both cases. In this case the process can be limited for such a low iron concentration. This is discussed later, analysing the kinetics. This decrease in the degradation rate occurred for TBZ and IMZ as well, but in a lower extend. Results indicated that ACTM's (Figure 3.18) and the other biocides' degradation profiles in cloudy conditions were analogous to the other profiles obtained for the higher irradiances, above  $15 \text{ W/m}^2$ . This is important as per the running of the process since working with solar energy usually implies uncertainty due to UV-light variation, which is more unpredictable in cloudy days.

Regarding hydrogen peroxide, the tendency observed in the consumption profiles (Figure 3.19) also showed three distinct groups: the one belonging to the Fenton reaction, another one for  $5 \text{ W/m}^2$  and a final set for higher radiations, regardless of the iron concentration, as occurred in deionised water. In addition, similarly to the biocides' degradation, its consumption was slower in simulated effluent: while in deionised water hydrogen peroxide was totally consumed in 35 min, with simulated effluent it happened in 60 min for  $20 \text{ mg Fe/L}$  for high radiation values (above  $15 \text{ W/m}^2$ ); for  $1 \text{ mg Fe/L}$  and high irradiance, 65% was consumed in 45 and 75 min with deionised water and simulated effluent, respectively.



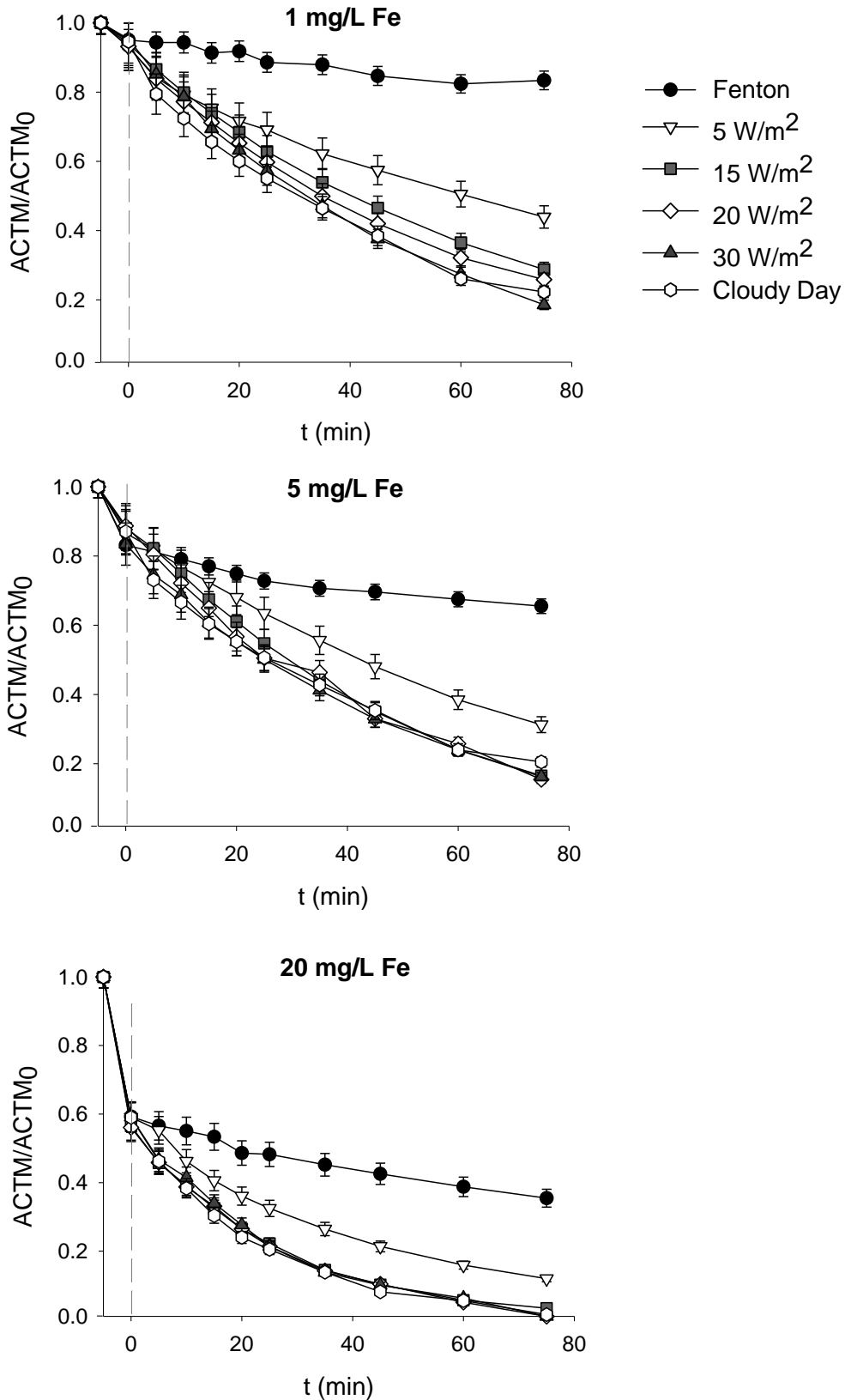


**Figure 3.18.** Acetamiprid degradation in simulated water at pilot plant scale under different operating conditions of iron concentration and irradiance.

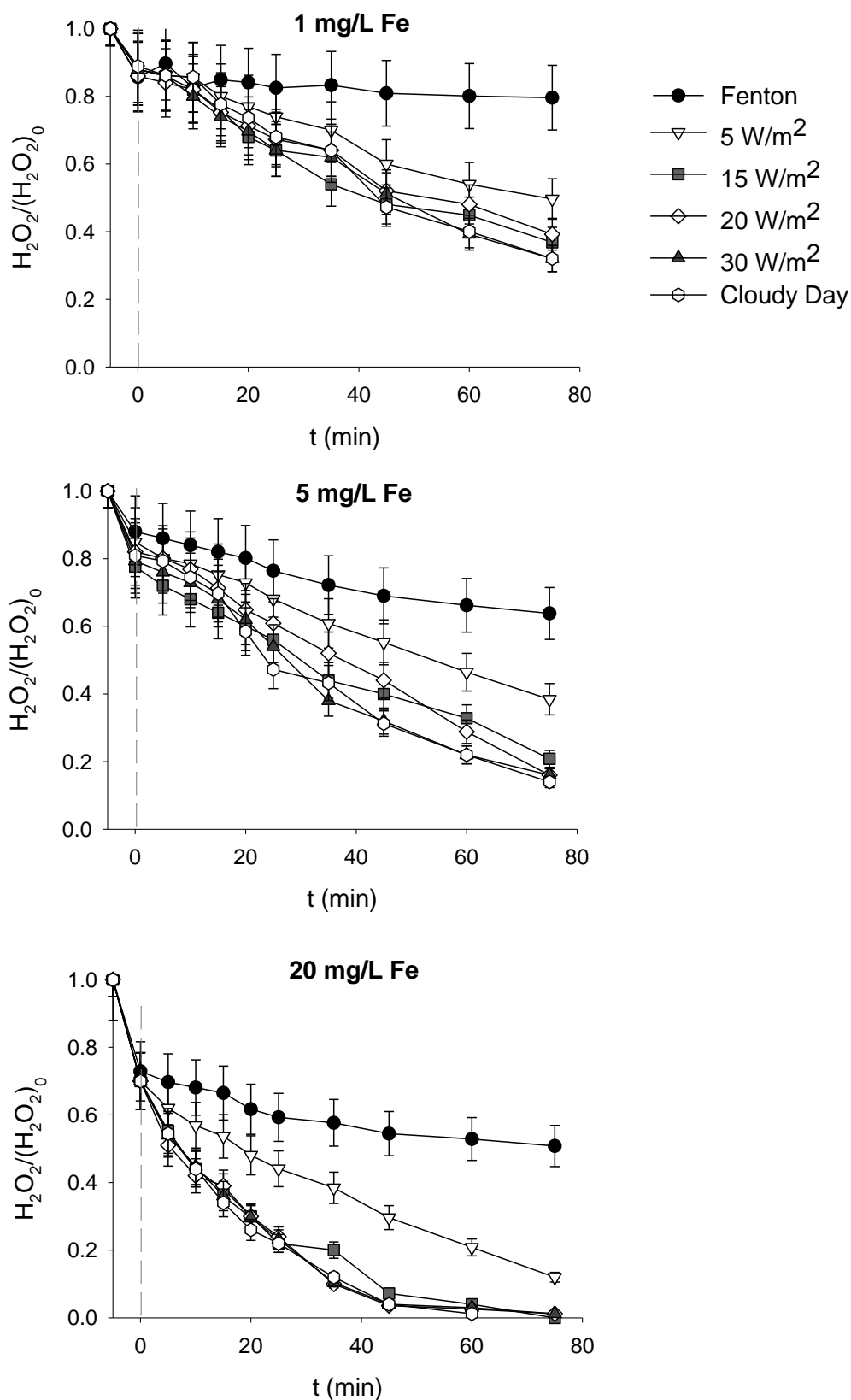


**Figure 3.19.** Hydrogen peroxide consumption profiles in simulated water at pilot plant scale under different operating conditions of iron concentration and irradiance.

### Kinetic analysis and determination of the limiting factor

Taking into account the obtained results, it is a worthwhile exercise to find out which variable, the operating (Fe concentration) or environmental (UV irradiance) one, limits the process. Nevertheless, a situation in which more than one variable limits a process may also occur. To determine the variable/s limiting the process it is necessary to know the effect of incident UV-light and Fe concentration on ACTM, TBZ and IMZ degradation kinetics.

The kinetic constants were calculated discarding the initial drop in pollutant concentration since it was only given by the first ferrous iron oxidation, as described in Equation 1.13, which yielded a great amount of HO<sup>•</sup>. This rapid reaction could also be observed in the hydrogen peroxide profiles (Figure 3.19). After this, the reaction rate decreased once the Fe redox cycle was established since ferric iron reduction is the slowest reaction in the cycle.

Reaction kinetics gives information not only on how operating parameters can affect the rate of the reactions, but also about the reaction mechanism. When working within the mg/L pollutant range, zero-order kinetics for pollutant concentrations usually fit contaminant removal during the first stages (McGinnis et al., 2000; Zapata et al., 2010). In this pollutant concentration range, a great amount of HO<sup>•</sup> is needed. Consequently, the process should usually be run at the optimal iron concentration so as to maximise photon absorption, which for CPCs' 5-cm path length is 20 mg Fe/L (Malato et al., 2004, Malato et al. 2009). As a result, UV-light is usually the limiting variable, as hydroxyl radical generation depends on irradiation power (in conditions of hydrogen peroxide excess). The limitation range of incident UV-light is especially important for the solar-driven photo-Fenton process as it can affect the reactor's operation and design. Under irradiance limitation, the solar collector surface determines the treatment plant capacity (Sánchez Pérez et al., 2013), and in this sense, 1-sun CPCs have proved to be the most efficient in maximising the capture of photons without solar irradiation concentration (Ajona and Vidal, 2000; Blanco et al., 1999). It should be noted that solar irradiation concentration is not recommended for economic (solar tracking is very expensive) and operational reasons (an increase in water temperature > 40°C is not desired to avoid iron precipitation) (Malato et al., 2009). However, when dealing with pollutants at the µg/L scale, the situation differs since the amount of organic matter to be degraded drastically decreases. The initial concentration of pollutant is essential to the phenomena occurring in the system. Indeed, the low concentration when dealing with micropollutants brings as a

consequence a difference in the rate of photons and hydroxyl radicals needed for degradation. Thus, the situation of iron and irradiance limitation is changed.

As a result, the process kinetics is not zero-order with regard to pollutant concentration. In fact, ACTM, TBZ and IMZ degradation adjusted pseudo-first order kinetics with respect to contaminant concentration. This meant the process rate was proportional to the pollutant concentration,  $C$ :  $-dC/dt = k' \cdot C$ . This places a significant restriction on efficiency when treating very low pollutant concentrations with AOPs, since treatment time will increase exponentially the greater the removal level required.

The influence of Fe concentration and UV irradiance on the biocide degradation kinetics in deionised water (plate reactor inside the solar box) and in simulated effluent (in the outdoor pilot plant) is illustrated in Figure 3.20. The kinetic constants represented are those obtained in deionised water and simulated effluent at 1, 5 and 20 mg Fe/L for ACTM; and in simulated effluent at 1, 5 and 20 mg Fe/L for TBZ. Rapid degradation of IMZ in simulated effluent and deionised water and TBZ in deionised water prevented their representation, as previously mentioned. Nevertheless, the same outcome was clearly observed in both matrices and biocides.

The first effect observed was that the increase in iron concentration for a given irradiance gave rise to an increase in the pseudo-first order kinetic constant regardless of the water matrix. For instance, in deionised water an increase in the catalyst amount from 1 to 5 mg Fe/L at  $30 \text{ W/m}^2$  involved a rise in  $k'$  from  $0.021$  to  $0.072 \text{ min}^{-1}$  for ACTM - coefficients of determination,  $r^2$ , were  $0.991$  and  $0.995$ , respectively. For TBZ, from 1 to 5 mg Fe/L at the same radiation, the increase in  $k'$  was from  $0.059$  to  $0.158 \text{ min}^{-1}$  ( $0.994$  and  $0.993$  as  $r^2$ , respectively).

For each irradiance, increasing the catalyst concentration also increases  $\text{HO}^\bullet$  generation. As a result, the higher the Fe concentration the greater  $k'$ , since there are more radicals to react with the biocides. Conversely,  $\text{HO}^\bullet$  generation is constant in the presence of hydrogen peroxide excess and the remaining variables constant; indeed, the radical concentration is included in the pseudo first order constant:  $k' = k \cdot C_{\text{OH}^\bullet}$  since hydroxyl radical generation is constant for a given Fe concentration. Nonetheless, hydroxyl radical concentration can be affirmed to be constant only when there is hydrogen peroxide excess, as previously mentioned, otherwise  $\text{H}_2\text{O}_2$  can also limit the process. This is further discussed below. This discussion is valid either for deionised water and simulated effluent. However, the presence of other compounds in simulated effluent resulted in smaller kinetic constants. The reduction in the degradation kinetics in a complex matrix is common due to competition between organic matter and the

biocides for hydroxyl radicals, to the formation of complexes between iron and organic matter, and also to the presence of inorganic ions such as chloride that slows down the process (De Laat et al., 2004). For example, at 15 W/m<sup>2</sup> and 20 mg Fe/L ACTM's  $k'$  was 0.038 min<sup>-1</sup> ( $r^2=0.998$ ) in simulated effluent and 0.299 min<sup>-1</sup> in deionised water ( $r^2=0.94$ ). Indeed,  $k'$  in the simulated effluent was more than three times lower for ACTM and almost twice as low for TBZ at 5 mg Fe/L. Also, as ACTM is the pollutant with the lowest reactivity, organic matter competition for HO<sup>•</sup> affects it more than the other two compounds.

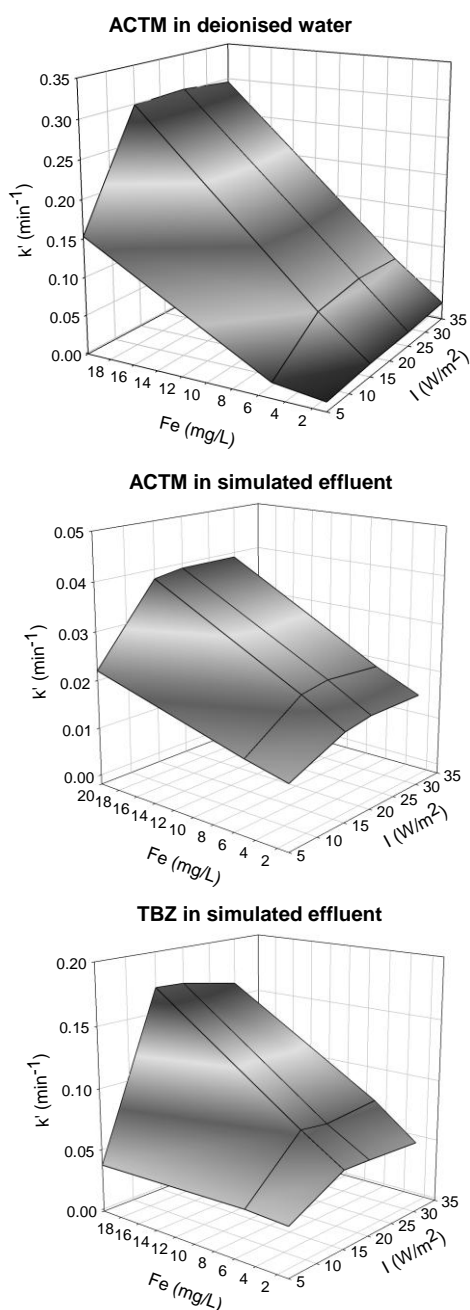


**Figure 3.20.** Influence of irradiance and iron concentration on the acetamiprid and thiabendazole degradation kinetic constant,  $k'$ .

The second effect observed was that the increase in irradiance above  $15 \text{ W/m}^2$  for a constant iron concentration did not result in an increase in  $k'$ , regardless of the matrix. This indicates there was irradiance excess or saturation above this value. That is to say, irradiance was not the limiting variable, but iron concentration for UV irradiance above  $15 \text{ W/m}^2$ . For instance, in simulated effluent ACTM's  $k'$  was 0.021, 0.022 and  $0.021 \text{ min}^{-1}$  for 5 mg Fe/L and 15, 20 and  $30 \text{ W/m}^2$ , respectively, with  $r^2$  0.991, 0.988 and 0.999, respectively.

Aside from the effects explained, for 1 mg Fe/L the kinetic constant  $k'$  was similar in deionised water and simulated effluent for all biocides, regardless of irradiance. This is due to the low amount of iron used, which radically limited the process, implying all the iron was photo-activated whatever the matrix, and therefore, it limited the process. Also, as increasing irradiance above  $5 \text{ W/m}^2$  also raises the kinetic constant, UV-light also limits the process. This would mean that the two factors, iron concentration and irradiation, were limiting the process at 1 mg Fe/L and  $5 \text{ W/m}^2$ .

Regarding hydrogen peroxide, to throw light on the fact of whether the reactant was really in excess or not, the consumption kinetic was analysed. The consumption profiles adjusted zero order kinetics. The results are presented in Table 3.6. The fact that hydrogen peroxide consumption adjusted zero-order ( $r=k$ ) kinetic implies that its consumption did not depend on its initial concentration but on the iron concentration whose redox cycle is activated by light. Thus, increasing hydrogen peroxide concentration would not have resulted in faster or greater hydroxyl radical generation since the reactant was in excess.

Either in deionised water or simulated effluent, the kinetic constant reflects the matrix effect described for the biocide degradation. On the one hand, rising Fe concentration increased hydrogen peroxide consumption rate: for 1, 5 and 20 mg Fe/L and  $15 \text{ W/m}^2$  the consumption rate was 0.015, 0.044 and  $0.240 \text{ M}\cdot\text{min}^{-1}$  in deionised water and 0.012, 0.016,  $0.046 \text{ M}\cdot\text{min}^{-1}$  in simulated effluent, respectively. On the other hand, the increase in UV irradiance did not involve an increase in the zero-order constant above  $15 \text{ W/m}^2$  due to UV-light saturation. For example, for 5 mg Fe/L, consumption rates were 0.044, 0.042 and  $0.041 \text{ M}\cdot\text{min}^{-1}$  in deionised water and 0.016, 0.018 and  $0.021 \text{ M}\cdot\text{min}^{-1}$  in simulated effluent for 15, 20 and  $30 \text{ W/m}^2$ . In addition, the consumption observed on the cloudy day for simulated effluent was also in line with the effects observed for the UV-light saturation range.

**Table 3.6.** Zero-order kinetic constant ( $M \cdot \text{min}^{-1}$ ) for hydrogen peroxide consumption in deionised and simulated water for all assayed conditions.

Water matrix	$I_{UV}$ ( $W/m^2$ )	Iron concentration					
		1 mg Fe/L		5 mg Fe/L		20 mg Fe/L	
		k	$r^2$	k	$r^2$	k	$r^2$
DW	5	0.006	0.959	0.005	0.982	0.066	0.995
	15	0.015	0.987	0.044	0.922	0.240	0.836
	20	0.017	0.927	0.042	0.88	0.257	0.895
	30	0.017	0.999	0.041	0.867	0.235	0.987
SW	5	0.008	0.978	0.010	0.988	0.021	0.98
	15	0.012	0.979	0.016	0.976	0.046	0.973
	20	0.010	0.982	0.018	0.912	0.055	0.973
	30	0.013	0.982	0.021	0.968	0.055	0.947
	Cloudy day	0.013	0.963	0.020	0.968	0.055	0.958

Altogether, the kinetic analysis of the biocides degradation and hydrogen peroxide consumption pointed out that above  $15 W/m^2$  iron was limiting the process rate (it was the limiting variable) regardless of the iron concentration used, the water matrix and the biocide. Two consequences come as a result to this situation. Firstly, as the process is easily iron-limited (irradiance excess) a constant degradation rate can be kept most of the year, favouring automatization of the process. Also, in the range of irradiance limitation ( $I_{UV} < 15 W/m^2$ ) iron concentration could be increased to keep the degradation rate. This is very important in solar-driven processes, where the efficiency strongly depends on an environmental (out of our control) variable, complicating automatization. Secondly, working in a situation of UV irradiance excess means there is an excess of photons. Thus, another alternative is increasing path length (reactor's diameter in this instance) to make out most of the irradiance reaching the system.

On the other hand, increasing UV irradiance from  $5$  to  $15 W/m^2$  actually increased the degradation rate for all iron concentrations. Thus, in these conditions we would be dealing with a situation where UV irradiance also limited the process. Yet, the fact that irradiance limitation occurred between  $5$  and  $15 W/m^2$  did not imply that the exact irradiance limitation range up to  $15 W/m^2$ , but only that it was in that interval.

### c) Influence of the light path length

With the aim to provide further insight into the effect of UV-light path length, additional experimentation with the simulated secondary effluent was carried out in the solar box. In contrast to the plate reactor system previously described, the tests were run in 1-L-stirred tank reactors wrapped with a dark cloth and a magnetic stirrer placed inside the solar box (Figure 2.7b). The wrapping cloth was used to ensure that the light entered the system only through the upper surface, permitting a correct evaluation of light path length as illumination comes from the top. The reactor was filled with the simulated secondary effluent containing the pollutant mixture (100 µg/L each biocide, as before) up to two different heights –two different light path lengths: 5cm and 10 cm height, which resulted in a volume of 400 and 800 mL, respectively. The 5-cm-path length (liquid depth in the reactor) was used to check the phenomena observed in the other two reactors (both the pilot plant and plate reactor had 5 cm of diameter as well). Iron concentration was set at 5 mg Fe/L and UV-light was set to 5, 15, 20 and 30 W/m<sup>2</sup>.

As mentioned, ACTM served the purpose of target pollutant, so its degradation is shown in Figure 3.21. For a proper comparison of both situations total mass of degraded ACTM was compared. It should be taken into account that volume was different (0.4 and 0.8 L) at different light path lengths, but irradiance (W/m<sup>2</sup>) and illuminated surface ( $\pi r^2$ , a cylindrical flask) were de same. With a path length of 5 cm and similarly to the other presented systems, increasing irradiance from 5 W/m<sup>2</sup> to 15 W/m<sup>2</sup> did indeed raise degradation rate; but increasing irradiance from 15 to 30 W/m<sup>2</sup> did not improve the process rate. On the other hand, degradation profiles proved to be remarkably different with a path length of 10 cm, as increasing irradiance from 5 W/m<sup>2</sup> to 30 W/m<sup>2</sup> indeed raised degradation rate in all the cases.

This confirmed the effects observed in the outdoor pilot plant, with 5 cm path length. On the other hand, the profile for 10 cm path length was outstandingly different. No irradiance saturation curve was observed. This was a result of UV irradiance limiting the process for this path length. Thus, in this case there was not irradiance excess.

Since the treated volume in both cases was different, it was especially interesting to compare the process rate taking into account the amount of ACTM degraded. For every irradiance value ACTM degradation with a path length of 10 cm was always over twice than with 5 cm, making the 10 cm path length the best operating choice.



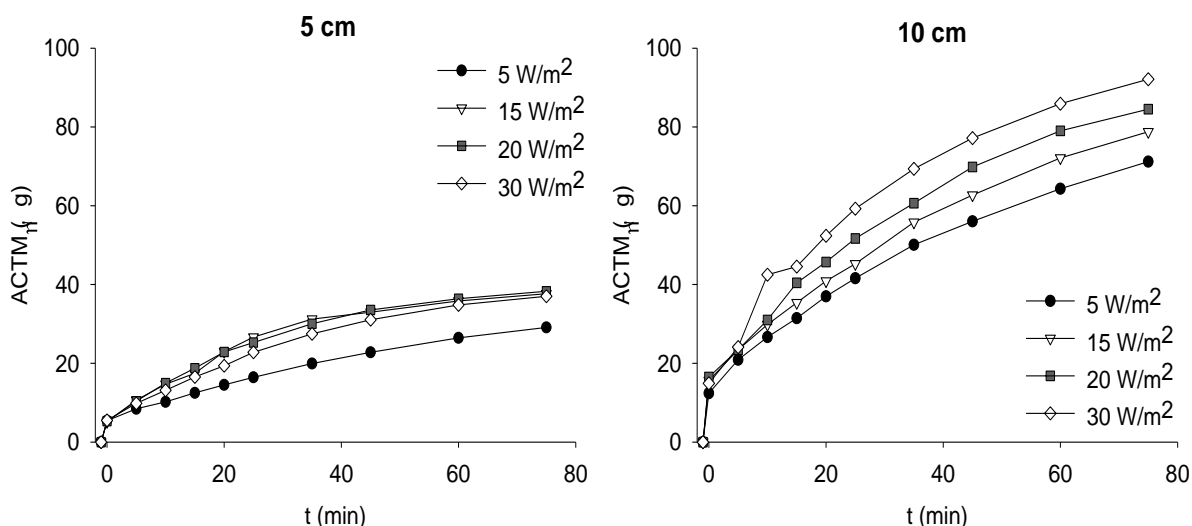


**Figure 3.21.** Mass of acetamidrid ( $C_0 = 100 \mu\text{g/L}$ ) degraded at different light path lengths in stirred tank reactor: at 5 cm height (total volume 0.4 L) and 10 cm height (total volume 0.8 L).

Consequently, working in a situation with wider path lengths than 5 cm would lead to new photoreactor configurations which would not necessarily be tubular as 10 cm or larger diameters (path lengths) are very often non-realistic due to costs or market availability of glass tubes (Malato et al., 2009). Concerning costs, tubular photoreactors are more expensive as higher diameter because glass tube wall should be thicker to withstand with pressure requirements. Therefore, tubular reactors perhaps are not the best solution when increasing light path and different configuration should be developed, for example, based on raceway ponds.

At the same time, it must be considered that, although increasing path length is recommended, the most significant point is to know with which situation we are dealing with – irradiance or iron limitation- in order to apply different operating strategies. In an existent plant where irradiance excess prevails during the year, process automatization is favoured by a fast and constant degradation rate. In contrast, with irradiance limitation, a function of wastewater volume with irradiance could be found to keep the fastest degradation rate such as increasing treated volume (light path length) in sunny days. At any rate, finding the optimal combined values of operating conditions and photoreactor path length should be aimed at obtaining the minimum process cost.

### 3.2.3 Modelling of the irradiance saturation effect

One of the keys to introduce the photo-Fenton process as technology at commercial scale is the automatization of the operation. Before this step is taken, we must be able to predict the outcome of the process (treatment time and reactant degradation) as well as the operating conditions. This is especially difficult for a solar-driven process, where irradiance is an environmental variable which cannot be controlled. Some attempts have been tried at higher pollutant concentrations (Li Puma et al., 2004; Kusic et al., 2009; Cabrera Reina et al., 2012).

The aim of this section was to obtain a reliable and simplified kinetic model which could predict the irradiance saturation effect observed in the experiments in the flat-reflector photoreactor described in Section 3.2.2.b. The model was focused on predicting micropollutant degradation and hydrogen peroxide consumption profiles in simulated secondary wastewater. Table 3.7 shows the experiments used for identification and validation.

**Table 3.7.** Experimental conditions for identification and validation runs

Run	Fe (mg/L)	Irradiance (W/m <sup>2</sup> )	Use
1	1	5	Identification
2	1	15	Identification
3	1	20	Validation
4	1	30	Identification
5	5	5	Validation
6	5	15	Identification
7	5	20	Identification
8	5	30	Identification
9	20	5	Identification
10	20	15	Validation
11	20	20	Identification
12	20	30	Identification

The model was based on a simplification of the reactions that take place in the photo-Fenton process and which are represented in Table 3.8. The reactions can be classified in three types: the iron redox cycle reactions (Equations 1.13-1.14 and 1.18); the oxidation of pollutant and other organic molecules (OM) (Equations 3.3-3.6); and

reactions of hydroxyl radicals with themselves and with hydrogen peroxide, which are considered inefficient as the radicals are not used to oxidise the pollutants (Equations 3.7-3.8) (Gogate and Pandit, 2004). The model assumes eight species:  $\text{Fe}^{2+}$ ,  $\text{Fe}^{3+}$ , hydrogen peroxide, ACTM, TBZ, IMZ, OM, and both hydroxyl and perhydroxyl radicals, which are named R in the model as both oxidise the organic compounds and the probability of reaction with them was assumed to be the same. The target was to degrade micropollutants not their mineralization or the mineralization of other organics. Therefore, oxidation till carbon dioxide release was not considered in this model.

The reaction rates and mass balances proposed for the system are shown in Tables 3.9 and 3.10. Note that solar UV irradiance was considered another variable in the kinetics and was denoted as  $I$  (Equation 3.10). This was necessary as the photo-Fenton process depends on the irradiance that reaches the reactor's surface. As explained in Section 3.2.2, there was irradiance saturation above  $15 \text{ W/m}^2$ . Thus, the kinetic corresponding to Reaction 1.14, which is where irradiance is directly involved in the process, had to include it. Indeed, in the kinetic rate expression (Equation 3.10) the term  $(I+k_{s2})$  was incorporated in the denominator to consider the saturation effect of irradiance, where  $k_{2s}$  is the saturation constant.

**Table 3.8.** Reaction scheme for the model.

<b>Iron redox cycle reactions</b>	
$\text{Fe}^{2+} + \text{H}_2\text{O}_2 \rightarrow \text{Fe}^{3+} + \text{HO}^\bullet + \text{HO}^-$	(1.13)
$\text{Fe}^{3+} + \text{H}_2\text{O} + h\nu \rightarrow \text{Fe}^{2+} + \text{HO}^\bullet + \text{H}^+$	(1.14)
$\text{Fe}^{3+} + \text{H}_2\text{O}_2 \rightarrow \text{Fe}^{2+} + \text{HOO}^\bullet + \text{H}^+$	(1.18)
<b>Parent compound and organic matter oxidation</b>	
$\text{HO}^\bullet + \text{ACTM} \rightarrow \text{ACTM}^*$	(3.3)
$\text{HO}^\bullet + \text{TBZ} \rightarrow \text{TBZ}^*$	(3.4)
$\text{HO}^\bullet + \text{IMZ} \rightarrow \text{IMZ}^*$	(3.5)
$\text{HO}^\bullet + \text{OM} \rightarrow \text{OM}^*$	(3.6)
<b>Inefficient reactions</b>	
$\text{H}_2\text{O}_2 + 2\text{HO}^\bullet \rightarrow 2\text{H}_2\text{O} + \frac{1}{2}\text{O}_2$	(3.7)
$\text{HO}^\bullet + \text{HO}^\bullet \rightarrow \text{H}_2\text{O} + \frac{1}{2}\text{O}_2$	(3.8)

In addition, the fraction of illuminated volume in the system was taken into account in the mass balances (ratio  $V_i/V_t = 0.65$ ) (Table 3.10). The aim of the model was to predict the time course variation in the main four process variables: ACTM,

TBZ, IMZ and H<sub>2</sub>O<sub>2</sub> concentrations. For this purpose, 10 parameters in the model had to be obtained. They were the kinetic constants  $k_1$ ,  $k_2$ ,  $k_{2s}$ ,  $k_3$ ,  $k_4$ ,  $k_5$ ,  $k_6$ ,  $k_7$ ,  $k_8$ ,  $k_9$ . The kinetic equations and mass balances were implemented in MATLAB® to find the best values for the 10 parameters to model the four aforementioned variables.

**Table 3.9.** Kinetic expressions for each reaction in the model.

<b>Kinetic equations</b>	
$r_1 = k_1 \cdot [\text{Fe}^{2+}] \cdot [\text{H}_2\text{O}_2]$	(3.9)
$r_2 = k_2 \cdot [\text{Fe}^{3+}] \cdot I / (k_{2s} + I)$	(3.10)
$r_3 = k_3 \cdot [\text{Fe}^{3+}] \cdot [\text{H}_2\text{O}_2]$	(3.11)
$r_4 = k_4 \cdot [\text{R}] \cdot [\text{ACTM}]$	(3.12)
$r_5 = k_5 \cdot [\text{R}] \cdot [\text{TBZ}]$	(3.13)
$r_6 = k_6 \cdot [\text{R}] \cdot [\text{IMZ}]$	(3.14)
$r_7 = k_7 \cdot [\text{R}] \cdot [\text{H}_2\text{O}_2]$	(3.15)
$r_8 = k_8 \cdot [\text{R}]^2$	(3.16)
$r_9 = k_9 \cdot [\text{R}] \cdot [\text{OM}]$	(3.17)

**Table 3.10.** Mass balances on the system for the model.

$$\frac{d[\text{Fe}^{2+}]}{dt} = -r_1 + \frac{V_i}{V_t} \cdot r_2 + \left(1 - \frac{V_i}{V_t}\right) \cdot r_3 \quad (3.18)$$

$$\frac{d[\text{Fe}^{3+}]}{dt} = r_1 - \frac{V_i}{V_t} \cdot r_2 - \left(1 - \frac{V_i}{V_t}\right) \cdot r_3 \quad (3.19)$$

$$\frac{d[\text{H}_2\text{O}_2]}{dt} = -r_1 - \left(1 - \frac{V_i}{V_t}\right) \cdot r_3 - r_8 \quad (3.20)$$

$$\frac{d[\text{R}]}{dt} = r_1 + \frac{V_i}{V_t} \cdot r_2 + \left(1 - \frac{V_i}{V_t}\right) \cdot r_3 - r_4 - r_5 - r_6 - r_7 - r_8 - r_9 \quad (3.21)$$

$$\frac{d[\text{ACTM}]}{dt} = -r_4 \quad (3.22)$$

$$\frac{d[\text{TBZ}]}{dt} = -r_5 \quad (3.23)$$

$$\frac{d[\text{IMZ}]}{dt} = -r_6 \quad (3.24)$$

$$\frac{d[\text{OM}]}{dt} = -r_9 \quad (3.25)$$

The modelling was executed implementing a Monte Carlo direct search with an error rate as objective function in a sequential search. Thus, the method searched randomly values for the parameters in a wide interval in the order of magnitude found

in literature for each constant. Then, the values were used to model the variables profiles in the experimental conditions of the identification runs (Table 3.7). The simulated profiles were then compared to the experimental data. The comparison was made by the error rate objective function:

$$E = \sum_{n=1}^4 e_n \quad (3.26)$$

Where  $E$  is the sum of the errors for each variable, subscript  $n$  stands for the modelled variable (ACTM, TBZ, IMZ and hydrogen peroxide); and  $e_n$  is the error of each variable and calculated through Eq. 3.27. This strategy has been used in previous work (Cabrera Reina et al., 2012).

$$e_n = \alpha_n \cdot \sum_{i=1}^9 \sum_{t=0}^{t=t_f} \left[ \frac{x_{sim,t} - x_{exp,t}}{x_{exp,t}} \right]^2 \quad (3.27)$$

The subscript  $i$  stands for each identification run;  $t$  is the time when the variable was measured; *sim* stands for the simulated value; and *exp*, for the measured value;  $\alpha$  is a weighting parameter to define the contribution and importance of each parameter to the model. The value of alpha was 4, 2, 1 and 3 for ACTM, TBZ, IMZ and hydrogen peroxide, respectively. Model validation was performed by comparing predicted and experimental data for the validation runs (Table 3.7). These runs were taken as representative of the assayed operating conditions.

The values obtained for model parameters are presented in Table 3.11. The highest kinetic constants corresponded to  $k_4$ - $k_6$  and  $k_8$ . The value of  $k_8$  is related to the radical-radical inefficient reaction (Equation 3.16), which in this case involves hydroxyl and perhydroxyl radicals. This agrees with the literature, where the kinetics between the radicals is very fast (Kusic et al., 2006; Ortiz de la Plata et al., 2010). As for the oxidation of ACTM, TBZ and IMZ, the corresponding constants met the condition  $k_4 < k_5 < k_6$ , as ACTM was the slowest to be oxidized, then TBZ and then IMZ. Certainly, IMZ's kinetic constant was over 10 times higher than ACTM's.

**Table 3.11.** Model parameters in  $\text{mM}^{-1} \text{s}^{-1}$ .

$k_1$	$k_2^a$	$k_{2s}^b$	$k_3$	$k_4$	$k_5$	$k_6$	$k_7$	$k_8$	$k_9$
350	3	7	0.05	1012	5053	12350	140	10276	34

<sup>a</sup> $k_2$  is expressed in  $\text{h}^{-1}$

<sup>b</sup> $k_{2s}$  is expressed in  $\text{W m}^{-2}$

The value of  $k_9$ , related to the oxidation of other organic molecules, was rather low ( $34 \text{ mM}^{-1} \text{ s}^{-1}$ ). This is reasonable since usually other organic molecules present in a secondary effluent have a high oxidation state, so their reactivity towards radicals would be smaller. The kinetic constants that showed the smallest values were those associated to the iron redox cycle,  $k_1$ - $k_3$  and  $k_{2s}$ . Values of  $k_1$  between  $53$  and  $76 \text{ M}^{-1} \text{ s}^{-1}$  and  $0.002 \text{ M}^{-1} \text{ s}^{-1}$  for  $k_3$  (Equations 1.13 and 1.14) can be found in the literature (Pérez-Moya et al., 2008). The value found for  $k_1$  in the model was  $350 \text{ M}^{-1} \text{ s}^{-1}$ , which is higher than the theoretical values. Nevertheless, the relationship between  $k_1$  and  $k_3$  is maintained ( $k_1/k_3 \sim 10^3$ ). As for  $k_2$ , the value in the model is  $3 \text{ h}^{-1}$ , higher than  $k_3$  as UV irradiance enhances the iron (III) reduction, and it is two orders of magnitude smaller than  $k_1$ , so it is also a consistent value. The value of  $k_{2s}$  is related with the saturation effect of UV irradiance. It corresponds to the value of irradiance which achieves half the maximum degradation rate. In this case, the value obtained was  $7 \text{ W m}^{-2}$ , which is consistent with the meaning of  $k_{2s}$  since the theoretical value would be the middle point between  $0$  and  $15 \text{ W m}^{-2}$ , which was where the irradiance saturation point was found. The values of parameters shown in Table 3.11 were used to validate the model, simulating the validation runs (which were not used to adjust the model) (Table 3.7). The results of the model fit are shown in Figure 3.22. Each of the figures corresponds to one iron concentration, each one with a different irradiance value to widen the validation range. During the search of the parameters, the weight of the error for each variable (ACTM, TBZ, IMZ or  $\text{H}_2\text{O}_2$ ) was not the same. The alpha value, which is a weighting parameter, was highest for ACTM and  $\text{H}_2\text{O}_2$ . Certainly, when ACTM is completely removed, the other two pollutants are removed as well, so it is important to effectively simulate this variable.

As for hydrogen peroxide, the successful prediction of its consumption is important for the process as it affects the process costs (Sánchez Pérez et al., 2013). Consequently, the parameter search was specially aimed at successfully modelling the two variables.

The model predicted remarkably well the hydrogen peroxide consumption in all the validation conditions (Figure 3.22). And ACTM degradation profiles could also be properly predicted for  $5$  and  $20 \text{ mg/L}$  of iron (in Figure 3.22b and 3.22c). However, the predicted profile for  $1 \text{ mg/L}$  Fe resulted in a slower degradation than the experimental values. This happened for IMZ and TBZ, although to a lesser extent, since the time for total removal could at least be predicted for these compounds. Their simulated profiles for higher iron concentrations were adequate.

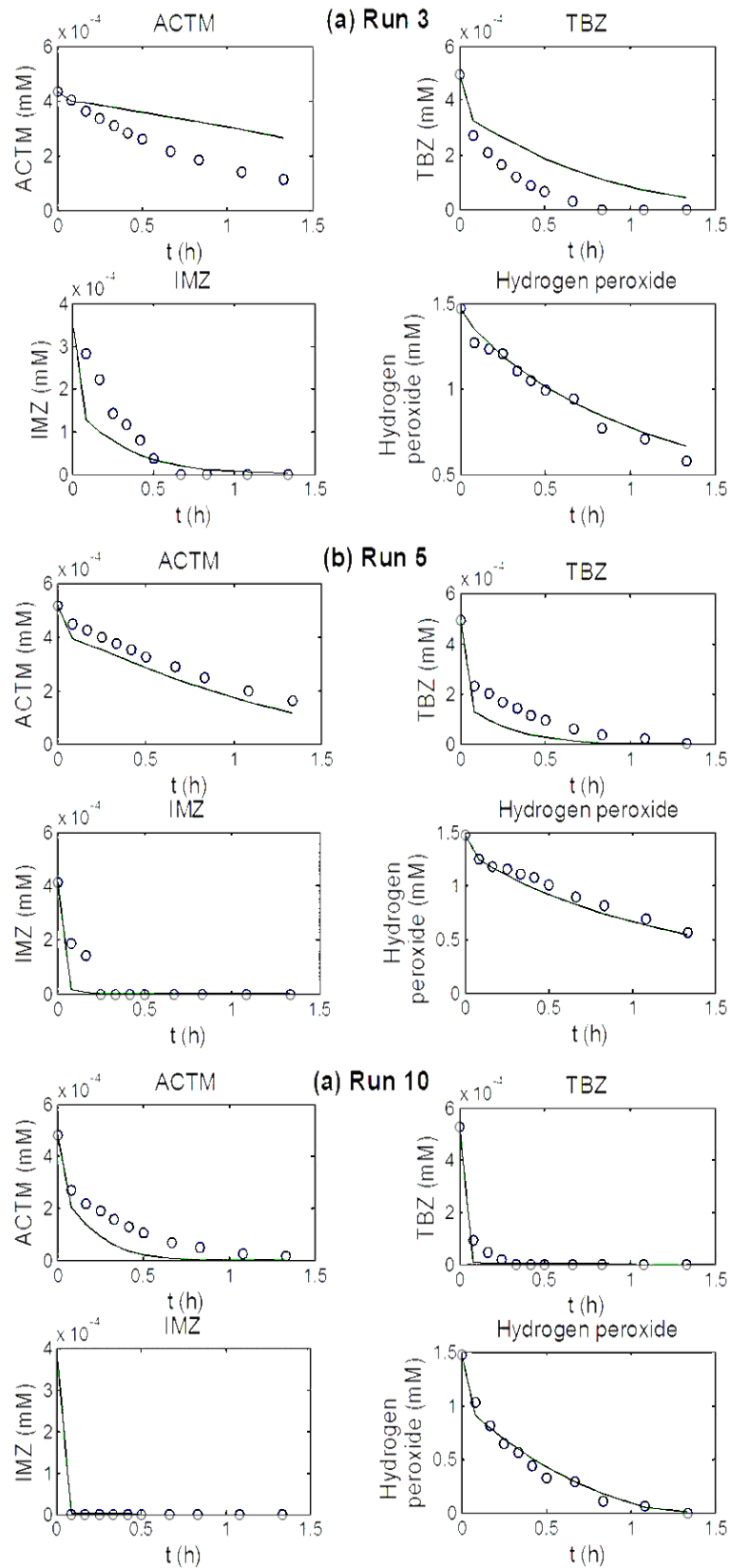


**Figure 3.22.** Experimental (dots) and predicted (lines) profiles for ACTM, TBZ and IMZ oxidation and hydrogen peroxide consumption for the model validation (runs 3, 5 and 10).

The deviation in the prediction of ACTM degradation with 1 mg/L Fe could be related to different factors. The most likely is that with only 1 mg/L Fe, hydroxyl radical generation rate is strongly limited by the low amount of catalyst and more reaction mechanisms could take place, which were not considered in the simplified model, such as the reactions with transformation products.

All in all, the model can be used to successfully predict micropollutant degradation in tubular solar photoreactors during the whole year with iron concentrations between 5 and 20 mg/L Fe, which is a common interval in this process. This model can also be taken as the first step to optimize micropollutant degradation and hydrogen peroxide dosage, permitting automatisation.

### **3.2.4 Raceway ponds as novel technology for micropollutant removal**

#### **3.2.4.1 Micropollutant removal in pilot plant scale raceway pond**

The use of photoreactors such as CPCs comes from the need of making the most of the solar beams that reach the system. Photon capture is crucial when the need of hydroxyl radicals is large such as for macropollutant (mg/L – g/L) removal, as is the case of industrial wastewater (Malato et al., 2013). When the treatment is aimed at micropollutant oxidation though, the pollutant concentration is at least a thousand times lower than for macropollutant oxidation. Therefore, the process needs less hydroxyl radicals and, consequently, less irradiance (less photons) to achieve removal (Section 3.2.2). From this arises the question whether other kind of photoreactors, less efficient in photon capture and more simple, could be used for micropollutant removal.

An interesting choice would be the raceway pond reactors (RPRs), which have been widely applied for microalgal mass culture (Chisti, 2007). In RPRs the liquid depth can be varied and the flow is controlled. They are extensive reactors with channels through which the water is recirculated. They are made of low cost materials, mainly plastic liners, giving rise to low construction costs of about 100,000 €/ha (Richardson et al., 2012). Additionally, the power requirements for mixing are also small –over 4 W/m<sup>3</sup>. Due to their flexibility and easy scale-up, raceway reactors are the most used devices for microalgal applications and production costs have been reported to be markedly lower than tubular photoreactors. Effective, extensive and low-cost (per surface unit)



photoreactors such as RPRs would spread the use of the photo-Fenton process as tertiary treatment.

In the light of these facts research was aimed at studying the applicability of extensive RPRs to remove micropollutants with solar photo-Fenton. In this case, a mixture of the commercial formulations of ACTM (EPIK®) and TBZ (TEXTAR 60®) (100 µg/L each) was used in natural water from the pumping network and simulated secondary effluent as model pollutant mixture, avoiding the disturbance of daily variations in real effluents. To assess the best process conditions, first the effect of iron concentration (1, 5.5 and 10 mg/L) and liquid depth (5, 10 and 15 cm, which corresponded to the same illuminated area but different water volume, up to 360 L) was studied using natural water as matrix instead of simulated secondary effluent to avoid disturbances due to other organics but with a ionic composition close to secondary effluents. Then the results were confirmed in simulated secondary effluent.

#### **a) Effect of liquid depth and iron concentration on pesticide removal**

The fiberglass-RPR has a maximum capacity of 360 L, a length of 3.85 m and width of 0.64 m. It is separated by a central wall, forming two canals. The RPR includes a paddle wheel connected to an engine to obtain a mixed and homogeneous system.

A one-factor-at-a-time strategy was followed, changing an individual variable and keeping the other one constant. Iron concentration was kept to low values, from 1 to 10 mg/L, typically used for micropollutant removal. Low concentrations of iron contribute to prevent large generation of iron sludge when neutralising the effluent after the treatment. Liquid depth, which determines irradiance path length, was varied from 5 cm to 15 cm. The first value was taken as the common diameter used in tubular reactors such as CPCs (Colina-Marqu ez et al, 2010). The last depth value is the maximum allowed by the configuration of the RPR reactor. The Reynolds number was estimated for each liquid height (Chisti et al., 2007) and a turbulent regime was used:  $6 \cdot 10^5$ ,  $7 \cdot 10^5$  and  $7 \cdot 10^5$  for 5 cm, 10 cm and 15 cm liquid depth, respectively. The Reynolds in a raceway pond is calculated as follows:

$$Re = \frac{\rho \cdot v \cdot d_h}{\mu} \quad (3.28)$$

$$d_h = \frac{4 \cdot w \cdot h}{w + 2h} \quad (3.29)$$

Where  $\rho$  is the density,  $v$  is the velocity of the flow,  $d_h$  is the hydraulic diameter,  $\mu$  is the viscosity,  $w$  is the width of the channel and  $h$  is the liquid depth.

The central operating condition (5.5 mg Fe/L and 10 cm height) was replicated five times to determine the experimental error. The experimental error, obtained from five replicates of the central operating condition was lower than 5% for ACTM, TBZ and hydrogen peroxide concentrations.

Hydrogen peroxide concentration was added at the beginning of the process in a concentration of 50 mg/L in all cases to ensure excess. As the liquid depth changes, so does the treated water volume in each case. To ensure similar mixing times the paddle wheel speed was changed according to the treated volume. The result was a ~2.5 min mixing time for all cases.

Prior to the beginning of the experiments, the reactor was covered and pH was adjusted to  $2.8 \pm 0.05$  with sulphuric acid. A recirculation time of 5 minutes was allowed for homogenisation after the addition of the pesticide mixture and iron salt, corresponding to twice the mixing time in the photoreactor. Then the reactor was uncovered and hydrogen peroxide was added, starting the reaction. The reactor was continuously mixed during the experiments with the paddle wheel. The experiments were always run at noon when solar irradiance was practically constant. The average UV irradiance was  $24 \pm 3 \text{ W/m}^2$ . Average temperature was  $28 \pm 2 \text{ }^\circ\text{C}$ .

The degradation profiles obtained for the commercial pesticide mixture during the photo-Fenton process are shown in Figures 3.23 and 3.24. Either for ACTM or TBZ, two oxidation steps were clearly detected, regardless of the liquid depth. The first step was always marked by high and fast oxidation of the compounds due to the initial reaction of  $\text{Fe}^{2+}$  with hydrogen peroxide (Equation 1.13) (Fenton effect). It is rather fast, directly proportional to  $\text{Fe}^{2+}$  concentration and generates a great amount of hydroxyl radicals (Gogate and Pandit, 2004). In said reaction,  $\text{Fe}^{2+}$  is oxidised. On the second reaction step,  $\text{Fe}^{3+}$  is reduced (Equation 1.14), establishing the continuous iron redox cycle. In this step, degradation is progressive, not as fast as in the first step because the ferric iron reduction is rate limiting.

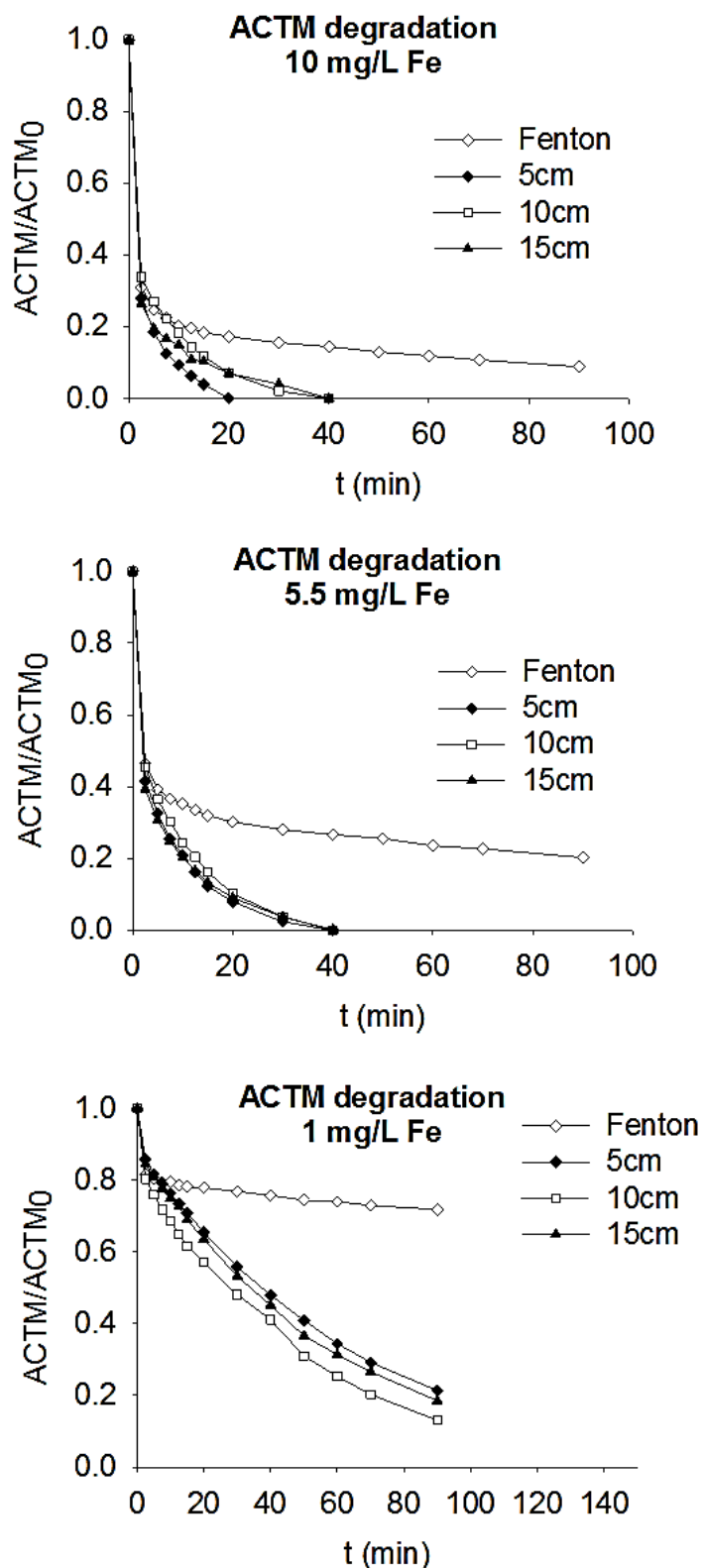


**Figure 3.23.** Acetamiprid degradation by solar photo-Fenton and Fenton with 1, 5.5 and 10 mg Fe/L ( $24 \pm 3 W_{UV}/m^2$  and  $28 \pm 2$  °C).

As in previous sections, the most persistent compound of the mixture, ACTM, was the one which gave further insight into the results. Figure 3.23a illustrates ACTM

oxidation with 1 mg Fe/L for all liquid depths (5, 10 and 15 cm). The first oxidation step, previously described, gave rise to 19% removal. As this step is dependent on iron concentration, it was the same for all liquid depths. The second oxidation step fitted an exponential decrease with similar degradation rates for the three liquid depths. In all cases approximately 75% ACTM removal was measured after 90 min of solar photo-Fenton.

For 5.5 mg Fe/L (Figure 3.23b) the first oxidation step is more significant than with 1 mg Fe/L as there was more initial  $\text{Fe}^{2+}$ , reaching 54% ACTM removal in 2.5 min. In addition, there was a significant increase in the process rate and complete removal was achieved in 40 min for all liquid depths with solar photo-Fenton. This short reaction time is an important fact as it is one of the factors which affects costs the most (Sánchez et al., 2013). As observed with 1 mg Fe/L, the profiles were analogous for the three liquid depths. This is also a significant effect. When the liquid depth was 5 cm, the treated volume was 120 L. When the liquid depth was increased to 10 cm and 15 cm, the treated volumes were 240 and 360 L, respectively. So, the number of iron ions present that needed to be photoactivated in the system was 2 and 3 times greater and so was the number of pesticide molecules. However, the photons reaching the system remain the same as the photoreactor surface did not change. Even so, the oxidation rate with solar photo-Fenton was the same, regardless of the volume. This meant that all iron ions were photoactivated for the three liquid depths and the concentration of hydroxyl radicals generated was similar.

When 10 mg Fe/L was used (Figure 3.23c), there was an increase in the process rate as well. However, it was not linearly proportional to the increase in iron concentration. The first degradation step involved 69% ACTM removal for all liquid depths, in comparison with the 54% achieved with 5.5 mg Fe/L. This first degradation step was the same for all liquid depths since it is independent of irradiation. However, in the second degradation step, there was a remarkable difference with respect to the two lowest iron concentrations: the oxidation of ACTM was faster in 5 cm than in 10 cm or 15 cm liquid depth. Indeed, complete removal time was 20 min in 5 cm liquid depth and 40 min in the other two. This can be explained as follows, taking into account that the amount of photons reaching the surface is the same for all liquid depths but not the amount of iron ions: in 5 cm depth with 10 mg/L of Fe there are  $1.3 \cdot 10^{22}$  iron ions in 120 L which need certain amount of photons to be photoactivated. When the treated volume is increased to 240 L or 360 L, the number of iron ions is  $2.6 \cdot 10^{22}$  or  $3.9 \cdot 10^{22}$ , respectively, but the amount of photons reaching the system remains the same. Thus, while for 1 and 5.5 mg Fe/L all iron ions were photoactivated for the three different

depths as shown in Figure 3.23a and 3.23b, for 10 mg/L that was not the case for 10 and 15 cm (Figure 3.23c) and the process became photo-limited. Consequently, hydroxyl radical generation per unit of volume was smaller for 240 L (10 cm) and 360 L (15 cm) than for 120 L (5 cm) with 10 mg Fe/L.

Figure 3.24 shows TBZ degradation profiles for 1 mg Fe/L and the three liquid depths. As previously mentioned, it was oxidised faster than ACTM and difficult to evaluate any effect at concentration  $> 1$  mg Fe/L. For 5.5 and 10 mg Fe/L degradation was so fast it could not be tracked. Indeed, for 5.5 mg Fe/L complete removal was achieved in 5 min; while for 10 mg Fe/L, the first degradation step (Fenton effect) was already enough to completely remove all TBZ. This is likely due to differences between the reactivity of hydroxyl radicals towards ACTM and TBZ (hydroxyl radical is more reactive towards TBZ than ACTM). This is important since if only TBZ had been used the effect of photo-limitation would not have been detected. The first degradation step for 1 mg Fe/L by Reaction 1 was more significant as TBZ is likely more reactive towards hydroxyl radicals than ACTM; and the second oxidation step also follows a fast exponential decrease. Nevertheless, the profiles tendency proved to be analogous to ACTM in the same conditions: the degradation rate was similar for the three treated volumes. The discussion of TBZ degradation follows the explanation given for ACTM above.

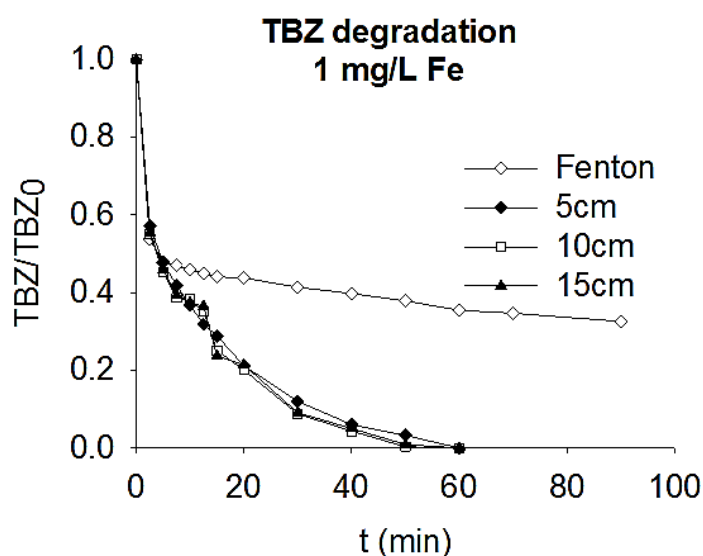


**Figure 3.24.** Thiabendazole degradation by solar photo-Fenton and Fenton with 1 mg Fe/L ( $24 W_{UV}/m^2$  and  $28 \pm 2$  °C).

In addition to the photo-Fenton tests, the Fenton process was also carried out as blank (Figures 3.23 and 3.24). The Fenton process is mainly dependent on the concentration of iron and the liquid depth is not a variable in this case. Additionally, the

reduction of  $\text{Fe}^{3+}$  takes place through Equation 1.18 instead of Equation 1.14. As Equation 1.18 is very slow (Ikehata et al., 2006), so the most significant degradation occurred in the first degradation step, which also happened in solar photo-Fenton. In no case was complete ACTM removal accomplished in 90 min, but high percentage was obtained with 10 mg Fe/L, 90%. This means the Fenton effect is rather important in micropollutant removal only if high iron concentration is used. As a result, a combination of solar photo-Fenton and Fenton (for cloudy days and nights) could be made to operate continuously. This is essential for the commercial development of this technology: extensive, less costly reactors which can operate in continuous mode.

Aside from micropollutant concentration, hydrogen peroxide consumption is crucial to corroborate the effects observed. In this case, the reactant concentration was in light excess, 50 mg/L, to ensure that the micropollutant oxidation was not conditioned by lack of hydrogen peroxide. The evolution of hydrogen peroxide concentration with time is shown in Figure 3.25. At first glance it can be appreciated that the effects observed in ACTM degradation were reflected in  $\text{H}_2\text{O}_2$  concentration.

The fact that ACTM and  $\text{H}_2\text{O}_2$  profiles matched is especially clear for 10 mg Fe/L, where profiles for the 5-cm liquid depth were different with respect to 10 cm and 15 cm (Figure 3.25c).  $\text{H}_2\text{O}_2$  consumption for different liquid depths with 10 mg Fe/L corroborates the idea that not all iron ions are photoactivated for 10-cm and 15-cm depth. With 1 and 5.5 mg Fe/L the degradation of  $\text{H}_2\text{O}_2$  was similar for all liquid depths (Figure 3.25a and 3.25b). At the end of the test, 10%  $\text{H}_2\text{O}_2$  was still in the system for 5.5 mg Fe/L. When 1 mg Fe/L was used, only 30%  $\text{H}_2\text{O}_2$  was consumed. This is consistent since  $\text{H}_2\text{O}_2$  consumption rate is proportional to the concentration of catalyst.

These results show the efficiency of the RPRs as extensive systems for micropollutant removal. A kinetic analysis was also made to compare the value of the constants. For the calculation of the kinetic constants, the first degradation step (Fenton) was omitted since it was mainly a result of the first ferrous iron oxidation, as described in Equation 1.13, yielding a great amount of  $\text{HO}^\cdot$ . It is in the second degradation stage (photo-Fenton) when the Fe redox cycle was established as iron reduction is the slowest reaction in the cycle and is seriously affected by radiation absorption and, therefore, liquid depth.

ACTM and TBZ profiles adjusted an exponentially decreasing function, following pseudo-first order degradation. ACTM pseudo-first order kinetic constants were calculated as well after the first degradation stage and included in Table 3.12. Hydrogen peroxide profiles adjusted a linear decrease after the first degradation stage,

so pseudo-zero order kinetic constants were calculated (Table 3.12). As kinetic constants for TBZ could not be obtained for 5.5 and 10 mg Fe/L due to fast degradation, only ACTM constants are presented. Since the degradation rate for 5, 10 and 15 cm liquid depth was the same for 1 and 5.5 mg Fe/L, a mean value was calculated. Standard deviation of ACTM and  $H_2O_2$  constants were included. For 10 mg Fe/L and 5 cm, there was only one experiment, so the kinetic values were not averaged.

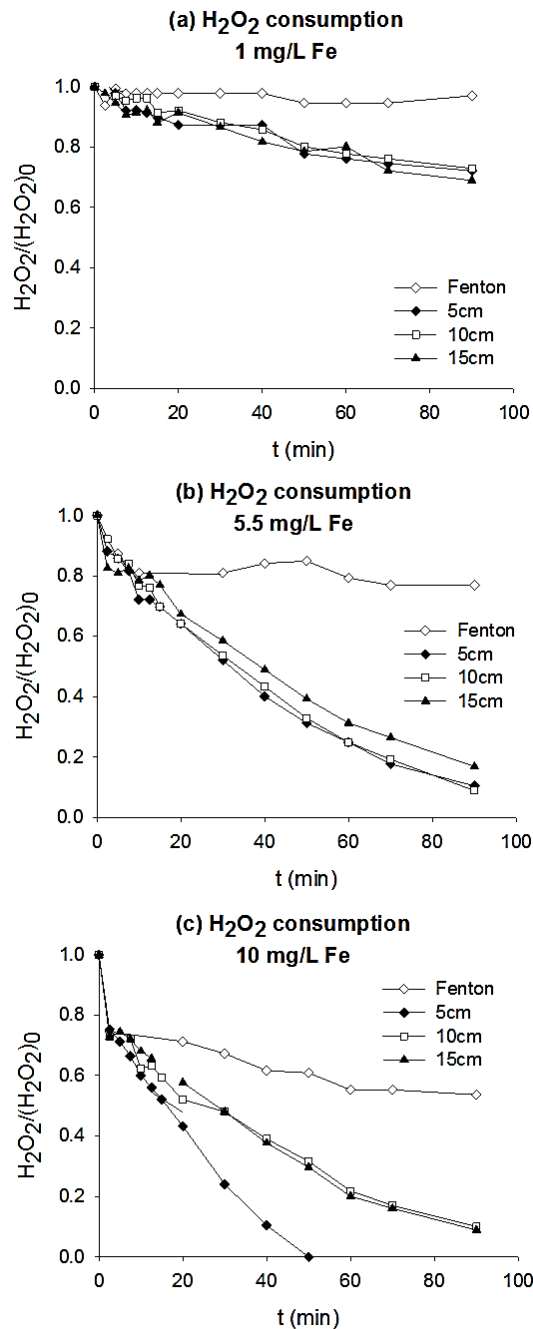


**Figure 3.25.** Hydrogen peroxide concentration profiles during pesticide degradation by solar photo-Fenton and Fenton with 1, 5.5 and 10 mg Fe/L.

**Table 3.12.** Kinetic constants for ACTM and H<sub>2</sub>O<sub>2</sub>.

Fe concentration (mg/L)	Liquid height (cm)	k <sub>ACTM</sub> (min <sup>-1</sup> )		k <sub>H<sub>2</sub>O<sub>2</sub></sub> (mM·min <sup>-1</sup> )	
		mean	Standard deviation	mean	Standard deviation
1	5, 10 and 15	0.02	0.002	0.003	0.0003
5.5	5, 10 and 15	0.08	0.004	0.012	0.0008
10	10 and 15	0.08	0.003	0.013	0.0009
10	5	0.13	-	0.021	-

It could be seen that either for ACTM and H<sub>2</sub>O<sub>2</sub> an increase in catalyst concentration from 1 to 5.5 mg/L raised the kinetic constant values four times: from 0.02 min<sup>-1</sup> to 0.08 min<sup>-1</sup> in the case of ACTM; and from 0.003 mM·min<sup>-1</sup> to 0.012 mM·min<sup>-1</sup> for H<sub>2</sub>O<sub>2</sub>. However, when the catalyst concentration was increased to 10 mg Fe/L, the kinetic constants were over 1.5 times greater only for 5 cm liquid depth (0.13 min<sup>-1</sup> and 0.021 mM·min<sup>-1</sup> for ACTM and H<sub>2</sub>O<sub>2</sub>, respectively); while at the higher liquid depths the constants remained practically the same than for 5.5 mg Fe/L. This contributes to the explanation given above that there was excess of catalyst for 10 mg Fe/L at 10 and 15 cm liquid depth. Therefore, with the fastest operating conditions (10 mg Fe/L and 5 cm liquid depth) 120 L of water were treated in 20 min. On the contrary, using 5.5 mg Fe/L with 10 cm depth, 240 L of water were treated in 40 min and 360 L with 15 cm liquid depth also in 40 min. As a result, the best operating condition was 5.5 mg/L of Fe concentration and 15 cm liquid depth.

### **b) Micropollutant removal in simulated secondary effluent**

In simulated secondary effluent, the RPR was operated at the highest liquid depth, 15 cm, and two iron concentrations, 5.5 and 10 mg Fe/L. The first as the best operating condition obtained in natural water and the second, to check if the use of a different matrix –with organic matter (10 mg/L DOC)- could have an effect on the process, for example, decreasing reaction rate as DOC scavenges HO<sup>•</sup> or augmenting water light absorption. In both cases, increasing Fe concentration would produce a clear effect increasing reaction rate.

Additionally, for comparison purposes, the same pesticide mixture was degraded in the CPC photoreactor (5 cm diameter, 0.48 m<sup>2</sup> collector area and 7 L total volume) with 5.5 mg/L of iron. ACTM and hydrogen peroxide concentrations are shown



in Figure 3.26. TBZ concentration is not shown as its degradation was too fast (it was removed in less than 5 min).

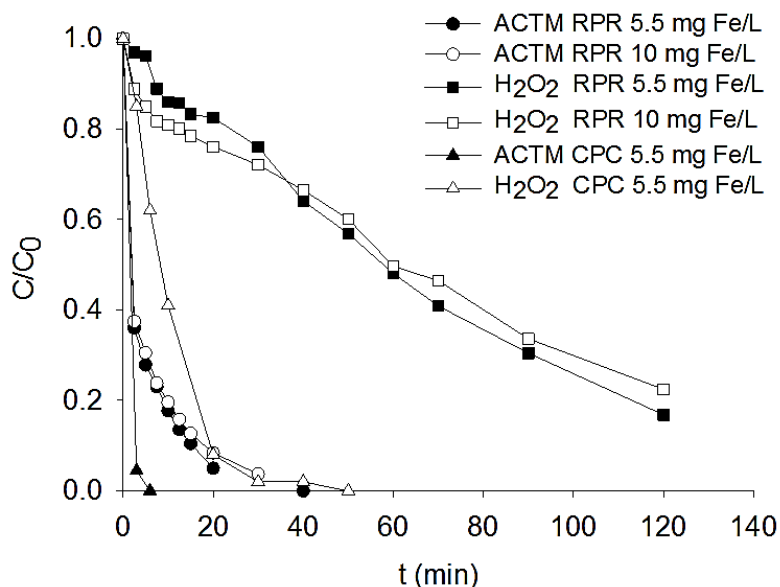


**Figure 3.26.** Acetamidiprid degradation and hydrogen peroxide consumption in simulated secondary effluent by solar photo-Fenton in 15 cm liquid-depth-RPR with 5.5 and 10 mg Fe/L, and in 5 cm diameter-CPC with 5.5 mg Fe/L.

In the RPR, ACTM as well as hydrogen peroxide degradation profiles were analogous for both iron concentrations, validating the effects observed in natural water and excluding a detrimental effect provoked by scavengers of HO<sup>•</sup> or light absorption. Nevertheless the ACTM degradation kinetic constant was 0.01 min<sup>-1</sup> in the secondary effluent; while the constant in natural water was 0.08 min<sup>-1</sup>. This is due to the difference in organic matter and salts in both water matrices. DOC mineralization was negligible. On the other hand, as expected, ACTM degradation and hydrogen peroxide consumption were faster in CPC than in RPR, due to the higher ratio area/volume in the CPC.

Another approach to take into account that the treated volume changes with depth is the treatment capacity, expressed as the mass of oxidised pollutant per unit of time and surface of reactor exposed to radiation, mg/h·m<sup>2</sup>. This parameter considers the photoreactor surface, volume and efficiency as it is important to compare with other reactors. For instance, for the RPR 150 L of water were treated per square meter for 15 cm depth (150 L/m<sup>2</sup>). The ratio volume/surface of the CPC reactor was 14.6 L/m<sup>2</sup>. This analysis allows knowing the reactor performance as a function of the mass of oxidised pollutant.

In this sense, from the discussion above it can be concluded that the treatment capacity to remove ACTM and TBZ increases linearly with liquid depth when the volumetric removal rate does not depend on liquid depth, as is the case for low iron concentration. As for the relationship between the capacity and Fe concentration, it is different for each liquid depth. For low depth (5 cm), treatment capacity increases with Fe concentration because for the same treated volume the addition of more catalyst produces faster removal rate. For deeper liquid depths though, increasing Fe concentration can give rise to a situation where not all iron ions can be photoactivated and process rate is not improved. This occurred with 15 cm liquid depth (360 L treated volume) and 10 mg Fe/L. The RPR treatment capacity was 48 mg/h·m<sup>2</sup> for 5.5 or 10 mg Fe/L, so the best condition corresponded to the lower iron concentration. On the other hand, although the CPC photoreactor with 5.5 mg Fe/L gave the highest pesticide removal rate, the treatment capacity was 29 mg/h·m<sup>2</sup>, 40% lower than RPR. It is necessary to remark that CPC optimal concentration for photo-Fenton is in the range of 20 mg Fe/L for 5-cm tube diameter (Malato et al., 2004). But 20 mg Fe/L is too high concentration for the treatment of micropollutants, reinforcing the idea that extensive and non-concentrating solar photoreactors could be a good alternative for working at high light path length, large volumes and short treatment time with low iron concentration.

The presented results showed the efficiency and feasibility of using RPRs at low iron concentration for micropollutant removal with solar photo-Fenton. RPRs involve simple design and materials and it would significantly reduce amortization costs compared with CPCs for this application.

In addition, at this pollutant concentration the Fenton process can have certain significance. As a result, the combination of solar photo-Fenton and Fenton for continuous operation could be worth studying in future works. These facts encourage the use of RPR at commercial scale as tertiary treatment.

#### **3.2.4.2 Monitoring of transformation products**

An important aspect of AOPs is that degradation occurs through oxidation steps, meaning that different transformation products (TPs) are generated during the treatment (Konstantinou et al., 2014). The parent molecule can be completely removed, but partially oxidised molecules remain. TPs generated during degradation can be persistent and even hazardous (Farré et al., 2008; Köck-Schulmeyer et al.,

2013). Nonetheless, the low concentration levels at which pollutants and their TPs are found in waters make them undetectable if advanced analytical techniques are not used.

In this Section, the transformation products of TBZ and ACTM were monitored in collaboration with the Environmental Analysis and Water Treatment Research Group in CIESOL with Prof. Ana Agüera as head researcher and Dr. Carla Sirtori from the Instituto de Química-UFRGS in Porto Alegre (Brazil), who used the advanced analytical techniques LC-QLiT-MS/MS (liquid chromatography-triple quadrupole-linear ion trap-mass spectrometer) and LC-QTOF-MS/MS (liquid chromatography-quadrupole time-of-flight mass spectrometry) for the monitoring and identification of TPs.

#### **a) Monitoring of thiabendazole transformation products at laboratory scale**

A first study was carried out at laboratory scale to determine if the transformation products could be monitored in real wastewater effluent. In this case, TBZ was used as model pollutant. TBZ is the most abundant micropollutant found in the effluent of the in-situ SBR placed in the agrofood industry Cítricos del Andarax S. A. As the production of the industry changes seasonally, the concentration of TBZ in the effluent varies during the year, but ~4 µg/L could be detected in some of the seasons.

In a first stage, TBZ's TPs were identified. The identification was performed with the same amount of TBZ as in Fenton and photo-Fenton experiments, 100 µg/L. For the identification of TPs, deionised water was used in a 5-L stirred tank reactor to avoid interferences caused by the complex real wastewater effluents. The study did not intend to propose a complete transformation pathway, but to identify those intermediates more relevant by their abundance or persistence, at the low concentration level used in the experiments. The treatment chosen for identification was Fenton with iron additions at natural pH every 15 min. Four additions of increasing amounts of Fe (5-5-10-20 mg/L) were used to avoid rapid disappearance of the TPs generated during the treatment. The lower iron concentration at the start would allow the process to be slowed down, favouring the persistence of the intermediates in solution and thus their identification. Four doses of 12.5 mg/L hydrogen peroxide were also added in order to guarantee the presence of a high enough quantity of this

reactive during the experiments. Figure 3.27 shows the details of the experiment as well as the evolution of the TBZ concentration.

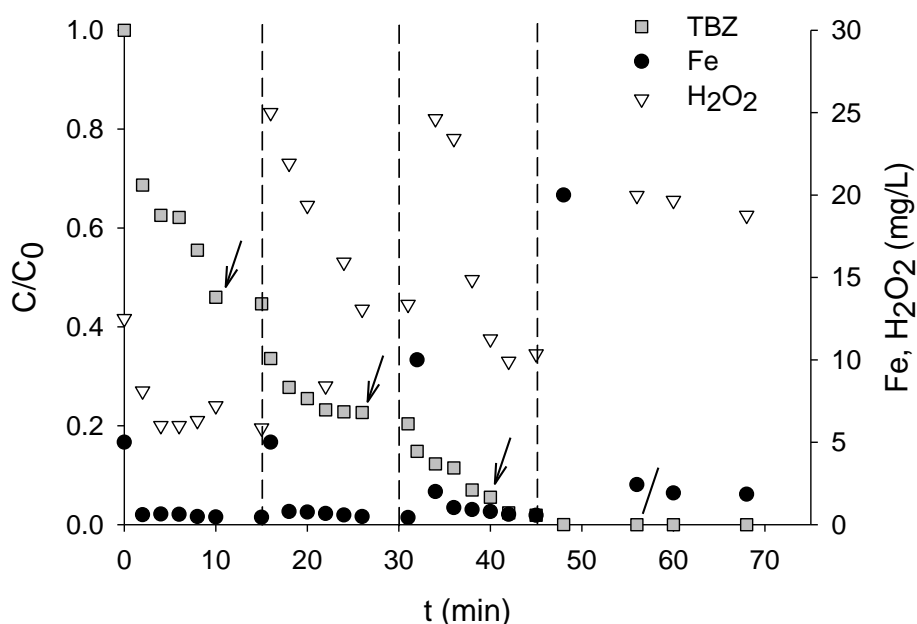


**Figure 3.27.** Details of thiabendazole degradation (100  $\mu\text{g/L}$ ) in deionised water and natural pH by Fenton with iron dosing (5-5-10-20 mg/L) for TPs identification.

Samples for TPs analysis are marked by arrows.

TBZ degradation was evaluated and monitored by direct injection of the filtered samples into a hybrid triple quadrupole/linear ion trap mass spectrometer system (5500 QTRAP® LC/MS/MS, AB Sciex Instruments, Foster City, CA) equipped with an electrospray ion (ESI) source and coupled to an Agilent 1200 Series HPLC system (Agilent Technologies, Wilmington, DE, USA). The analytical column employed was a reversed-phase. Identification of TPs was performed by liquid chromatography-time-of-flight mass spectrometry (LC-TOF-MS).

Because of the low initial concentration of TBZ and in order to increase the detectability of the TPs, the samples were pre-concentrated. However, direct injection of the samples was also done in order to identify compounds that could escape to the extraction procedure applied. Up to four TPs (TP1-TP4) could be detected in the samples. Figure 3.28 shows the evolution of the four TPs identified during the Fenton experiment. They reach their maximum concentration after the second addition of 5 mg/L iron, corresponding with a disappearance of around 75% of TBZ, TP formation rate being higher at this time than the degradation rate. Conversely, TP formation rate decreases with the two following iron additions. The structure of TP1 and TP2 were

determined by the Environmental Analysis and Water Treatment research group (Figure 3.28). TP1 and TP2 corresponded to the hydrolysis of the TBZ molecule. TP3 and TP4 corresponded to mono-hydroxylated derivatives, typically generated under hydroxyl radicals driven processes. However, available information was not enough to determine position in which the HO<sup>•</sup> radical attack occurred, and therefore their structure could not be determined.

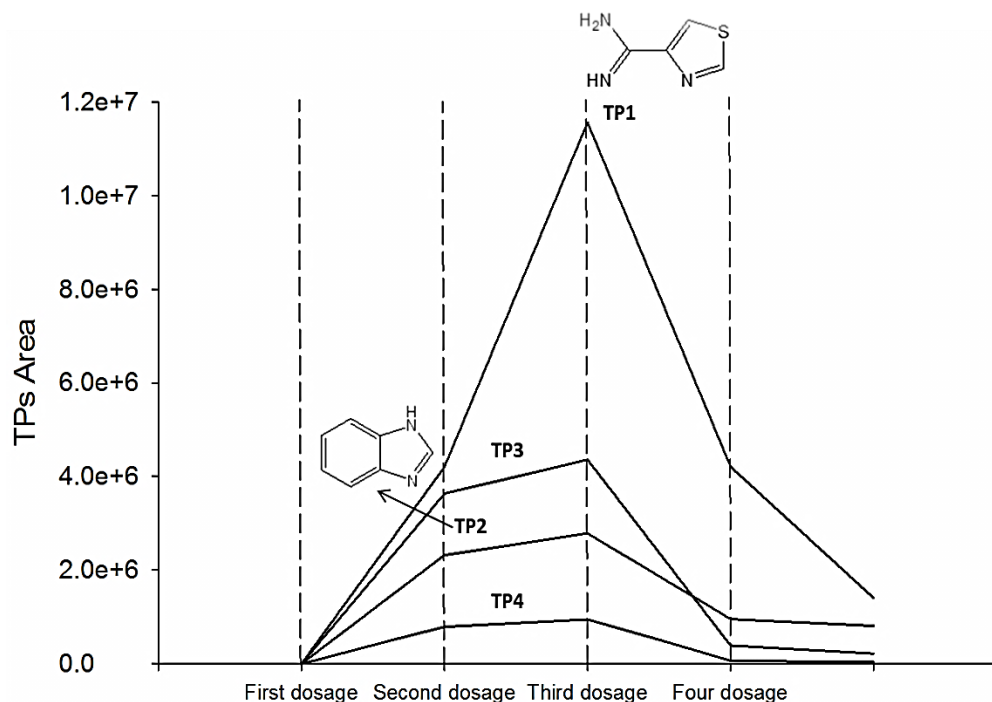


**Figure 3.28.** Evolution of TPs formed during thiabendazole degradation by Fenton.

In order to evaluate their persistence under the Fenton and photo-Fenton conditions, new degradation experiments were carried out. The water matrix was the effluent of a laboratory scale 7-L MBR operated in CIESOL. The MBR was fed with simulated wastewater: 3.2 mg/L of beef extract, 6.4 mg/L yeast extract, 16 mg/L of peptone, 0.8 mL/L of glycerol (87% v/v) and mineral salts (16 mg/L NaCl, 0.5 g/L K<sub>2</sub>HPO<sub>4</sub>, 0.5 g/L KH<sub>2</sub>PO<sub>4</sub>, 0.5 g/L MgSO<sub>4</sub>·7H<sub>2</sub>O and 10 mL/L of trace mineral solution). DOC was 350 mg/L in the influent and 11 mg/L in the effluent. The concentration of mixed liquor volatile suspended solids (MLVSS) was 11 g/L and mixed liquor total suspended solids (MLTSS) concentration was always lower than 15 g/L in the MBR. The mean pH value was 7.5.

Solar photo-Fenton and Fenton treatments were carried out at pH 7 without bicarbonates in borosilicate cylindrical stirred reactors. Total volume was 5 L. Both Fenton and photo-Fenton were run with MBR effluent as the water matrix and doped

with 100 µg/L TBZ. Photo-Fenton was also carried out at pH 2.8 in deionised water and MBR effluent as references. The experimental conditions are shown in Table 3.13.

**Table 3.13.** Experimental conditions for the degradation experiments.

Experimental conditions			
<b>Water matrix</b>	MBR effluent	MBR effluent	Deionised water
<b>Treatment</b>	Fenton	Photo-Fenton	Photo-Fenton
<b>pH</b>	7	7, 2.8	2.8
<b>Iron dosage (mg/ L)</b>	20-20-20	20-20-20	20
<b>H<sub>2</sub>O<sub>2</sub> dosage (mg/L)</b>	100-50	100-50	100-50

Hydrogen peroxide additions were made every 10 min. For the Fenton treatment the reactors were completely covered and for photo-Fenton experimentation was carried out outdoors at noon, when solar radiation was mostly constant. Mean UV radiation and temperature values were  $21 \pm 2 \text{ W m}^{-2}$  and  $25.0 \pm 0.3^\circ\text{C}$ , respectively. Iron additions were made every five minutes using iron solutions prepared before each test. Results are shown in Figure 3.29.

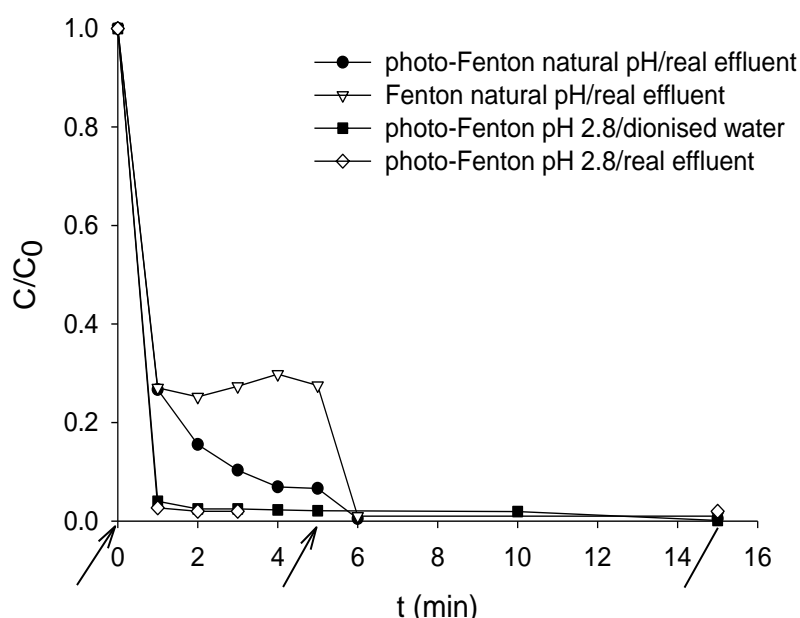


**Figure 3.29.** Thiabendazole degradation in MBR effluent treated by Fenton and photo-Fenton at initial neutral pH; in MBR effluent at pH 2.8 by photo-Fenton; and in deionised water at pH 2.8 by photo-Fenton. Iron additions are marked by arrows.

The MBR effluent treatment with Fenton and photo-Fenton at natural pH resulted in 99.9 % TBZ degradation with only two iron additions in both processes. After that, TBZ concentration was stabilized in both Fenton and photo-Fenton at around 0.09 µg/L (Figure 3.29). Nevertheless, degradation profiles were not the same for either treatment. When the first addition is made, regardless of whether the reactor is irradiated or not, the ferrous iron oxidation takes place yielding hydroxyl radicals (Equation 1.13). This reaction occurs in both Fenton and photo-Fenton and the effect can be observed after 1 min of treatment, where TBZ concentration drops to the same value in both processes (~27 µg/L). Subsequently, Fe<sup>2+</sup> reduction to Fe<sup>3+</sup> takes place through Reaction 1.14 for the photo-Fenton process and through Reaction 1.18 for Fenton, which is slower. However, iron reduction is hindered at natural pH in both cases due to Fe<sup>3+</sup> hydrolysis and subsequent precipitation of iron hydroxide. As a result, pH decreases from 7.0 to 3.4.

As a consequence of the kinetic difference between Reactions 1.14 and 1.18, iron precipitation is slowed down during the photo-Fenton process due to the rapid iron reduction. Thus, between minute 1 and minute 5 (just before the second iron addition) TBZ degradation by dark Fenton stops since iron is precipitated; while the degradation in that interval by photo-Fenton still continues and fits a first-order kinetic, with a constant  $k = 0.402 \text{ min}^{-1}$  ( $r^2 = 0.92$ ).

The second iron addition causes quick new generation of hydroxyl radicals (Reaction 1.13) which degrade TBZ down to the final concentration of 0.09 µg/L. This concentration remained stable in spite of the third iron addition. The identified TPs were sought in the samples taken after the second and third iron additions, which was when residual concentrations of the parent molecule were detected, but none could be detected after the second addition of iron, confirming the efficacy of the treatment for the elimination not only of TBZ but also of its TPs.

To check TBZ degradation under optimal photo-Fenton conditions, an assay with 100 µg/L TBZ dissolved in deionised water and pH 2.8 was carried out. 99.9% TBZ degradation was achieved in 2 min, while at initial neutral pH 93.4% TBZ removal was reached in 5 min using the same iron dose (20 mg/L). As commented above, to reach 99.9% TBZ degradation, a second iron dose was necessary in the experiment without pH adjustment and MBR effluent. For the three oxidation alternatives assayed the same trace concentration of 0.09 µg/L TBZ was detected at the end of the experiments.

Concerning hydrogen peroxide concentration, reactant consumption was greater in DW than in the MBR effluent. This is to be expected, since inorganic ions and organic matter present in the MBR effluent react with hydroxyl radicals in competition with the target pollutant and hydrogen peroxide.

Nevertheless, it must be pointed out that although iron profiles in both processes are analogous at the beginning of treatment, after the third addition iron concentration was over 5 mg/L higher with photo-Fenton. This is so because at that point the pH is already acidic and iron hydrolysis is not so strong, so the iron redox cycle takes place more often in the photo-Fenton process, partially preventing precipitation. The difference in iron concentration between Fenton and photo-Fenton after 10 min of treatment would also involve differences in TBZ degradation, but this compound is already degraded by this time. Indeed, if the conditions needed were stronger or the process required more time (e.g. when working at a concentration level of mg/L instead of  $\mu\text{g/L}$ ), differences between pollutant degradation in the Fenton and photo-Fenton processes would be quite significant. Following this, it could also be interpreted that the treatment at  $\mu\text{g/L}$  scale of a pollutant with a more persistent nature than TBZ (which would also need a longer treatment) would involve more noteworthy differences between Fenton and photo-Fenton as well.

From a general analysis of the presented results, 99.9% TBZ removal was achieved with two iron additions (40 mg/L Fe) and one dose of hydrogen peroxide (100 mg/L  $\text{H}_2\text{O}_2$ ) with both Fenton and photo-Fenton processes, the precipitated iron hydroxides being further removed by sedimentation/ filtration. Therefore, no significant differences were observed to justify the application of photo-Fenton to this pollutant. Nonetheless, a case by case study is recommended as differences between both processes will depend on the concentration scale and the persistent nature of the target compound

Since TBZ's TPs could be monitored during the treatment of real effluent at the low concentration used in the experiments, the next stage of research was the monitoring of ACTM's and TBZ's TPs during the treatment of real wastewater in the RPR.



### **b) Monitoring of acetamiprid and thiabendazole transformation products during the treatment of industrial effluent in the raceway pond reactor**

In the previous Section it was proved that TBZ TPs could be monitored in real wastewater at micropollutant concentration (100 µg/L). The aim of this research was to monitor the TPs of TBZ and ACTM during their degradation under solar photo-Fenton in the raceway at pH 2.8. This work was also done in collaboration with the Environmental Analysis and Water Treatment Research Group in CIESOL. In this case, the LC-QLiT-MS/MS instrument was used to monitor the TPs.

The water matrix was the effluent from the in-situ SBR in Cítricos del Andarax S. A, with high conductivity. The properties of the effluent were: pH 8.7, 12 mg/L DOC, 214 mg/L carbonates, 5.2 mS/cm, 511 mg/L chloride and 1133 mg/L sulphate, 2 mg/L nitrate, 3 mg/L phosphate. In this work, 120 L (5 cm liquid depth in the RPR) were used.

Before the tests, the effluent went through a filtration system comprising two cartridge filters. The first one had a pore diameter of 100 µm and it was connected to a second filter with a pore diameter of 20 µm. It was then enriched with 100 µg/L of commercial ACTM (EPIK®) and TBZ (TEXTAR 60®) (200 µg/L in total).

A set of laboratory tests was carried out with the aim of determining a combination of hydrogen peroxide and iron concentrations which resulted in rapid degradation of the pollutant mixture, and subsequently using it in the RPR at pilot plant scale. The experimental conditions are displayed in Table 3.14. 1-L borosilicate stirred tank reactors were used for the solar photo-Fenton assays. High concentrations of hydrogen peroxide and iron were tried due to the high salinity of water. The central condition was replicated five times to determine the experimental error, which was determined to be below 7%. Average UV irradiance was  $14\pm 2$  W/m<sup>2</sup> and average temperature was  $25\pm 2$  °C.

The results after 120 min are shown in Figure 3.30. Approximately 98% of TBZ was removed under all conditions in less than 5 min. ACTM, however, proved to be more persistent. The least efficient condition in terms of ACTM removal was 10 mg Fe/L - 50 mg H<sub>2</sub>O<sub>2</sub>/L. In this instance, approximately 70% of ACTM was degraded, consuming over 30 mg/L of hydrogen peroxide. With 15 mg Fe/L - 75 mg H<sub>2</sub>O<sub>2</sub>/L

approximately 80% of ACTM was degraded and 50 mg/L hydrogen peroxide consumed.

**Table 3.14.** Experimental conditions used with 1-L reactors.

Fe <sup>2+</sup> (mg/L)	H <sub>2</sub> O <sub>2</sub> (mg/L)
10	50
15	75
15	75
15	75
25	100

The operating condition 25 mg Fe/L-100 mg H<sub>2</sub>O<sub>2</sub>/L it allowed 91% ACTM degradation. Hydrogen peroxide consumption in this case was close to 80 mg/L. In the presence of hydrogen peroxide excess inefficient reactions between radicals and hydrogen peroxide-radicals are favoured and this increases consumption (Figure 3.30). As a result, this combination was used for the experiment at pilot plant scale in the RPR.

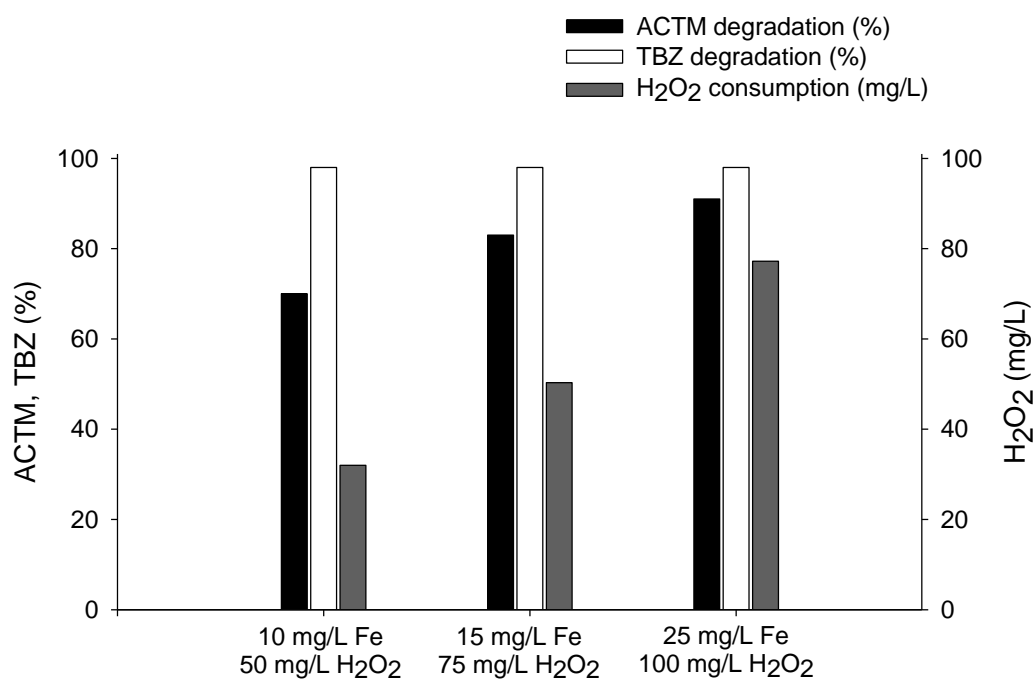


**Figure 3.30.** Acetamiprid and thiabendazole degradation and hydrogen peroxide consumption after 120 min of solar photo-Fenton (14 W/m<sup>2</sup>).

At pilot plant scale in the RPR both the photo-Fenton and Fenton processes were carried out (120 L, 5 cm liquid depth), keeping the RPR covered for Fenton. The average UV irradiance was  $15\pm 1$  W/m<sup>2</sup>. Average temperature was  $26\pm 2$  °C. ACTM and TBZ degradation in these conditions during Fenton and photo-Fenton treatments are shown in Figure 3.31.

Adding the catalyst in the form of ferrous iron, as was the present case, initiated the process through Equation 1.13. This reaction is independent of UV-light, so its effect was the same for both Fenton and photo-Fenton. This effect can be seen in the first degradation step in Figure 3.31. Thanks to this reaction high ACTM and TBZ removal was achieved during the first few minutes. Almost 40% oxidation was achieved for ACTM and more than 99% of TBZ was degraded.

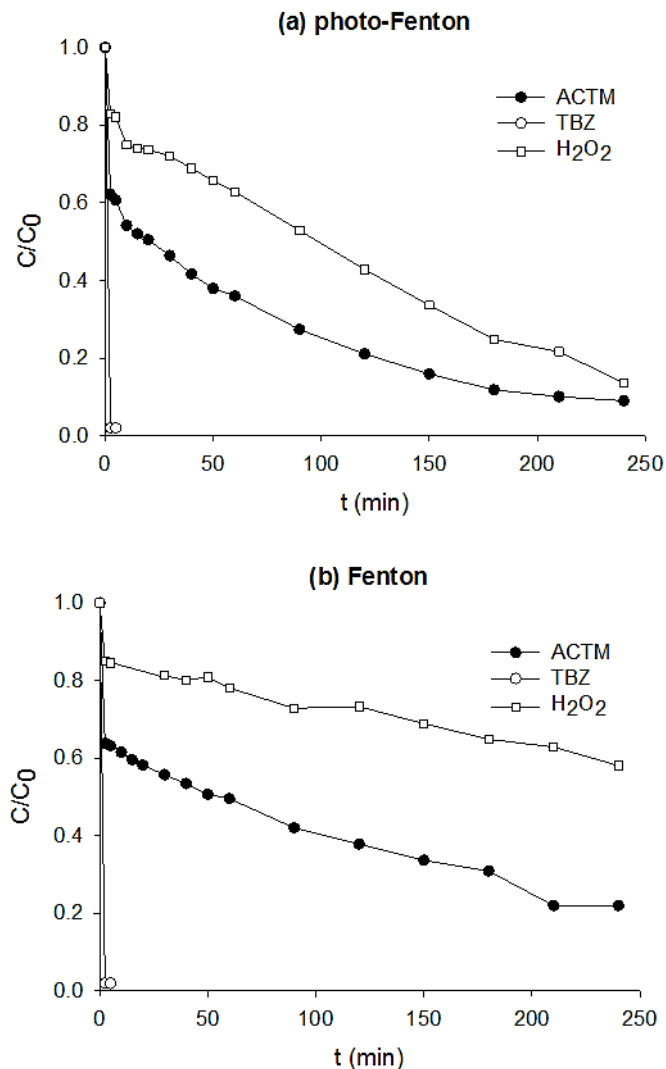


**Figure 3.31.** ACTM and TBZ degradation in industrial effluent by (a) solar photo-Fenton ( $15$  W/m<sup>2</sup>) and (b) Fenton in the RPR, both with  $25$  mg Fe/L- $100$  mg H<sub>2</sub>O<sub>2</sub>/L.

After the first reaction stage takes place, ferric iron is reduced to ferrous iron, thus, closing the redox iron cycle and degradation is progressive. In the Fenton process this reduction happens through Equation 1.18, which yields perhydroxyl radicals and consumes hydrogen peroxide. These radicals are less oxidant than hydroxyl radicals. In the photo-Fenton process, however, ferric iron reduction occurs via solar radiation (Equation 1.14), which is faster. After the initial degradation, ACTM profiles in both Fenton and photo-Fenton adjusted a pseudo-first order rate. For TBZ this effect could not be appreciated since its degradation was very fast.

After 120 min of photo-Fenton reaction, 80% ACTM degradation could be observed. However, after twice that length of time, in 240 min, it was 91%. As the number of parent molecules decrease, so does the probability of reaction with hydroxyl radicals. On the other hand, after 120 min of Fenton reaction ACTM oxidation was 62% and 78% after 240 min. Hydrogen peroxide consumption was also different in both processes: 85 mg/L were consumed during photo-Fenton and 40 mg/L in Fenton.

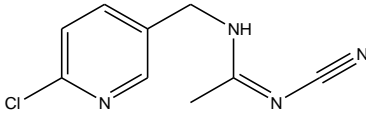
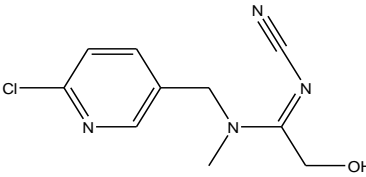
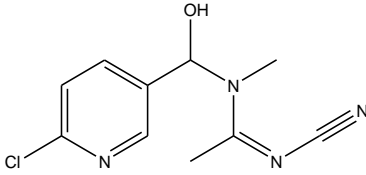
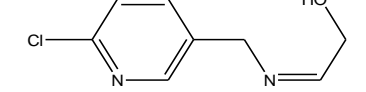
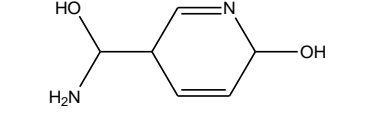
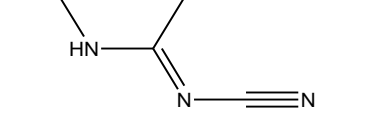
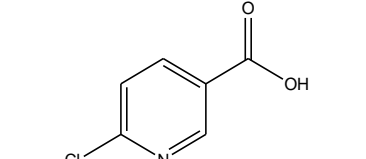
As for the kinetics, 0.54 and 0.30 h<sup>-1</sup> were the calculated pseudo-first order constants for ACTM degradation in photo-Fenton and Fenton, respectively. Although the difference between Fenton and photo-Fenton was significant, the use of 25 mg Fe/L was enough to achieve relatively high oxidation with Fenton. This is an important fact since it means the process could also be run in a RPR on cloudy days, although at a lower rate.

The slow kinetics was due to the complexity of the water matrix. DOC concentration was not high (12 mg/L), but it presented high conductivity mainly due to sulphate ions and chloride ions. The latter are detrimental to Fenton and photo-Fenton (Buxton et al., 1988). As a consequence, the presence of all these species and compounds in the industrial effluent bring about as a consequence a decrease in the efficiency of the process and the kinetics. Also, the most photoactive and abundant iron species in demineralised water at pH 2.8 is the iron aqua-complex Fe(OH)<sup>2+</sup>. However, in the presence of other ions and organic matter the distribution of iron species in water may change. Chloride ions can form iron complexes. These species can absorb light, forming chlorine radicals, which are less oxidant than hydroxyl radicals ( $E^0_{OH}=2.80$  V versus  $E^0_{Cl}=1.36$  V) but they are reacting with Fe, precluding the participation of Fe in Fenton and photo-Fenton reactions. Additionally, chloride ions act as a radical scavenger (Laat et al., 2004) (see Section 1.4.2).

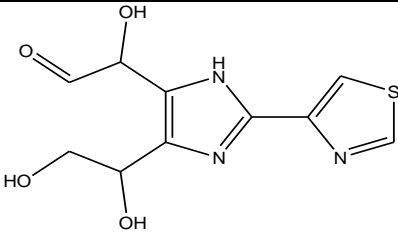
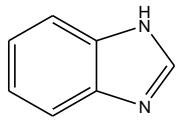
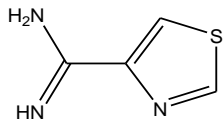
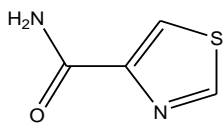
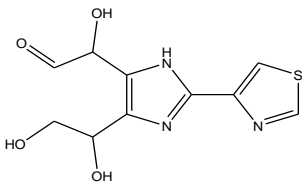
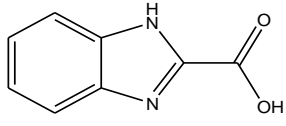
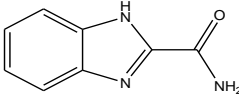
Regarding the effect of sulphate ions, analogous with chloride, iron complexes may be formed, reacting with Fe, absorbing photons and generating sulphate radicals, which are also less oxidant than hydroxyl radicals. Additionally, sulphate ions can also act as hydroxyl radical scavengers (Laa et al., 2004) (See Section 1.4.2).

Additionally, during the photo-Fenton treatment, samples were taken to monitor ACTM's and TBZ's TPs. Previous studies reported the identification of major TPs of ACTM and TBZ, seven TPs for each (Sirtori et al., 2014a; Sirtori et al., 2014b). They are shown in Tables 3.15 and 3.16. In the case of TBZ, two of them corresponded to TP1 and TP4 in Section 3.2.4.2.1 (TBZ-TP129 and TBZ-TP270, respectively).

**Table 3.15.** Structure of acetamiprid transformation products during photo-Fenton treatment analyzed by LC-QqLIT-MS.

TP	Structure
ACTM-TP209	
ACTM-TP239a	
ACTM-TP239b	
ACTM-TP185	
ACTM-TP143	
ACTM-TP98	
ACTM-TP158	

**Table 3.16.** Structure of thiabendazole transformation products during photo-Fenton treatment analyzed by LC-QqLIT-MS.

TP	Structure
TBZ-TP270	
TBZ-TP119	
TBZ-TP128	
TBZ-TP129	
TBZ-TP268	
TBZ-TP163	
TBZ-TP162	

The higher level of stability of some of the TPs identified with respect to the parent compound and the influence of the matrix composition in the degradation behavior were in evidence (Figure 3.32), highlighting that monitoring of both parents and TPs is mandatory to provide a comprehensive assessment of water treatment efficiency.

Most of ACTM's TPs showed an appearance/disappearance profile, consequence of their efficient elimination by the oxidative treatment (Figure 3.32a).

Such is also the case of TP239a, TP185, TP143 and TP158. In contrast, TP209, TP239b and TP98 resulted in being more stable compounds, persisting at the end of the treatments. TP209 corresponded to a demethylated derivative and was the most abundant intermediate detected. TP98 could only be detected only after 120 min of treatment, during that time experiencing a continuous increase in concentration until the end of the experiments.

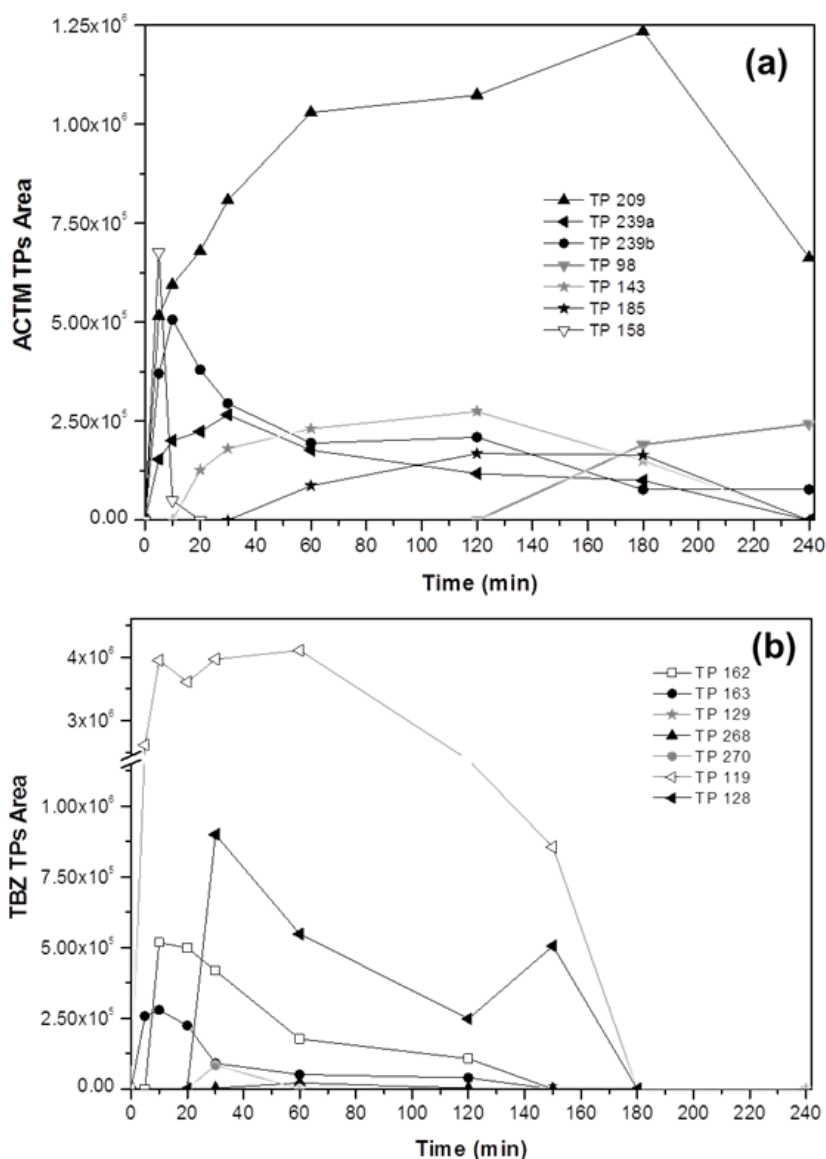


**Figure 3.32.** Time profile of (a) acetamiprid TPs; (b) and thiabendazol TPs during photo-Fenton treatment of the SBR effluent from the agro-food industry.

Another seven additional TPs were also observed from the transformation of TBZ (Figure 3.32b). They appeared at the first stages of the treatment and after reaching a maximum, between the 10 to 50 minutes of photo-Fenton reaction, going

through a continuous decrease until their total disappearance after 180 min. TP119 and TP128 were the most abundant TPs.

The results obtained indicate that the photo-Fenton process is an efficient treatment for eliminating pesticides and their TPs in industrial wastewater, although monitoring of the TPs must be taken into account in the optimization of the treatments as a consequence of the higher stability exhibited by the TPs identified. These results showed the feasibility of the RPR as technology for the removal of micropollutants in industrial effluent with high conductivity. Fenton and photo-Fenton proved to be similar in terms of degradation rate, although it should be noted that the experiments were carried out in winter with low irradiance. Summer conditions should no doubt increase the difference between both processes.

Thanks to the use of the advanced analytical instrument LC-QqLIT-MS/MS the monitoring of selected TPs of TBZ and ACTM during the treatment was possible. From the results it can be concluded that the process operation should take into consideration the degradation of TPs, since some of them proved to be as persistent as the parent molecule and treatment times can change depending on the objective (parent molecule removal or TPs removal).

### **3.2.5 Use of lamps to run the photo-Fenton process**

Bearing in mind the strategies learned the operation of the photo-Fenton process was also studied under artificial light. This study was made during a three-month placement in the Water Science Institute in Cranfield University (United Kingdom). Firstly, UVC low pressure lamps were used to compare the performance of the photo-Fenton process with other AOP systems such as persulphate, hydrogen peroxide photolysis and heterogeneous photocatalysis ( $\text{TiO}_2$ ) to remove the most persistent model pollutant used in this thesis, acetamiprid. Secondly, high intensity UVC light emitting diodes (LEDs) were also tested as low energy-consuming technology for photo-Fenton applications.

#### **a) UVC low pressure lamps**

The way in which AOPs generate radicals changes from one AOP to another. For instance, UV/ $\text{TiO}_2$  yields hydroxyl radicals through a semiconductor; while the photo-Fenton process generates them by a photochemical process. This gives a



difference in radical generation efficiency. This difference is also affected by the water matrix. For instance, the performance of AOPs in drinking water is influenced mainly by ions such as bicarbonates. However, their performance in wastewater effluent is more complex since the concentration of salts and organic matter is higher. As a result, a comparison of AOPs will vary in each matrix.

In this Section the performance of several AOPs as tertiary treatment to remove acetamiprid in different water matrices was evaluated. Specifically, UVC /TiO<sub>2</sub>, UVC/H<sub>2</sub>O<sub>2</sub>/Fe. Two systems with persulphate (PS) were also assessed: UVC/PS and UVC/PS/Fe. UV photolysis was also tested as reference. AOP operation was assessed in deionised water and in simulated secondary treated wastewater. The operating condition for each AOP which resulted in the fastest degradation rate was then used in real conventional activated sludge (CAS) effluent (Table 3.17). The system H<sub>2</sub>O<sub>2</sub>/Fe was also included as reference for the photo-Fenton process. Additionally, the effect of humic acids, lignin-derivate compound and lauryl sulphate on acetamiprid degradation was investigated.

The UV experiments were conducted with the UVC low pressure lamp system described in Section 2.6.3, emitting at 254 nm. The UV irradiance used in all experiments was 20 W/m<sup>2</sup>, except when UVC photolysis was studied. In that case, irradiance values of 10 and 27 W/m<sup>2</sup> were also used. ACTM degradation by hydrogen peroxide and PS in the dark was also assessed and shown to be insignificant. Adsorption of the pesticide on to TiO<sub>2</sub> and the organic matter studied was also shown to be negligible. The experimental error for measurement of acetamiprid, hydrogen peroxide, PS and iron concentrations was determined by replicating the central condition for each AOP (Table 3.17). The error was 5%, 8%, 10% and 6% for acetamiprid, hydrogen peroxide, PS, and iron, respectively.

#### Acetamiprid degradation in deionised water and simulated effluent

The acetamiprid degradation over time for each operating condition in deionised water (Figure 3.33) and simulated effluent (Figure 3.34) was very different depending on the AOP under investigation. UV photolysis was the slowest process (Figure 3.33a). Three UV intensities were investigated (10, 20 and 27 W/m<sup>2</sup>). Complete acetamiprid removal was achieved in deionised water at 90 min at 10 W/m<sup>2</sup> and after 60 min with the two highest intensities, indicating irradiance saturation. This meant that at 20 W/m<sup>2</sup> enough photons were added to the water to degrade acetamiprid molecules and so the

reaction could not be made any faster. This irradiation value was used for the rest of the systems studied. Irradiance saturation was again observed in simulated effluent (Figure 3.34a), corroborating this effect. However, in simulated effluent acetamiprid removal was much slower and achieved only after 180 min.

**Table 3.17.** Operating conditions assayed in deionised and simulated water with the low pressure lamps.

Process	I (W/m <sup>2</sup> )	H <sub>2</sub> O <sub>2</sub> (mg/L)	pH	TiO <sub>2</sub> (mg/L)	PS (mg/L)
UV photolysis	10		natural		
	20	-	natural	-	
	27		natural		
TiO <sub>2</sub> /UV			natural	50	
	20	-	natural	100	
			neutral	200	
UV/H <sub>2</sub> O <sub>2</sub>		25	natural		
	20	50	natural	-	
		100	natural		
UV/H <sub>2</sub> O <sub>2</sub> /Fe (1 mg Fe/L)		50	2.8		
	20	50	natural	-	
		50	natural		
H <sub>2</sub> O <sub>2</sub> /Fe (1 mg Fe/L)	20	50	natural	-	
UV/PS			natural		25
	20	-	natural	-	50
			natural		100
UV/PS/Fe (1 mg Fe/L)	20	-	natural	-	50

UV/TiO<sub>2</sub> was run using 50, 100 and 200 mg TiO<sub>2</sub>/L at 20 W/m<sup>2</sup> UVC, which are concentrations similar to those reported in other works for micropollutants (Autin et al., 2013; Jiménez et al., 2014). In deionised water, photocatalysis proved to be one of the fastest AOPs, removing acetamiprid in less than 1 min for all catalyst concentrations (data not shown due to fast degradation). Blank tests were run to determine acetamiprid adsorption on the catalyst and it was found negligible. However, in a more complex matrix (Figure 3.34b) acetamiprid degradation took 60 min in all cases,

matching the profile observed for photolysis at the same intensity (20 W/m<sup>2</sup>), showing that the photocatalytic reaction was slowed by components of the simulated effluent.

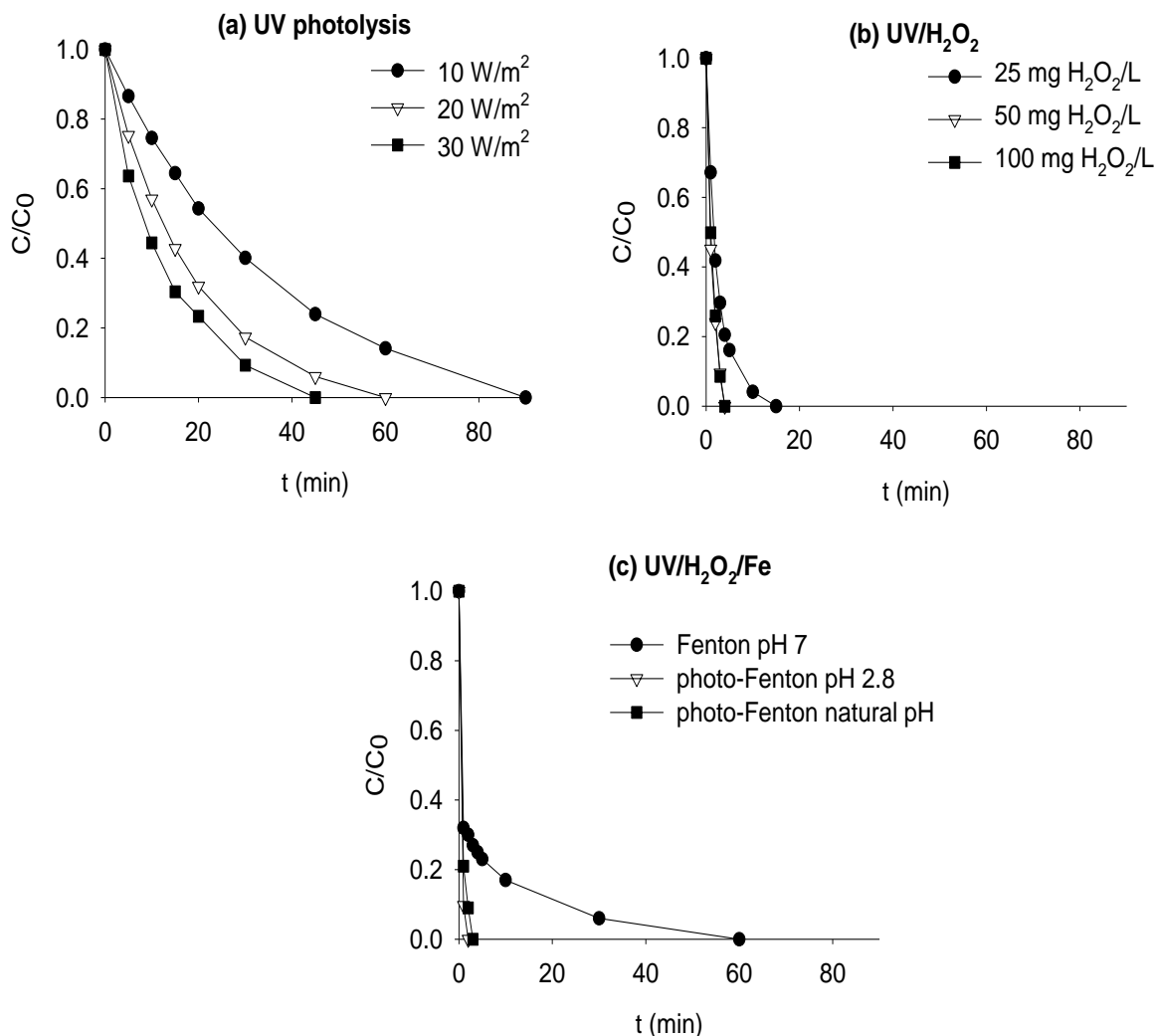


**Figure 3.33.** Acetamidrid degradation in deionised water and by (a) UV (10, 20, 27 W/m<sup>2</sup>); (b) UV/ H<sub>2</sub>O<sub>2</sub> (25, 50, 200 mg/L); (c) UV/H<sub>2</sub>O<sub>2</sub>/Fe (1mg Fe/L and 50 mg H<sub>2</sub>O<sub>2</sub>/L at pH 2.8; and at natural pH), H<sub>2</sub>O<sub>2</sub>/Fe (1 mg Fe/L and 50 mg H<sub>2</sub>O<sub>2</sub>/L at natural pH).

Pollutant degradation by heterogeneous photocatalysis involves the migration of electrons from the valence to the conduction band, leaving a charged hole in the valence band, and creating an electron–hole pair. Holes oxidise water and hydroxyl groups, yielding hydroxyl radicals that become available for oxidative reactions or directly oxidise organic compounds adsorbed on the solid surface. As a result, the efficiency of heterogeneous photocatalysis is highly dependent on the available holes on the catalyst surface. The presence of organic matter and anions in complex water matrices like simulated effluent can be detrimental for photocatalysis efficiency as they

can block or compete for sites on the catalyst surface (Blanco and Malato, 2003) and reduce the absorption of photons by the  $\text{TiO}_2$  (Gogate and Pandit, 2004).

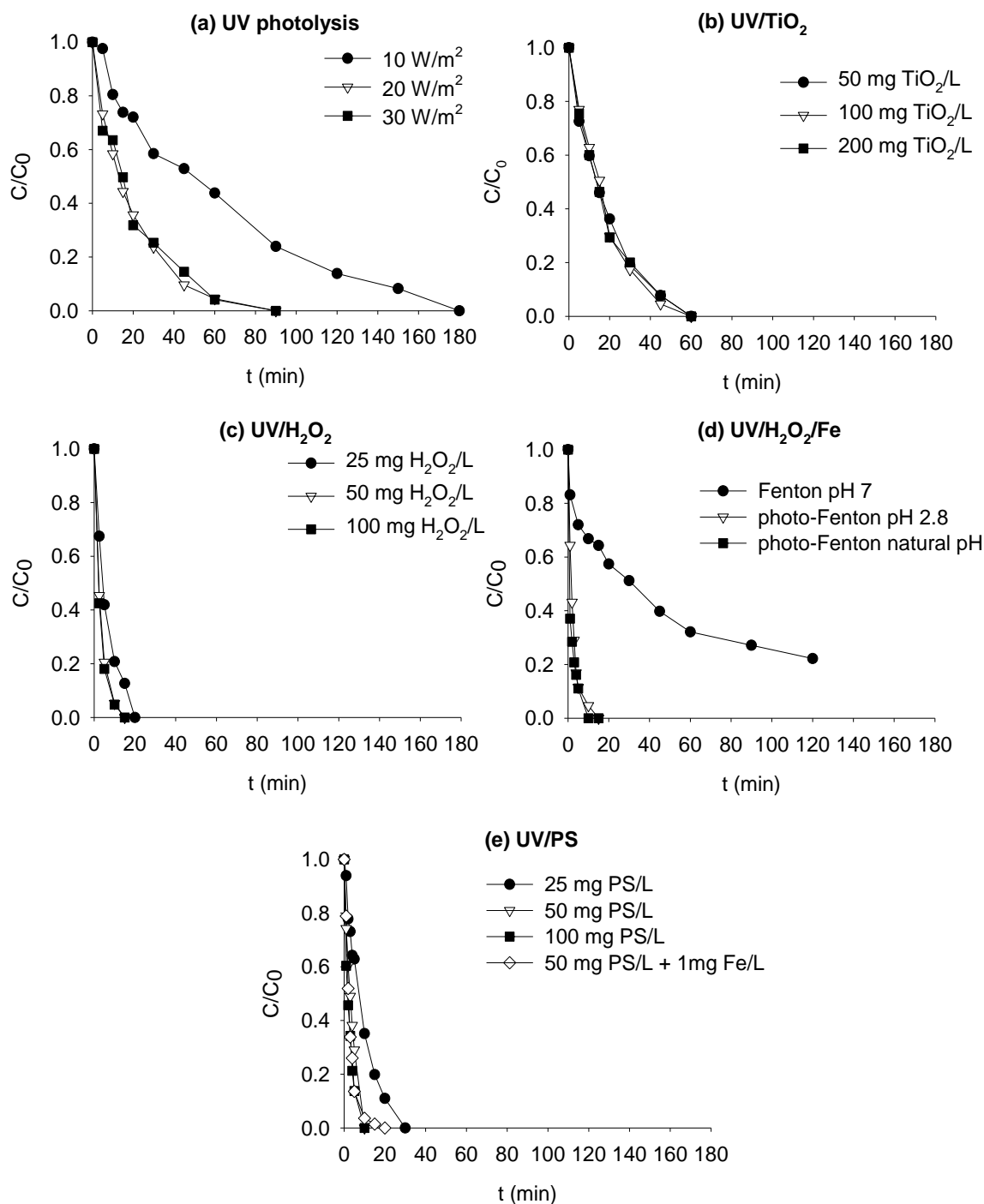


**Figure 3.34.** Acetamiprid degradation in simulated effluent by (a) UV (10, 20, 27  $\text{W/m}^2$ ); (b) UV/ $\text{TiO}_2$  (50, 100, 200  $\text{mg TiO}_2/\text{L}$ ); (c) UV/ $\text{H}_2\text{O}_2$  (25, 50, 100  $\text{mg/L}$ ); (d) UV/ $\text{H}_2\text{O}_2/\text{Fe}$  (1  $\text{mg Fe/L}$  and 50  $\text{mg H}_2\text{O}_2/\text{L}$  at pH 2.8 and at natural pH),  $\text{H}_2\text{O}_2/\text{Fe}$  (1  $\text{mg Fe/L}$  and 50  $\text{mg H}_2\text{O}_2/\text{L}$  at natural pH); (e) UV/PS (25, 50, 100  $\text{mg PS/L}$ ); UV/PS/Fe (50  $\text{mg PS/L}$  and 1  $\text{mg Fe/L}$ ).

In addition, the presence of alkalinity in the water causes  $\text{TiO}_2$  to aggregate, reducing the area available for surface reactions. This is an effect seen previously for degradation of the pesticide metaldehyde where degradation reduced by 93 to 45% from a low to high alkalinity water source (Keen and Linden, 2013).

Hydrogen peroxide photolysis was also assayed (UV/ $\text{H}_2\text{O}_2$ ) with a concentration of oxidant of 25, 50, 100 mg/L. This system has been reported as effective in the degradation of micropollutants from wastewater effluents using UV lamps (Keen and Linden, 2013). The acetamiprid removal profile was similar for 50 and 100 mg  $\text{H}_2\text{O}_2$ /L in either deionised water (Figure 3.33b) or simulated effluent (Figure 3.34c) (but slower in simulated effluent with complete removal in 5 and 15 min, respectively); while with 25 mg  $\text{H}_2\text{O}_2$ /L removal was much slower, but the pesticide was still degraded after 15 and 20 min for deionised water and simulated effluent respectively. Thus, the concentration of hydrogen peroxide which enabled the fastest removal with less oxidising agent was 50 mg/L.

This AOP is based on the cleavage of hydrogen peroxide (Section 1.3.2). This reaction yields two  $\text{HO}^\bullet$  by photon absorption at 254 nm. However, it should be noted that the molar absorption coefficient of hydrogen peroxide at 254 nm is approximately  $25 \text{ M}^{-1} \text{ cm}^{-1}$ . This means that the concentration of hydrogen peroxide required to generate enough radicals has to be high, especially in more complex matrices (Virikutyte et al., 2010). In fact, hydrogen peroxide consumption for complete pesticide removal was less than 15 mg/L in deionised water and 18 mg/L in simulated effluent in all cases.

To compare UV/ $\text{H}_2\text{O}_2$  and the photo-Fenton process (UV/ $\text{H}_2\text{O}_2$ /Fe), 1 mg  $\text{Fe}^{2+}$ /L was added to the best operating condition obtained from hydrogen peroxide photolysis (50 mg  $\text{H}_2\text{O}_2$ /L). This combination of low concentration of Fe and  $\text{H}_2\text{O}_2$  was assayed at pH 2.8 and the natural pH of the system, as well as in the absence of light (Fenton process) for reference. In both water matrices (Figure 3.33c and Figure 3.34d) acetamiprid degradation was fast and similar at both pH (5 min in deionised water and 15 min in simulated effluent). Although removal times were similar to hydrogen peroxide photolysis, degradation after 1 min of reaction was greater in the iron-catalysed systems. However, consumed hydrogen peroxide after removal was higher at pH 2.8 (38 and 30 mg/L in deionised water and simulated effluent) than at natural pH (29 and 20 mg/L in deionised water and simulated effluent). It should also be noted that the reagent consumption is due to the reaction with ferrous iron and hydrogen peroxide photolysis. In this system the main contribution to degradation came from hydrogen

peroxide photolysis, but even so, using a low iron concentration improved removal and reduced residual hydrogen peroxide concentration.

The reason why pesticide removal was analogous in photo-Fenton at both pH values was because degradation was too fast to observe any differences between the systems. The change in iron concentration was assessed during the different treatment conditions. At pH 2.8, the iron concentration was constant during the test since ferric iron is soluble at the acidic pH. At natural pH the iron concentration changed during the process due to ferric hydroxide precipitation. The measured iron concentration was 0.5 mg/L after the first minute and remained at that value over the duration of the reaction.

Other systems assayed were UV/PS and UV/PS/Fe. These AOPs generate sulphate radical anions,  $\text{SO}_4^{\cdot-}$ . To generate the radicals, PS was activated by irradiance (UV/PS) and electron transfer with iron (UV/PS/Fe). Sulphate radical anions present the advantage of being highly oxidative (2.6 V). They have also been reported to be more selective than hydroxyl radicals, with a higher affinity to remove electrons from aromatic rings (Anipsitakis and Dionysiou, 2010). This could mark a difference from oxidation by hydroxyl radical since acetamiprid has a ring in its molecular structure. Indeed, with 25 and 50 mg PS/L, acetamiprid degradation in deionised water was as fast as the photo-assisted Fenton, needing less than 5 min for complete removal (data not shown due to fast degradation). With 100 mg PS/L the process was faster, achieving removal in 1 min. The fact that the UV/PS system was slightly more effective than UV/H<sub>2</sub>O<sub>2</sub> was due to the higher molar absorption coefficient of PS at 254 nm, over two times higher than that of hydrogen peroxide (Anipsitakis and Dionysiou, 2010). To see the effect of Fe in the system, 1 mg Fe/L was added together with 50 mg PS/L. Results were analogous to 100 mg PS/L, needing half of the PS concentration. In simulated effluent (Figure 3.34e), 25 mg PS/L was not enough to result in rapid degradation (30 min for removal), but with 50 and 100 mg/L, the pesticide was oxidised in 10 min, similarly to the photo-assisted Fenton process (Figure 3.34d). In this case, adding Fe did not result in an improvement of the process. Also, similarly to UV/H<sub>2</sub>O<sub>2</sub>, PS consumption without iron was less than 10% in all cases, while it increased to 25% when iron was present.

Acetamiprid followed first-order degradation in all cases, although for some conditions in deionised water removal was so fast that it was not possible to obtain consistent kinetic data ( $k' > 2.3 \text{ min}^{-1}$ ). The pseudo-first order kinetic constants are shown in Table 3.18. A comparison of the kinetic constants corroborated the effects

observed in the degradation profiles and helped determine the operating condition for each AOP to apply on CAS effluent.

**Table 3.18.** Acetamidrid pseudo-first order degradation constants in deionised water, simulated effluent and CAS water for each operating condition and consumed H<sub>2</sub>O<sub>2</sub> or PS.

AOP	Operating condition		simulated					
			deionised water		effluent		CAS	
			k' (min <sup>-1</sup> )	r <sup>2</sup>	k' (min <sup>-1</sup> )	r <sup>2</sup>	k' (min <sup>-1</sup> )	r <sup>2</sup>
UV	I (W/m <sup>2</sup> )	10	0.032	0.998	0.016	0.993	-	-
		20	0.060	0.996	0.051	0.998	0.035	0.983
		27	0.073	0.995	0.049	0.974	-	-
UV/TiO <sub>2</sub>	TiO <sub>2</sub> (mg/L)	50	>2.334	-	0.055	0.996	0.034	0.995
		100	>2.334	-	0.056	0.977	-	-
		200	>2.334	-	0.056	0.995	-	-
UV/H <sub>2</sub> O <sub>2</sub>	H <sub>2</sub> O <sub>2</sub> (mg/L)	25	0.386	0.999	0.146	0.996	-	-
		50	0.764	0.995	0.301	0.977	0.082	0.992
		100	0.769	0.981	0.313	0.995	-	-
UV/H <sub>2</sub> O <sub>2</sub> /Fe	pH	2.8	>2.334	-	0.482	0.914	-	-
		Neutral	>2.334	-	0.351	0.988	0.140	0.946
UV/PS	PS (mg/L)	25	>2.334	-	0.104	0.999	-	-
		50	>2.334	-	0.245	0.996	-	-
		100	>2.334	-	0.339	0.988	0.073	0.992
		50 (+1mg Fe/L)	>2.334	-	0.383	0.984	0.087	0.990

The constant for photolysis at 10 W/m<sup>2</sup> in deionised water was approximately twice its value in simulated effluent (0.032 and 0.016 min<sup>-1</sup> respectively). The difference at 20 and 27 W/m<sup>2</sup> was not so marked since, as discussed, there was an excess of photons at that intensity. For that reason, 20 W/m<sup>2</sup> was chosen to use on CAS effluent. Likewise, for hydrogen peroxide photolysis a saturation effect for hydrogen peroxide concentration (H<sub>2</sub>O<sub>2</sub>>50 mg/L) was further corroborated. Indeed, increasing hydrogen peroxide concentration significantly above this value would lead to a decrease in the reaction rate due to inefficient reactions between hydroxyl radicals and hydrogen peroxide. Thus, a concentration of 50 mg H<sub>2</sub>O<sub>2</sub>/L was selected to treat the CAS effluent. UV/TiO<sub>2</sub> was not tested with CAS effluent due to the slow kinetics in simulated effluent.

For the UV/H<sub>2</sub>O<sub>2</sub>/Fe system, degradation in deionised water was too fast to enable calculation of the reaction kinetics. In simulated effluent the constant at pH 2.8 was higher than at natural pH (0.482 vs 0.351 min<sup>-1</sup>) but the kinetic constants for the two processes were the highest obtained from the AOPs assayed. Taking into account that both kinetic constants were high, that working at acidic pH involves an increase in costs (firstly to acidify and then neutralise the effluent) and an impact in the receiving environment due to change in ionic strength, the operating condition at natural pH was selected for the treatment of CAS water.

For UV/PS, the highest kinetic constant was achieved at 100 mg PS/L (0.339 min<sup>-1</sup>), although with half that concentration a constant of 0.245 min<sup>-1</sup> was already observed. Adding iron increased slightly the kinetic constant using 50 mg PS/L. Consequently, the UV/PS/Fe system (50 mg PS/L and 1 mg Fe/L) was also used on CAS effluent, as well as the UV/PS (50 mg PS/L) to act as a reference to check the effect of iron.

### Acetamiprid degradation in CAS effluent

CAS effluent was taken from the activated sludge pilot plant at Cranfield University (Table 3.19). In all cases acetamiprid degradation in CAS effluent resulted in removal times that were longer than for simulated effluent (Figure 3.35). This was due to the higher absorption of UV light at 254 nm by the CAS effluent in comparison with simulated effluent, as well as different proportions of ions and organic matter in the different waters. This resulted in more interference from background compounds in the CAS, which reduced the efficiency of all AOPs.

From all of the processes assayed, the UV/H<sub>2</sub>O<sub>2</sub>/Fe system was the fastest, reaching complete pesticide removal in 20 min (Table 3.18). Iron species like Fe(OH)<sup>2+</sup> have been found to absorb UV<sub>254</sub> strongly (Anipsitakis and Dionysiou, 2010). UV/PS and UV/PS/Fe had slower reaction times, both resulting in complete degradation after 30 min, although the pseudo-first kinetic constant for UV/PS/Fe was slightly higher than without iron. The next process in terms of kinetic rate was UV/H<sub>2</sub>O<sub>2</sub>, with a similar kinetic constant to the PS system. The fact that adding iron to UV/H<sub>2</sub>O<sub>2</sub> significantly increased the process rate but not when it was added to UV/PS was due to the inefficient reaction between the sulphate radical anion and the ferrous iron (Liang et al., 2004).



**Table 3.19.** CAS effluent properties.

Parameter	Value
pH	8.6
DOC (mg/L)	18.5
TIC (mg/L)	44
COD (mg/L)	71
Nitrate (mg/L)	2.1
Nitrite (mg/L)	0.02
Sulphate (mg/L)	58
Phosphate (mg/L)	4.1

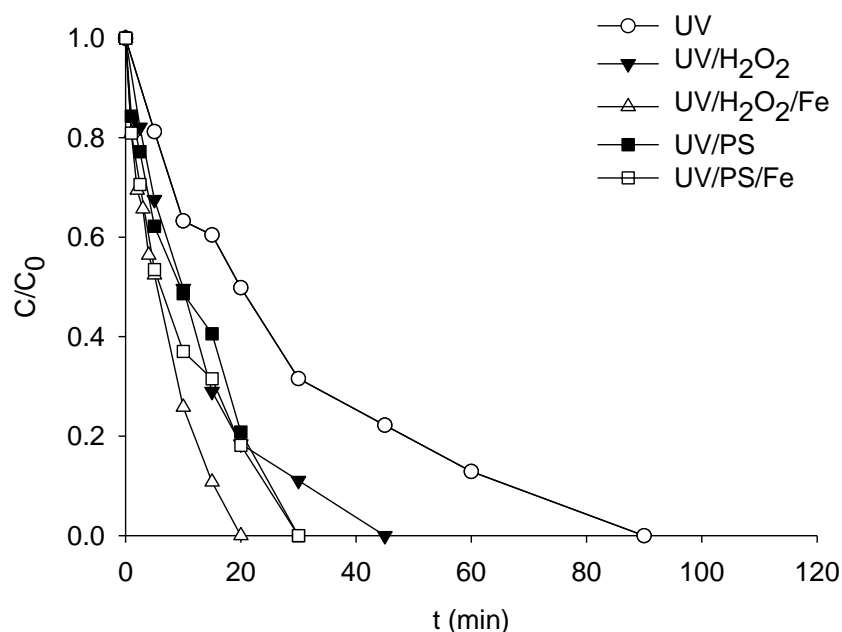


**Figure 3.35.** Acetamiprid degradation profiles in CAS effluent at  $20 \text{ W/m}^2$  by direct photolysis (UV), UV/ $\text{H}_2\text{O}_2$  (50 mg  $\text{H}_2\text{O}_2/\text{L}$ ), UV/ $\text{H}_2\text{O}_2/\text{Fe}$  (1 mg  $\text{Fe}/\text{L}$  natural pH and 50 mg  $\text{H}_2\text{O}_2/\text{L}$ ), UV/PS (50, 100 mg PS/L), UV/PS/Fe (50 mg PS/L and 1 mg  $\text{Fe}/\text{L}$ ).

The study of all the AOPs showed that the photo-assisted Fenton was the fastest system, this fact being consistent through the three water matrices –deionised water, simulated effluent and CAS effluent. In deionised water, the UV/ $\text{TiO}_2$ , UV/ $\text{H}_2\text{O}_2$  or UV/PS systems did not show any differences, resulting in the same degradation kinetics. However, in simulated effluent and CAS effluent, where the water matrix is closer to real application and where there was high alkalinity and organic matter, the differences between the AOPs were more marked. UV/ $\text{TiO}_2$  was only effective in deionised water and UV/ $\text{H}_2\text{O}_2$ , demonstrated the same degradation rate as for UV/PS in deionised water and simulated effluent, but was slower in real effluent.

### Effect of humic acids, lignin-derivate and lauryl sulphate on acetamiprid degradation

The type and oxidation state of organic matter has a significant effect on AOP operation. In the case of tertiary treatment, mostly non-biodegradable compounds are present in the water. Compounds such as humic acids and lignin-derivatives are usually present either in secondary effluents or in the receiving environment (Dignac et al., 2000; Her et al., 2003; Mesfioui et al., 2012). Lignin is the second most abundant plant-derived polymer in the world and it is formed by phenil monomers. Humic acids are major components of the natural organic matter in water. They are generated by reactions formed during the decay of dead plant material, including lignin, and they tend to be resistant to further bio-degradation. Both compounds present the additional complexity in that there are many possible bonding patterns within individual molecules (mainly aromatic rings) (Adler, 1977; Amir et al., 2006). Other compounds commonly found in secondary effluent are surfactants. For instance, lauryl sulphate is an anionic surfactant used as a foaming and viscosity control agent, and as a detergent in personal care products including shampoos and shower gels. It is toxic and resistant to biodegradation in conventional activated sludge (CAS) (Kroschwitz and Howe-Grant, 2004) and found in wastewater effluents (Cantero et al., 2005). Its degradation by AOPs has been previously studied, but not its effect on AOPs as background organic matter (Lea and Adesina, 1998).

To evaluate the effect of humic acids, lauryl sulphate and lignin-derivate on acetamiprid degradation, each was added separately in deionised water to obtain a concentration of 10 mg DOC/L, the same DOC as for the simulated effluent (Figure 3.36).

Humic acids had the most significant detrimental effect on pesticide degradation when using UV photolysis (Figure 3.36a). Complete acetamiprid removal was measured after 120 min; while with lignin and lauryl sulphate it was removed in 60 min (Figures 3.36b and 3.36c). This was because absorptivity of humic acids at 254 nm was 92% higher than that of the other two compounds. As UV photolysis effectiveness is based on the absorption of light by acetamiprid, humic acid molecules present such high absorptivity; they act as a filter of the UV light. The other AOPs resulted in faster degradation than for UV photolysis, giving degradation in less than 20 min for all systems. Using Fe with either UV/H<sub>2</sub>O<sub>2</sub> or UV/PS did not significantly enhance degradation. Humic acids have been reported to improve the process when the redox iron cycle is taking place at natural pH due to the enhanced reduction of Fe<sup>3+</sup>-humate

complexes by  $\text{H}_2\text{O}_2/\text{HO}_2^\bullet/\text{O}_2^\bullet$  in comparison to the  $\text{Fe}^{3+}$  aquo-complexes (Vione et al., 2004). Such enhancement occurs because the ligand (humate in this case) affects the reactivity of the iron complex in two ways: by ligand-field effects on iron redox properties and by labile coordination position on iron for complexation in the case of UV/ $\text{H}_2\text{O}_2$ /Fe system (Sun and Pignatello, 1992). On the other hand, a radical scavenging effect can also take place in the presence of high concentrations of humic acids.

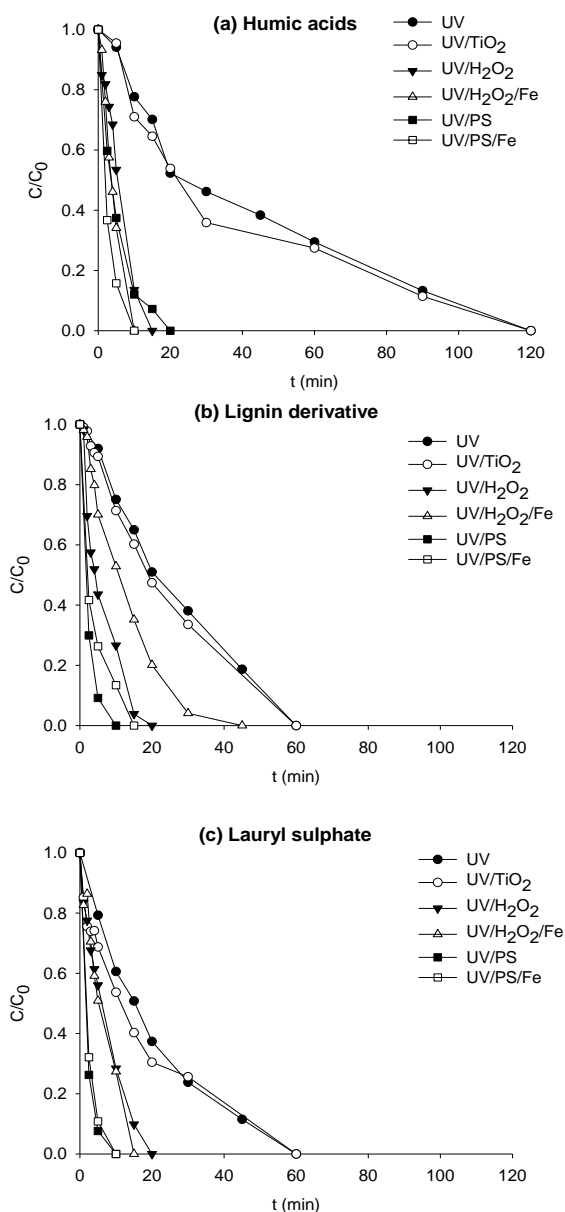


**Figure 3.36.** Acetamiprid degradation in the presence of 10 mg DOC/L of (a) humic acids; (b) lignin-derivative; and (c) lauryl sulphate at  $20 \text{ W/m}^2$  by direct photolysis (UV), UV/ $\text{H}_2\text{O}_2$  (50 mg  $\text{H}_2\text{O}_2$ /L), UV/ $\text{H}_2\text{O}_2$ /Fe (1mg Fe/L natural pH and 50 mg  $\text{H}_2\text{O}_2$ /L at natural pH), UV/PS (50, 100 mg PS/L), UV/PS/Fe (50 mg PS/L and 1 mg Fe/L).

The effect of the lignin-derivative on acetamiprid degradation was different than for the humic acids. In this case, the presence of Fe (UV/H<sub>2</sub>O<sub>2</sub>/Fe or UV/PS/Fe), along with the lignin derivative had a negative impact on the degradation of acetamiprid (Figure 3.36b), especially for the photo-assisted Fenton process. However, the UV/PS system was not as affected by the lignin derivative because of the high selectivity of sulphate radical anions towards acetamiprid. Lignin-derivatives are likely to have an analogous effect as for tannins, since they have a similar chemical structure, and are known to form Fe<sup>2+</sup> complexes (Lopes et al., 1999). Moreover, the complexes formed tend to exhibit high light absorptivity, acting also as a light filter (Lopes et al., 1999).

In the case of lauryl sulphate, acetamiprid degradation was still fast (less than 20 min) (Figure 3.36c) with UV/H<sub>2</sub>O<sub>2</sub> or UV/PS, but the addition of iron did not affect the overall outcome. Lauryl sulphate is an anionic surfactant with a 12-carbon aliphatic tail and sulphate group. This structure does not allow for the formation of iron complexes to keep it in solution for long, which results in a similar degradation with iron and without it.

The results have shown a comprehensive direct comparison of five AOP as a tertiary treatment technology for micropollutant removal from wastewater prior to discharge. UV/H<sub>2</sub>O<sub>2</sub>/Fe and UV/PS were shown to be the most effective AOP across all of the water sources investigated, with near complete removal of the pesticide under all conditions within 30 minutes. However the composition of water is important because the nature of organic matter in secondary effluent has a significant effect on treatment times. Although the highest overall reaction rates were observed for UV/H<sub>2</sub>O<sub>2</sub>/Fe across all conditions tested, this work has identified that organic compounds that act as ligands or light filters reduce the effectiveness of the AOP. Consequently, careful consideration of water matrix is needed prior to implementation of iron based AOP along with a focus on upstream removal of compounds that exhibit similar properties to humic acid and lignin. Although giving overall lower removal rates than for UV/H<sub>2</sub>O<sub>2</sub>/Fe, the PS/UV system was proven to be less affected by variations in organic matter than the rest of the systems thanks to persulphate selectivity. As a less studied AOP, PS/UV, has shown that it offers a method for selective micropollutant removal from water sources. There may also be a role for considering complimentary AOP to provide the most robust treatment for differing wastewater characteristics. But implementing the best UV-AOP at full scale for tertiary wastewater treatment will require engineering cost effective equipment and in understanding the nature of the by-products formed following AOP treatment.

### **b) UVC high intensity LED**

The effectiveness of the lamp-driven photo-Fenton to remove acetamiprid was proven in the previous section. The most frequently used lamps are low pressure lamps like the ones used. However, a short bulb life, low energy efficiency (which increases electrical costs) and used or damaged lamps being a possible source of mercury contamination in the environment are drawbacks of this kind of lamp (Vilhunen and Sillanpää, 2010). This has encouraged the search for more efficient devices for delivering UV light, such as light emitting diodes (LEDs). LEDs contain a semiconducting material that emits light in a narrow spectrum when a voltage is applied (Hu et al., 2006; Khan, 2006). They are more energetically efficient than conventional UV lamps since they transform less energy into heat and have a much longer life than conventional bulbs (Vilhunen and Sillanpää, 2010). LEDs are still under development, but low-intensity UVC-LEDs (UV irradiance below  $5 W_{UV}/m^2$ ) have been effectively applied for water treatment. For example, for water decontamination to remove pollutants such as metaldehyde using heterogeneous photocatalysis (Autin et al., 2013) or phenol with hydrogen peroxide photolysis (Vilhunen and Sillanpää, 2009).

One of their most important applications is water disinfection (Chatterley and Linden, 2010; Würtele et al., 2011; Ibrahim et al., 2014). However, the relatively low intensity of UV LEDs increases the number of bulbs needed. Chatterley and Linden (2010) reported in a case study based on a UV-LED prototype to inactivate *Escherichia coli* that the development of high-intensity LED systems could decrease the number of bulbs needed from 201 (low-intensity LED, 0.36 mW/lamp) to 8 (high-intensity LED, 10 mW/lamp). This significantly improves the likelihood of applying LED based AOPs at full scale. High-intensity UVC-LEDs have recently been developed but, as far as the authors are aware, no studies about their application to water treatment have yet been published. This is in part due to their high cost, which is the greatest limitation of this technology at present. However, thanks to their numerous potential applications, reliability and low operational costs, UVC-AOPs using high intensity LEDs are a very promising process worthy of further investigation (He et al., 2014).

In this Section, the aim was to study the efficiency of high-intensity UVC LED lamps for photo-Fenton. The pesticide acetamiprid was used as model pollutant at a concentration of 100 µg/L in the simulated secondary effluent. Experimentation was carried out in a high intensity UVC LED system and in the low-pressure UVC lamp (LPL) system used in Section 3.2.5.1 for comparative purposes, using both systems at a UV intensity of  $20 W/m^2$ . The comparison was carried out at natural pH with low iron

concentration, since these conditions are more operative for real applications. A sequential iron dosage strategy was also assayed. Tests were run at pH 2.8 in the high intensity LED system, which is the conventional pH of the photo-Fenton process, to estimate the volumetric photon absorption (VRPA) since iron is soluble at this pH and evaluate the influence of hydrogen peroxide and iron in acetamiprid degradation. The experimental conditions are shown in Table 3.20.

UV photolysis was also tested as a control since photolysis in the UVC spectrum has been shown to effectively remove pollutants from water (Legrini et al., 1993; Pera-Titus et al., 2004). At natural pH, iron was added sequentially to study the effect of degradation efficiency. The iron additions were made in increments of 1 mg Fe<sup>2+</sup>/L each to make up to 2 mg Fe<sup>2+</sup>/L (1+1 mg Fe/L) or 3 mg Fe<sup>2+</sup>/L (1+1+1 mg Fe/L). Each addition was made every 30 seconds. Experiments with one initial addition 3 mg Fe/L were also assayed to compare with the iron dosage strategy.

**Table 3.20.** Operating conditions assayed.

pH	system	Fe (mg/L)	H <sub>2</sub> O <sub>2</sub> (mg/L)	Ratio H <sub>2</sub> O <sub>2</sub> :Fe
Natural pH	LED and LPL	3	6	2:1
		1+1	4	2:1
		1+1+1	6	2:1
		3	12	4:1
		1+1	8	4:1
		1+1+1	12	4:1
2.8	LED	1	2	2:1
		2	4	2:1
		3	6	2:1
		1	4	4:1
		2	8	4:1
		3	12	4:1

#### Acetamiprid degradation at natural pH

Working at natural pH is more realistic in terms of process operation since costs associated with neutralisation of the treated water would not be required and an acidic effluent would not be discharged to the environment. Two operating strategies were followed in the LED and LPL systems to degrade acetamiprid using relatively low iron concentrations to avoid iron sludge: firstly, an initial addition of 3 mg Fe/L was used (Figure 3.37); secondly, an iron dosage strategy was evaluated. Iron was added in a sequential dosage to add a total of 2 and 3 mg Fe/L. Low iron concentrations are

enough to keep certain amount of iron in solution and they are in the commonly used range for micropollutant removal (Bernabeu et al., 2012; Klamerth et al., 2013).

When iron was added to the system the Fenton reaction with hydrogen peroxide rapidly yielded radicals, which resulted in rapid acetamiprid degradation (Equation 1.13). However, iron hydrolysis also occurred at the same time due to the higher pH (Equation 3.1). From this reaction, iron precipitates as ferric hydroxide, resulting in a loss of catalyst. Thus, when one initial addition of 3 mg Fe/L was used, acetamiprid degradation mainly occurred in the first few minutes of treatment, both in the LED or LPL systems when there was opportunity for the soluble fraction of iron to react through Equation 1.14 prior to precipitation. Degradation was similar regardless of the  $\text{H}_2\text{O}_2$ :Fe ratio. For instance, in the LED system and for 3 mg Fe/L, the removal was 57% and 60% after 30 min for a  $\text{H}_2\text{O}_2$ :Fe ratio of 2:1 and 4:1 respectively. In the same conditions, acetamiprid removal in the LPL system was 68% and 72% respectively.

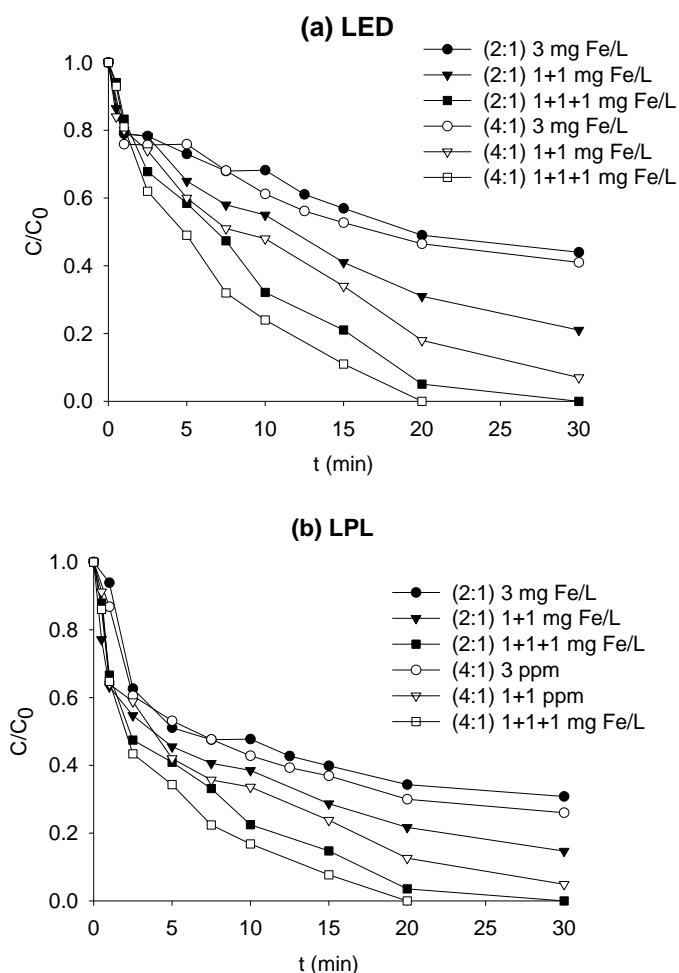


**Figure 3.37.** Acetamiprid degradation by photo-Fenton in the (a) LED system and (b) LPL system at natural pH with one and sequencing iron additions every 30 seconds at a  $\text{H}_2\text{O}_2$ :Fe ratio of 4:1 and 2:1.

The process was then operated using sequential iron additions (Figure 3.20). Indeed, with three additions of 1 mg Fe/L complete removal was achieved in 20 min and 30 min for the  $\text{H}_2\text{O}_2$ :Fe ratio of 4:1 and 2:1 in both UVC systems. With two iron additions a high level of removal was also obtained: more than 90% degradation with a  $\text{H}_2\text{O}_2$ :Fe ratio of 4:1 and more than 80% with a 2:1 ratio.

When working at natural pH, the effect of the non-UV dependent Fenton process can be significant. The amount of hydroxyl radicals generated through Equation 1.13 between ferrous iron and hydrogen peroxide, which takes place in the dark, can be the main source of radicals at natural pH, as observed in the previous study of iron dosage (Section 3.2.1). To evaluate the effects of acetamiprid degradation due to radical generation in the dark, the Fenton process was carried out as a blank. In the strongest conditions ( $\text{H}_2\text{O}_2$ :Fe ratio of 4:1 and iron addition sequence of 1+1+1 mg Fe/L), acetamiprid removal after 30 min was over 35%. In the same operating conditions but in the presence of UVC light acetamiprid was completely removed in 20 min in the LED and LPL systems. This means that, although a fraction of the radicals generated came from the non-UV dependent reaction (Equation 1.13), most of the radicals were yielded by the UV-driven reactions.

The results show that the LED system was efficient in the removal of acetamiprid in a complex water matrix with additional organic matter and ions at natural pH using the iron dosage strategy.

### Acetamiprid degradation at acidic pH

The LED showed analogous efficiency to the LPL system in realistic conditions at natural pH. However, part of the aim of the study was to evaluate the influence of hydrogen peroxide and iron in acetamiprid degradation with the LED through the estimation of the photon absorption. At natural pH iron precipitates, so the catalyst concentration changes during the experiment and estimation of the photon absorption is more complex since iron photon absorption changes with time. Therefore experiments were carried out at pH 2.8, when iron solubility is high (Pignatello, 1992), so its concentration is constant for the duration of the experiments. To simplify calculations, it was assumed that UVC beams were all parallel and perpendicular to the water surface, so only the direction in one axis was considered, similarly to collimated beam systems (Baeza and Knappe, 2011).



At the maximum wavelength of the LED, 256 nm, ferrous iron strongly absorbs UV light, but during the experiments, the iron was mainly as the ferric iron due to rapid oxidation by H<sub>2</sub>O<sub>2</sub>. Therefore, the predominant absorbing species considered in the system were hydrogen peroxide and ferric iron.

The absorption spectra of ferric iron in the synthetic effluent were obtained at different iron concentrations and the absorption coefficients,  $\epsilon$  (mM<sup>-1</sup> m<sup>-1</sup>), at 256 nm were determined through Equation 3.29. Similarly, hydrogen peroxide absorption coefficients were calculated at both wavelengths.

$$\epsilon_{i,\lambda} = \frac{Abs_{i,\lambda}}{C_i \cdot x} \quad (3.29)$$

where  $\epsilon_{i,\lambda}$  is the absorption coefficient for each absorbing species in the system (ferric iron and hydrogen peroxide);  $Abs_{i,\lambda}$  is the absorption of each specie dissolved in synthetic water at the specific wavelength;  $C_i$  is the concentration of the absorbing species; and  $x$  is the optical path (cuvette width). The absorption coefficient for ferric iron species at pH 2.8 was 1730 M<sup>-1</sup> cm<sup>-1</sup> 256 nm, respectively. The coefficient for hydrogen peroxide was 18 M<sup>-1</sup> cm<sup>-1</sup> at 256 nm.

The attenuation of UVC radiation is a function of the main absorbing species, iron and hydrogen peroxide concentrations, and light path length (Equation 3.30).

$$I_{att} = I_0 10^{-(\epsilon_{Fe} \cdot C_{Fe} + \epsilon_{H_2O_2} \cdot C_{H_2O_2}) \cdot p} \quad (3.30)$$

Where  $I_0$  is the measured UVC radiation on the water surface; and  $p$  is the optical path (liquid depth in the reactor, 1.64 cm).

Based on the above description on light attenuation, the volumetric rate of photon absorption for each absorbing species (VRPA<sub>*i*</sub>, W/m<sup>3</sup>) in the photochemical reactor was determined through Equation 3.31 (Rivas et al., 2014).

$$VRPA_i = \frac{S_R}{V_R} \int_0^p \epsilon_i \cdot C_i \cdot I_{att} \cdot dp \quad (3.31)$$

The acetamiprid degradation profiles at the conditions assayed at acidic pH are shown in Figure 3.38. In all cases degradation followed a pseudo-first order trend, as reported in the literature for micropollutant degradation by the photo-Fenton process (Barreca et al., 2014; Neamțu et al., 2014).

An increase in the catalyst concentration increased the process rate; although the increase in the rate also depended on the hydrogen peroxide concentration. For the same iron concentration, increasing the ratio  $\text{H}_2\text{O}_2:\text{Fe}$  always improved degradation. Complete acetamiprid removal could only be achieved using a ratio of  $\text{H}_2\text{O}_2:\text{Fe}=4:1$  (2 and 3 mg Fe/L). Hydrogen peroxide concentration was also measured at the end of each assay, and a residual concentration between 4-7% remained in all cases. UV photolysis was carried out as a control experiment where acetamiprid removal was low, achieving 22% degradation in 20 min.

Acetamiprid degradation principally depended on two light-absorbing effects that resulted in  $\text{HO}^\bullet$  formation. On the one hand, light absorption by ferric iron (Equation 1.14); and on the other hand, light absorption by hydrogen peroxide in the photolysis reaction (Equation 1.3).

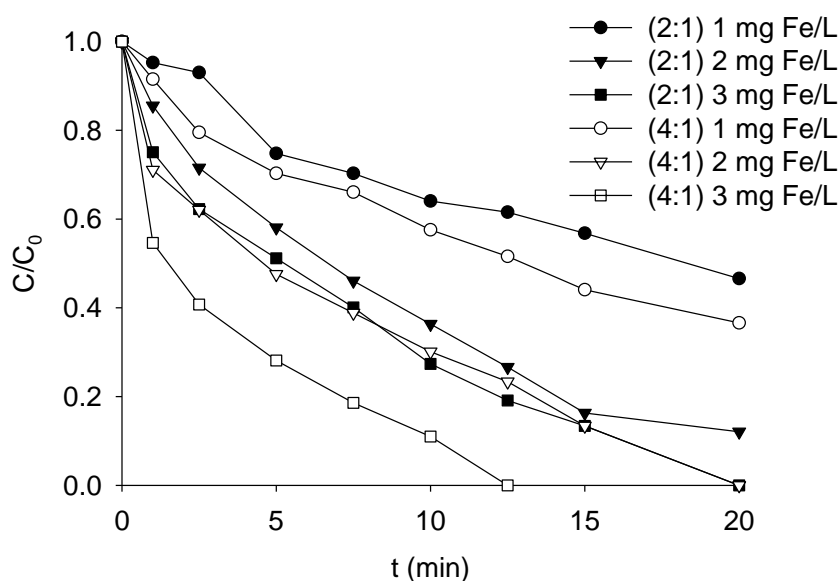
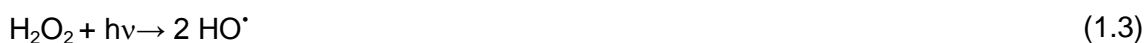


**Figure 3.38.** Acetamiprid degradation by photo-Fenton in the UVC-LED system using 1, 2 and 3 mg Fe/L and a  $\text{H}_2\text{O}_2:\text{Fe}$  ratio of 2:1 and 4:1 in synthetic secondary effluent at pH 2.8.

Acetamiprid degradation can therefore be expressed as a function of the  $[\text{HO}^\bullet]$ , following Equation 3.32, showing that it is proportional to hydroxyl radical generation, which at the same time is dependent on reaction rates  $r_1$  and  $r_2$  (Equation 3.33). Here  $r_1$  is the radical generation rate due to the iron redox cycle which is rate limited by the ferric iron reduction by light and  $r_2$  is the radical generation rate due to light absorption

and photolysis of hydrogen peroxide. Each reaction was affected by the volumetric rate of photon absorption of each species,  $VRPA_{Fe}$  and  $VRPA_{H_2O_2}$  (Equations 3.34 and 3.35). Therefore, acetamiprid degradation rate could be expressed as a function of both light-absorbing effects with the overall apparent kinetic constant,  $k' = k [HO^*] = \alpha \cdot VRPA_{Fe} + \beta \cdot VRPA_{H_2O_2}$  (Equation 3.36).

$$-\frac{d[Acetamiprid]}{dt} = k \cdot [HO^*] \cdot [Acetamiprid] \quad (3.32)$$

$$[HO^*] \propto r_1 + r_2 \quad (3.33)$$

$$r_1 = k_{Fe} \cdot VRPA_{Fe} \quad (3.34)$$

$$r_2 = k_{H_2O_2} \cdot VRPA_{H_2O_2} \quad (3.35)$$

$$-\frac{d[Acetamiprid]}{dt} = (\alpha \cdot VRPA_{Fe} + \beta \cdot VRPA_{H_2O_2}) \cdot [Acetamiprid] \quad (3.36)$$

Consequently, acetamiprid degradation would follow a non-linear model as described in Equation 3.37.

$$\frac{[Acetamiprid]}{[Acetamiprid]_0} = e^{-(\alpha \cdot VRPA_{Fe} + \beta \cdot VRPA_{H_2O_2}) \cdot t} \quad (3.37)$$

The model was adjusted using the results from all operating conditions except those used to validate the model, which were 3 mg Fe/L and a  $H_2O_2:Fe$  ratio of 2:1; and 1 mg Fe/L with a  $H_2O_2:Fe$  ratio of 4:1. The data of each experiment was adjusted to the non-linear model (Equation 3.37) to obtain  $\alpha$  and  $\beta$ . The model would serve to elucidate the importance of iron and hydrogen peroxide adsorption in the degradation of acetamiprid. The results obtained from the model fit are shown in Table 3.21.

**Table 3.21.** Model parameters and fitting.

UVC System	$\alpha$ ( $m^3 W^{-1} min^{-1}$ )	$\beta$ ( $m^3 W^{-1} min^{-1}$ )	$r^2$
LED	$7.4 \cdot 10^{-4}$	$7.2 \cdot 10^{-4}$	0.935

The model served to determine an understanding of the balance of the iron and hydrogen peroxide absorption in the LED system. Coefficients  $\alpha$  and  $\beta$  represent the

significance of iron and hydrogen peroxide on photon absorption to yield radicals and degrade acetamiprid. The coefficients were similar, so the contribution of iron and hydrogen peroxide to generate radicals and degrade acetamiprid was practically the same.

The model validation was made using the calculated  $\alpha$  and  $\beta$  to simulate the profiles of the validation experiments (Figure 3.39). The validation showed an acceptable fit to the experimental results, corroborating the discussion above. The model served to bring light to the weight of iron and hydrogen peroxide absorption in the LED system. The value of  $\alpha$  and  $\beta$  was similar in the LED system, showing that the contribution of iron and hydrogen peroxide to generate radicals and degrade acetamiprid was the same.

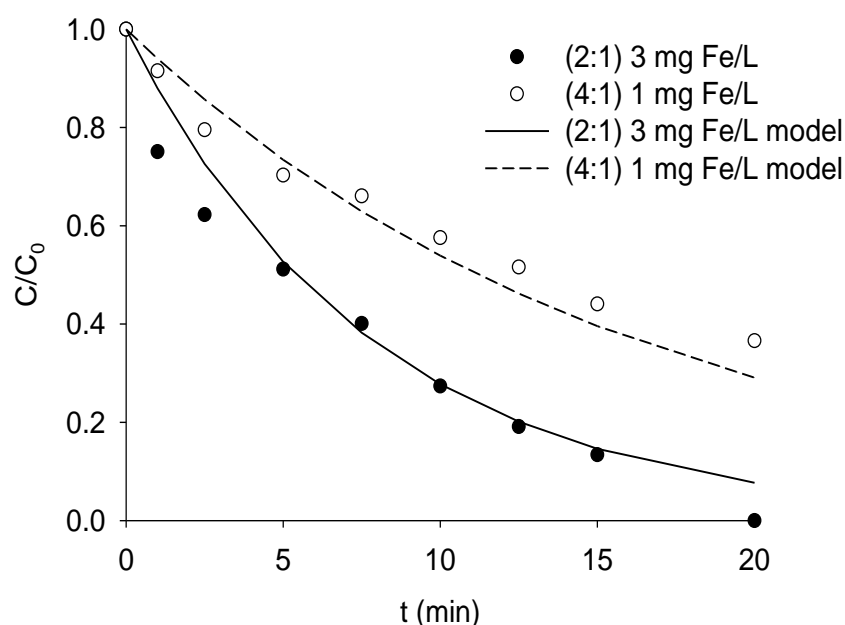


**Figure 3.39.** Model validation for acetamiprid degradation in the LED system with a  $\text{H}_2\text{O}_2$ :Fe ratio of 2:1 (3 mg Fe/L) and 4:1 (1 mg Fe/L).

The study of the process at acidic pH provided information on the effect of hydrogen peroxide and iron on acetamiprid degradation in the simulated water, indicating that the contribution of both to generate hydroxyl radicals was the same in the LED system.

Results show the efficiency of UVC-LED systems for AOP applications. Specifically, the use of LEDs in the photo-Fenton process enables acetamiprid to be degraded in short reaction times at natural pH using iron additions in steps of 1 mg Fe/L. Specifically, acetamiprid could be removed in 20 min adding a total of 3 mg Fe/L

(1+1+1 mg Fe/L every 30 s). The results at natural pH were similar to those achieved with the LPL, which is promising for the future of UV-AOPs.

UV LEDs are a potential technology for UV-based AOPs, which still needs to be developed in terms of process scale and cost. The manufacture of high intensity LEDs constitutes already a step in this direction, reducing the effective surface and bulbs needed in comparison to low intensity LEDs. LED's can reduce amortization and maintenance costs in a plant due to their longer lifespan. As they do not require warm-up time, operating costs can also be reduced. These advantages will be seen in the near future as the commercial uptake of LED systems increases exponentially and the cost of LED bulbs commensurately decreases, making their implementation financially more attractive in comparison to LPLs. However, this technology is still under development and more research should be made on the design of new photoreactors at pilot plant scale to implement LEDs and consider the economy of scale in the process before comparing it to solar-driven processes.



## ***CONCLUSIONS***

---





## 4. CONCLUSIONS

The problem of water scarcity has encouraged the investigation of advanced oxidation technologies to remove persistent pollutants from wastewater and increase the volume of reclaimed water. The photo-Fenton process has been deemed effective in the oxidation of organic pollutants. Nevertheless, the operation of the process is not yet fully optimised. The complexity and variability of wastewater effluents make this matter difficult. The main goal of this Ph.D. thesis was to develop new operating strategies to operate the photo-Fenton process to remove persistent pollutants. The strategies were focused on the pH of water (natural or acidic pH) and on the phenomenology between iron concentration and solar irradiance. These studies were complemented with an insight into the determination of the main intermediates of contaminants treated by photo-Fenton using highly sensitive analytical techniques (LC/MS) and the comparison of photo-Fenton with other AOPs using artificial UV to gain a deeper understanding of the process.

The following specific conclusions could be drawn from the results obtained in this PhD thesis:

1. To operate the photo-Fenton process at natural pH, iron dosage is an efficient strategy for both mg/L and  $\mu\text{g/L}$  ranges of pollutants. Expressly, continuous addition of ferrous iron salt following a decreasing exponential function has been shown to be the best dosage strategy.
2. The use of iron D-gluconate, lactate, mesylate deferoxamine and ferroactive are not recommended as iron sources for the removal of mg/L of pollutants at natural pH since their effectiveness in degradation is analogous or lower than iron salt dosage.

3. For micropollutant removal, the photo-Fenton process can be operated in photoreactors with optical paths wider than 5 cm since the requirement of photons is small in comparison with macropollutant removal. Specifically, for the removal of micropollutants in the range of a few hundred  $\mu\text{g/L}$ , there was an excess of irradiance for an average solar irradiance above  $15 \text{ W/m}^2$  (for a concentration of ferrous iron between 1 and 20 mg/L and 5 cm of optical path).
4. The situation of irradiance excess can be simulated by a simplified model using the main reactions and mass balances as well as including the hyperbolic function  $k_m \cdot I / (k_s + I)$  to express in the kinetic constant the effect of irradiance on the ferric iron photoreduction ( $\text{Fe}^{3+} + \text{H}_2\text{O} + h\nu \rightarrow \text{Fe}^{2+} + \text{HO}^\bullet + \text{H}^+$ ).
5. Raceway ponds are proposed as photoreactors for the operation of solar photo-Fenton to remove micropollutants since the optical path can be adjusted to irradiance requirements. As such, this gives rise to a higher treatment capacity per surface area than for tubular photoreactors. They were successfully used for the treatment of real agrofood industry effluent enriched with commercial formulations of acetamiprid and thiabendazole in the range of a few hundred  $\mu\text{g/L}$ .
6. The monitoring of acetamiprid and thiabendazole transformation products indicated that when the aim of the process is to remove parent molecules as well as by-products, treatment times would be significantly lengthened.
7. The study of lamp-driven photo-Fenton indicated that the degradation due to hydrogen peroxide photolysis is high, but the addition of ferrous iron improves the process rate. Additionally, the water matrix is crucial for the comparison of AOPs since their efficiency is differently affected by anions and organic matter. That aside, the photo-Fenton process was affected to a lesser extent by the

water matrix (deionised, simulated effluent or real effluent) than heterogeneous photocatalysis and hydrogen peroxide photolysis.

8. The use of UVC-LED-driven photo-Fenton is effective in the degradation of micropollutants at both natural and acidic pH. This technology is still under development but the promising results indicate LEDs could be a competitive source of radiation for AOP applications.

The main contribution of this research and core of the PhD thesis is the finding of the irradiance saturation effect on the removal of micropollutants. So far, tubular photoreactors with a 5-cm optical path have been used for micropollutant oxidation, which was the design optimised for macropollutant removal. However, in this PhD thesis it was proved that irradiance requirements for micropollutant oxidation are lower, so the optical path can be enlarged, increasing treated volume per surface area. This has led to the successful application of raceway ponds as a novel and low-cost technology involving the use of solar photo-Fenton for micropollutant removal. The photoreactor is of simple design and made of economical materials and one of its main advantages is that it has already been applied at commercial scale for other solar applications, so in this way it can be seen as a developed technology in this sense. This kind of photoreactor brings solar photo-Fenton closer to being commercially applied.



## ***CONCLUSIONES***

---



## 5. CONCLUSIONES

El problema de la escasez de agua ha impulsado la investigación en técnicas de oxidación avanzada para eliminar contaminantes persistentes del agua e incrementar el volumen de agua reutilizada. Se ha demostrado que el proceso foto-Fenton es eficaz en la oxidación de contaminantes orgánicos. Sin embargo, la operación del proceso no está optimizada aún. La complejidad y variabilidad de efluentes de agua residual complican este hecho. El objetivo principal de esta tesis doctoral ha sido desarrollar nuevas estrategias para operar el proceso foto-Fenton para eliminar contaminantes persistentes. Las estrategias se han enfocado a pH natural y ácido y en la fenomenología entre la concentración de hierro y la radiación solar. Esto se complementó con el estudio de la determinación de los principales intermedio de los contaminantes tratados con foto-Fenton mediante LC/MS y con la comparación de foto-Fenton con otros procesos de oxidación avanzada utilizando luz UV artificial para entender mejor el proceso.

Se han obtenido las siguientes conclusiones específicas a partir de los resultados obtenidos en esta tesis:

1. Para operar el proceso foto-Fenton a pH natural, la dosificación de hierro es una estrategia eficiente tanto a nivel de mg/L como de  $\mu\text{g/L}$  de contaminante. En concreto, la adición continua de hierro ferroso siguiendo una función exponencial decreciente ha sido la mejor estrategia de dosificación.
2. El uso de D-gluconato y lactato de hierro, mesilato de deferoxamina y ferroactive no están recomendados como fuentes de hierro para eliminar mg/L de contaminante a pH natural, ya que su eficacia para degradar es análoga o más baja que la dosificación de hierro.

3. Para la eliminación de microcontaminantes, el proceso foto-Fenton puede ser operado con pasos ópticos mayores que 5 cm ya que el requerimiento de fotones es pequeño en comparación con la eliminación de macrocontaminantes. En concreto, para la eliminación de microcontaminantes a nivel de unos cientos de  $\mu\text{g/L}$  había exceso de irradiancia para una radiación solar media por encima de  $15 \text{ W/m}^2$  (para una concentración de hierro ferroso entre 1 y 20  $\text{mg/L}$  y un paso óptico de 5 cm).
4. La situación de exceso de radiación solar puede ser simulada con un modelo simplificado utilizando los principales balances de materia y reacciones así como incluyendo la función hiperbólica  $k_m \cdot I / (k_s + I)$  para expresar en la constante cinética el efecto de la irradiancia en la fotorreducción del hierro férrico ( $\text{Fe}^{3+} + \text{H}_2\text{O} + h\nu \rightarrow \text{Fe}^{2+} + \text{HO}^\bullet + \text{H}^+$ ).
5. Se propone a los reactores tipo “raceway” como fotorreactores para operar el proceso foto-Fenton solar para eliminar microcontaminantes, ya que el paso óptico puede ajustarse a las necesidades de irradiancia. Por tanto, esto da lugar a una capacidad de tratamiento por unidad de área mayor que los reactores tubulares. Se han utilizado con éxito en el tratamiento del efluente de una industria agroalimentaria enriquecida con formulaciones comerciales de acetamiprid y tiabendazol en el rango de  $\mu\text{g/L}$ .
6. El seguimiento de los productos de transformación de acetamiprid y tiabendazol ha mostrado que cuando el objetivo del proceso es eliminar las moléculas iniciales y los productos de transformación, los tiempos de tratamiento pueden verse alargados significativamente.
7. El estudio de foto-Fenton con lámpara indicó que la degradación debida a la fotólisis de peróxido de hidrógeno es alta, pero la adición de hierro mejora la



velocidad del proceso. Además, la matriz de agua es fundamental a la hora de comparar procesos de oxidación avanzada, ya que su eficacia se ve afectada de manera diferente por aniones y materia orgánica. En cualquier caso, el proceso foto-Fenton fue el menos afectado por la matriz de agua (desionizada, efluente simulado de proceso secundario o efluente real) en comparación con la fotocatalisis heterogénea o la fotólisis de peróxido de hidrógeno.

8. El uso de LEDs UVC para foto-Fenton es efectivo para la degradación de microcontaminantes a pH natural y ácido. Esta tecnología se está desarrollando aún, pero los resultados son prometedores e indican que los diodos LEDs pueden ser una fuente de radiación competitiva en aplicaciones de proceso de oxidación avanzada.

La principal contribución y núcleo de esta tesis es el hallazgo del efecto de saturación de irradiancia en la eliminación de contaminantes. Hasta ahora, los fotorreactores tubulares con un paso óptico de 5 cm se han utilizado para la eliminación de microcontaminantes, que es el diseño optimizado para macrocontaminantes. Sin embargo, en esta tesis doctoral se ha demostrado que los requerimientos de irradiancia para eliminar microcontaminantes son menores, por lo que el paso óptico se puede agrandar, incrementando el volumen tratado por área de superficie. Esto ha llevado a la aplicación de los reactores “raceway” como tecnología novedosa y de bajo coste para la aplicación de foto-Fenton solar en la eliminación de microcontaminantes. El fotorreactor es de diseño sencillo y hecho de materiales económicos y una de sus principales ventajas es que ya se aplica a escala comercial para otras aplicaciones solares, así que es una tecnología ya desarrollada. Este tipo de fotorreactor lleva al proceso foto-Fenton solar más cerca de ser implantado a nivel comercial.



## ***REFERENCES***

---



## 6. REFERENCES

- Abida, O., Kolar M., Jirkovsky J., Mailhot, G., 2012. Degradation of 4-chlorophenol in aqueous solution photoinduced by Fe(III)-citrate complex. *Photochemical and Photobiological Sciences* 11, 794-802.
- Adler, E., 1977. Lignin chemistry-past, present and future. *Wood Science and Technology* 11, 169-218.
- Ajona, J. I., Vidal, A., 2000. The use of CPC collectors for detoxification of contaminated water: Design, construction and preliminary results. *Solar Energy* 68, 109-20.
- Alfano, O. M., Bahnemann, D., Cassano, A. E., Dillert, D., Goslich, R., 2000. Photocatalysis in water environments using artificial and solar light. *Catalysis Today*, 58, 199-230.
- Alkan, U., Teksoy, A., Atesli, A., Baskaya, H. S., 2007. Efficiency of the UV/H<sub>2</sub>O<sub>2</sub> process for the disinfection of humic surface waters. *Journal of Environmental Science and Health, Part A: Toxic/Hazardous Substances and Environmental Engineering* 42, 497-506.
- Almeida, L. C., Garcia-Segura, S., Bocchi, N., Brillas, E., 2011. Solar photoelectro-Fenton degradation of paracetamol using a flow plant with a Pt/air-diffusion cell coupled with a compound parabolic collector: Process optimization by response surface methodology. *Applied Catalysis B: Environmental* 103, 21-30.
- Amir, S., Hafidi, M., Lemee, L., Merlina, G., Guiresse, M., Pinelli, E., Revel, J., Bailly, J., Ambles, A., 2006. Structural characterization of humic acids, extracted from sewage sludge during composting, by thermochemolysis-gas chromatography-mass spectrometry. *Process Biochemistry* 41, 410-22.
- An, J., Zhu, L., Zhang, Y., Tang, H., 2013. Efficient visible light photo-Fenton-like degradation of organic pollutants using in situ surface-modified BiFeO<sub>3</sub> as a catalyst. *Journal of Environmental Sciences* 25, 1213-1225.
- Anipsitakis, G. P., Dionysiou, D. D., 2004. Transition metal/UV-based advanced oxidation technologies for water decontamination. *Applied Catalysis B: Environmental* 54, 155-63.
- Anipsitakis, G. P., Dionysiou, D. D., Gonzalez, M. A., 2006. Cobalt-mediated activation of peroxymonosulphate and sulfate radical attack on phenolic compounds. Implications of chloride ions. *Environmental Science and Technology* 40, 1000-1007.
- Arslan, I., Balcioglu, I. A., 2001. Advanced oxidation of raw and biotreated textile industry wastewater with O<sub>3</sub>, H<sub>2</sub>O<sub>2</sub>/UV-C and their sequential application. *Journal of Chemical Technology and Biotechnology* 76, 53-60.
- Autin, O., Hart, J., Jarvis, P., MacAdam, J., Parsons, S. A., Jefferson, B., 2013. Comparison of UV/TiO<sub>2</sub> and UV/H<sub>2</sub>O<sub>2</sub> processes in an annular photoreactor for

- removal of micropollutants: Influence of water parameters on metaldehyde removal, quantum yields and energy consumption. *Applied Catalysis B: Environmental* 138-139, 268-75.
- Ayoub, G., Ghauch, A., 2014. Assessment of bimetallic and trimetallic iron-based systems for persulfate activation: Application to sulfamethoxazole degradation. *Chemical Engineering Journal* 256, 280-292.
- Bahnemann, D., 2004. Photocatalytic water treatment: Solar energy applications. *Solar Energy* 77, 445-459.
- Ballesteros Martín, M. M., Sánchez Pérez, J. A., García Sánchez, J. L., Casas López, J. L., Malato Rodríguez, S., 2009. Effect of pesticide concentration on the degradation process by combined solar photo-Fenton and biological treatment. *Water Research* 43, 3838–3848.
- Ballesteros Martín, M. M., Casas López, J. L., Oller, I., Malato, S., Sánchez Pérez, J. A., 2010. A comparative study of different tests for biodegradability enhancement determination during AOP treatment of recalcitrant toxic aqueous solutions. *Ecotoxicology and Environmental Safety* 73, 1189-1195.
- Birus, M., Kujundzic, N., Pribanic, M., 1993. Kinetics of complexation of iron (III) in aqueous solution (Volume 18 of Progress in reaction kinetics), Oxford, Pergamon.
- Blanco, J., Malato, S., Fernández, P., Vidal, A., Morales, A., Trincado, P. et al., 1999. Compound parabolic concentrator technology development to commercial solar detoxification applications. *Solar Energy* 67, 317-30.
- Blanco Gálvez, J., Malato, S., 2003. *Solar Detoxification*, ISBN 92-3-103916-4 ed., UNESCO Publishing, France.
- Blanco, J., Malato, S., Fernández-Ibañez, P., Alarcón, D., Gernjak, W., Maldonado, M.I., 2009. Review of feasible solar energy applications to water processes. *Renewable and Sustainable Energy Reviews* 13, 1437-1445.
- Bockelmann, D., Weichgrebe, D., Goslich, R., Bahnemann, D. W., 1995. Concentrating vs. non-concentrating reactors for solar water detoxification. *Solar Energy Materials and Solar Cells* 38, 441–451.
- Bolton, J. R., 1991. *EPA Newsletter* 43, 40-45.
- Bontoux, J., Picot, B., 1994. Possibilités et limites des bassins lagunaires dans l'épuration des eaux usées. *Water Pollution Research Journal of Canada* 29, 545–556.
- Bossmann, S. H., Oliveros, E., Göb, S., Siegwart, S., Dahlen, E. P., Payawan, L., Straub, M., Wörner, M., Braun, A. M., 1998. New evidence against hydroxyl radicals as reactive intermediate in the thermal and photochemically enhanced Fenton reaction. *Journal of Physical Chemistry A* 102, 5542–5550.
- Buxton, G. V., Greenstock, C. L., Helman, W. P., Ross, A. B., 1988. Critical review of rate constants for reactions of hydrated electrons, hydrogen atoms and hydroxyl

- radicals in aqueous solution. *Journal of Physical and Chemical Reference Data* 17, 513–886.
- Cabrera Reina, A., Santos-Juanes Jordá, L., García Sánchez, J. L., Casas López, J.L., Sánchez Pérez, J.A., 2012. Modelling photo-Fenton process for organic matter mineralization, hydrogen peroxide consumption and dissolved oxygen evolution. *Applied Catalysis B: Environmental* 119–120, 132-138.
- Cabrera Reina, A., Casas López, J. L., Maldonado Rubio, M. I., Santos-Juanes Jordá, L., García Sánchez, J. L., Sánchez Pérez, J. A., 2014a. Effects of environmental variables on the photo-Fenton plant design. *Chemical Engineering Journal* 237, 469-477.
- Cabrera Reina, A., Santos-Juanes Jordá, L., Casas López, J. L., Maldonado Rubio, M. I., García Sánchez, J. L., Sánchez Pérez, J. A., 2014b. Biological oxygen demand as a tool to predict membrane bioreactor best operating conditions for a photo-Fenton pretreated toxic wastewater. *Journal of Chemical Technology and Biotechnology*, Article in Press.
- Calderón-Preciado, D., Jiménez-Cartagena, C., Matamoros, V., Bayona, J.M., 2011. Screening of 47 organic microcontaminants in agricultural irrigation waters and their soil loading. *Water Research* 45, 221-231.
- Cantero, M., Rubio, S., Pérez-Bendito, D., 2005. Determination of non-ionic polyethoxylated surfactants in wastewater and river water by mixed hemimicelle extraction and liquid chromatography-ion trap mass spectrometry. *Journal of Chromatography A* 1067, 161-70.
- Carra, I., Ortega-Gómez, E., Santos-Juanes, L., Casas López, J. L., Sánchez Pérez, J. A., 2013. Cost analysis of different hydrogen peroxide supply strategies in the solar photo-Fenton process. *Chemical Engineering Journal* 224, 75-81.
- Chan, K. H., Chu, W., 2009. Degradation of atrazine by cobalt-mediated activation of peroxymonosulfate: Different cobalt counteranions in homogenous process and cobalt oxide catalysts in photolytic heterogeneous process. *Water Research* 43, 2513-2521.
- Chatterley, C. and Linden, K., 2010. Demonstration and evaluation of germicidal UV-LEDs for point-of-use water disinfection. *Journal of Water Health* 8, 479-86.
- Cheng, H., Chou, S., Chen, S., Yu, C., 2014. Photoassisted Fenton degradation of phthalocyanine dyes from wastewater of printing industry using Fe(II)/ $\gamma$ -Al<sub>2</sub>O<sub>3</sub> catalyst in up-flow fluidized-bed. *Journal of Environmental Sciences* 26, 1307-1312.
- Chisti, Y., 2007. Biodiesel from microalgae. *Biotechnology Advances* 25 (2007) 294-306.
- Colina-Márquez, J., Machuca-Martínez, F., Li Puma, G., 2010. Radiation adsorption and optimisation of solar photocatalytic reactors for environmental applications. *Environmental Science and Technology* 44, 5112-5120.

- Cornell, R. M., Schwertmann, U., 2003. Iron Oxides: Structure, Properties, Reactions, Occurrences and Uses. Second ed., Wiley-VCH, Weinheim.
- Cromar, N. J., Fallowfield, H. J., Martin, N. J., 1996. Influence of environmental parameters on biomass production and nutrient removal in a high rate algal pond operated by continuous culture. *Water Science and Technology* 34, 133–140.
- Datta, N. C., 1981. Chemistry of Iron(III) Oxides and Oxyhydroxides. *Journal of Scientific & Industrial Research* 40, 571-583.
- De la Cruz, N., Giménez, J., Esplugas, S., Grandjean, D., de Alencastro, L. F., Pulgarín, C., 2012. Degradation of 32 emergent contaminants by UV and neutral photo-fenton in domestic wastewater effluent previously treated by activated sludge. *Water Research* 46, 1947-5.
- De Luca, A., Dantas, R. F., Esplugas, S., 2014. Assessment of iron chelates efficiency for photo-Fenton at neutral pH. *Water Research* 61, 232-242.
- Decision No 2455/2001/EC of the European Parliament and of the Council of 20<sup>th</sup> November 2001.
- Decree, 2008. Decree MAM/85/2008 of 16<sup>th</sup> January, regarding the technical criteria for the evaluation of the damage to the Hydraulic Public Domain and the regulation for the taking of samples and wastewater discharge analysis.
- Deng, Y., Ezyske, C.M., 2011. Sulfate radical-advanced oxidation process (SR-AOP) for simultaneous removal of refractory organic contaminants and ammonia in landfill leachate. *Water Research* 45, 6189-6194.
- Dias, I. N., Souza, B. S., Pereira, J.H.O.S., Moreira, F. C., Dezotti, M., Boaventura, R.A.R., Vilar, V. J.P., 2014. Enhancement of the photo-Fenton reaction at near neutral pH through the use of ferrioxalate complexes: A case study on trimethoprim and sulfamethoxazole antibiotics removal from aqueous solutions. *Chemical Engineering Journal* 247, 302-313.
- Dignac, M., Ginestet, P., Rybacki, D., Bruchet, A., Urbain, V., Scribe, P., 2000. Fate of wastewater organic pollution during activated sludge treatment: Nature of residual organic matter. *Water Research* 34, 4185-94.
- Dillert, R., Cassano, A. E., Goslich, R., Bahnemann, D., 1999. Large scale studies in solar catalytic wastewater treatment. *Catalysis Today* 54, 267-282.
- Directive 2000/60/EC of the European Parliament and of the Council establishing a framework for the Community action in the field of water policy.
- Directive 2008/32/EC of the European Parliament and of the Council of 11 March 2008
- Directive 2008/105/EC of the European Parliament and of the Council of 16 December 2008
- Directive 2009/31/EC of the European Parliament and of the Council of 23 April 2009



- Djeffal, L., Abderrahmane, S., Benzina, M., Siffert, S., Fourmentin, S., 2014. Efficiency of natural clay as heterogeneous Fenton and photo-Fenton catalyst for phenol and tyrosol degradation. *Desalination and Water Treatment* 52, 2225-2230.
- Dorfman, L. M., Bühler, R. E., Taub, I. A., 1962. Absolute rate constant for the reaction of hydroxyl radicals with benzene in water. *The Journal of Chemical Physics* 36, 549-550.
- Durán, A., Monteagudo, J. M., Sanmartín, I., Valverde, A., 2014. Solar photodegradation of antipyrine in a synthetic WWTP effluent in a semi-industrial installation. *Solar Energy Materials and Solar Cells* 125, 215-222.
- El Ouarghi, H., Boumansour, B. E., Dufayt, O., El Hamouri, B., Vassel, J. L., 2000. Hydrodynamics and oxygen balance in a high-rate algal pond. *Water Science and Technology* 42, 349–356.
- EIshafei, G. M. S., Yehia, F. Z., Dimitry, O. I. H., Badawi, A. M., Eshaq, G.h, 2010. Degradation of nitrobenzene at near neutral pH using Fe<sup>2+</sup>–glutamate complex as a homogeneous Fenton catalyst. *Applied Catalysis B: Environmental* 99, 242-247.
- EPA, 2002a. EPA, Office of Prevention, Pesticides and Toxic Substances (7508W) EPA-738-F-02-002
- EPA, 2002b. EPA, Office of Prevention, Pesticides and Toxic substances, OPP-2002-0333.
- EPA, 2002c. EPA, Office of Prevention, Pesticides and Toxic Substances, Conditional Registration (7501C).
- European Commission, 2014. Report on the EU water framework directive in 2014. ISBN: 978-92-79-36449-5
- Fallmann, H., Krutzler, T., Bauer, R., Malato, S., Blanco, J., 1999. Applicability of the Photo-Fenton method for treating water containing pesticides. *Catalysis Today* 54, 309-319.
- Farré, M. I., Pérez, S., Kantiani, L., Barceló, D., 2008. Fate and toxicity of emerging pollutants, their metabolites and transformation products in the aquatic environment. *Trends in Analytical Chemistry* 27, 991-1007
- Faust, B. C., Hoigné, J., 1990. Photolysis of Fe (III)-hydroxy complexes as sources of OH radicals in clouds, fog and rain. *Atmospheric Environment* 24, 79-89.
- Feng, W., Nansheng, D., 2000. Photochemistry of hydrolytic iron (III) species and photoinduced degradation of organic compounds. A minireview. *Chemosphere* 41, 1137-1147.
- Fernández Sevilla, J. M., Ación Fernández, F. G., Molina Grima, E., 2010. Biotechnological production of lutein and its applications. *Applied Microbiology and Biotechnology* 86, 27–40.

- Fitzgerald, J., Jay, C., 2011. Chemical control of the European tarnished plant bug, *Lygus rugulipennis*, on strawberry in the UK. *Crop Protection* 30, 1178-1183.
- García, J., Green, B.F., Lundquist, T., Mujeriego, R., Hernández-Mariné, M., Oswald, W. J., 2006. *Bioresource Technology* 97, 1709–1715.
- García-Reyes, J. F., Gilbert-López, B., Molina-Díaz, A., 2008. Determination of Pesticide Residues in Fruit-Based Soft Drinks. *Analytical Chemistry* 80, 8966-8974.
- Ghatak, H. R., 2014. Advanced oxidation processes for the treatment of biorecalcitrant organics in wastewater. *Critical Reviews in Environmental Science and Technology* 44, 1167-1219.
- Gernjak, W., Krutzler, T., Glaser, A., Malato, S., Cáceres, J., Bauer, R., Fernández-Alba, A.R., 2003. Photo-fenton treatment of water containing natural phenolic pollutants. *Chemosphere* 50, 71-78.
- Gernjak, W., Fuerhacker, M., Fernandez-Ibañez, P., Blanco, J., Malato, S., 2006. Solar photo-Fenton treatment - Process parameters and process control. *Applied Catalysis B: Environmental* 64, 121-130.
- Gogate, P. R., Pandit, A. B., 2004. A review of imperative technologies for wastewater treatment II: hybrid methods. *Advances in Environmental Research* 8, 553-597.
- González, O., Sans, C., Esplugas, S., 2007. Sulfamethoxazole abatement by photo-Fenton: Toxicity, inhibition and biodegradability assessment of intermediates. *Journal of Hazardous Materials* 146, 459-464.
- Gonzalez-Olmos, R., Martin, M. J., Georgi, A., Kopinke, F., Oller, I., Malato, S., 2012. Fe-zeolites as heterogeneous catalysts in solar Fenton-like reactions at neutral pH. *Applied Catalysis B: Environmental* 125, 51-58.
- Goswami, D. Y., 1997. A Review of Engineering Developments of Aqueous Phase Solar Photocatalytic Detoxification and Disinfection Processes. *Journal of Solar Energy Engineering* 119, 101-107.
- Green, B., Lundquist, T., Oswald, W. J., 1995. Energetics of advanced integrated wastewater pond systems. *Water Science and Technology* 31, 9–20.
- Grundl T., Delwiche, J., 1993. Kinetics of ferric oxyhydroxide precipitation. *Journal of Contaminant Hydrology* 14, 71-97.
- Gupta, S. S., Stadler, M., Noser, C. A., Ghosh, A., Steinhoff, B., Lenoir, D., Horwitz, C. P., Schramm, K. W., Collins, T. J., 2002. Rapid total destruction of chlorophenols by activated hydrogen peroxide. *Science* 296, 326-328.
- Hadjltaief, H. B., Da Costa, P., Beaunier, P., Gálvez, M. E., Zina, M. B., 2014. Fe-clay-plate as a heterogeneous catalyst in photo-Fenton oxidation of phenol as probe molecule for water treatment. *Applied Clay Science* 91–92, 46-54.

- He, X., de la Cruz, A. A., O'Shea, K. E., Dionysiou, D. D., 2014. Kinetics and mechanisms of cylindrospermopsin destruction by sulfate radical-based advanced oxidation processes. *Water Research* 63, 168-178.
- Her, N., Amy, G., McKnight, D., Sohn, J., Yoon, Y., 2003. Characterization of DOM as a function of MW by fluorescence EEM and HPLC-SEC using UVA, DOC, and fluorescence detection. *Water Research* 37, 4295-303.
- Hernández-Sancho, F., Molinos-Senante, M., Sala-Garrido, R., 2011. Cost modelling for wastewater treatment processes. *Desalination* 268, 1–5.
- Huang, K., Couttenye, R. A., Hoag, G. E., 2002. Kinetics of heat-assisted persulfate oxidation of methyl tert-butyl ether (MTBE). *Chemosphere* 49, 413-420.
- Huang, W., Brigante, M., Wu, F., Hanna, K., Mailhot, G., 2012. Development of a new homogenous photo-Fenton process using Fe(III)-EDDS complexes. *Journal of Photochemistry and Photobiology A: Chemistry* 239, 17-23.
- Huang, W., Brigante, M., Wu, F., Mousty, C., Hanna, K., Mailhot, G., 2013. Assessment of the Fe(III)-EDDS complex in Fenton-like processes: From the radical formation to the degradation of bisphenol A. *Environmental Science and Technology* 47, 1952-1959.
- Ibrahim, M.A.S., Macadam, J., Autin, O., Jefferson, B., 2014. Evaluating the impact of LED bulb development on the economic viability of ultraviolet technology for disinfection. *Environmental Technology* 35, 400-406.
- Ikehata, K., El-Din, M.G., 2006. Aqueous pesticide degradation by hydrogen peroxide/ultraviolet irradiation and Fenton-type advanced oxidation processes: a review. *Journal of Environmental Engineering and Science* 5, 81-135.
- ISO 6332:1988, Water quality – Determination of iron –Spectrometric method using 1,10-phenantroline
- Jayson, G. G., Parsons, B. J., Swallow, A. J., 1973. Some simple, highly reactive, inorganic chlorine derivatives in aqueous solution. Their formation using pulses of radiation and their role in the mechanism of the Fricke dosimeter. *Journal of the Chemical Society, Faraday Transactions 1: Physical Chemistry in Condensed Phases* 69, 1597-1607.
- Ji, F., Li, C., Zhang, J., Deng, L., 2011. Heterogeneous photo-Fenton decolorization of methylene blue over LiFe(WO<sub>4</sub>)<sub>2</sub> catalyst. *Journal of Hazardous Materials* 186, 1979-1984.
- Jiang, C., Xu, Z., Guo, Q., Zhuo, Q., 2014. Degradation of bisphenol A in water by the heterogeneous photo-Fenton. *Environmental Technology (United Kingdom)* 35, 966-972.
- Jiménez, M., Maldonado, M. I., Rodríguez, E. M., Hernández-Ramírez, A., Saggiaro E., Carra, I., Sánchez Pérez, J. A., 2014. Supported TiO<sub>2</sub> solar photocatalysis at semi-pilot scale: Degradation of pesticides found in citrus processing industry wastewater,

- reactivity and influence of photogenerated species. *Journal of Chemical Technology & Biotechnology*, In Press.
- Katsoyiannis, I. A., Ruettimann, T., Hug, S. J., 2008. pH dependence of Fenton reagent generation and As(III) oxidation and removal by corrosion of zero valent Iron in aerated water. *Environmental Science and Technology* 42, 7424–7430.
- Keen, O. S., Linden, K. G., 2013. Degradation of antibiotic activity during UV/H<sub>2</sub>O<sub>2</sub> advanced oxidation and photolysis in wastewater effluent. *Environmental Science and Technology* 47, 13020-13030.
- Kiwi, J., Lopez, A., Nadochenko, V., 2000. Mechanism and kinetics of the OH Radical intervention during Fenton oxidation in the presence of a significant amount of radical scavenger (Cl<sup>-</sup>). *Environmental Science and Technology* 34, 2162–2168.
- Klamerth, N., Malato, S., Maldonado, M.I., Agüera, A., Fernández-Alba A.R., 2011. Modified photo-Fenton for degradation of emerging contaminants in municipal wastewater effluents. *Catalysis Today* 161, 241-246.
- Klamerth, N., Malato, S., Agüera, A., Fernández-Alba, A. R., Mailhot, G., 2012. Treatment of municipal wastewater treatment plant effluents with modified photo-fenton as a tertiary treatment for the degradation of micro pollutants and disinfection. *Environmental Science and Technology* 46, 2885-2892.
- Klamerth, N., Malato, S., Agüera, A., Fernández-Alba A., 2013. Photo-Fenton and modified photo-Fenton at neutral pH for the treatment of emerging contaminants in wastewater treatment plant effluents: A comparison. *Water Research* 47, 833-40.
- Klavarioti, M., Mantzavinos, D., Kassinos, D., 2008. Removal of residual pharmaceuticals from aqueous systems by advanced oxidation processes. Review article. *Environment International* 35, 402-417.
- Ko, J., Day, J. W., Lane, R. R., Day, J. N., 2004. A comparative evaluation of money-based and energy-based cost-benefit analyses of tertiary municipal wastewater treatment using forested wetlands vs. sand filtration in Louisiana. *Ecological Economics* 49, 331– 347.
- Köck-Schulmeyer, M., Villagrasa, M., López de Alda, M., Céspedes-Sánchez, R., Ventura, F., Barceló, D., 2013. Occurrence and behavior of pesticides in wastewater treatment plants and their environmental impact. *Science of the Total Environment* 458–460, 466–476.
- Kolthoff, I.M., Carr, E.M., 1953. Volumetric determination of persulfate in the presence of organic substances. *Analytical Chemistry* 25, 298–301.
- Konstantinou, I. K., Antonopoulou, M., Lambropoulou, D. A., 2014. Transformation products of emerging contaminants formed during advanced oxidation processes. In: Transformation products of emerging contaminants in the environment. D.A. Lambropoulou and L.M.L. Nollet (Eds) John Wiley and Sons Ltd., United Kingdom.
- Kroschwitz, J. I., Howe-Grant, M., 2004. Kirk-othmer encyclopedia of chemical technology, 4th ed., Wiley vol. 7–8.

- Kunai, A., Hata, S., Ito, S., Sasaki, K., 1986. The role of oxygen in the hydroxylation reaction of benzene with Fenton's reagent. 18O tracer study. *Journal of the American Chemical Society* 108, 6012-6016.
- Kusic, H., Koprivanac, N., Loncaric, A., Selanec, I., 2006. Photo-assisted Fenton type processes for the degradation of phenol: a kinetic study. *Journal of Hazardous Materials* 136, 632–644.
- Kusic, H., Koprivanac, N., Horvat, S., Bakija, S., Bozic, A. L., 2009. Modeling dye degradation kinetic using dark- and photo-Fenton type processes. *Chemical Engineering Journal* 155, 144-154.
- Laat, J., Le, G. T., Legube, B., 2004. A comparative study of the effects of chloride, sulfate and nitrate ions on the rates of decomposition of H<sub>2</sub>O<sub>2</sub> and organic compounds by Fe(II)/H<sub>2</sub>O<sub>2</sub> and Fe(III)/H<sub>2</sub>O<sub>2</sub>. *Chemosphere* 55, 715–723.
- Law, 1985. Law 29/1985 of 2<sup>nd</sup> August, establishing the Water Law in Spain.
- Law, 1988. Law 10/1988 of December 29<sup>th</sup>, regarding wastewater sanitation in Navarra, published in Official Bulletin of Spain, 1989, no. 32, pages 3669-3679, from 7<sup>th</sup> of January, 1989.
- Law, 1992. Law 2/1992 of March 26<sup>th</sup>, regarding wastewater sanitation in the region of Valencia, published in Official Bulletin of Spain, 1992, no. 128, pages 18195-18199, from 28<sup>th</sup> of May, 1992.
- Law, 1993. Law 10/1993 of October 26<sup>th</sup>, regarding industrial liquid waste into the sanitary network in the region of Madrid, published in Official Bulletin of Spain, 1993, no. 312, pages 37578-37587, from 30<sup>th</sup> of December, 1993.
- Law, 1994. Law 1/1994 of February 21<sup>st</sup>, regarding water sanitation and supply in the Principality of Asturias, published in Official Bulletin of the Principality of Asturias, 1994, no. 43, pages 1141-1447, from 25<sup>th</sup> of June, 1994.
- Law, 2000. Law 3/2000 of July 12<sup>th</sup>, regarding wastewater sanitation and depuration, and the establishment of the sanitary tax in the region of Murcia, published in Official Bulletin of Spain, 2001, no. 8, pages 883–891, from 9<sup>th</sup> of January, 2001.
- Law, 2000. Law 5/2000 of October 25<sup>th</sup>, regarding wastewater sanitation and depuration in La Rioja, published in Official Bulletin of Spain, 2000, no. 273, pages 39588–39603, from 14<sup>th</sup> of November, 2000.
- Law, 2001. Law 6/2001 of May 17<sup>th</sup>, 2001, regarding water management in Aragón, published in Official Bulletin of Aragón, no. 64, pages 3866-3883, from 1<sup>st</sup> of June, 2001.
- Law, 2002. Law 2/2002 of April 29<sup>th</sup>, 2002, regarding wastewater sanitation and depuration in the region of Cantabria, published in Official Bulletin of Cantabria, no. 86, pages 4275-4287, from 7<sup>th</sup> of May, 2002.

- Law, 2007. Law 7/2007 of July 9<sup>th</sup>, regarding the management of environmental quality, published in the Official Bulletin of Spain, 2007, no. 190, pages 34118 a 34169 from 9<sup>th</sup> August, 2007.
- Law, 2010. Law 9/2010 of November 4<sup>th</sup>, regarding waters in the region of Galicia, published in Official Diary of Galicia, 2010, no. 222, pages 18886-18924, from 18<sup>th</sup> of November, 2010.
- Lea, J., Adesina, A. A., 1998. The photo-oxidative degradation of sodium dodecyl sulphate in aerated aqueous TiO<sub>2</sub> suspension. *Journal of Photochemistry and Photobiology A* 118, 111-22.
- Lee, Y. K., 1997. Commercial production of microalgae in the Asia-Pacific rim. *Journal of Applied Phycology* 9, 403-411.
- Lee, C., Sedlak, D. L., 2009. A novel homogeneous Fenton-like system with Fe(III)–phosphotungstate for oxidation of organic compounds at neutral pH values. *Journal of Molecular Catalysis A: Chemical* 311, 1-6.
- Lee, Y., Lee, W., 2010. Degradation of trichloroethylene by Fe (II) chelated with cross-linked chitosan in a modified Fenton reaction. *Journal of Hazardous Materials* 178, 187-193.
- Lee, S., Park, S., 2013. TiO<sub>2</sub> photocatalyst for water treatment applications. *Journal of Industrial and Engineering Chemistry* 19, 1761-1769.
- Legislative Decree, 2003. Legislative Decree 3/2003 of November 4<sup>th</sup>, regarding waters in the region of Cataluña, published in Official Diary of Cataluña, 2003, no. 4015, pages 22823-22839, from 21<sup>st</sup> of November, 2003.
- Legrini, O., Oliveros, E., Braun, A. M., 1993. Photochemical processes for water treatment. *Chemical Reviews* 93, 671-698.
- Lam, F. L., Hu, X., Ming-Hung Lee, T., Chan, K. Y., 2009. A combined technique of photo-doping and MOCVD for the development of heterogeneous photo-Fenton catalyst. *Separation and Purification Technology* 67, 233-237.
- Li, Y., Bachas, L. G., Bhattacharyya, D., 2005. Kinetics studies of trichlorophenol destruction by chelate-based Fenton reaction. *Environmental Engineering Science* 22, 756-771.
- Li, L., Chen, X., Zhang, D., Pan, X., 2010. *Pesticide Biochemistry and Physiology* 98, 300-304.
- Li Puma, G., Khor, J. N., Brucato, A., 2004. Modeling of an Annular Photocatalytic Reactor for Water Purification: Oxidation of Pesticides. *Environmental Science and Technology* 38, 3737–3745.
- Liang, C., Bruell, C. J., Marley, M. C., Sperry, K. L., 2004. Persulfate oxidation for in situ remediation of TCE. I. Activated by ferrous ion with and without a persulfate-thiosulfate redox couple. *Chemosphere* 55, 1213-1223.

- Liao, C., Kang, S., Wu, F., 2001. Hydroxyl radical scavenging role of chloride and bicarbonate ions in the H<sub>2</sub>O<sub>2</sub>/UV process. *Chemosphere* 44, 1193-1200.
- Lin, S.H., Lo, C. C., 1997. Fenton process for treatment of desizing wastewater. *Water Research* 31, 2050-2056.
- Liu, S., Cheng, S., Feng, L., Wang, X., Chen, Z., 2010. Effect of alkalications on heterogeneous photo-Fenton process mediated by Prussian blue colloids. *Journal of Hazardous Materials* 182, 665-671.
- Lopes, G. K. B., Schulman, H. M., Hermes-Lima, M., 1999. Polyphenol tannic acid inhibits hydroxyl radical formation from fenton reaction by complexing ferrous ions. *Biochimica et Biophysica Acta: General Subjects* 1472, 142-52.
- Lu, M., Chen, J., Chang, C., 1997. Effect of inorganic ions on the oxidation of dichlorvos insecticide with Fenton's reagent. *Chemosphere* 35, 2285-2293.
- Malato, S., Blanco, J., Vidal, A., Richter, C., 2002. Photocatalysis with solar energy at a pilot-plant scale: An overview. *Applied Catalysis B: Environmental* 37, 1-15.
- Malato, S., Blanco, J., Vidal, A., Alarcón, D., Maldonado, M. I., Cáceres, J., Gernjak, W., 2003. Applied studies in solar photocatalytic detoxification: an overview. *Solar Energy* 75, 329-336.
- Malato Rodríguez, S., Blanco Gálvez, J., Maldonado Rubio, M. I., Fernández Ibáñez, P., Alarcón Padilla, D., Collares Pereira, M., Farinha Mendes, J., Correrira de Oliveira, J., 2004. Engineering of solar photocatalytic colectors. *Solar Energy* 77, 513-524.
- Malato, S., Fernández-Ibáñez, P., Maldonado, M. I., Blanco, J., Gernjak, W., 2009. Decontamination and disinfection of water by solar photocatalysis: Recent overview and trends. *Catalysis Today* 147, 1-59.
- Malato, S., Fernández-Ibáñez, P., Maldonado, M. I., Oller, I., Polo-López, M. I., 2013. Chapter 15. Photocatalysis solar pilot plants. Commercially available reactors In *Photocatalysis and water purification: From Fundamentals to Recent Applications*. Ed. Wiley-VCH, Weinheim-Germany, 377-397.
- Malato, S., Maldonado, M. I., Fernández Ibáñez, P., Oller, I., Polo, I., 2014. Chapter I, "Decontamination of water by solar irradiation", in *Advanced Oxidation Technologies: Sustainable Solutions for Environmental Treatments*, CRC Press.
- McGinnis, B. D., Adams, V. D., Middlebrooks, E. J., 2000. Degradation of ethylene glycol in photo Fenton systems. *Water Research* 34, 2346-54.
- McKay, A., Förster, H., Adaskaveg, J.E., 2012. Efficacy and Application Strategies for Propiconazole as a New Postharvest Fungicide for Managing Sour Rot and Green Mold of Citrus Fruit. *Plant Disease* 96, 235-242.
- Méndez-Arriaga, F., Esplugas, S., Giménez, J., 2010. Degradation of the emerging contaminant ibuprofen in water by photo-Fenton. *Water Research* 44, 589-595.

- Mesfioui, R., Love, N. G., Bronk, D. A., Mulholland, M. R., Hatcher P. G., 2012. Reactivity and chemical characterization of effluent organic nitrogen from wastewater treatment plants determined by fourier transform ion cyclotron resonance mass spectrometry. *Water Research* 46, 622-34.
- Minella, M., Marchetti, G., De Laurentiis, E., Malandrino, M., Maurino, V., Minero, C., Vione, D., Hanna, K., 2014. Photo-Fenton oxidation of phenol with magnetite as iron source. *Applied Catalysis B: Environmental* 154–155, 102-109.
- Miralles Cuevas, S., Oller, I., Sánchez Pérez, J. A., Malato, S., 2014a. Removal of pharmaceuticals from MWTP effluent by nanofiltration and solar photo-Fenton using two different iron complexes at neutral pH. *Water Research* 64, 23-31.
- Miralles Cuevas, S., Prieto Rodríguez, L., De Torres Socías, E., Polo López, M. I., Fernández Ibáñez, P., Oller, I., Malato, S., 2014b. Strategies for hydrogen peroxide dosing based on dissolved oxygen concentration for solar photo-fenton treatment of complex wastewater. *Global NEST Journal* 16, 553-560.
- Molina Grima, E., Fernández, F. G. A., García Camacho, F., Chisti, Y., 1999. Photobioreactors: Light regime, mass transfer, and scaleup. *Journal of Biotechnology* 70, 231-247.
- Murray, K. E., Thomas, S. M., Bodour, A. A., 2010. Prioritizing research for trace pollutants and emerging contaminants in the freshwater environment. *Environmental Pollution* 158, 3462-3471.
- Nemetz, P., 1980. System solutions to urban wastewater control. *Journal of Environmental and Economic Management* 7, 108-122.
- Neppolian, B., Choi, H.C., Sakthivel, S., Arabindoo, B., Murugesan, V., 2002. Solar light induced and TiO<sub>2</sub> assisted degradation of textile dye reactive blue 4. *Chemosphere* 46, 1173-1181.
- Nogueira, R. F. P., Silva, M. R. A., Trovo, A. G., 2005a. Influence of the iron source on the solar photo-Fenton degradation of different classes of organic compounds. *Solar Energy* 79, 384-392.
- Nogueira, R.F.P., Mirela, C.O., Paterlini, W.C., 2005b. Simple and fast spectrophotometric determination of H<sub>2</sub>O<sub>2</sub> in photo-Fenton reactions using metavanadate. *Talanta* 66, 86-91.
- Norman, R. O. C., Storey, P. M., West, P. R., 1970. Electron spin resonance studies. Part XXV. Reactions of the sulphate radical anion with organic compounds. *Journal of the Chemical Society B: Physical Organic*, 1087-1095.
- OECD, 1999. Guidelines for Testing of Chemicals, Simulation Test-Aerobic Sewage Treatment 303A.
- Oliveros, E., Legrini, O., Hohl, M., Müller, T., Braun, A.M., 1997. Industrial waste water treatment: Large scale development of a light-enhanced Fenton reaction. *Chemical Engineering and Processing: Process Intensification* 36, 397-405.



- Oller, I., Malato, S., Sánchez-Pérez, J. A., 2011. Combination of Advanced Oxidation Processes and biological treatments for wastewater decontamination-A review. *Science of the Total Environment* 409, 4141-4166.
- Orbeci, C., Untea, I., Nechifor, G., Segneanu, A. E., Craciun, M. E., 2014. Effect of a modified photo-Fenton procedure on the oxidative degradation of antibiotics in aqueous solutions. *Separation and Purification Technology* 122, 290-296.
- Ortega-Gómez, E., Moreno Úbeda, J. C., Álvarez Hervás, J. D., Casas López, J. L., Santos-Juanes Jordá, L., Sánchez Pérez, J. A., 2012. Automatic dosage of hydrogen peroxide in solar photo-Fenton plants: Development of a control strategy for efficiency enhancement. *Journal of Hazardous Materials* 237–238, 223-230.
- Ortiz de la Plata, G. B., Alfano, O. M., Cassano, A. E., 2010. Decomposition of 2-chlorophenol employing goethite as Fenton catalyst II: Reaction kinetics of the heterogeneous Fenton and photo-Fenton mechanisms. *Applied Catalysis B: Environmental* 95, 14-25.
- Oswald, W. J., Gotaas, H. B., 1957. Photosynthesis in sewage treatment. *Transactions of the American Society of Civil Engineers* 122.
- Pecsok, R. L., Sandera, J., 1955. The gluconate complexes. II. The ferric-gluconate system. *Journal of the American Chemical Society* 77, 1489–1494.
- Pereira, V. J., Linden, K. G., Weinberg, H. S., 2007a. Evaluation of UV irradiation for photolytic and oxidative degradation of pharmaceutical compounds in water. *Water Research* 41, 4413-4423.
- Pereira, V. J., Weinberg, H. S., Linden, K. G., Singer, P. C., 2007b. UV degradation kinetics and modeling of pharmaceutical compounds in laboratory grade and surface water via direct and indirect photolysis at 254 nm. *Environmental Science and Technology* 41, 1682-1688.
- Pereira, J.H.O.S., Queirós, D. B., Reis, A. C., Nunes, O. C., Borges, M. T., Boaventura, R.A.R., Vilar, V.J.P., 2014. Process enhancement at near neutral pH of a homogeneous photo-Fenton reaction using ferricarboxylate complexes: Application to oxytetracycline degradation. *Chemical Engineering Journal* 253, 217-228.
- Pérez-Estrada, L. A., Maldonado, M. I., Gernjak, W., Agüera, A., Fernández-Alba, A. R., Ballesteros, M. M., Malato, S., 2005. Decomposition of diclofenac by solar driven photocatalysis at pilot plant scale. *Catalysis Today* 101, 219-226.
- Pérez-Moya, M., Graells, M., Buenestado, P., Mansilla, H. D., 2008. A comparative study on the empirical modeling of photo-Fenton treatment process performance. *Applied Catalysis B: Environmental* 84, 313–323.
- Picot, B., Moersidik, S., Casellas, C., Bontoux, J., 1993. Using diurnal variations in a high rate algal pond for management pattern. *Water Science and Technology* 28, 209–215.

- Pignatello, J. J., 1992. Dark and photoassisted iron(3+)-catalyzed degradation of chlorophenoxy herbicides by hydrogen peroxide. *Environmental Science and Technology* 26, 944-951.
- Pignatello, J. J., Oliveros, E., MacKay, A., 2006. Advanced Oxidation Processes for Organic Contaminant Destruction Based on the Fenton Reaction and Related Chemistry. *Critical Reviews in Environmental Science and Technology* 36, 1-84.
- Pouran, S. R., Aziz, A. R. A., Daud, W. M. A. W., 2014. Review on the main advances in photo-Fenton oxidation system for recalcitrant wastewaters. *Journal of Industrial and Engineering Chemistry*, In Press.
- Prieto-Rodríguez, L., Oller, I., Zapata, A., Agüera, A., Malato, S., 2011. Hydrogen peroxide automatic dosing based on dissolved oxygen concentration during solar photo-Fenton. *Catalysis Today* 161, 247–254.
- Prieto-Rodríguez, L., Miralles-Cuevas, S., Oller, I., Agüera, A., Puma, G.L., Malato, S., 2012. Treatment of emerging contaminants in wastewater treatment plants (WWTP) effluents by solar photocatalysis using low TiO<sub>2</sub> concentrations. *Journal of Hazardous Materials* 211-212, 131-137.
- Prieto-Rodríguez, L., Oller, I., Klamerth, N., Agüera, A., Rodríguez, E.M., Malato, S., 2013. Application of solar AOPs and ozonation for elimination of micropollutants in municipal wastewater treatment plant effluents. *Water Research* 47, 1521-1528.
- Rastogi, A., Al-Abed, S. R., Dionysiou, D. D., 2009. Sulfate radical-based ferrous–peroxymonosulfate oxidative system for PCBs degradation in aqueous and sediment systems. *Applied Catalysis B: Environmental* 85, 171-179.
- Ratola, N., Cincinelli, A., Alves, A., Katsoyiannis, A., 2012. Occurrence of organic microcontaminants in the wastewater treatment process. A mini review. *Journal of Hazardous Materials* 239–240, 1-18.
- Richardson, J. W., Johnson, M. D., Outlaw, J. L., 2012. Economic comparison of open pond raceways to photo bio-reactors for profitable production of algae for transportation fuels in the Southwest. *Algal Research* 1, 93-100.
- Román Sánchez, I. M., Molina Ruiz, J. M., Casas López, J. L., Sánchez Pérez, J. A., 2011. Effect of environmental regulation on the profitability of sustainable water use in the agro-food industry. *Desalination* 279, 252-257.
- Román Sánchez, I. M., Carra, I., Sánchez Pérez, J. A., 2014. Promoting environmental technology using sanitary tax: the case of agro-food Industrial wastewater in Spain. *Environmental Engineering and Management Journal* 13, 961-969.
- Rodríguez, S., Vasquez, L., Costa, D., Romero, A., Santos, A., 2014. Oxidation of Orange G by persulfate activated by Fe(II), Fe(III) and zero valent iron (ZVI). *Chemosphere* 101, 86-92.
- Royal Decree, (2001), Royal Legislative Decree 1/2001 of 20<sup>th</sup> July, establishing the Consolidated Water Law

- Royal Decree, 2007. Royal Decree 1620/2007 of December the 7<sup>th</sup>, regarding water reclamation of depurated waters
- Ruppert, G., Bauer, R., Heisler, G., 1994. UV-O<sub>3</sub>, UV-H<sub>2</sub>O<sub>2</sub>, UV-TiO<sub>2</sub> and the photo-Fenton reaction - comparison of advanced oxidation processes for wastewater treatment. *Chemosphere* 28, 1447-1454.
- Safarzadeh-Amiri, A., Bolton, J. R., Cater, S. R., 1996. Ferrioxalate-mediated solar degradation of organic contaminants in water. *Solar Energy* 56, 439-443.
- Sanches, S., Barreto Crespo, M. T., Pereira, V. J., 2010. Drinking water treatment of priority pesticides using low pressure UV photolysis and advanced oxidation processes. *Water Research* 44, 1809-1818.
- Sánchez-Martínez, M. T., Rodríguez-Ferrero, N., Salas-Velasco, M., 2011. La gestión del agua en España. La unidad de Cuenca, revista de estudios regionales 92, 199-220. ISSN: 0213-7585.
- Sánchez Pérez, J. A., Román Sánchez, I. M., Carra, I., Cabrera Reina, A., Casas López, J. L., Malato, S., 2013. Economic evaluation of a combined photo-Fenton/MBR process using pesticides as model pollutant. Factors affecting costs. *Journal of Hazardous Materials* 244-245, 195-203.
- Santos-Juanes, L., García, J. L., Casas, J. L., Oller, I., Malato, S., Sánchez Pérez, J. A., 2011. Dissolved oxygen concentration: A key parameter in monitoring the photo-Fenton process. *Applied Catalysis B: Environmental* 104, 316-323.
- Sapieszko, R. S., Patel, R. C., Matijevic, E., 1977. Ferric hydrous oxide sols. 2. Thermodynamics of aqueous hydroxo and sulfato ferric complexes. *The Journal of Physical Chemistry A* 81, 1061-1068.
- Schenk, P., Thomas-Hall, S., Stephens, E., Marx, U., Mussgnug, J., Posten, C., et al., 2008. Second generation biofuels: high efficiency microalgae for biodiesel production. *Bioenergy Research* 1, 20-43.
- Sharma, R., Singhal, S., 2014. Photodegradation of textile dye using magnetically recyclable heterogeneous spinel ferrites. *Journal of Chemical Technology and Biotechnology*, in Press.
- Sharpless, C. M., Linden, K. G., 2003. Experimental and model comparisons of low- and medium-pressure Hg lamps for the direct and H<sub>2</sub>O<sub>2</sub> assisted UV photodegradation of N-nitrosodimethylamine in simulated drinking water. *Environmental Science and Technology* 37, 1933-1940.
- Sirtori, C., Agüera, A., Carra, I., Sánchez Pérez, J. A., 2014. Application of liquid chromatography quadrupole time-of-flight mass spectrometry to the identification of acetamiprid transformation products generated under oxidative processes in different water matrices. *Analytical and Bioanalytical Chemistry* 406, 2549-2558.
- Sirtori, C., Agüera, A., Carra, I., Sánchez Pérez, J. A., 2014. Identification and monitoring of thiabendazole transformation products in water during Fenton

- degradation by LC-QTOF-MS (2014) *Analytical and Bioanalytical Chemistry*, Article in Press.
- Sorokin, A., Meunier, B., Seris, J. L., 1995. Efficient oxidative dechlorination and aromatic ring cleavage of chlorinated phenols catalyzed by iron sulfophthalocyanine. *Science* 268, 1163-1166.
- Spolaore, P., Joannis-Cassan, C., Duran, E., Isambert, A., 2006. Commercial applications of microalgae. *Journal of Bioscience and Bioengineering* 101, 87–96.
- Steer, D., Aseltyne, T., Fraser, L., 2003. Life-cycle economic model of small treatment wetlands for domestic wastewater disposal. *Ecological Economics* 44, 359-369.
- Sun, Y., Pignatello, J. J., 1992. Chemical treatment of pesticide wastes. Evaluation of Fe(III) chelates for catalytic hydrogen peroxide oxidation of 2,4-D at circumneutral pH. *Journal of Agricultural and Food Chemistry* 40, 322-327.
- Tekbaş, M., Yatmaz, H. C., Bektaş, N., 2008. Heterogeneous photo-Fenton oxidation of reactive azo dye solutions using iron exchanged zeolite as a catalyst. *Microporous and Mesoporous Materials* 115, 594-602.
- Thomas, A., 1995. Regulating pollution under asymmetric information: the case of industrial wastewater treatment. *Journal of Environmental Economical Management* 28, 357-373.
- Toor, R., Mohseni, M., 2007. UV-H<sub>2</sub>O<sub>2</sub> based AOP and its integration with biological activated carbon treatment for DBP reduction in drinking water. *Chemosphere* 66, 2087-2095.
- Trovó, A. G., Nogueira, R. F. P., Agüera, A., Fernandez-Alba, A. R., Sirtori, C., Malato, S., 2009. Degradation of sulfamethoxazole in water by solar photo-Fenton. *Chemical and toxicological evaluation. Water Research* 43, 3922-3931.
- Tu, Y., Xiong, Y., Descorme, C., Kong, L., Tian, S., 2014. Heterogeneous photo-Fenton oxidation of acid orange II over iron-sewage sludge derived carbon under visible irradiation. *Journal of Chemical Technology and Biotechnology* 89, 544-551.
- USGS, 2014. U. S. Geological Studies, Glacier Studies Project, <http://www.glaciers.er.usgs.gov/>
- Van Well, M., Dillert, R. H. G., Bahnemann, D. W., Benz, V. W., Müller, M. A., 1997. A novel non-concentrating reactor for solar water detoxification. *Journal of Solar Energy Engineering* 119, 114-119.
- Vione, D., Merlo, F., Maurino, V., Minero, C., 2004. Effect of humic acids on the fenton degradation of phenol. *Environmental Chemistry Letters* 2, 129-33.
- Virkutyte, J., Varma, R.J., Jegatheesan, V., 2010. *Treatment of micropollutants in water and wastewater*. IWA Publishing, ISBN 10: 1843393166.
- WWF, 2014. *World Wildlife, Water Scarcity Report*, <http://www.worldwildlife.org/threats/water-scarcity>

- Wu, Y., Brigante, M., Dong, W., De Sainte-Claire, P., Mailhot, G., 2014a. Toward a better understanding of Fe(III)-EDDS photochemistry: Theoretical stability calculation and experimental investigation of 4- tert -butylphenol degradation. *Journal of Physical Chemistry A* 118, 396-403.
- Wu, Y., Passananti, M., Brigante, M., Dong, W., Mailhot, G., 2014b. Fe(III)-EDDS complex in Fenton and photo-Fenton processes: from the radical formation to the degradation of a target compound. *Environmental Science and Pollution Research*, Article in Press.
- Würtele, M. A., Kolbe, T., Lipsz, M., Külberg, A., Weyers, M., Kneissl, M., Jekel, M., 2011. Application of GaN-based ultraviolet-C light emitting diodes – UV LEDs – for water disinfection. *Water Research* 45, 1481-1489.
- Yuan, F., Hu, C., Hu, X., Qu, J., Yang, M., 2009. Degradation of selected pharmaceuticals in aqueous solution with UV and UV/H<sub>2</sub>O<sub>2</sub>. *Water Research* 43, 1766-1777.
- Zapata, A., Velegraki, T., Sánchez Pérez, J.A., Mantzavinos, D., Maldonado, M.I., Malato, S., 2009. Solar photo-Fenton treatment of pesticides in water: Effect of iron concentration on degradation and assessment of ecotoxicity and biodegradability. *Applied Catalysis B*: 88, 448–454.
- Zapata, A., Oller, I., Rizzo, L., Hilgert, S., Maldonado, M.I., Sánchez-Pérez, J.A., Malato, S., 2010. Evaluation of operating parameters involved in solar photo-Fenton treatment of wastewater: Interdependence of initial pollutant concentration, temperature and iron concentration. *Applied Catalysis B: Environmental* Volume 97, 292-298.
- Zepp, R. G., Faust, B.C., Holgné, J., 1992. Hydroxyl radical formation in aqueous reactions (pH 3-8) of iron(II) with hydrogen peroxide: The photo-fenton reaction. *Environmental Science and Technology* 26, 313-319.
- Zhang, R., Vigneswaran, S., Ngo, H., Nguyen, H., 2007. A submerged membrane hybrid system coupled with magnetic ion exchange (MIEX®) and flocculation in wastewater treatment. *Desalination* 216, 325-333.
- Zhoua, T., Lib, Y., Wongb, F., Lu, X., 2008. Enhanced degradation of 2,4-dichlorophenol by ultrasound in a new Fenton like system (Fe/EDTA) at ambient circumstance. *Ultrasonics Sonochemistry* 15, 782-790.



## **GLOSSARY**

---





---

## 7. GLOSSARY

<b>ACTM</b>	Acetamiprid
<b>AOP</b>	Advanced Oxidation Process
<b>BOD</b>	Biological Oxygen Demand
<b>COD</b>	Chemical Oxygen Demand
<b>CWL</b>	Consolidated Water Law
<b>CAS</b>	conventional activated sludge
<b>DOC</b>	Dissolved Organic Carbon
<b>EDDS</b>	ethylenediamine-N,N'-disuccinic acid
<b>EDTA</b>	Ethylenediaminetetraacetic acid
<b>FC</b>	Fixed Cost
<b>HM</b>	Heavy Metals
<b>HKCH</b>	Hexaketocyclohexane
<b>HEIDA</b>	Hydroxyethyliminodiacetic acid
<b>IMZ</b>	Imazalil
<b>IWWTP</b>	Industrial Wastewater Treatment Plant
<b>IS</b>	Inhibitory Substances
<b>LOD</b>	Limit of Detection
<b>LED</b>	Low Emitting Diode
<b>LPL</b>	Low Pressure Lamp
<b>MBR</b>	Membrane Bioreactor
<b>MLTSS</b>	mixed liquor total suspended solids
<b>MLVSS</b>	mixed liquor volatile suspended solids
<b>PTC</b>	Parabolic Trough Collector
<b>PS</b>	Persulfate
<b>PL</b>	Pollution Load
<b>RPR</b>	Raceway Pond Reactor
<b>ST</b>	Sanitary Tax
<b>SBR</b>	Sequencing Batch Reactor
<b>FePcS</b>	Sulfophthalocyanine
<b>THQ</b>	Tetrahydroxy-1,4quinone hydrate
<b>TBZ</b>	Thiabendazole
<b>TC</b>	Total Carbon
<b>TIC</b>	Total Inorganic Carbon
<b>TOC</b>	Total Organic Carbon

<b>TP</b>	Transformation product
<b>UPLC</b>	Ultra Performance Liquid Chromatography
<b>UWWTP</b>	Urban Wastewater Treatment Plant
<b>VC</b>	Variable Cost
<b>WCT</b>	Waste Control Tax
<b>WWTP</b>	Wastewater Treatment Plant
<b>WFD</b>	Water Framework Directive
<b>WRL</b>	Water Reclamation Law

# ***SCIENTIFIC PRODUCTION***

---



## 8. SCIENTIFIC PRODUCTION

As a result of the research presented in this PhD thesis, the following works were published or submitted for publication:

1. I. Carra, J. A. Sánchez Pérez, S. Malato, O. Autin, B. Jefferson, P. Jarvis. Application of high intensity UVC-LED for the removal of acetamiprid with the photo-Fenton process. *Chemical Engineering Journal*, Submitted.
2. I. Carra, L. Ponce-Robles, A. Agüera, J. A. Sánchez Pérez, S. Malato, C. Sirtori. Acetamiprid and thiabendazole degradation and monitoring of their transformation products in an agro-food industry effluent by using solar photo-Fenton in raceway ponds. *Chemosphere*, Submitted.
3. I. Carra, J. A. Sánchez Pérez, S. Malato, O. Autin, B. Jefferson, P. Jarvis. Performance of different Advanced Oxidation Processes for tertiary wastewater treatment to remove the pesticide acetamiprid. *Journal of Chemical Technology & Biotechnology*, Accepted.
4. I. Carra, L. Santos-Juanes, F. G. Ación, S. Malato, J. A. Sánchez Pérez. Raceway ponds as tertiary treatment technology. *Journal of Hazardous Materials* 279 (2014) 322–329.
5. I. Carra, S. Malato, J.L. Casas López, J.L. García Sánchez, J.A. Sánchez Pérez. Phenomenological study and application of the combined influence of iron concentration and irradiance on the photo-Fenton process to remove micropollutants. *Science of the Total Environment* 15 (2014) 123-132.
6. I. Carra, J. L. García Sánchez, S. Malato, J. A. Sánchez Pérez. Modelling Micropollutant Removal By Solar Photo-Fenton. *Global NEST Journal* 16 (2014) 445-454.
7. I. Carra, S. Malato, M. Jiménez, M. I. Maldonado, J.A. Sánchez Pérez. Microcontaminant removal by solar photo-Fenton at natural pH run with sequential and continuous iron additions. *Chemical Engineering Journal* 235 (2014) 132–140.

8. J.A. Sánchez Pérez, I. Carra, C. Sirtori, A. Agüera, B. Esteban. Fate of thiabendazole through the treatment of a simulated agro-food industrial effluent by combined MBR/Fenton processes at  $\mu\text{g/L}$  scale. *Water Research* 51 (2014) 55-63.
9. I. Carra, J.L. Casas López, L. Santos-Juanes, S. Malato, J.A. Sánchez Pérez. Iron dosage as a strategy to operate the photo-Fenton process at initial neutral pH. *Chemical Engineering Journal* 224 (2013) 67–74.
10. I. Carra, S. Malato, L. Santos-Juanes, J.L. Casas López, J. A.Sánchez Pérez. Study of iron sources and hydrogen peroxide supply in the photo-Fenton process using acetaminophen as model contaminant. *Journal of Chemical Technology and Biotechnology* 88 (2013) 636–643.



